Παρακολούθηση ψυχοσωματικής κατάστασης οδηγού με χρήση βιοσημάτων

Η ΔΙΔΑΚΤΟΡΙΚΗ ΔΙΑΤΡΙΒΗ

υποβάλλεται στην

ορισθείσα από την Γενική Συνέλευση Ειδικής Σύνθεσης

του Τμήματος Πληροφορικής Εξεταστική Επιτροπή

από τον

Γεώργιο Ρήγα

ως μέρος των Υποχρεώσεων για τη λήψη του

ΔΙΔΑΚΤΟΡΙΚΟΥ ΔΙΠΛΩΜΑΤΟΣ ΣΤΗΝ ΠΛΗΡΟΦΟΡΙΚΗ

Δεκέμβριος 2009

Dedication

I would like to dedicate this thesis to my parents, who all these years are supporting my dreams and my effort.

Acknowledgements

First of all, I sincerely need to thank, my supervisors Dr. D.I. Fotiadis, Professor at the Departmert of Materials Science and Engineering, University of Ioannina, and Dr. C. Nikou, Assistant Professor at the Department of Computer Science, University of Ioannina, for their support and greet assistance in order to complete this work. I would also thank the member of my advisory committee Dr. A. Likas, Associate Professor at the Department of Computer Science, University of Ioannina, for his support and cooperation. Furthermore, I should also thank all my colleagues I worked with, Dr. Y. Goletsis, Lecturer at the Department of Economics, University of Ioannina, P. Bougia, Dr. C. Katsis, Dr. A. Koutlas and K. Exarchos, as well as the people in the office, S. Petsios and V. Oikonomou, with whom we spent many years together, sharing good and bad times.

I would like especially to thank Dr. D.I. Fotiadis and Dr. C. Katsis for their actions for the funding of my research from the research program PENED 2003 of the Greek General Secretariat of Research and Technology.

Μέλη τριμελούς επιτροπής

Χριστόφορος Νίκου, Επίκουρος Καθηγητής Τμήματος Πληροφορικής του Παν/μίου Ιωαννίνων

Αριστείδης Λύκας, Αναπληρωτής Καθηγητής Τμήματος Πληροφορικής του Παν/μίου Ιωαννίνων

Δημήτριος Φωτιάδης, Καθηγητής Τμήματος Μηχανικών Επιστήμης Υλικών του Παν/μίου Ιωαννίνων

Μέλη επταμελούς επιτροπής

Μιχάλης Ζερβάκης, Καθηγητής Τμήματος Ηλεκτρονικών Μηχανικών και Μηχανικών Υπολογιστών Πολυτεχνείου Κρήτης

Κωνσταντίνα Νικήτα, Καθηγήτρια Σχολής Ηλεκτρολόγων Μηχανικών και Μηχανικών Ηλεκτρονικών Υπολογιστών του Ε.Μ.Π.

Γεώργιος Μανής, Επίκουρος Καθηγητής Τμήματος Πληροφορικής του Παν/μίου Ιωαννίνων

Κων/νος Μπλέκας, Επίκουρος Καθηγητής Τμήματος Πληροφορικής του Παν/μίου Ιωαννίνων

Table of Contents

List of Figures

List of Tables

Abstract

George Rigas. PhD, Computer Science Department, University of Ioannina, Greece. December, 2009. Assessment of driver's physiological state using physiological signals. Thesis Supervisor: Christophoros Nikou.

Among the most important factors in accident provocation is the human factor. Driver's loss of attention, aggressiveness and inefficient decision making, often lead to hazardous situations. A common reason of all the above is the physiological state of the driver. The last few decades several studies have designated the role of physiological state in driving performance and accident provocation. However the design of in-vehicle systems, able to assess physiological state with high credibility and in a rather unobtrusive way is still an ambitious goal.

This thesis makes a contribution towards the goal of driver's status recognition in a real-car application. Based mainly on the monitoring of driver's physiological signals and using additional sources such as video from driver's face as well as driving environment information, we focused on the detection of driver's fatigue and stress levels. The data used were collected during a long-lasting experimental protocol on a real driving environment and under different weather, traffic and road conditions. During the real-world experiments a set of physiological signals have been recorded, in particular: electrocardiograph (ECG), respiration and electrodermal activity (EDA), from which a number of features from both time and frequency space were extracted. The set of features were examined in terms of their contribution to the detection of fatigue and stress and the most powerful indicators for each state of interest were selected following a feature selection technique. Four different classifiers were employed and the classification results were evaluated in terms of sensitivity, specificity and accuracy. Our results indicate good performance for both fatigue and stress classification problems. The evaluation of features' contribution to the detection of the two states revealed that all information sources contribute equally to the two-class stress classification problem, while a three-class fatigue classification is feasible by using physiological features only, as those are the features with the major contribution.

Although the majority of relevant works concentrate on the detection of high levels of fatigue (drowsiness) with our methodology we can achieve also detection of early fatigue stages (low fatigue). To quantify the impact of these early fatigue stages on driving performance, we built a driving simulation environment, which allowed us to monitor driving performance measures (i.e. reaction times) and correlate them with the states under investigation. The outcomes of the simulation study verified the association of the different fatigue levels and the physiological features used for their classification with the degree of impairment in driver's performance. This finding demonstrates the value and potential of an in-vehicle system able to recognize progressive fatigue levels and predict driver's reaction time based on physiological signals monitoring.

Unlike fatigue which is a progressive state, driver stress is a more time-variant condition which is highly dependent on the driving context and it is temporarily influenced by events occurring en-route. We call the driving environment-related events (such as overtake, hard braking, junction, curve, etc) "driving events" and the temporal stress that may impose to the driver, "stress events". The detection of stress events can contribute to the driver's state estimation in the sense that the frequent occurrence of stress events could have more prolonged effects on driver's state, i.e. increase the overall driver's stress level. In our thesis, we developed a methodology for online detection of stress events, using the same set of physiological signals (ECG, Respiration, EDA) as well as driving behavior parameters (position, velocity, acceleration, deceleration) acquired from car equipment (GPS and CAN bus). We achieved 95% accuracy in the detection of stress events which is expected to increase with the introduction of visual information from the road environment.

A very important requirement for a system for driver physiological state assessment, is the adaptation of system's parameters on the physiological features of new drivers. We consider a system based on a Gaussian mixture model, and the basic assumption is that the feature distribution of the new driver is a geometric transformation of the feature distribution used for the training of the system. The method is based on the Expectation-Maximization (EM) approach for the estimation of the geometric transformation applied on the initial Gaussian Mixture model. We evaluated the proposed method using artificial dataset. Since EM is a local optimization algorithm, the method does not guarantee the correct solution identification. To confront this limitation we proposed a multiple start EM algorithm which increased the method performance. Next we extended the model allowing each mixture component to have an individual (local) transformation, and applied a MAP-EM approach for estimating both the common (global) transformation as well as the local ones. We evaluated the proposed method using both artificial and real driver's data, collected in a simulation environment. Apart from adaptation to new drivers, the proposed method can be applied also to other problems, such as image registration and

tracking.

Based on the fact that driver's state is a significant factor for road safety, we made a step further and designed the building blocks of an advanced driver support systems that exploits driver's state estimation as well as vehicle communication abilities for increasing safety in every day driving. As a first step we developed a simulation environment of vehicle to vehicle (V2V) and vehicle to infrastructure (V2I) communication. Experiments on the simulation environment confirmed that the exploitation of those types of communication can increase driving safety. Moreover, it helped to define minimum requirements for communication characteristics (range, latencies and broadcasting frequency) in realistic scenarios of co-operative driving. The second step was the implementation of two basic subsystems: a) the information handler and b) the decision maker. The information handler applies information fusion of low confidence sensors (other vehicles) and employs Bayesian Networks for the extraction of high-level information, useful for the driver. The decision maker is based upon sampling of Dynamic Bayesian networks for driving risk evaluation and decides upon the best warning strategy, taking into account both environmental conditions and driver's state. Concluding, this thesis studies the assessment of driver's psycho-physiological state exploiting mainly physiological signals as well as other information sources towards the development of a real-application driver support system that contributes to the increase of driving safety.

Εκτενησ Περιληψη στα Ελληνικα

Γεώργιος Ρήγας του Αντωνίου και της Βασιλικής. PhD, Τμήμα Πληροφορικής, Πανεπιστήμιο Ιωαννίνων, Δεκέμβριος, 2009. Αναγνώριση της ψυχοσυναισθηματικής κατάστασης του οδηγού με χρήση βιοσημάτων. Επιβλέποντας: Χριστόφορος Νίκου.

Από τους πιο σημαντικούς παράγοντες στην πρόκληση ατυχημάτων είναι ο ανθρώπινος παράγοντας. Μεταξύ άλλων, η μείωση της προσοχής του οδηγού, η επιθετικότητα στην οδήγηση και οι λανθασμένες αποφάσεις, συχνά μπορούν να οδηγήσουν στην πρόκληση ατυχημάτων. Ένα κοινό αίτιο όλων των παραπάνω είναι η ψυσοσυναισθηματική κατάσταση του οδηγού. Τις τελευταίες δεκαετίες έχουν γίνει αρκετές μελέτες που τονίζουν τον ρόλο της ψυχοσυναισθηματικής κατάστησης στην απόδοση του οδηγού και στην πιθανή πρόκληση ατυχημάτων. Ωστόσο η ανάπτυξη συστήματων που θα βρίσκονται μέσα στο όχημα και θα ανιχνεύουν την κατάσταση του οδηγού με μεγάλη αξιοπιστία και χωρίς να επιβαρύνουν ή να ενοχλούν τον οδηγό, είναι ακόμα σε πρώιμα στάδια.

Αντικείμενο έρευνας της παρούσας διατριβής είναι η αναγνώριση της ψυχοσυναισθηματικής κατάστασης του οδηγού σε πραγματικές οδηγικές συνθήκες. Βασιστήκαμε κυρίως στην λήψη και επεξεργασία βιοσημάτων του οδηγού, όπως επίσης σε παρακολούθηση του προσώπου του οδηγού και σε μεταβλητές του περιβάλλοντος οδήγησης για την αναγνώριση των καταστάσεων κούρασης και στρες του οδηγού. Τα δεδομένα που χρησιμοποιήθηκαν συλλέχθηκαν σε ένα μακροχρόνιο στάδιο διεξαγωγής πειραμάτων σε πραγματικές οδηγικές συνθήκες. Στην διάρκεια αυτών των πειραμάτων συλλέξαμε ένα σύνολο από βιοσήματα του οδηγού, και συγκεκριμένα ηλεκτροκαρδιογράφημα, αναπνοή και ηλεκτροδερμική δραστηριότητα. Από τα βιοσήματα, το βίντεο και τις συνθήκες οδήγησης εξάγαμε έναν σημαντικό αριθμό από χαρακτηριστικά και τα αξιολογήσαμε ως προς την συνεισφορά τους στην αναγνώριση τόσο της κούρασης όσο και του στρες. Σε μια διαδικασία επιλογής χαρακτηριστικών, μόνο αυτά με την μεγαλύτερη συνεισφορά χρησιμοποιήθηκαν στο επόμενο βήμα της ταξινόμησης. Τέσσερεις διαφορετικοί ταξινομητές αξιολογήθηκαν ώς προς την ακρίβεια ταξινόμησης, την ευαισθησία και την εξειδίκευση. Τα αποτελέσματα μας ήταν πολύ ικανοποιητικά τόσο για την αναγνώρισης της κούρασης και του στρες. Στην συνέχεια αξιολογήσαμε την συνεισφορά του κάθε αισθητήρα στην αναγνώριση της κούρασης και του στρες. Μία τέτοια μελέτη είναι σημαντική στον σχεδιασμό ενός συστήματος αναγνώρισης της κατάστασης του οδηγού, τόσο για την μείωση της πολυπλοκότητας όσο και του κόστους. Τα πειράματα που πραγματοποιήσαμε έδειξαν ότι στην αναγνώριση της κούρασης τα βιοσήματα είναι αυτά

που συνεισφέρουν περισσότερο και ειδικότερα το ηλεκτροκαρδιογράφημα φαίνεται να είναι ο σημαντικότερος αισθητήρας, ενώ για το στρες όλοι σχεδόν οι αισθητήρες έχουν παρόμοια συνεισφορά.

Ενώ οι περισσότερες σχετικές εργασίες εστιάζουν στην αναγνώριση υψηλών επιπέδων κούρασης (υπνηλία) με την μεθοδολογία μας επιτυγχάνεται επίσης η αναγνώριση των πρόιμων σταδίων της κούρασης (μέτρια κούραση). Για να ποσοτικοποιήσουμε την επίδραση των χαμηλών επιπέδων κούρασης στην οδηγική απόδοση, αναπτύξαμε ένα περιβάλλον εξομοίωσης, το οποίο μας επέτρεψε την καταγραφή μέτρων οδηγικής απόδοσης (όπως χρόνοι αντίδρασης) και την συσχέτιση τους με τα επίπεδα κούρασης. Τα αποτελέσματα από την μελέτη στο περιβάλλον εξομοίωσης επαλήθευσαν την συσχέτιση των διαφορετικών επιπέδων κούρασης και των χαρακτηριστικών από τα βιοσήματα με τον βαθμό μείωσης της οδηγικής απόδοσης. Αυτό το εύρημα επιδεικνύει την αξία και την προοπτική ενός συστήματος ικανού να αναγνωρίζει τα προοδευτικά επίπεδα κούρασης και να προβλέπει τον χρόνο αντίδρασης του οδηγού, βασιζόμενο στην καταγραφή βασικών βιοσημάτων. Αντίθετα με την κούραση, η οποία είναι μία προοδευτική κατάσταση το στρες είναι πιο ευμετάβλητο, καθώς επηρεάζεται σε μεγάλο βάθμο από το περιβάλλον οδήγησης και από γεγονότα που λαμβάνουν χώρα σε αυτό. Ονομάζουμε αυτά τα γεγονότα κατα την διάρκεια της οδήγησης (προσπέραση, απότομη πέδηση κ.α.) "οδηγικά γεγονότα" και το παροδικό στρες που αυτά προκαλούν στον οδηγό "γεγονότα στρες". Η ανίχνευση των γεγονότων στρες συμβάλει στην εκτίμηση της ψυχοσωματικής κατάστασης του οδηγού, καθώς η συχνή εμφάνιση τέτοιων γεγονότων μπορεί να προκαλέσει παρατεταμένο στρες στον οδηγό. Σε αυτήν την διατριβή αναπτύξαμε μία μεθοδολογία για την αναγνώριση γεγονότων στρες σε πραγματικό χρόνο, χρησιμοποιώντας το ίδιο σύνολο βιοσημάτων (ηλεκτροκαρδιογράφημα, αναπνοή και ηλεκτροδερμική δραστηριότητα) καθώς και παραμέτρους της οδηγικής συμπεριφοράς (θέση, ταχύτητα, επιβράδυνση κ.α.) τα οποία συλλέξαμε από τον εξοπλισμό του αυτοκινήτου (GPS και Can-Bus). Με την χρήση Bayesian δικτύων αναγνωρίζουμε με ακρίβεια 95% τα γεγονότα στρες.

Ένα πρόβλημα που συχνά παρουσιάζεται με παρόμοια συστήματα, είναι η ανάγκη για "προσαρμογή" του συστήματος σε ένα νέο οδηγό. Προς αυτήν την κατεύθυνση παρουσιάζουμε μία μέθοδο για την εκτίμηση των παραμέτρων μία μεικτής κανονικής κατανομής η οποία υφίσταται έναν γεωμετρικό μετασχηματισμό. Η μέθοδος βασίζεται στον αλγόριθμο EM. Καθώς ο αλγόριθμος EM είναι ένας αλγόριθμος τοπικής βελτιστοποίησης, η μέθοδος δεν εγγυάται την εύρεση της πραγματικής λύσης. Για να αντιμετώπισουμε αυτόν τον περιορισμό, προτείναμε την χρήση του αλγορίθμου EM με πολλαπλές εκκινήσεις. Αυτή η προσέγγιση αυξάνει σημαντικά την πιθανότητα εύρεσης της πραγματικής λύσης. Στην συνέχεια επεκτείνουμε το αρχικό μοντέλο, όπου έχουμε έναν κοινό μετασχηματισμό σε όλες τις συνιστώσες, αναθέτοντας έναν τοπικό μετασχηματισμό σε κάθε συνιστώσα. Στις παραμέτρους των τοπικών μετασχηματισμών, θεωρούμε μία εκ των προτέρων κατανομή και χρησιμοποιούμε μία προσέγγιση MAP-EM για την εκτίμηση των παραμέτρων του ολικού και των τοπικών μετασχηματισμών. Δοκιμάσαμε την μέθοδο στην προσαρμογή ενός μοντέλου αναγνώρισης της κατάστασης του οδηγού, το οποίο έχει εκπαιδευθεί σε ένα συγκεκριμένο σύνολο οδηγών,

σε νέους οδηγούς. Τα πρώτα αποτελέσματα είναι αρκετά υποσχόμενα. Επίσης πρέπει να τονίσουμε ότι η συγκεκριμένη μέθοδος μπορεί κάλιστα να εφαρμοστεί σε παρόμοια προβλήματα αλλά και σε άλλα όπως η υπέρθεση εικόνων.

Βασιζόμενοι στο γεγονός ότι η κατάσταση του οδηγού είναι σημαντική στην οδηγική ασφάλεια, προχωρήσαμε ένα βήμα παραπέρα και μελετήσαμε τα βασικά μέρη ενός "έξυπνου" συστήματος υποβοήθησης του οδηγού το οποίο μπορεί να εκμεταλλευτεί τόσο την κατάσταση του οδηγού όσο και δίκτυα επικοινωνίας μεταξύ αυτοκινήτων. Τέτοια συστήματα στοχεύουν στην αύξηση της οδηγικής ασφάλειας, αφενός επεκτείνοντας το πεδίο αντίληψης του οδηγού και αφετέρου παρέχοντας κατάλληλα ειδοποιητικά μηνύματα στον οδηγό για προσεχείς κινδύνους. Το πρώτο βήμα ήταν ο σχεδιασμός ενός προγράμματος μακροσκοπικής εξομοίωσης ενός οδηγικού περιβάλλοντος με επικοινωνία μεταξύ οχημάτων καθώς και οχημάτων με την υποδομή του δρόμου. Πειράματα σε αυτό το περιβάλλον έδειξαν ότι τέτοια συστήματα μπορούν πράγματι να αυξήσουν την οδηγική ασφάλεια, κάτω από ορισμένες τιμές των παραμέτρων επικοινωνίας (καθυστέρηση, εμβέλεια, συχνότητα εκπομπής). Σε αυτό το σύστημα υπάρχουν δύο βασικά υπομέρη, που στα αρχικά πειράματα θεωρούνταν δεδομένα αλλά χρίζουν εκτενέστερης μελέτης. Το πρώτο είναι ο τρόπος με τον οποίο χειριζόμαστε την πληροφορία. Μελετήσαμε μία μέθοδο με χρήση Bayesian δικτύων για χειρισμό της πληροφορίας από πηγές χαμηλής αξιοπιστίας και εξαγωγής νέας πληροφορίας. Το δεύτερο κομμάτι του συστήματος που εξετάζουμε είναι ο μηχανισμός λήψης αποφάσεων ο οποίος είναι υπεύθυνος για τον τρόπο και τον χρόνο προώθησης μηνυμάτων για την έγκαιρη ειδοποίηση του για πιθανούς κινδύνους. Ο μηχανισμός απόφασης βασίστηκε σε δειγματολεψία δυναμικών Bayesian δικτύων για την εκτίμηση της αναμενόμενης τιμής μίας συνάρτησης κόστους και την εκτίμηση της βέλτιστης ενέργειας.

Η συγκεκριμένη διατριβή συνοψίζοντας, μελετά την αναγνώρισης της ψυχοσυναισθηματικής κατάστασης του οδηγού μελετώντας κυρίως βιοσήματα αλλά και άλλες πηγές πληροφοριών και προχωρά στην αξιοποίηση αυτής της πληροφορίας μεταξύ άλλων για την επίτευξη συστημάτων που εντέλει θα συνεισφέρουν στην μείωση των ατυχημάτων και στην αύξηση της ασφάλειας στην οδήγηση.

Chapter 1

Introduction

The human physiological state is well studied in many fields of science and industry, such as medicine, human factors, aviation, and automotive. Generally in any critical task involving a decision process by a human, the quality of the decision and hence the successful execution of the task strongly depends on human's physiological state. Such a task, which daily perils the life of millions of people is driving. Driving in a real-world environment is a difficult task, because decisions are made given only incomplete information in real time. A great number of fatalities occurring in motor vehicles could be avoided if behaviors such as driver inattention, stress, fatigue, and sleepiness were detected. The inability to manage one's condition during driving is identified as one of the major causes of accidents [57]. The task to determine the driver state in a vehicle is an active topic both for the scientific community and research institutes as well as software companies for real world applications. The most common aspects of physiology that contribute greatly to degradation of driving performance and consequently increase road risk are the mental fatigue and stress. High stress influences adversely drivers' reactions in critical situations, thus it is one of the most important reasons for car accidents according to the American Highway Traffic Safety Administration. Recent findings have shown that stress is not only tightly intertwined neurologically with the mechanisms responsible for cognition, but also plays a vital role in decision making, problem solving and adapting to unpredictable environments such as driving [95]. When drivers are overwhelmed by anger or stress, their thinking, perceptions, and judgments are impaired, leading to misinterpretation of events. In addition, drivers often lack the ability to calm themselves when they are angry or frustrated [67]. In the context of everyday driving, similar situations are not even tolerable since they may not only compromise the performance of the drivers but also endanger

their lives. On the other hand, fatigue impairs human performance elements, which are critical for safe driving [6]. More specifically, the most common fatigue effects identified in in-vehicle studies include:

- Increased reaction time: Drowsy drivers appear to have slower reaction times, which hinders effective braking to avoid a collision. At high speeds in particular, even small impairments in reaction time can have a profound effect on crash risk.
- Hypo-vigilance: Performance of tasks requiring attention declines with fatigue, including prolonged periods of non-responding or delayed responding.
- Information processing impairment: Processing and integration of information needs more time, the accuracy of short-term memory is reduced, and the overall performance of situation perception declines.

Having the most negative impact on road safety, driver fatigue and stress constitute the two physiological states of interest for this study. However, since both terms may be assigned with several interpretations, it is considered fundamental to provide hereby definitions of fatigue and stress that describe best the conditions studied in this work. A review of the impact of each state on driving performance is also given, in order to justify the necessity of the detection of these two states, regarding the driver and the driving task.

1.1 Definition of Fatigue

Fatigue is a general term which has been used to describe several expressions of this psycho-physiological state. The most common are mental fatigue and muscle fatigue. In this thesis we focus on mental fatigue. However, even for mental fatigue there are several definitions. According to Brown [18], "physiological fatigue is defined as a subjectively experienced disinclination to continue the task". Another definition from NASA [126], states than "fatigue may refer to feeling tired, sleepy or exhausted". Hancock's [2] definition of fatigue is "an individual's multi-dimensional physiological-cognitive state associated with stimulus repetition which results in prolonged residence beyond a zone of performance comfort". A more comprehensive definition given by Hancock [2], that fulfills a number of criteria necessary for a complete definition of fatigue is that "fatigue refers to the state of an organism's muscles, viscera, or central nervous system, in which prior physical activity and/or mental processing, in the absence of sufficient rest, results in insufficient cellular capacity or system wide energy to maintain the original level and/or processing by using normal resources". In this thesis the studied fatigue is well described by all the above definitions. From the definition of fatigue, as well as from personal experience, the most probable symptoms of fatigue on a driver's performance are rather expected.

1.1.1 Fatigue and Driving performance

According to the previous definitions, mental fatigue is a cumulative and gradual process that is highly related with loss of alertness. It is associated with reluctance for any effort, with reduced efficiency and impaired mental performance [39]. Although the factors that influence mental fatigue could vary from physical health and nutrition [156] to physical activity and environmental factors [137] or even to recuperation periods [108], the symptoms of mental fatigue are quite common: unwillingness for any physical or mental effort, feeling of weariness, and impaired activity. According to Grandjean [38], the functional states of a person range from deep sleep, light sleep, drowsy, weary, hardly awake, relaxed, resting, fresh, alert, very alert, stimulated and a state of alarm. In this context, mental fatigue is a condition grading in one direction into sleep, and in the other direction into a relaxed, resting state. Both directions, though, are considered likely to reduce attention and decline alertness. When individuals are allowed to rest, these resting conditions are not considered unpleasant; but they can be distressing if one needs to deal with a demanding task such as driving. When mental fatigue leads to drowsiness it becomes significant contributing factor to road crashes. According to NCSDR/NHTSA Expert Panel on Driver Fatigue and Sleepiness[138] there are 56,000 crashes each year (in the United States) in which drowsiness or fatigue was cited by police as a causal factor. These crashes lead to, on average, 40,000 nonfatal injuries and 1,550 fatalities per year. Data from the U.S.-based 100-car naturalistic driving study indicated that drowsy driving (compared to alert driving) resulted in a five-fold increase in risk of a crash or near-crash [73]. MacLean *et al.* [92] concluded that "while estimates of the number of crashes due to sleepiness have varied widely, there is converging evidence that about 20% of crashes are related to sleepiness". Taken together, these statistics indicate that driver drowsiness imposes a significant burden on society, and constitutes a serious public health issue. All the above indicate that mental fatigue and especially drowsiness is a high risk physiological state in the driving context. Apart from late fatigue stages such as drowsiness, even earlier fatigue states, which are characterized by a reduced driver's arousal are followed by a driving performance impairment [25]. In neurological research the terms vigilance and arousal are used interchangeably, both referring to a general state of wakefulness, characterized as alertness [110]. An important factor related to fatigue and hypovigilance is the circadian rhythm. It is the biological clock that normally has a 24 h period. Physiological parameters such as motor activity, body temperature, blood pressure and work performance are disturbed from disruptions to the circadian rhythm [127]. Apart from circadian rhythm, a number of environmental factors affect vigilance, such as noise, vibration, ambient temperature, frequency and variety of stimulations during driving. For instance, the higher levels of noise during driving can lead to driver fatigue. This type of mental fatigue, also known as "cognitive fatigue", results from the higher demand for driver's attention imposed by the presence of such stressors [25]. Driver performance is also deteriorated with long hours of continuous driving, with monotonous driving environment and during night/early morning hours driving [100].

In a road environment, drivers' fatigue can be severe before its effects in routine driving performance become noticeable. This is because, even lower fatigue levels can still cause declines in physiological vigilance/arousal, slow sensorimotor functions (i.e. slower perception and reaction times) and information processing impairments, which in turn diminish driver's ability to respond to unexpected and emergency situations [94]. Therefore, the impact of fatigue on driver performance cannot be measured using only direct indices of driving task, like speed maintenance and steering control, but additional parameters, associated with driving performance, are needed (such as perceptual, motor and cognitive skills). [154]. This is also the main drawback of approaches measuring physical appearance measures, such as eye blinking, head movement and yawning. Those are symptoms of late fatigue stages and the driving performance has already a significant reduction. It is therefore critical for a real-time operational driving environment to develop strategies for early fatigue detection and provide countermeasures that optimize performance and maintain an adequate margin of safety.

1.2 Definition of Stress

According to European ISO 10075 [1], mental stress is defined as: "The total of all assessable influences impinging upon a human being from external sources and affecting it mentally." Situational influences on mental stress include: task requirements (e.g. sustained concentration, responsibility for others), physical conditions (e.g. lighting, noise), social and organisational factors (e.g. control structure, communication structure, organisational environment), social factors, external to the organisation (e.g. economic situation). Another definition by Lazarus and Folkman [3] states that: "stress is a feeling experienced when a person thinks that the demands exceed the personal and social resources the individual is able to mobilize".

1.2.1 Stress and driving performance

Moderate levels of stress appear to be fairly common in everyday driving. In a diary study of company car drivers, around 50% of drivers reported adverse affective reactions on any given day [40]. Although negative moods experienced during driving are often relatively mild, strong emotional reactions to driving also occur in forms of driving phobias and in so-called road rage. Stress appears to predispose drivers to a heightened risk of motor vehicle accidents. Variables that discriminate between accident-involved and non accident-involved drivers include specific sources of stress, such as interpersonal and job problems, as well as overall assessments of recent exposure to stressful life events. Accident likelihood is also connected to personality characteristics that are associated with stress vulnerability, such as personal maladjustment, depression, anxiety, and aggression (see [40]). Stress effects can sometimes be quite large in magnitude. Brenner and Selzer [16] estimated that drivers who have experienced a recent stressful event are five times more

likely to cause fatal accidents than are unstressed drivers. There are two limitations of current research. First, stress is often used as a vague, umbrella term. However, a variety of distinct emotional and cognitive components of stress reactions can be distinguished that might have differing consequences for performance [150]. Second, existing works provide little information on the behavioral mechanisms that might link stress to increased accident risk[136]. Accident research suggests a variety of mechanisms for human error in driving, such as impairment of attentional efficiency and change in strategy [96], but it is unclear how these mechanisms are influenced by stress reactions. Hence, to understand how stress influences safety, it is necessary to discriminate different aspects of driver stress and then to link these different aspects of stress to behavioral measures.

1.3 Outline of this thesis

The literature reports many attempts to develop safety systems for reducing the number of automobile accidents: these systems detect both the "driving behavior" by monitoring lane keeping, steering movements, acceleration, braking and gear changing, and also the "driver status" by such means as tracking the driver's head and the eye movements, monitoring the heart and breathing rates, the brain activity, and recognizing the torso and arm/leg motion. An in-depth literature review focused on specific aspects of driver stress and fatigue estimation was conducted. Different methodologies based on biosignal and machine vision driver monitoring along with their experimental protocols and their achieved results were studied and analyzed. Both advantages and limitations of state-of-the-art methods are defined. Before proceeding with the presentation of literature review the basic physiological measures used in the majority of similar works are described in section 2.2 along with their association to the human physiology. Moreover, in Chapter 2 the most insightful research studies are presented. Those constitute the baseline for our research and they have contributed significantly to move beyond the state-of-the art in the field of driver state recognition based mostly on physiological signals.

Discussions with neurologists and human factor experts helped in the definition of the stress and fatigue classification problems. As previously mentioned stress influences driving performance through nervous reactions and has negative effects on drivers' judgment. From human factor point of view, a driver assistance system should be able to discriminate *stress* from *normal* driver state and alternate its warning strategy accordingly. Stress detection is therefore tackled as a two-class classification problem. Driver fatigue, on the other hand, although it is the subject of numerous studies in literature, the majority of the existing works focus mainly on the detection of late stages of fatigue (drowsiness), when driver experiences micro sleep episodes, which is most probable to lead to potential accidents. However, as noticed before, according to experts in the human physiology, even earlier stages of fatigue (low-fatigue) may have significant impact on driving performance

and the detection of those stages could be very useful for driver assistance systems. In our work we tackle the fatigue detection as a three-class problem, i.e. discriminate: *normal*, *low-fatigue* and *high-fatigue* states.

The collection of experimental data for different driver states (stress and fatigue) requires a protocol which ensures that driver experiences these states. The major part of our experiments was conducted in real-world considering the difficulty in controlling the driver's state since it highly depends on the prevailing driving environment. A series of experiments were also conducted in a simulation environment, specially built for studying the impact of human physiology on driving performance. In Chapter 3 we present the dataset collection which was performed in both real driving conditions and a simulation environment. Details about the equipment of the study, the experimental protocol and software developed for data acquisition and annotation are also presented.

Making use of the data collected during real driving conditions we developed a methodology for the aforementioned stress and fatigue classification problems. The validation and quantification of the impact of the different levels of fatigue on degradation of driving performance was achieved through a series of experiments conducted in a simulation environment, which we built specifically for this purpose. In Chapter 4 we present the methodology for fatigue and stress estimation based on physiological signals and video monitoring of driver's face.

An important aspect of driver physiology related to driving behavior, is stress reactions to specific driving events. The term stress used here does not refer to the permanent stress condition, which determines the long-term driver's psycho-physiological state but rather addresses the temporal increase of stress level of the driver that is directly related with a specific stimulation, i.e. a driving event. However, the detection of those stress events is rather significant since they contribute to the overall stress state of the driver, and can provide an indication of the driver's behavior and the quality of the decisions taken during driving. Analyzing the intermediate en-route self-annotated data, interesting findings could come out regarding the temporal stress experienced by driver during driving and its connection to the occurrence of driving events on-route (e.g. overtaking, hard braking, high speeding). We call these non-permanent stressful conditions stress events, to discriminate them from the psychological state that one experiences for relatively longer period of time. Although the causes of driver stress events and stress state may differ (the former is due to events occurring on road while the second is perhaps the result of deeper psychological factors), their impact on safety is quite similar since in both cases the driver becomes more vulnerable to driving errors, which can lead to accidents. The analysis of the collected data has shown high association of the stress events occurrence

and the physiological signal responses. This finding is of high importance in the sense that such stress events could be easily detected when observing the variation of the driver's physiological signals during en-route recordings. To this end we developed a methodology for real time stress events detection, described in Chapter 5. The methodology is based on the incorporation of features extracted from physiological signals and vehicle information into a Bayesian network model.

The main difficulty in developing a reliable system for driver's physiological state assessment lies on the fact that each human has a different baseline on his/her physiological signals and we need to have a reliable adaptation procedure of the system to the new subject-driver. In Chapter 6 we describe a study on the adaptation of a classifier based on mixture of Gaussians. The classifier is trained on an initial dataset and needs fitting to a new dataset which is obtained through a geometric transformation of the initial dataset. We derive an EM based algorithm and a schema with multiple starts in order to increase the probability of convergence to the correct solution. We extended the initial transformation to a more generic, where each component has a local also transformation and we tested both approaches on data collected in a driving simulation environment.

The cutting-edge technology of driver assistance systems is moving towards the cooperative driving that exploits wireless communications (vehicle -to- vehicle communication and road infrastructure -to- vehicle communication) with the scope to extend driver's perception through the information coming from the external environment and to develop more accurate pre-crash warning systems. The incorporation of driver psychophysiological state into the pre-crash warning mechanisms can evolve further this technology by increasing the safety margins with the provision of alerts tailored to the current driver state. The rationale is that a driver under stress or fatigue should be notified of a road hazard earlier and in a different way, comparing to a driver of normal status, because the former would need more time to process the information and make decisions. Therefore, monitoring the driver and performing on-line evaluation of his/her state is a necessity for a system targeting at preparing the driver in the best way for upcoming risks. In Chapter 7 we present a study towards an advanced cooperative driving system, which incorporates information of driver's state and external information coming from other vehicles and road infrastructure, with the scope to provide timely and useful notifications and alerts to the driver. The first step towards this direction is the development of a simulation environment of vehicle to vehicle communication. Based on this simulation environment we performed a study on communication requirements in order to achieve a safety gain. The second step was the implementation of two basic subsystems: a) the information handler and b) the decision maker. The information handler applies information fusion of low confidence sensors (other vehicles) and employs Bayesian Networks for the extraction of high-level information (e.g. Traffic congestion due to road works).

The decision maker is based on sampling of Dynamic Bayesian networks for driving risk evaluation and decides upon the best warning strategy, taking into account both environmental conditions and driver's state. The decision mechanism is evaluated on a user interactive simulation environment.

Chapter 2

Literature Review

2.1 Introduction

In this chapter we present an introduction to the physiological signals mainly used in similar works, and their relation to the physiological state of interest (fatigue/stress). Then we present the most important works in literature for fatigue and stress detection.

2.2 Physiological Signals

A variety of physiological signal have been used in the literature, for physiological state assessment. However, the most informative and therefore gained the larger attention are: i) electrocardiogram , ii) electrodermal activity, iii) respiration, iii) electromyogram and iv) electroencephalography. From the aforementioned signals, in this study we employed the first three and in the following section we provide a detailed description of their physiology and their use in physiological mental state assessment.

2.2.1 Electrocardiography

The heart is innervated both by the Parasympathetic Nervous System (PNS) and the Sympathetic Nervous System (SNS) and each heart contraction forces the blood through

the circulatory system. The contraction is produced by electrical impulses that can be measured in the form of the electrocardiogram (ECG). From the ECG signal (a) time domain measures, (b) frequency measures and (c) amplitude measures can be derived. In the time domain the R-waves[76, 103] of the ECG are detected, and the time between these peaks, the Inter-Beat-Interval (IBI), is calculated. Heart Rate (HR) is directly related to Heart Period (HP) or IBI , however, this relation is non-linear and IBI is more normally distributed in samples compared with HR [59]. Therefore, IBI scores should be used for detection and testing of differences between mean HR scores, the IBI scale is less influenced by trends than the HR scale [49]. Average heart rate during task performance compared to rest-baseline measurements is a fairly accurate measure of metabolic activity [115]. Not only physical effort affects heart rate level [81], emotional factors, such as high responsibility or the fear of failing for a test, also influence mean heart rate [63]. Other factors affecting cardiac activity are speech and high G-forces [155]. The effect of sedative drugs and time-on-task resulting in fatigue is a decrease in average HR [94], while low amounts of alcohol are reported to increase HR [93]. A continuous feedback between the central nervous system (CNS) and peripheral autonomic receptors causes irregularities in heart rate. Heart rate variability is a marker of performance of this feedback system and in healthy humans this is reflected in large deviations from the mean rate [115]. Compared to time-domain analysis, frequency analysis of IBI has as a major advantage that HRV is decomposed into components that are associated with biological control mechanisms [76, 115]. Three frequency bands have been identified [104, 105]: A low frequency band (0.02 - 0.06 Hz) believed to be related to the regulation of the body temperature, a mid frequency band (0.07 - 0.14 Hz) related to the short-term blood-pressure regulation and a high frequency band (0.15 - 0.50 Hz) believed to be influenced by respiratory-related fluctuations (vagal, PNS influenced)[76]. A decrease in power in the mid frequency band (also called the "0.10 Hz component" after the main frequency component), and in the high frequency band have been shown to be related to mental effort and task demands [105, 63, 9]. Jorna [62] and Paas *et al.* [109], however, conclude that spectral measures are primarily sensitive to task-rest differences, and not to moderate increases in difficulty within a task. Measurement of heart rate is not very complex, the ECG signal needs little amplifying (about 10 to 20 times less as ongoing EEG) and if measurement is limited to R-wave detection and registration then electrode placement is not very critical. Heart rate may provide an index of overall workload, spectral analysis of heart rate variability is more useful as index of cognitive, mental workload [155]. A restriction in the use of heart rate measures is that, due to the idiosyncratic nature of the measure, operators are usually required to serve as their own control in stress assessment. Another major restriction to the use of ECG measures is the effect speech has on blood pressure, and therefore on the 0.10 Hz component of heart rate variability [105, 135]. If verbalization is a predominant aspect of operator performance the 0.10 Hz component may be less suitable for mental load assessments. However, speech is not necessarily a disturbing factor, Porges and Byrne [115] recommend no corrective action in cases in which the verbalization duration is short

(less than 10 s) or in the case that speech is relatively infrequent (one to five times per minute).

2.2.2 Respiration

Respiration is indispensable to supply the blood with oxygen and to expel carbon dioxide. Measures of respiration could provide an index of energy expenditure. Recently, evidence has been found supporting the hypothesis that cognitive effort coincides with a small but significant increase in energy expenditure [9]. The most frequently used measure of respiration is respiration rate [155]. Respiration rate increases under stressful attention conditions[115] and as a result of increased memory load or increased temporal demands [9]. Wientjes [152], [153] states that respiration rate without information about tidal volume is meaningless and has led to inconclusive results. The multiplication of respiration rate (i.e. timing) with tidal volume (i.e. intensity) gives the minute ventilation, the quantity of air breathed per minute. Wientjes [153] found an increase in minute ventilation (and an increase in respiration rate and a decrease in tidal volume) as a result of mental effort or mild stress. Moreover, the measure is, just as many other physiological measures, not uniquely sensitive to mental effort and is affected by, for instance, speech and physical effort. It is also closely linked to emotions and personality characteristics. Wientjes [152] as well as Backs and Seljos [9], however, consider the use of respiration measures to be undervalued in psychophysiological research. In applied settings, respiration measures, in particular respiration rate, have been used several times as measures of mental load. Use of the measures has been confined to aviation, mainly to (simulated) highspeed jet-flight [125, 155]. In these field studies it was also found that, in general, a decrease in respiration rate coincided with increases in cognitive activity.

2.2.3 Electrodermal activity

Electrodermal activity (EDA) refers to the electrical changes in the skin. These changes are the result of Autonomic Nervous System (ANS) activity. Two techniques arein use, exosomatic and endosomatic measurement. With exosomatic measurement a small current from an external source is led through the skin and is measured, while the less frequently applied endosomatic measurement makes no use of an external source. EDA is expressed in terms of skin conduction or resistance, which are (nonlinearly) inversely related. Electrodermal activity can be further distinguished in tonic and phasic activity [48], while Kramer [76] adds spontaneous or non-specific EDA to these two. Tonic EDA, the Electrodermal Level (EDL) or Skin Conduction Level (SCL), is the average level of EDA or baseline activity. Phasic EDA includes the Electrodermal Response (EDR), which is most similar to the formerly common measure GSR (Galvanic Skin Resistance). EDR is the result of an external stimulus. Response is fairly slow, a latency of 1.3 to 2.5 sec to the occurrence of stimulation is to be expected [76]. EDR is expressed either as Skin Resistance Response (SRR) or as Skin Conduction Response (SCR). Spontaneous EDA, EDA

in response to unknown stimuli, has predominantly been used as an indicator of arousal or emotion, and not as a measure of car driver's stress. Kramer [76] in his review refers to several studies that show sensitivity of SCR to information processing. He concludes that spontaneous EDA appears to be sensitive to general levels of arousal while SCRs seem to index the allocation of an undifferentiated form of processing resources. The main problem with electrodermal activity measures are a global sensitivity, or as Heino et al. [48] state "all behaviour (emotional as well as physical) that affects the sympathetic nervous system can cause a change in EDA". EDA is usually measured on the palm of the hand or on the sole of the foot where Sympathetic Nervous System (SNS)-controlled eccrine sweat glands are most numerous [26, 76]. Activity of these glands is sensitive to respiration, temperature, humidity, age, sex, time of day, season, arousal and emotions. The measure is therefore not very selective.

2.3 Fatigue detection

Many countermeasures to driver fatigue have been proposed, such as the use of bright light, caffeine, or naps. However, these countermeasures rely on drivers' self-monitoring of their level of drowsiness, and such subjective measures may be unreliable [122]. An alternative related approach has been to develop countermeasures based on objective driver-performance data. A number of technological countermeasure systems have been designed to detect driver drowsiness [68, 72, 157]. There are three main approaches for fatigue detection, based on the information exploited:

1. Physiological signals (ECG, EEG)
2. Physical appearance (eye blinking, yawning etc.)
3. Driving behavior (lane deviation)

Apart from studies focusing on any of the three approaches, there are methods which used a combination of the above information. In this thesis we have concentrated on the use of physiological signals and driver's physical appearance. In the following sections we describe the most important works on fatigue detection based on physiological signals and video monitoring of the driver.

2.3.1 Fatigue detection from physiological signals

R. Bittner *et al.*. [12] presented a first approach for detection of fatigue based on biosignals acquired from driver (EEG, ECG, EOG) and video monitoring. They examined different features that might be correlated with fatigue, as the spectrum of the EEG, the PERCLOS and fractal properties of HRV. They concluded that the former ones are more correlated with instant fatigue levels of the driver, while the latter is most suitable for the detection of the permanent state of the driver.

Zengyong Li [85] in his work, aimed to estimate mental fatigue of a driver using the HRV spectrum analysis. He used a simulator for data collection which produced situations of high mental effort. In his experiments took part 8 healthy subjects and the duration of each session was 90 minutes. The features from HRV indicated high correlation with mental fatigue of the driver.

Qiang Ji *et al.* [117] proposed a probabilistic framework based on the Bayesian networks for modeling and real-time inferring human fatigue by integrating information from various sensory data and certain relevant contextual information. In their approach they used the existing literature for defining the variables of the model. Furthermore they used a Dynamic Bayesian Network which encapsulates the time dependent development of fatigue symptoms. The estimation is based on visual cues and behavioral variables.

In another approach [161], fatigue detection was based on heterogeneous information sources such as subject specific information (fitness, sleep deprivation etc.), environmental information (traffic, road condition etc.), physiological signals (ECG, EEG) and video monitoring (head movement, blink rate and facial expressions). In order to combine all the abovementioned information they used the Dempster-Shafer theory and rules for determining whether the driver is fatigued or not.

Shen *et al.* [131] developed an EEG-based mental-fatigue monitoring system using a probabilistic-based support vector-machines (SVM) method. Ten subjects underwent 25-h sleep deprivation experiments with EEG monitoring. EEG data were segmented into 3-s long epochs and manually classified into 5 mental-fatigue levels, based on subjects' performance on an auditory vigilance task (AVT). Using probabilistic-based multi-class SVM and confidence estimates aggregation, an accuracy of 91.2% in discriminating mental-fatigue in five levels. This work, in combination with similar studies demonstrated the feasibility of an automatic EEG method for assessing and monitoring of mental fatigue.

Lal *et al.* [78] describe a EEG-based fatigue countermeasure algorithm and reported its reliability. They employed changes in all major EEG bands during fatigue in order to develop the algorithm for detecting different levels of fatigue. In this study ten subjects participated and using the EEG-based detector, the percentage of time the subjects were detected to be in a fatigue state was significantly different than the alert phase (P¡.01).

Summarizing the results of the existing literature, physiological signals are very promising indicators of mental-fatigue, a result also indicated by Crawford[23]. Cardiac related signals such as ECG, respiration and BVP are good indicators of the circadian rhythm

and therefore of the current alertness of the driver. EEG is a very good indicator of mental-fatigue and mental activity. Also a increase in EEG's Theta activity was observed during long monotonous tasks [52]. However, in real-world driving, it is rather difficult to perform real-time monitoring of driver's EEG activity, since this would require special sensor equipment attached to the driver and would raise a number of safety related issues concerning the obtrusive driving monitoring procedure. On the other hand ECG and BVP could be acquired from the steering wheel [129] of the vehicle and respiration could be acquired from sensors on the safety belt. In combination with video monitoring, systems predicting fatigue and detecting drowsiness are feasible.

2.3.2 Fatigue detection from face and eye measures

We dedicate one section in fatigue detection, and more precisely drowsiness detection from physical appearance measures, such as blinking, yawning, head movement etc. One of the most important drowsiness indicators is the percentage of eye closure (PERCLOS). This measures has a significant correlation with the psychomotor vigilance task (PVT) which varies from 0.67 to 0.7 [41]. In order to extract PERCLOS, a method for accurate estimation of eye opening is needed. Accurate estimation of eye opening can be estimated though EOG measurements. However this is an obtrusive method and cannot be applied on a vehicle context. Therefore, the most common approach is based on the video monitoring of driver's face which is an unobtrusive and relatively low cost method. The methods usually consist of two basic steps: i) the face detection and ii) the detection of eyes. The face detection is used for tracking head movements which are used for detecting driver's awareness and loss of attentions and the second for blink detection and PERCOS estimation. Several methods are proposed in the literature to detect the face from single images or sequences. These include knowledge based methods which encode human knowledge about the facial features associations such as facial geometry[162]; template based methods such as deformable models[51];appearance based methods which utilize information based on higher order features of the face [132]. Rowley et al. [128] employed a neural network to classify a region either as a face or non face using as features the pixel intensities as well as spatial relationships between pixels. Waring and Liu [148] employed an appearance based method utilising information from spectral histograms and classified into face or non-face regions using Support Vector Machines. One of the most commonly employed face detector is the real time face detector proposed by Viola and Jones [145]. The face detector does not operate directly with image intensities but extracts a set of features which are based on Haar functions. Fasel *et al.* [32] extended the work by Viola and Jones to detect both the face and the eyes. A large number of studies extended Fasel's work [77, 147, 80] using other features instead of Haar or applying the method on video sequences. Template based methods are simple to implement but are usually prone to failure when large variations in pose or scale exist [162].

Anderson and McOwan [7] employed the Ratio Template Algorithm to locate and track the face and Optical Flow via the multichannel gradient model to create the feature vector. Deformable models are template methods that provide the mechanisms to partly tackle the problem of variations in pose or scale. Kass *et al.* [65] used the Active Contour Models or snakes. Snakes are initialized at the proximity of the structure and are fitted onto nearby edges. Active Shape Models proposed by Cootes *et al.* [22] work similarly with snakes but enforce global shape constraints on the deformable model.

Asteriadis *et al.* [8] presented a work for eye and mouth detection based on a distance vector fields [24] and distance transform [17]. The accuracy of the detection of the three regions (two eyes and mouth) was 95.48% in images from XM2VTS database [98].

2.4 Stress Detection

Stress and fatigue are affecting the same regulation mechanism of the organism, therefore, we need to search in similar places for stress evidence. As in the case of fatigue, literature has focused mainly on physiological measures. Some approaches have used also physical appearance measures but the relation of those measures with stress is ambiguous. This can be explained since stress has many different aspects and leads to different behaviors. However a measure identified as rather indicative of stress is the pupil diameter[163, 64]. Even though effects of mental load on pupillary response were found, the largest changes in pupil diameter occur as a result of other factors, e.g., a change in ambient illumination and the near reflex. These factors make the measure best suitable for laboratory situations [75]. Another promising approach is based on biomarkers and two pioneering works in this direction are presented.

2.4.1 Stress detection from physiological signals

Healey *et al.*. [43] used a driving task related data collection protocol. Each subject had to perform a specific sequence of driving maneuvers-tasks (in total 15 including parking, reversing and other). According to a questionnaire given to driver, for each task a difficulty degree was assigned which also corresponded and the level of stress stimulation of each task. From the physiological signals numerous features were extracted. Using feature selection method and K-NN a 88.6% accuracy of four stress levels was achieved. The selected features, mainly included heart rate and skin conductivity related features.

In another study, Healey *et al.*. [46] specified an experimental protocol for data collection. Each driver followed a pre-specified route through fifteen different events, from which four stress level categories were created according to the results of the subjects self report questionnaires. In total, 545 one-minute segments were classified. A linear

discriminant function was used to rank each feature individually based on recognition performance and a sequential forward floating selection (SFFS) algorithm was used to find an optimal set of features for recognizing driver stress. Moreover, in another work [5] a slightly different protocol was followed: Data from 24 drives of at least 50-min duration were collected for analysis. The data were analyzed in two ways. In the first case they used features from 5-min intervals of data during resting, highway and city driving conditions to distinguish three levels of driver stress within multiple drivers and driving days. The average accuracy was 97%. In the second case they compared continuous features, calculated at 1-s intervals throughout the entire drive with a metric of observable stressors created by independent coders from videotapes. The results showed that for most drivers studied, skin conductivity and heart rate metrics are most closely correlated to driver stress level.

Rani *et al.*. [120] presented a real time method for stress detection based on heart rate variability using Fourier and Wavelet analysis. They used fuzzy logic methods for determining the activation level of parasympathetic and sympathetic nervous systems. They collected limited data to test their method and they pointed out challenges in stress detection, such as stress stimulation and the daily and subject variability.

Lee *et al.*. [83] developed a PDA application of stress detection. The physiological signal acquisition unit had four electrodes, one for PPG (for monitoring heart rate), one for EDA and one for SKT (for measuring variations in electrodermal activity). From those signals a number of features was extracted. Those include the mean value of EDA and SKT as well as the LF/HF ratio extracted from the heart rate variability. The method for data collections was based on the presentation of images and analogous vocal tones (a method based "stroop color-naming task" [36]). The collected data from 80 healthy subjects. The annotation of the data was performed manually be inspecting physiological signals. Based on this annotation they trained three classifiers: i) Multilayer perceptron (MLP), ii) Generalized regression neural network (GRNN) and iii) adaptive network based fuzzy inference network (ANFIS). They split the dataset in half for training and testing. The obtained accuracy was 96.67%. Next they developed a system for acquisition and preprocessing of physiological signals, feature extraction and stress detection on a PDA. The main drawback of this work is the annotation process. If the annotation is based on an indicator, i.e. looking at the increases of the EDA and categorizing large increases as stress, then this feature alone could easily provide a very large accuracy.

Zhai *et al.*. [164] developed a similar system for stress detection using blood volume pressure, skin temperature variation, electrodermal activity and pupil diameter [1]. They

[1]The measure through the center of the adjustable opening in the iris of the eye, terminated at both

used the same data collection protocol which included 6 healthy subjects. The experimental protocol was divided in three phases. In the first phase subjects were getting familiar with the environment, in the second phase stress was elicited and in the third the subject was relaxing. This procedure was repeated three times. The data in the second phase were labeled as stress, whereas the data of the third phase was labeled as normal. In total they collected 36 segments, 18 with stress and 18 normal. They used more features than Rani *et al.*. [120]. However no method of feature selection or feature reduction was considered. This could be necessary regarding the number of dimensions (10) and the number of data (36). The classification using SVM with different kernels (linear, RBF and sigmoid) using a leave one out method, gave an accuracy of 57.14% for the linear, 60% for RBF and 80% for the sigmoid kernel. Those differences are very large considering only a change in the kernel of the classifier.

In another study Zhai *et al.*. [163] using more subjects (32 healthy subjects) and the same methodology had better results (90.1% accuracy). Pupil diameter was proven as the most dominant feature, whereas other physiological features did not have a significant contribution to classification performance. However, the normalization and the handling of the inter and intra subject variations was not clear and may have lead to the small value of those measures.

Liao *et al.* [86] estimated stress levels from evidences of different modalities. The evidences include physical appearance (facial expression, eye movements, and head movements) extracted from video via visual sensors, physiological conditions collected from an emotional mouse, behavioral data from user interaction activities with the computer, and performance measures. They were based on a Dynamic Bayesian Network (DBN) framework to model the user stress and these evidences. They described the computer vision techniques used to extract the visual evidences, the DBN model for modeling stress and the associated factors, and the active sensing strategy to collect the most informative evidences for efficient stress inference. In their experiments they show that the inferred user stress level by their system is consistent with that predicted by psychological theories.

Liao *et al.*. [87] presented a general unified decision-theoretic framework based on Influence Diagrams for simultaneously modeling user affect recognition and assistance. Affective state recognition is achieved through active probabilistic inference from the available multi-modality sensory data (physical appearance features, physiological measures, user performance, and behavioral data). User assistance is automatically accomplished through a decision-making process that balances the benefits of keeping the user in productive affective states and the costs of performing user assistance. The validation of the

ends by its circumference.

proposed framework was based on a simulation study. A significant correlation of the estimated stress levels from the DBN model and the ground truth was presented. However the model was trained each time with data from each subject on the same experimental session and thus the generalization ability of the proposed method is questionable. They also presented some initial results for fatigue estimation. However, the incorporation of performance variables for the specific task, which are very correlated with the state of the subject, puts under question the extracted results for both fatigue and stress estimation. However is was apparent that both physiological and appearance features (hand movement, blinking rate e.t.c.) were highly correlated with stress.

Wilson and Russell [155], used artificial neural networks and physiological signals to continuously monitor, in real time, the functional state of 7 participants while they performed the Multi-Attribute Task Battery with two levels of task difficulty. Six channels of brain electrical activity and eye, heart rate and respiration measures were evaluated on line. The accuracy of the classifier was determined to test its utility as an on-line measure of operator state. The mean classification accuracies were 85%, 82%, and 86% for the baseline, low task difficulty, and high task difficulty conditions, respectively. The high levels of accuracy suggest that these procedures can be used to provide accurate estimates of operator functional state that can be used to provide adaptive aiding. The relative contribution of each of the 43 psychophysiological features was also determined.

Kim *et al.*. [70] indicated that long term patterns of heart rate variability (HRV) features were decreased in subjects with higher self reporting stress scores. For mobile applications, short term analysis of HRV features may be ideal since conventional heartbeat recordings (3 5 min) might be inadequately long. In this study, short term analysis has been performed for heartbeat data obtained at five different time points from two subject groups (15 under high and 18 under low mental stress). The reliability of short term heartbeat data was demonstrated by detecting significant differences in long term patterns of HRV features between two groups. Fifteen to thirty second heartbeat measurements were long enough to produce reliable long term patterns of HRV features. Thus, short and intermittent recordings of heartbeats could be used to detect long term HRV patterns and offer a convenient method to monitor mental stress in mobile environments.

As we have noticed in mental fatigue detection, EEG was a very good indicator. Considering that stress and intense workload, according to Grandjean (1979) scale, is the opposite state of mental fatigue, EEG could be also expected to be a good indicator of stress. The first two studies presented in this section, include both ECG and EEG recordings. Hankins and Wilson [42] presented a study on mental workload during flight. They used EEG, face monitoring and ECG which were collected during an during an actual

flight scenario designed to provide tasks that required different piloting skills imposing different mental workload. They found that heart rate was sensitive to the demands of flight but not diagnostic with regard to determining the cause of the workload. Heart rates increased during take offs and landings and to an intermediate level during instrument flight rules (IFR) segments. By showing sensitivity to only the visual demands of the various segments of flight eye activity was more diagnostic. The theta band of the EEG demonstrated increased power during those flight segments which required inflight mental calculations.

Dussault *et al.* [29] evaluated the effects of mental workload without actual physical risk. They studied the cortical and cardiovascular changes, using ECG and EEG respectively, that occurred during simulated flight. 12 pilots (8 novices and 4 experts) attended a simulated flight composed of 10 sequences that induced several different mental workload levels. Theta band activity was lower during the two simulated flight rest sequences than during visual and instrument flight sequences. On the other hand, rest sequences resulted in higher beta and gamma power than active segments. The mean heart rate (HR) was not found significantly different during any simulated flight sequence, but HR was lower for expert subjects than for novices. The subjective tests revealed no significant anxiety and high values for vigilance levels before and during flight, explaining the small variations of HR.

From the above two studies we can conclude that EEG measures are more sensitive two workload and are better discriminants of workload levels. However, heart rate measures could be used in order to differentiate the no or low workload states from the intense workload states or stress. Taking into consideration that ECG could be more easily acquired in a vehicle context we consider that further studying of ECG and Heart rate measures is necessary in order to build a reliable stress detector. EEG on the other hand could be used as an objective workload metric, since self-assessment especially on workload and stress annotation has some disadvantages, such as that it provides an additional workload on the subject and in cases of intense workload the probability of misjudgment is higher. Another approach that could be used as an objective workload metric is based on biomarkers. There are limited works presented on workload estimation and biomarkers but the results obtained are very promising. Those are presented in the next section.

2.4.2 Stress detection from biomarkers

Yamaguchi and Sakakima [160] used salivary amylase as a biomarker, an oculomotor angle, a subjective evaluation and examined the acute, psychological effect human stress of driving using a motor-vehicle driving simulator. 20 healthy female subjects in their

early twenties were enrolled in this study. The time-course change of their salivary amylase activity (sAMY) was analyzed before and during the driving. The results indicated that the psychological effect of driving-induced stress was quickly quantified using a biomarker in saliva.

Nomura *et al.* [107] we used the cortisol as a biomarker of mental stress. 10 male subjects were inscribed to conduct a simple, easy, and monotonous mental arithmetic task for about an hour with intermissions, so as to emulate a mild mental workload. As a result, salivary cortisol depicted an accumulative increase during mild mental workloads, while no marked difference was obtained in the heart rate and its variability. It suggests the slow and long-lasting properties in the stress-response of the cortisol unlike as in autonomous nervous system indices, and therefore plausibly demonstrates the possible candidacy of cortisol as a biomarker for a mild mental load.'

2.5 Contribution of this thesis

The majority of the reported works in literature, towards drivers' physiological state assessment, are performed in a simulation environment. In a controlled and isolated simulation environment is easier to monitor a subject under a specific physiological state. However the physiological reaction of the subjects is expected to have significant differences from real driving conditions. When a subject is asked to participate in a scientific experiment, it is expected to be rather alerted, even in late fatigue stages. Our main effort was to minimize this effect, monitoring drivers in repeated experiments in real driving conditions, where the driver was alone in the vehicle, in order to have his usual behavior, and ignore the fact that his is monitored, through a special equipped vehicle. Those repeated experiments in real unrestricted driving conditions , allows to monitor the driver under different combination of physiological states, such as fatigue and stress. The possibility of simultaneous presence of more than one physiological states, is another factor ignored in the majority of related studies. The experiments in real driving conditions, gave us the opportunity to monitor the physiological signals of the driver under specific stressful driving events, and relate events with stress reaction, using a methodology presented in Chapter 5. Furthermore, in this thesis, the driver's physiological state recognition is performed using information that is or can be available in a real vehicle. This excludes from this study, physiological signals such as EEG, as well as information about driver's context, used in similar works. Another serious limitation of existing methodologies is the necessity of a resting period, or a period where the driver is at a normal physiological state. Physiological signals of this period, are considered as baseline, and are compared to signals of the physiological state of interest. This approach cannot be applied on a real driver physiological state recognition system. In order to overcome this limitation, we present in Chapter 6 a methodology with promising results. The information about

current driver status could be exploited by the advanced driver assistance systems in order to adjust their warning strategies accordingly. In Chapter 7 we study a new generation co-operative driver support system, able to monitor drivers' physiological state, communicate with infrastructure or other vehicles and infer driving conditions. This study is performed in terms of safety gain, information handling and advanced decision making for optimal warning.

Chapter 3

Data Collection

3.1 Introduction

Collection of experimental data for different driver states (stress and fatigue) requires a protocol which ensures that driver experiences these states. This process can take place either in real driving or simulation environment. Each approach has both advantages and disadvantages, which was discussed in the previous Chapter. In this thesis we have performed both types of experiments:

1. Experiments in real driving conditions.
2. Experiments using a simulator.

In the following sections each of the experimental phases are described in detail.

3.2 Experiments in real driving conditions

This was the earliest and longest phase of the experiments, which lasted more than one year. We first describe the equipment used for the experiments in real driving conditions, we proceed with the description of the data collection protocol and the final dataset description.

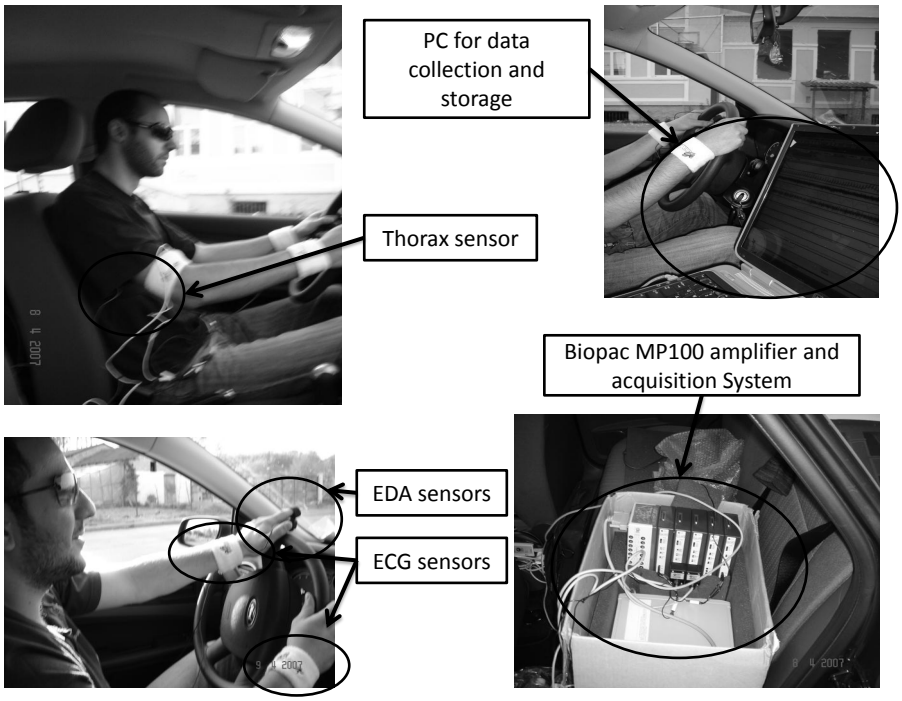

(a)

(b)

(c)

Figure 3.1: a) The sensors installation for the real driving experiments. b) A snapshot from the camera monitoring drver's face. c) The SONY DCR -HC94E for road monitoring and annotation.

3.2.1 Equipment

In this type of experiments, a custom vehicle was used for execution of experiments in real driving conditions. The data collection was performed using off-the-shelf equipment,

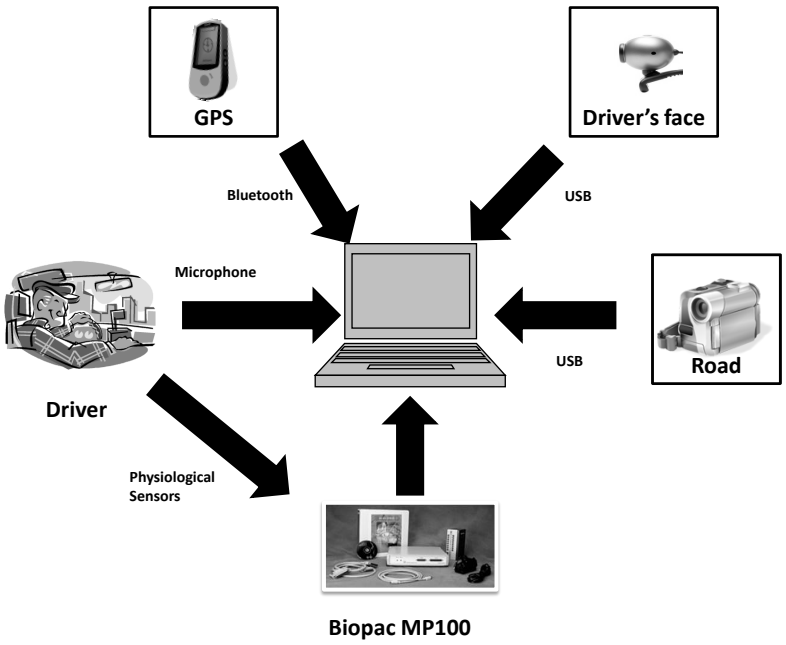

Figure 3.2: The equipment used for the data collection.

which was set up in the car formulating a data acquisition system for driver monitoring during real-world driving. The basic equipment for data acquisition is depicted in Fig. 3.2, in real driving conditions. The equipment includes:

1. Biopac MP-100 for physiological signal acquisition. The sensor placement is depicted in Fig. 3.1(a).

2. A camera monitoring driver's face. We used a simple web-cam with frame size 320-240 and 15fps. It is installed right behind the wheel and a snapshot taken with this camera is given in Fig. 3.1(b).

3. A SONY DCR -HC94E camera monitoring road (Fig. 3.1(c)). This camera was installed on co-drivers seat.

4. A GPS device with bluetooth connection.

5. An ELM327 adaptor for data acquisition from the vehicle's CAN-bus.

6. A microphone for driver's self-assessment recording.

7. A laptop for device synchronization and data storage.

For signal acquisition we selected the Biopac MP-100 system, since it is used in a number of similar studies. A further description acquisition system and technical specifications can be found in [10]. The following physiological signals were acquired:

1. Electrocardiogram (ECG) through a g.ECG sensor which is placed on the subject's chest.

2. Electrodermal Activity (EDA) through two Ag/Ag.Cl electrodermal activity sensors attached on the subject's middle and index fingers of the right hand.

3. Respiration signal through the contraction of the thorax, measured by a belt fastened to subject's chest.

We should also notice that initially, we also acquired a EMG signal from driver's arm, however it proved a rather obtrusive measurement and raised safety issues, forcing us to remove it.

3.2.2 Data collection protocol

The data were collected during real driving conditions in Greek national roads. Two types of routes were selected to work on different stress and mainly fatigue levels:

- Ioannina - Arta (75 kms). This is a high speed provincial road (considered highway) with one lane per direction, not barrier separated, yielding potential stress.

- Ioannina - Aridea (397 kms). This route is composed of 180 km of closed highway (with minimum two lanes per direction, barrier separated) and 217 km of rural road (one lane, not barrier separated with curves). This second route was selected for combining both curved narrow road and monotonous non-congested motorway, which was considered ideal for yielding both stress and fatigue conditions to the driver.

The map in Fig. 5.28 indicates the routes driven during the conducted experiments.

In the beginning of every experimental procedure the ECG, EDA and respiration sensors were attached to the driver and the two cameras were calibrated to monitor the driver face and the road scenery respectively. From the laptop PC the acquisition software was initiated and the recording of signals and videos (driver, road) started simultaneously. After 60 min of driving the recording procedure was stopped and signals and videos were stored for processing in batch mode. In the end of each session the driver made a shelf-assessment of his state (in a three level scale for fatigue and in a two scale for stress) to indicate the actual psycho-physiological condition.

In addition for stress annotation, intermediate on-route self-reports were given by the driver in cases when he experienced short-term stress events due to situations/events occurring on the road. These short-term stress events affected only temporarily his state and they were reported vocally by the driver. The vocal report was used to avoid subject's distraction from the driving task and it was recorded by a speech recognition system. To annotate this dataset (driving event and driver stress), both video recording and self annotation of the driver was used.

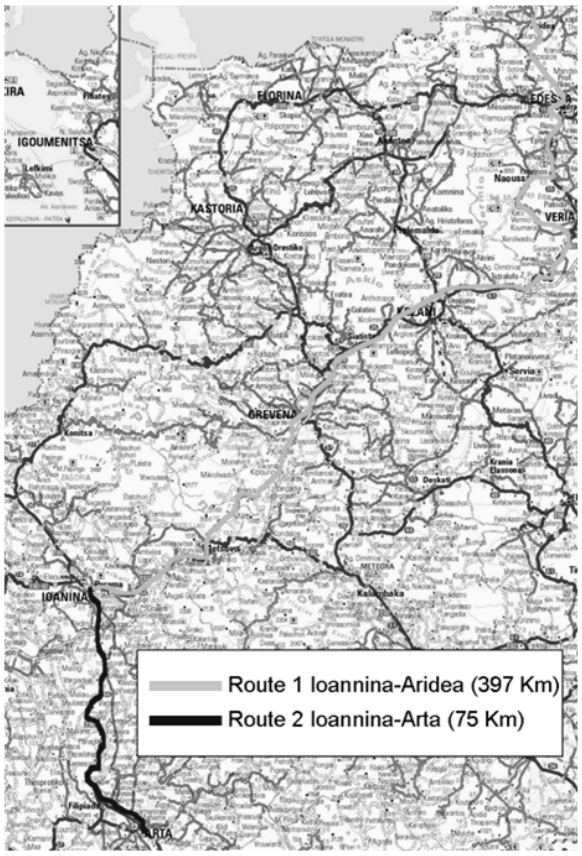

Figure 3.3: The equipment used for the data collection.

Driving took place in various hours of the day, so that recordings were collected along different phases of the day cycle. The experiments had an average duration of 60 minutes. The route no.1 (Ioannina - Aridea) was divided into subsequent one-hour-experiments which were conducted in different roadway parts (motorway/ rural congested road) and covered the whole distance of 397 kms. The self- annotation was again performed both during driving and at the end of each 1-hour session. A significant number of experiments were conducted at 6 am and 6 pm of the same day after few sleeping hours, with the drowsiness of the subject reaching high level. Others were conducted with bad weather conditions (heavy rain, fog) and intense traffic flow (high-speed vehicles, frequent braking, overtaking) making the driver experience high levels of stress.

3.2.3 Dataset description

Eight subjects participated in the experiments performed in real driving conditions. The majority of the data collected are from one subject. He performed more than 60 tours during one-year-experiments. After some first testing sessions, he was rather familiar with the equipment and allowed to be alone in the sessions. Thus the effect of monitoring process on his physiological state was negligible. The subject participated in a large number of sessions under different traffic and weather conditions.

Table 3.1: Description of the dataset for real driving conditions.

Tour info	Number of tours	37
	Average Duration of Each Tour	50 min.
Condition	States	Number of Tours
Stress	No	13
	Yes	24
Fatigue	Normal	9
	Medium	15
	High/Drowsiness	13
Environmental conditions	No Rain	26
	Rain	8
	Heavy Rain	3
	Normal Visibility	29
	Medium Visibility (Late Evening)	6
	Low Visibility (Fog/Night)	2

The dataset collected from the one year experiments is summarized in the Table 3.1, where the total number of tours, average duration of each tour and number of road events in all tours are indicated.

Figure 3.4(a) provides the average number of particular driving events per hour. We observe that the most frequent event is the overtaking, which obviously has to do with the driver's behavior, the type of the road and the traffic conditions.

Figure 3.4(b) presents for each event, the percentage of instances annotated as a stressful event. We observe that *overtaking* and *hard braking* are the events which are mostly related with stressful situation in our dataset.

3.3 Experiments with a simulator

Although the initial setting of the algorithms was performed using the data gathered from a single subject, a robust driver state recognition method should be able to apply to subjects of different age, sex, lifestyle or experience. However, the biosignals and facial features, used as inputs for driver status monitoring, vary significantly from subject to subject, making the training of the system with multiple drivers mandatory. Considering the difficulties in involving many subjects in the real-driving data collection procedure, especially when fatigue is one state of interest, an additional phase of experiments was introduced, monitoring subjects during driving in a simulated environment.

For this type of experiments a simulation environment was built to serve the execution of experiments. Having as a baseline the simulator-based training used in similar research works, our purpose was to built a rather simple simulator, that would allow us to monitor

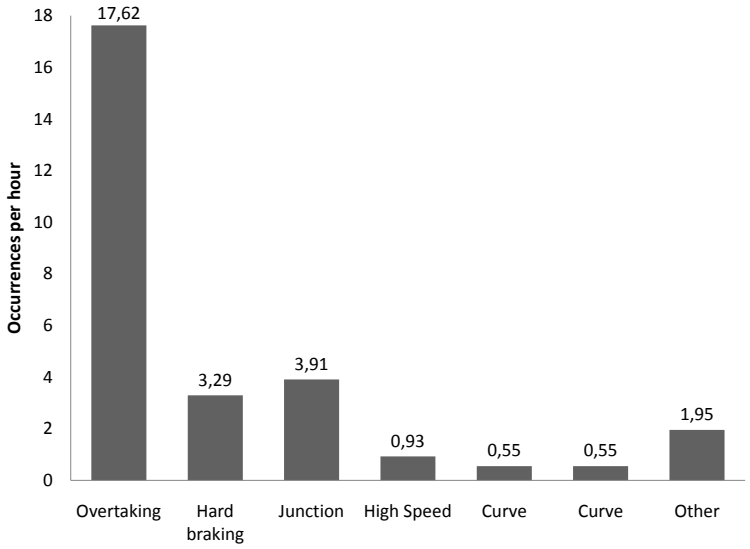

(a)

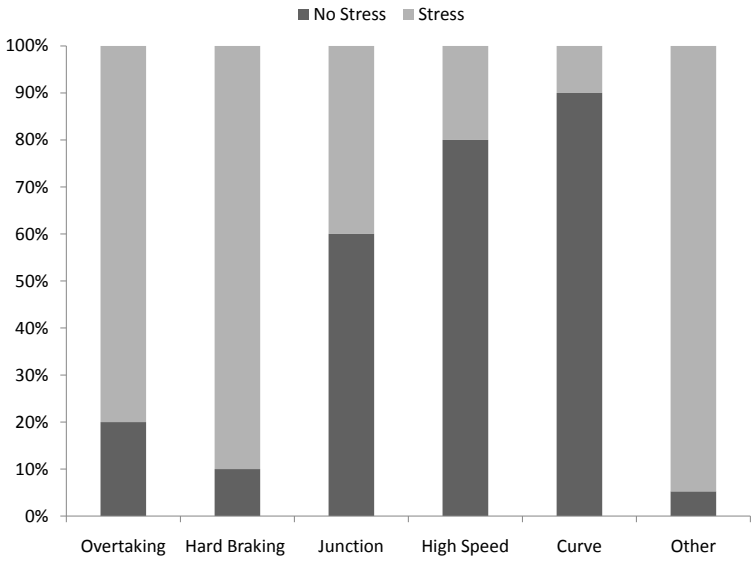

(b)

Figure 3.4: a) The number of specific event occurrences per hour b) The percentage of each event instances that was annotated as stressful events.

the driver while performing the driving task under different psycho-physiological conditions (varying from very stressful to normal and to high drowsiness states). Additionally, the simulator could serve the monitoring of driving behavior parameters (steering, braking, lateral position) and the extraction of useful features, such as reaction time, reversal rate, which could not be measured during real-world driving with the custom car.

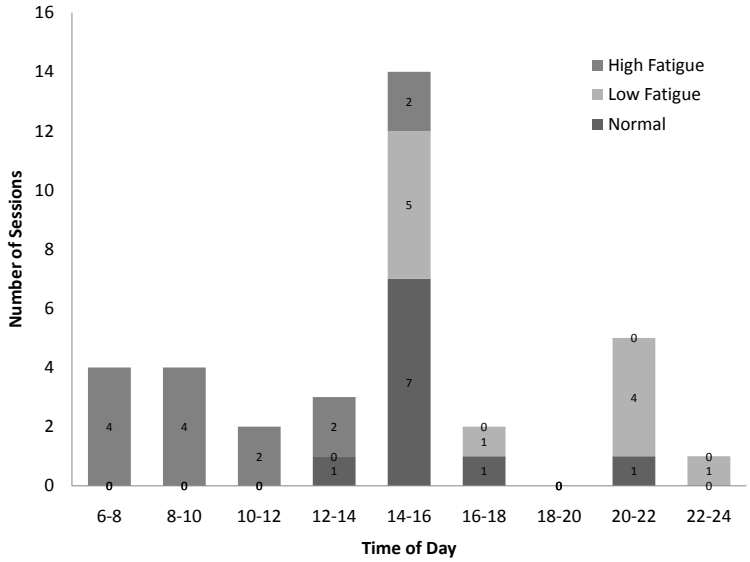

(a)

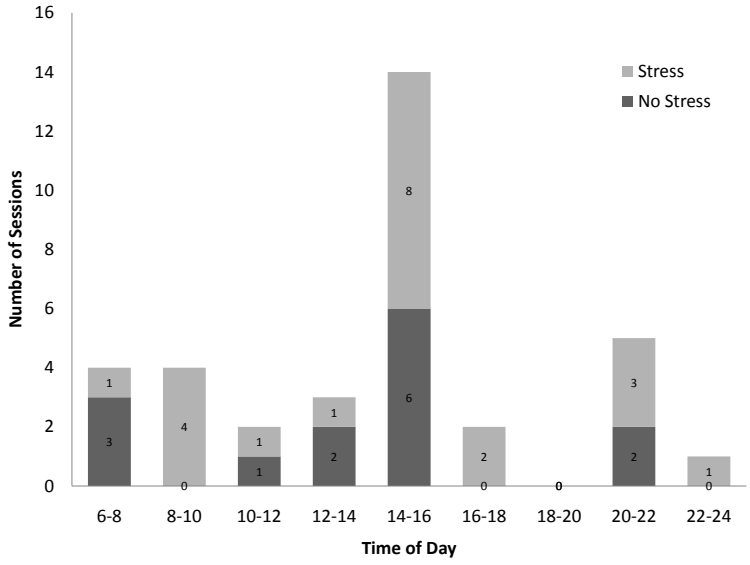

(b)

Figure 3.5: a) The number of instances of different fatigue levels and b) stress levels, for every hour of day.

3.3.1 Equipment

In the laboratory driving experiments, the Logitech realistic force feedback wheel was used allowing the controlling of:

- Force Feedback: supporting direct guidance of one's way

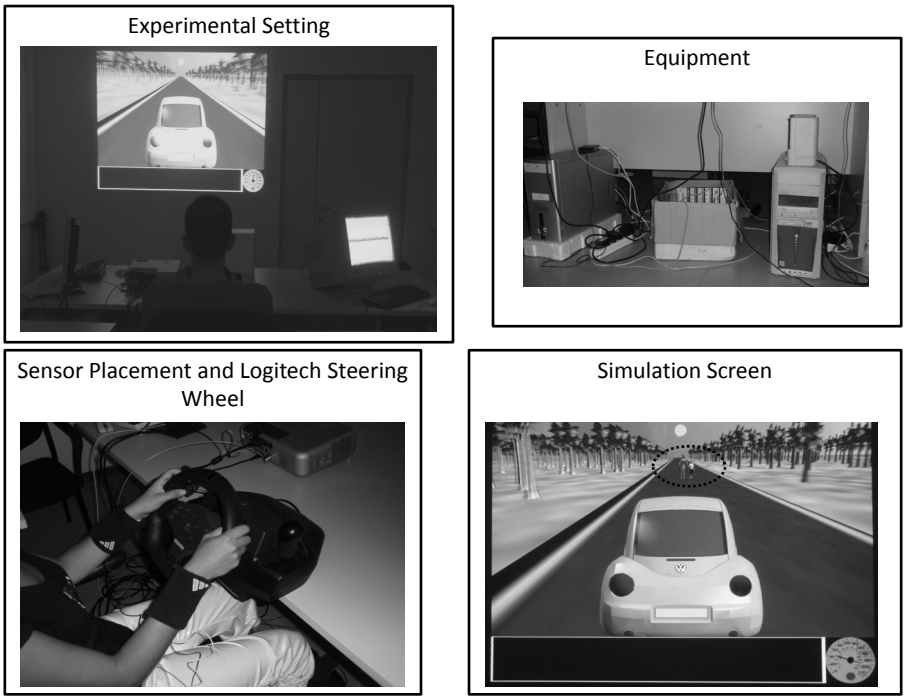

Figure 3.6: The simulation environment.

- Gas and Brake Pedals: getting instant response and feedback with carpet-grip foot pedals
- Shifting: using paddle shifters or the manual knob for sequential precision
- Six Programmable Buttons

The force feedback wheel set is illustrated in the figure below.

A 3D driving simulation environment was developed (Fig. 3.6) using the Microsoft XNA framework, which is based on the Directx3d. The world of this environment consists of a roadway with a single lane, a vehicle moving in a constant speed on the road and virtual obstacles. The software of the virtual driving world ran on a PC Pentium III workstation.

3.3.2 Signal Acquisition

The physiological signals monitored in the laboratory experiments are similar to the ones measured during real-world experiments (ECG, EDA and respiration). The same off-the-shelf equipment (Biopack MP-100) described in section3.2.1, is used in this type of experiments. The equipment was now set up in the laboratory formulating a data acquisition system for driver monitoring during simulated driving. The signal acquisition software ran on a second workstation (PC Pentium III) together with the video acquisition software.

3.3.3 Video Acquisition

In laboratory testing a single camera was used to take video recordings from drivers' faces. The camera that equipped the custom car for the real driving experiments was also used in the lab experiments. The camera was calibrated every time to focus on the subject's face and the video acquisition software run on the PC Pentium III that served also for signal acquisition.

3.3.4 Software synchronization

To run the simulation experiments, the three separate software parts: i) the virtual driving world (simulator), ii) the acquisition of physiological signals from the Biopack device and iii) the acquisition of video recordings of driver's face, should be synchronized. The basic coordinator of the whole process was the signal acquisition which writes the data file in a specific folder. The other two applications (video acquisition and simulator) run a file watcher monitoring the same folder. The start of the signal acquisition triggers also the start of the other two applications. The small delay introduced by the time the file watchers need for triggering, is negligible, considering the synchronization requirements of the applications.

3.3.5 Data collection protocol

In the beginning of every experimental procedure the subject completed a questionnaire composed by an expert psycho-physiologist from well-established results regarding stress scaling [40] and fatigue scaling [47]. Apart from profiling information (age, sex, experience, frequency of exercise, etc), the subject was asked to answer questions about his/her psychological status of the resent period. The questions were focalized on estimation of subjects' stress and fatigue levels and were used as an additional annotation measure for experienced states to allow for further evaluation by experts in the field. The last part of the questionnaire urged the subject to make a self-assessment of his/her current status using the same scales for stress and fatigue used also in real experiments.

After completing the questionnaire, the subjects attached the biosensors (ECG, EDA and respiration measurements) and the camera was calibrated for face monitoring. From the PC-II the signal acquisition software was initiated and the recording of bio-signals and face-video started simultaneously with the simulator running in the PC-I.

Every experiment was of 15 minutes duration. The subject was asked to focus on the driving task, i.e. keep the vehicle within the road lane and avoid crashes with pedestrians that appeared unexpectedly on the road, by pressing the brake pedal and stopping the vehicle. From this primary task, measurements of and reaction times and lane keeping were monitored. In addition to the primary driving task, a secondary-task request has been used following the well-established PDT (Peripheral Detection Task) technique [55]. During driving sessions apart from pedestrians, other objects (animals) randomly appeared

Table 3.2: The description of the dataset in the simulation environment.

Subject #	Sex	Age	# of Sessions	Stress				Fatigue			
				0	**1**	**2**	**3**	**0**	**1**	**2**	**3**
1	Female	32	7	0	5	2	0	1	4	0	2
2	Male	25	19	2	9	2	6	3	4	1	11
3	Male	28	17	6	4	3	4	3	3	3	8
4	Female	28	14	2	9	2	1	3	2	2	7
5	Male	26	17	7	2	5	3	7	5	1	4
6	Male	25	10	2	2	5	1	1	0	6	3
7	Male	26	14	2	6	3	3	2	3	2	7
8	Male	29	12	7	2	2	1	2	2	2	6
9	Male	28	11	2	2	4	3	1	1	9	0

outside the roadway (among trees). Once the objects perceived, the subject should respond by pressing one of the control buttons of the steering wheel and the respective reaction time was measured as well.

At the end of the experiment the signals and videos were stored in the subject's data folder. The same folder kept also the simulation measurement files (primary reaction time, lane keeping, and secondary reaction time).

The same experiment was repeated 3 times along the day with the same subject: the first session early in the morning when a reduced alertness and thus slow reaction times were expected, the second at midday with the subjects typically fully alerted and the last one late in the evening/night when fatigue is present.

3.3.6 Dataset description

Fifteen subjects participated in the experiments around the simulator and a total of 114 sessions were conducted. The Table 3.2 below summarizes the annotated dataset gathered from 9 out of 15 subjects participating in the lab experiments. In Fig. 3.7(a) the distribution of the subject's age is provided, whereas in Fig. 3.7(b) the distribution of the sleep hours before a session is also provided. The sleep hours are a very important information, which is highly correlated with alertness and subject's fatigue.

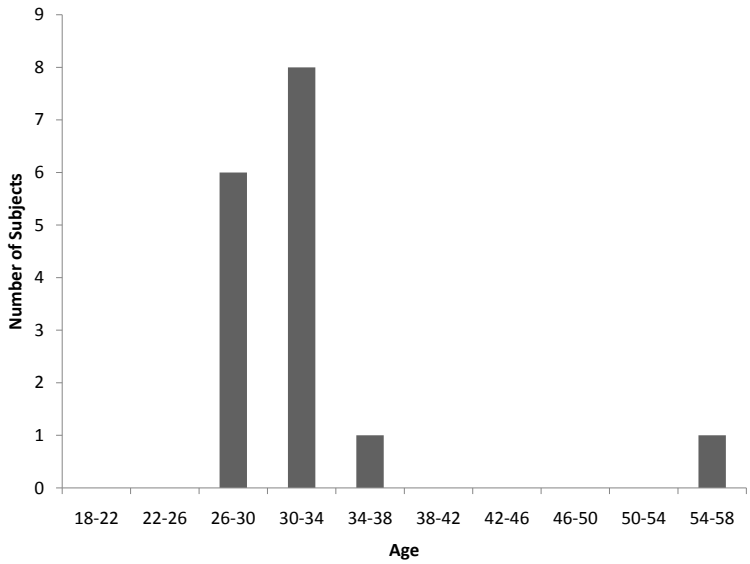

(a)

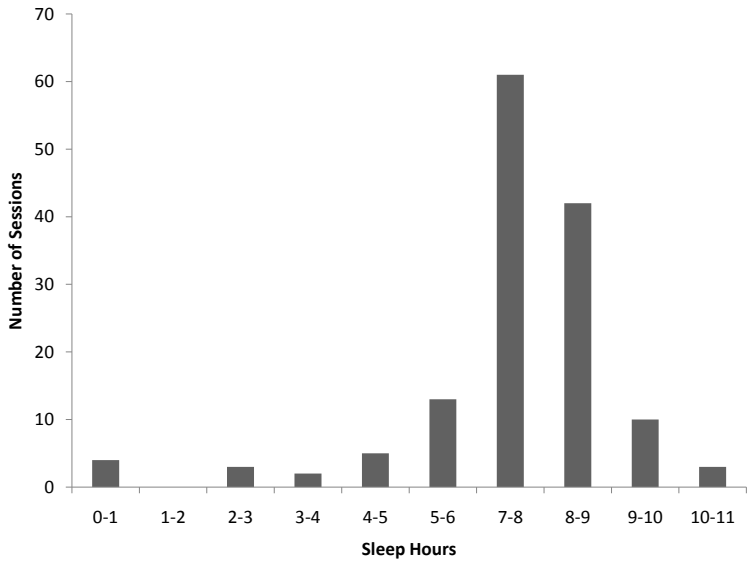

(b)

Figure 3.7: a) The distribution of the subject's age is provided, and b) the distribution of the sleep hours before a session.

Chapter 4

Driver state detection

4.1 Introduction

Real-life car driving requires accurate and fast decisions by the driver, given only incomplete information in real time. A large number of fatalities occurring during car driving could be avoided if behaviors such as driver inattention, stress, fatigue and drowsiness were detected and appropriate countermeasures were produced. The determination of the driver status in a vehicle is an active topic for the scientific community. However, the detection of stress and fatigue level in drivers is a complex task, which requires expertise in biosignal processing, computer vision, human factors, etc. The estimation of fatigue is well-studied in the literature. The majority of relative works is based on in-lab experiments, mainly focusing on face monitoring and blink detection to calculate eye activation [142], while the vehicular experiments serve for indirect fatigue recognition through its impact on driving issues (speed maintenance, steering control). These methods, however, are suitable for the recognition of rather late stages of the fatigue (drowsiness) when the effects on driver's face are quite noticeable and performance change has already become

critical. In the road environment, even earlier fatigue stages can affect driving performance. This is because even lower fatigue levels still cause declines in physiological vigilance/arousal, slow sensorimotor functions (i.e. slower perception and reaction times) and information processing impairments, which in turn diminish driver's ability to respond to unexpected and emergency situations [94]. Therefore, the impact of fatigue on the driver's performance should not be estimated using only driving measures, but additional parameters, associated with the driving performance, are needed (such as perceptual, motor and cognitive skills) [154]. According to Crawford [23], physiological measures are the most appropriate indicators of driver fatigue. This has been confirmed by numerous studies, which followed similar approaches for driver fatigue estimation, making use of biosignals obtained from the driver [5]-[8].

Bittner *et al.* [12] presented an approach for the detection of fatigue based on biosignals acquired from the driver electroencephalogram (EEG), electrocardiogram (ECG), electrooculogram (EOG) and video monitoring. They examined different features that might be correlated with fatigue, such as the spectrum of the EEG, the percentage of eye closure (PERCLOS) and the fractal properties of heart rate variability (HRV). They concluded that the first two are more correlated with instant fatigue levels of the driver, while the last is most suitable for the detection of the permanent state of the driver. Li [85] addressed the estimation of driver's mental fatigue using HRV spectrum analysis using a simulator for data collection. The features obtained from HRV indicated high correlation with the mental fatigue of the driver. Yang *et al.* [161] used heterogeneous information sources to detect driver's fatigue. The information sources included fitness, sleep deprivation, environmental information (traffic, road condition, etc), physiological signals (ECG, EEG) and video monitoring parameters (head movement, blink rate and facial expressions). In order to combine all the above-mentioned information they used the Dempster-Shafer theory and rules for determining whether the driver is in fatigue state or not. Ji *et al.* [117] proposed a probabilistic framework for modelling and real-time inferencing of human fatigue by integrating data from various sources and certain relevant contextual information. They used a Dynamic Bayesian Network which encapsulates the time dependent development of fatigue symptoms. The estimation is based on visual cues and behavioural variables. As research in the field progresses, a variety of physiological signals has been used for fatigue detection. The most informative measures in terms of fatigue recognition are those extracted from the EEG signal, which have been used for the quantification of task specific performance changes [9]-[17]. However, the idea of near future vehicles, capable of acquiring drivers' EEG, is quite optimistic. Indicators coming from measurements taken in a less obtrusive manner should be exploited in a real life system.

Physiological measurements are also good indicators of the driver's stress. Several works in the literature focus on driver stress recognition based on biosignal processing. ECG, electromyogram (EMG), respiration, skin conductivity, blood pressure and body temperature are the most common signals collected from the driver in order to estimate

the workload and the levels of stress he/she experiences. Healey *et al.* [43] presented a real time method for data collection and analysis in real driving conditions to detect the driver stress status. According to them, there is a strong correlation between driver status and selected physiological signals (EMG, ECG, skin conductivity and respiration effort). In another study, Healey *et al.* [46] specified an experimental protocol for data collection. Four stress level categories were created according to the results of the subjects self report questionnaires. A linear discriminant function was used to rank each feature individually based on the recognition performance and a sequential forward floating selection (SFFS) algorithm was used to find an optimal set of features to recognize driver stress. Healey *et al.* [45], proposed a slightly different protocol, while the results showed that for most drivers, the skin conductivity and the heart rate are most closely correlated to driver stress level. Zhai *et al.* [163] developed a system for stress detection using blood volume pressure, skin temperature variation, electrodermal activity and pupil diameter[1]. Rani *et al.* [120] presented a real time method for driver's stress detection based on the heart rate variability using Fourier and Wavelet analysis. Liao *et al.* [86] presented a probabilistic model for driver's stress detection based on probabilistic inference using features extracted from multiple sensors.

The well-established literature in stress and fatigue detection problems has revealed a number of features, highly correlated to the one or the other state. However, according to our knowledge, all studies focus only on one specific driver affective state (either fatigue or stress), although in practice they both influence the physiology of the driver and hence his physiological responses. Putting such systems in practice could make the estimation of drivers state less effective compared to experimental settings, as in real driving simultaneous presence of both fatigue and stress could occur making discrimination of different possible states more difficult.

Having this in mind, we developed a driver status recognition methodology for simultaneous stress and fatigue detection. Our methodology employs features coming from (i) a set of driver's biosignal recordings (ECG, electrodermal activity, respiration), ii) video recordings from driver's face, iii) environmental conditions (weather, visibility and traffic). In our work we select the features with higher contribution to the classification of the states under investigation. Furthermore, we evaluate the contribution of different groups of features (biosignals, video and environmental features), in order to investigate which group is more associated to a specific driver's state (fatigue and stress). Using the selected features, we examine the performance of four different classifiers (namely the SVMs, the Decision Trees, the Naive Bayes and General Bayesian classifier) on the driver state recognition accuracy. The proposed methodology allows for simultaneous estimation of stress and fatigue levels using the minimum set of physiological signals in the less obtrusive manner. Applying our methodology, changes in driver's state are estimated at an early stage before they critically affect driving performance.

[1]The measure through the center of the adjustable opening in the iris of the eye, terminated at both ends by its circumference.

Having developed a sound methodology for driver's state estimation we also study whether the estimated changes of driver's state affect driving performance. To perform this study, we have developed a driving simulation environment, which allows us to monitor a set of driving performance measures (steering, braking, lane keeping, reaction time) and examine their association with the subject's physiological state. A series of laboratory experiments are conducted around the driver simulator. As drivers are not easily stressed when using a simulator, our study focuses only on the association of the estimated fatigue and the deterioration of driving performance.

In the following sections we first describe the proposed methodology (Section 4.2). The dataset obtained in real driving conditions is then presented (Section 4.3). In section 4.4 the obtained results are presented. In section 4.5 we shortly present our study of fatigue impact on driving performance. A discussion on the methodology and the results follows (Section 4.6).

4.2 Methodology

The methodology consists of three main steps (depicted in Fig. 4.1):

(I). *Preprocessing and feature extraction* which is decomposed in three streams: (I-a) signal acquisition, preprocessing and feature extraction, (I-b) video acquisition processing and feature extraction and (I-c) environment information extraction.

(II). *Feature selection.*

(III). *Classification.*

These steps are described in details in the following paragraphs.

4.2.1 Step I-a: Signal acquisition/pre-processing and feature extraction

The physiological signals which are reported in the literature as the most significant indicators of subjects' fatigue and stress, are: blood pressure, EEG, EOG, ECG, heart rate variability, skin conductivity and respiration [163, 141, 66]. However, in order to set up a real time system for driver stress and fatigue monitoring in real driving conditions, the sensors for the physiological signal acquisition should be minimally obtrusive. Taking this into consideration, the recorded physiological signals in our work are limited to the following signals: (i) Electrocardiogram (ECG) through a g.ECG sensor which is placed on the subject's chest, (ii) Electrodermal Activity (EDA) through two Ag/Ag.Cl electrodermal activity sensors attached on the subject's middle and index fingers of the right hand and (iii) the respiration rate using a g.RESP Piezoelectric Respiration Sensor which

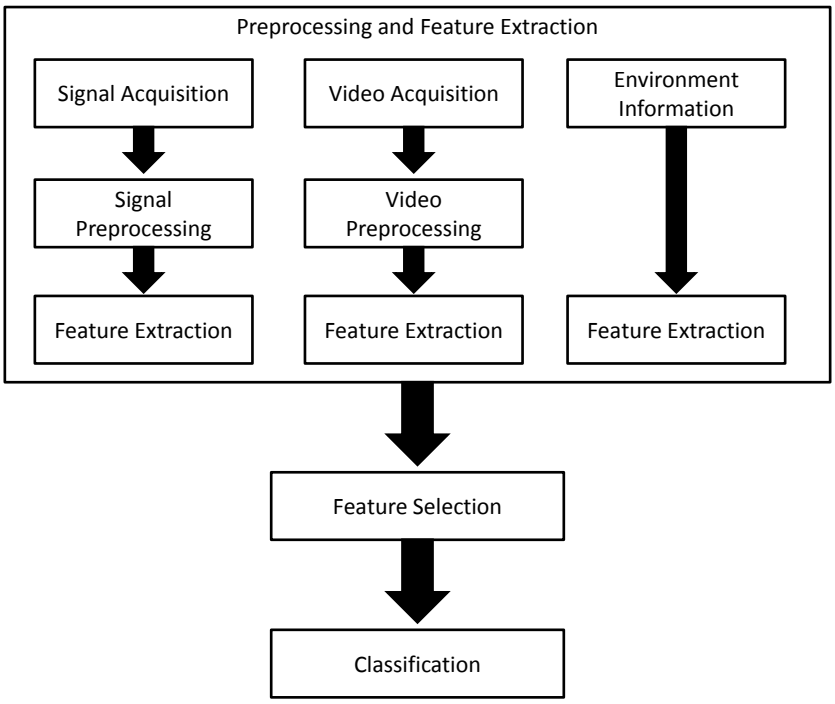

Figure 4.1: The steps of the methodology for driver stress and fatigue classification.

is placed around the subject's thorax. The Biopac MP-100 system is used for signal acquisition. The ECG signal is acquired at sampling frequency 300Hz while the EDA and the respiration signal at 50 Hz. The resolution is set to 12-bit for all signals.

ECG signal

The Biopac system, has an option of acquiring only the R-waves of ECG signals, which are more robust to noise[2]. This option is used in the real driving conditions, since the noise from the subject's movement introduces high noise in the ECG signal. In order to obtain useful indicators of the subject's states under investigation (fatigue and stress) we first perform some necessary preprocessing steps on the raw signals. The features are extracted in time windows of 5 minutes, that is a reasonable compromise between the need of sufficient sample size in order to have reliable statistic properties and the need of small window to capture the changes in the psycho-physiology of the driver [26]. In order to extract the RRV signal from the ECG, an accurate estimation of R peaks is needed. Initially, a lowpass ButterWorth Filter is applied to the ECG signal to remove the baseline wonder. Then the R peaks are detected, using the procedure described in [119]. Furthermore, since the errors in the RR interval estimation and in RRV extraction can have serious impact in the spectrum estimation and thus in the features calculated from the spectrum, we also visually correct the initial R estimation of the algorithm through

[2]The output signal is a positive peak only when a R-wave is detected. This function is useful for heart rate calculations when a well-defined peak is desired as it tends to remove any components of the waveform that might be mistaken for peaks.

a specifically built application. After ECG preprocessing and R peak detection, the R-R intervals are estimated as the time differences between successive R peaks. Those R-R intervals constitute the RR variability signal (RRV). The next step is the interpolation of the RRV series in 4 Hz samples and downsampling to 1 Hz. This is an important step if ordinary spectrum estimation methods are to be applied (FFT, AR)[3]. After interpolation the low frequency (0.01 Hz) trend of the signal is removed using a ButterWorth filter. The FFT transform $H(f)$, of the signal (calculated at 1024 samples) is extracted and the spectrum of the signal is obtained as $P(f) = |H(f)H(f)^*|$. The following features are calculated from the spectrum:

- The ratio of the very low frequency (VLF) [0.01-0.05 Hz] energy to the total signal energy.
- The ratio of the low frequency (LF) [0.05-0.2 Hz] energy to the total signal energy minus the VLF energy.
- The ratio of the high frequency (HF) [0.2-0.4 Hz] energy to the total signal energy minus the VLF energy.
- The ratio of the LF to the HF components.

We also calculate the Spectrum Entropy (SE) of the signal,

$$p(f) = \frac{P(f)}{\sum_{f'} P(f')}, \tag{4.1}$$

$$SE = \sum_{f} p(f) \log p(f). \tag{4.2}$$

The SE can be considered as a measure of the deterministic behavior of the RRV. The Detrended Fluctuation Analysis (DFA) [113, 14, 30] and Lyapunov exponent analysis [116] are applied on our 5 min intervals of the RRV recordings.

EDA signal

The EDA signal is downsampled to 1 Hz. A smoothing filter is applied, since in many cases noise is evident in the signal; then the low frequency 0.01 Hz of the signal is removed which is considered as the skin conductance level (SCL). The first absolute difference (FAD) of the remaining signal is calculated, giving a measure of the skin conductance response (SCR):

$$FAD = \sum_{i} |y_{i+1} - y_i|. \tag{4.3}$$

[3]FFT: Fast Fourier Transform, AR: AutoRegressive spectrum estimation methods.

Respiration signal

The respiration signals have high signal to noise ratio and only in cases with subject's sudden movements, noise exists. The signal is downsampled to 10 Hz and the wonder is removed. The power spectrum of the signal, using FFT transform, is extracted. A smoothing of the power spectrum follows, and the maximum energy frequency between 0.1 Hz and 1.5 Hz is selected as the dominant respiration frequency (DRF). Furthermore, we extract another feature which is the ratio of the heart rate to the respiration rate. As respiration is a main modulator of the cardiac function, the hypothesis is that for normal/relaxed conditions the ratio of heart to respiration rate is constant and changes are observed only in abnormal conditions, such as stress and fatigue. Given the mean RR intervals and the dominant respiration frequency the ratio of the heart rate to the respiration rate is calculated as:

$$\begin{aligned} \frac{HeartRate}{RespirationRate} &= \frac{60/(MeanRR)}{60 \cdot D.R.F.} \\ &= \frac{1}{(MeanRR)(D.R.F.)}. \end{aligned} \tag{4.4}$$

4.2.2 Step I-b:Video acquisition/processing and feature extraction

The video of the face of the driver is processed following the approach described in [145, 32]. The first step is the detection of the face and the second is the detection of eyes. The information of interest is: (i) the movement of the head, which could be an indicator for both stress and fatigue and (ii) the mean level of eye opening as an indicator of fatigue. We also calculate an estimation of PERCLOS, considering eye closure when the confidence of eye presence is less than zero. As a measure of head movement, the standard deviation of the face position in the video frame is used, and as a measure of eye opening we use the confidence of eye detection (provided in [145]). If the eyes are wide open this confidence is high, while for near close eyes it is quite low. As video is not available for all sessions (e.g. due to low quality recordings) the sessions without video recordings, can be treated as missing values. The K-NN algorithm is used for replacing the missing data in the combined data for video and physiological features for all sessions. K is set to 3 and the weighted Euclidean distance is employed.

4.2.3 Step I-c: Environment information extraction

In our methodology we introduce driving environmental information. For this purpose, a forward looking camera for road monitoring is employed. From road monitoring video, useful information about driving environment conditions during each session is manually extract. This information concerns weather, road visibility and traffic conditions. Bad weather and low visibility are reported as important stress factors [20]. Another important stress factor is traffic density [151, 50]. Using the video recordings of the road scenery, we manually extract a metric of the traffic load of the road during the 5 min interval. All

Table 4.1: The features used in this study and the code name assigned to each feature.

Source	Feature	Code
Physiological	Mean RR	F1
Signals	Std of detrended RR	F2
	Proportion of RRV energy on very low frequency band (VLF)	F3
	Proportion of RRV energy on low frequency band (LF)	F4
	Proportion of RRV energy on high frequency band (HF)	F5
	LF/HF	F6
	Mean EDA level	F7
	First absolute differences	F8
	Mean Respiration Rate	F9
	RRV Detrended Fluctuation Analysis (DFA)	F10
	Respiration Spectrum Entropy	F11
	RRV Lyapunov Mean exponent	F12
	RRV Lyapunov Max exponent	F13
	HR (bpm)/Resp. Rate (bpm)	F14
Face Video	Mean Eye Activation	V1
	Std of Eye Activation	V2
	Std of Head Position	V3
	PERCLOS	V4
Environment	Weather conditions	S1
	Visibility	S2
	Traffic conditions	S3

environmental variables are categorized in three states (*good/bad/very bad* weather, *very low/low/good* visibility and *low/medium/high* traffic density).

4.2.4 Step II: Feature selection

The majority of the features extracted in Step I are the most common features used in similar studies. However, a classifier using all those features would lack robustness. For this reason we employ feature selection. Such an approach is a prerequisite in cases where the ratio of data to features is low. Furthermore, introducing redundant features or features highly correlated can deteriorate the classification performance. Therefore, to build a robust classifier for stress and fatigue detection, we have to evaluate the contribution of each feature as an indicator of these states. We used four measures for ranking features with respect to their discrimination power for the problems under investigation: i) Relief [134], ii) Information Gain, iii) Information Gain Ratio and iv) the difference in the area under curve (AUC) of a classifier based on the specific feature and a random classifier (DAUC). We follow with a more detailed description of the four measures.

Input: m training vectors on n attribute and class label for each vector.
Output: $\mathbf{w} = \{\mathbf{w_1}, \cdots, \mathbf{w_n}\}$
Set all weights to zero $\mathbf{w} := \mathbf{0}$
for all data point $\mathbf{x}$ **do**
  Find nearest hit sample NH and nearest miss sample NM.
  for $j = 1 \cdots n$ **do**
    $w_j = w_j + dist(x^{(j)}, NM^{(j)} - dist(x^{(j)}), NH^{(j)})$

Algorithm 1: Relief

Relief

The Relief algorithm [134] iteratively estimates the feature weights according to their ability to discriminate between neighboring data points. In each iteration, for a random sample $\mathbf{x}$, two nearest neighbors of $\mathbf{x}$ are found. The first one belongs to the same class with $\mathbf{x}$, which is referred as the nearest hit (NH), whereas the second one to a different class, which is referred as the nearest miss (NM). The goal of the Relief algorithm, outlined in Algorithm 1, is to rank features according to their minimum nearest hit average distance and maximum nearest miss average distance.

Information Gain and Information Gain Ratio

We should first introduce the entropy of a discrete random variable X with K discrete states, denoted as $H(X)$:

$$H(X) = -\sum_{i=1}^{K} P(X = x_i) \log P(X = x_i), \tag{4.5}$$

where $P(X = x_i)$ the probability of the i-th state. The conditional entropy of a variable Y, conditioned on variable X is defined as

$$H(Y|X) = -\sum_{i=1}^{K} P(X = x_i) \log P(Y|X = x_i), \tag{4.6}$$

where $P(Y|X)$ is the conditional distribution of Y given X. Now given a variable C the information gain (IG) of the variable X with respect to C is defined as

$$IG(C|X) = H(C) - H(C|X). \tag{4.7}$$

This is a measure of how informative is a variable X about the distribution of the variable C, which is the problem's class in our case. The information gain ratio (IGR) is a variant of the information ratio, defined as:

$$IGR(C|X) = H(C) - H(C|X)/H(X). \tag{4.8}$$

In order to apply the above measures in our data, we discretize our data in ten bins with equal width.

Difference of area under curve (DAUC)

The DAUC is the difference of are under curve of a classifier based on a specific feature and a random classifier. The output of the classifier based on a specific feature $C(x)$, for a binary problem with two possible outcomes C_1 and C_2, is defined as:

$$C(x) = \begin{cases} C_1, x \leq t \\ C_2, x > t \end{cases}, \tag{4.9}$$

where t is a threshold. The ROC of this classifier is extracted, modifying the value of t. The area under curve of an optimal classifier is 1. Extracting the area under curve of a random classifier which is 0.5, the DAUC of the optimal classifier is 0.5. Thus, features with DAUC near 0.5 are considered to be optimal. In order to select the optimal feature set for more than one classification problems, the average DAUC of each feature is calculated. Then features are sorted according to their average DAUC, obtaining a feature ranking (see Section 4.4).

Based on the abovementioned measures, we obtain a weight w_{ij} of each feature i, and j corresponds to the measure used for the feature ranking. We then normalize the weights:

$$w'_{ij} = \frac{w_{ij}}{\sum_k w_{kj}}, \tag{4.10}$$

and the final weight of each feature W_i is the average of the normalized weights:

$$W_i = \sum_j w'_{ij}. \tag{4.11}$$

Finally we rank the features according to their weight W_i. The final number of the features incorporated in the classification process, was determined after a test and trial experimental procedure, in order to obtain the best accuracy in both fatigue and stress classification.

4.2.5 Step III: Classification

The third step of our methodology is classification. The performance of four different classifiers is examined. In this section we briefly describe the classifiers used for fatigue and stress classification.

Support vector machines (SVM): Each instance in the training set contains one "target value" (class labels) and several "attributes". The goal of the SVM is to produce a model which predicts the target value of data instances in the testing set in which only the attributes are given. Let a training set of instance-label pairs be (x_i, y_i), where $x_i \in \mathbf{R}$ is the training vector, belonging to one of the classes generating the data, N is the number of the extracted features in the training set and y_i indicates the class of x_i. The support

vector machine requires the solution of the following optimization problem:

$$\min_{\mathbf{w},b,\xi}(\frac{1}{2}\mathbf{w}^T\mathbf{w} + c\sum_{i=1}^{N}\xi_i), \tag{4.12}$$

subject to:

$$y_i(\mathbf{w}^T\phi(x_i) + b) \geq 1 - \xi_i, \tag{4.13}$$

$$\xi_i \geq 0, \tag{4.14}$$

where b is the bias term, $\mathbf{w}$ is a vector perpendicular to the hyperplane separating the classes, ξ is the factor of classification error and $c > 0$ is the penalty parameter of the error term. The training vectors x_i are mapped into a higher dimensional space F by the function $\phi : R^n \rightarrow F$. SVM finds a separating hyperplane with the maximal geometric margin and minimal empirical risk R_{emp} in the higher dimensional space. R_{emp} is defined as:

$$R_{emp} = \frac{1}{2N}\sum_{i=1}^{N}|y_i - f(x_i, a)|, \tag{4.15}$$

where f is the decision function defined as:

$$f(x) = \sum_{i=1}^{N} y_i a_i K(x_i, x) + b, \tag{4.16}$$

where $K(x_i, x_j) = \phi(x_i)^T\phi(x_j)$ is the kernel function, a_i are weighting factors and b is the bias term. In our case the kernel is a radial basis function (RBF) which is defined as:

$$K(x_i, x_j) = \exp(-\gamma\|x_i - x_j\|^2), \gamma > 0, \tag{4.17}$$

where $\gamma = \frac{1}{2\sigma^2}$ is the standard deviation. The RBF kernel, which is used in our experiments, non-linearly maps samples into a higher dimensional space, thus, it can handle the case when the relation between class labels and attributes is nonlinear. In our case $\gamma = 1$ and $c = 10$. In the case of more than two classes classification, the one-against-all strategy is followed.

Decision Trees: To construct the decision tree we use the C4.5 inductive algorithm [118]. The construction of the tree is based on a greedy approach. At each step there will be some number of candidate regions in input space that can be split, corresponding to the addition of a pair of leaf nodes to the existing tree, which initially is empty. In our problem, the features are continuous valued. Therefore, they can be incorporated into the decision tree by partitioning them into a set of discrete intervals. For each continuous feature x, a new Boolean feature is created:

$$X_t = \begin{cases} 1, & x \leq t \\ 0, & \text{otherwise.} \end{cases} \tag{4.18}$$

The selection of the threshold t is conducted through a process of generation of a set of candidate thresholds which produce a high information gain (see section 4.2.4). Those

candidate thresholds are evaluated and the one that produces the maximum information gain is finally chosen. The algorithm of [118] has the advantage of solving the over-fitting problem by using a post pruning method.

Naive Bayes Classifier: The Naive Bayes classifier is based on the Bayes Theorem and the assumption of independence among variables. Despite the fact that the independence assumption is considered as poor in general, this classifier works well even in complex situations. Let again a set of instance-label pairs (x_i, y_i) where $x_i \in \mathbf{R}$ and $y_i \in Y$ the class producing x_i. The probability model for a classifier is abstractly a conditional model:

$$p(y|X) = p(y|x_1, ..., x_N). \tag{4.19}$$

Applying the Bayes' Theorem:

$$p(y|x_1, ..., x_N) = \frac{p(y)p(x_1, ..., x_N|y)}{p(x_1, ..., x_N)}. \tag{4.20}$$

The denominator of the fraction is effectively constant. Thus, in practice we are only interested in the numerator of that fraction, which is equivalent to the joint probability model:

$$p(y, x_1, ..., x_N). \tag{4.21}$$

Using the conditional independence assumptions we can write the joint probability as:

$$p(y, x_1, ..., x_N) = p(y) \prod_{i=1}^{N} p(x_i|y). \tag{4.22}$$

Then, under the aforementioned independence assumptions, the conditional distribution can be expressed as:

$$p(y|x_1, ..., x_n) = \frac{1}{Z} p(y) \prod_{i=1}^{N} p(x_i|y), \tag{4.23}$$

where Z is a scaling factor. This is a more manageable form, requiring $(C-1) + NRC$ parameters where R is the number of parameters for the $p(x_i)$ model and C is the number of classes.

General Bayesian Classifier: This classifier is based on the same philosophy as the Naive Bayes, without the hypothesis of feature independence. For example, in cases of continuous features following a Gaussian distribution, in the Naive bayes case the covariance matrix is diagonal while in the General Bayes classifier the covariance is a full positive definite matrix.

4.3 Dataset

The dataset collection was performend driving conditions, which helps to recognize and understand the true physiology of the driving task, and measure the subject's reactions to common driving conditions, such as bad weather and traffic congestion. The subject

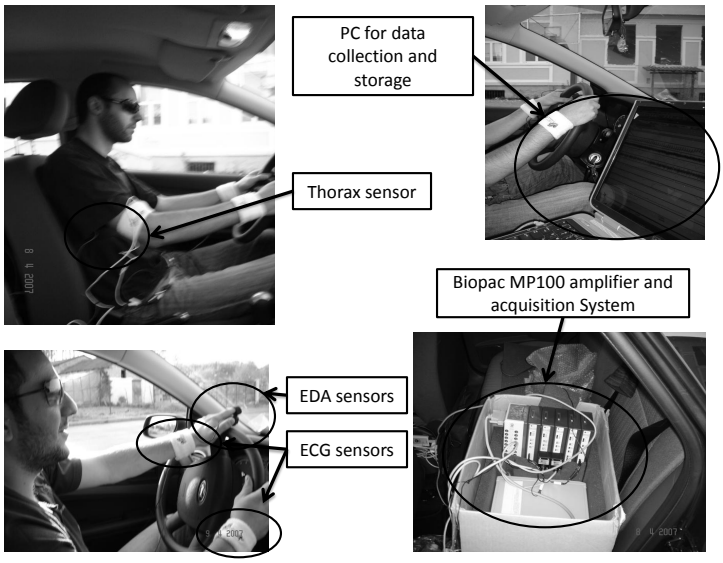

Figure 4.2: The acquisition system for real driving conditions.

under investigation is a 28 years old, healthy male, with two years of driving experience. Next, the experimental settings and protocols for the data collection is described.

The equipment that was used in order to acquire the needed information included: (i) a Biopac MP-100 for signal acquisition of the driver (ECG, EDA and Respiration). This equipment was installed on the back seat of the vehicle and the sensors were attached to the driver as depicted in Fig. 4.2. (ii) A camera monitoring the road is used only for annotation reasons, (iii) a camera monitoring driver's face. Before the begining of the annotated sessions, the subject conducted a number of long lasting sessions in order to familiarize with the equipment. The duration of the data collection in real conditions was approximately 18 months and a sufficient number of driving events under different conditions was encountered. The total number of tours (37 experiments), average duration of each tour and encountered conditions in all tours are shown in Table 5.1. Sessions are covering the whole day duration (07.00 - 24.00) so as to capture different fatigue levels (Fig. 4.3). The driver annotation was performed at the end of each session, by self annotating his state. A three scale of fatigue levels (*normal*, *low fatigue*, *high fatigue*) and a two scale for stress levels (*normal*, *stress*) are used, following a human factors expert's suggestion.

4.4 Results

The first step of our methodology is the preprocessing and feature extraction described in sections 4.2.1 and 4.2.2. The features extracted, are summarized in Table 4.1. The next step in our methodology is feature selection. In section 4.2.4 the DAUC measure, is described for a two class classification problem. For stress classification the application of the described method is straightforward since two classes exist. For fatigue classification,

Table 4.2: Description of the dataset for real driving conditions.

Tour info	Number of tours	37
	Average Duration of Each Tour	50 min.
Condition	States	Number of Tours
Stress	No	13
	Yes	24
Fatigue	Normal	9
	Medium	15
	High/Drowsiness	13
Environmental conditions	No Rain	26
	Rain	8
	Heavy Rain	3
	Normal Visibility	29
	Medium Visibility (Late Evening)	6
	Low Visibility (Fog/Night)	2

which is a three class classification problem, the problem is decomposed in four two-class subproblems (*normal* vs *low fatigue*, *normal* vs *high fatigue* and *low fatigue* vs *high fatigue*). The DAUC of each feature for all abovementioned classification problems is given in Fig. 4.4(a). Sorting the features according to their average DAUC we obtain a ranking of the features, depicted in Fig. 4.4(a).

The average ranking of the four measure described in Section 4.2.4, is depicted in Fig. 4.4(b). The physiological features with higher average ranking are *mean RR* (F1), *std of RR* (F2), *LF/HF ratio* (F6), *mean EDA level* (F7), *First absolute differences of EDA* (F8), *mean respiration rate* (F9) and *HR (bpm)/Resp. Rate (bpm)* (F14). From the video features, *std of eye activation* (V2) and PERCLOS (V4) are better indicators for fatigue, whereas *std of head positions* (V3) is a better indicator of stress. Finally from the environmental conditions, the weather conditions (S1) seem to be the most important. In Table 4.3 we present the correlation among physiological and video features. Correlation analysis shows that the indicators F1-F2, F1-F6, F1-F9 and F7-F8 are rather correlated. Finally, all these features were kept, as removal of any of them did not increase the performance of the selected classifiers; instead it tended to decrease the accuracy.

The third step of our methodology is classification. The classifiers tested are described in section 4.2.5. To provide unbiased results we followed two procedures. The steps of the first one are:

- 50 balanced datasets from the original one were extracted. Let K the number of samples for the class containing the fewer samples. K random samples are selected from all other classes and are combined in one dataset having which includes $K \times C$

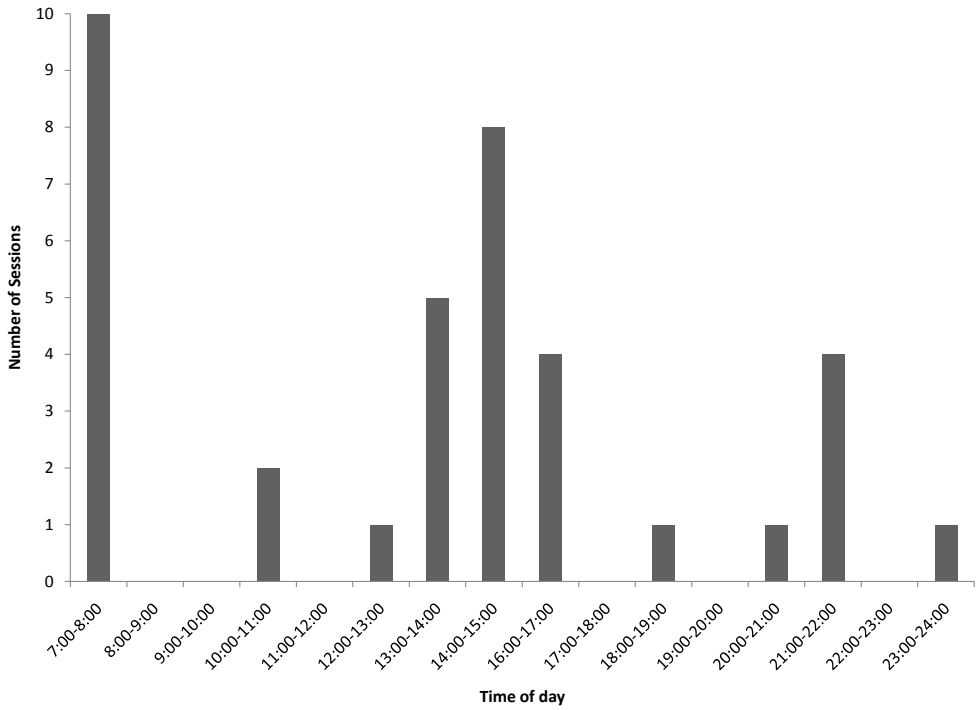

Figure 4.3: The distribution of the sessions during the day.

samples, where C is the number of classes.

- For each of the 50 datasets we perform stratified 10-cross validation using the classifiers described in section 4.2.5 and we obtain the confusion matrix.
- The mean of each entry of the confusion matrix is calculated.

In the second procedure, we perform a leave one session out method, each time keeping one session for testing and the rest for training. The use of two different classification procedures, will allow to investigate possible bias in the presented results.

The measures used to evaluate the performance of the different classifiers are the following:

- Confusion Matrix: A $C \times C$ matrix, where C is the number of classes. The element c_{ij} corresponds to the instances of the class i which are classified as class j. The diagonal elements c_{ii} are the correct classified instances.
- Sensitivity per class: The fraction of correctly classified instances of a class to the total number of instances belonging to that class.
- Specificity per class: The fraction of the correctly classified instances for a class to the total number of instances classified as the specific class.
- Overall accuracy: The fraction of the total number of correctly classified instances to the total number of instances

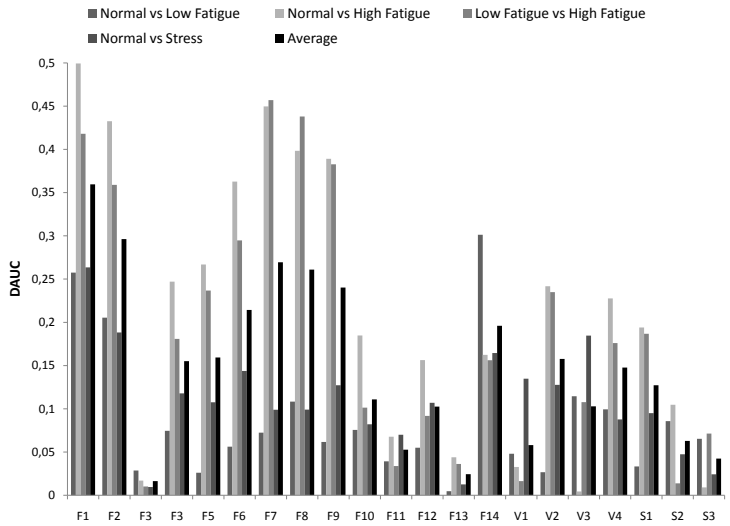

(a)

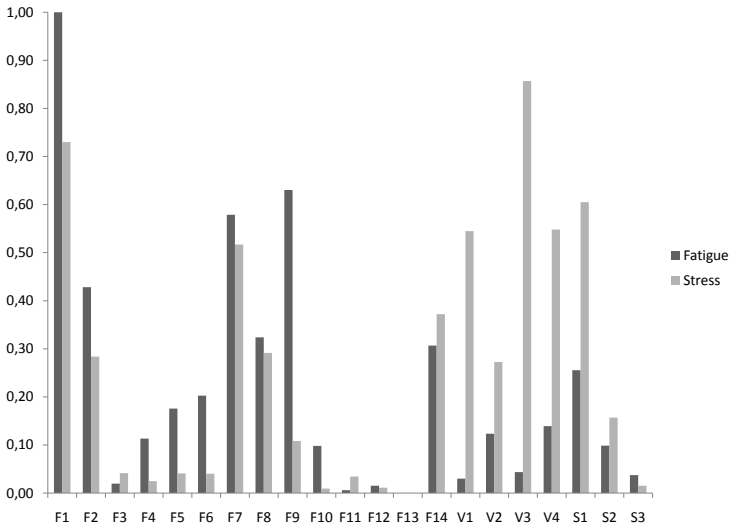

(b)

Figure 4.4: (a) The DAUC of physiological and video features for *normal* vs *high fatigue*, *normal* vs *low fatigue*, *low fatigue* vs *high fatigue* and *normal* vs *stress*, as well as the average DAUC for all problems. (b) The average feature ranking with the four ranking measures for the problems of fatigue and stress classification.

Table 4.3: The correlation among features.

	Physiological Features													Video Features			
	F2	F3	F4	F5	F6	F7	F8	F9	F10	F11	F12	F13	F14	V1	V2	V3	V4
F1	0.7	0.0	-0.4	0.5	-0.6	-0.6	-0.4	-0.7	-0.2	0.1	0.3	0.1	-0.2	0.0	-0.4	0.2	0.1
F2		0.0	-0.5	0.1	-0.4	-0.5	-0.4	-0.6	-0.3	0.0	0.0	0.0	-0.1	-0.1	-0.2	0.0	0.2
F3			0.3	0.1	0.0	0.0	0.0	0.0	-0.2	-0.1	-0.1	-0.1	0.0	0.1	0.0	0.0	0.2
F4				-0.1	0.6	0.3	0.1	0.4	0.6	0.1	0.0	0.0	0.0	0.0	0.4	-0.1	0.0
F5					-0.7	-0.4	-0.2	-0.4	0.0	-0.1	0.4	0.1	0.0	0.1	-0.4	0.2	0.0
F6						0.5	0.2	0.5	0.3	0.1	-0.3	-0.1	-0.1	0.0	0.7	-0.2	-0.1
F7							0.8	0.7	0.1	-0.1	-0.1	0.0	-0.2	0.0	0.3	-0.1	-0.1
F8								0.4	0.0	-0.1	-0.1	0.0	0.0	-0.1	0.1	-0.2	0.0
F9									0.1	-0.1	-0.2	-0.1	-0.5	0.0	0.3	-0.2	0.0
F10										0.1	0.1	0.0	0.1	0.0	0.2	0.0	0.0
F11											-0.1	0.0	0.1	-0.1	0.1	-0.1	0.0
F12												0.3	-0.1	0.1	-0.1	0.2	0.0
F13													0.0	0.1	0.0	0.0	0.1
F14														0.1	0.0	0.1	-0.1
V1															0.2	0.5	-0.7
V2																0.0	-0.2
V3																	-0.6

In Tables 4.4 and 4.5, we present the results for fatigue and stress classification using three sets of features: (i) only physiological features, (ii) physiological and video features and (iii) physiological, video and environmental features. In these tables the sensitivity and specificity per class, as well as the total accuracy for all classifiers and feature sets are given. For the two-class stress problem the information provided is sufficient to evaluate the performance of the classification. However for the three-class fatigue problem a better insight is given through the confusion matrix of the classification. From Tables 4.4 and 4.5 we observe that SVM had the best performance in all feature sets for classification of both states, whereas Naive Bayes classifier had the worst (up to 12% lower accuracy compared to SVM in some cases). In Table 4.4 we observe that the highest accuracy for fatigue classification was obtained using the full feature set (88% with SVM). When limited feature sets are employed the difference is rather small (85% with physiological features and 87% with physiological and video features, both obtained using SVM). In Table 4.8 detailed classification results (containing also the confusion matrix) are given using the full set of features. It can be noticed that the main source of misclassification is in the *low* fatigue class. From Table 4.5 we observe that for stress classification the incorporation of additional features, in contrast to fatigue detection, significantly increased the obtained accuracy. The 78% accuracy obtained by physiological features climbs to 86% using physiological, video and environment features.

In Tables 4.6 and 4.7 we present the results obtained using the second classification procedure, where one session was kept for test and the rest for training. In these results we use the full set of selected features (physiological, video and environmental features). We observe that there is no significant difference in the obtained accuracies compared to Tables 4.5 and 4.4 where the first classification procedure was used. This is a strong indication that the results presented here, are not biased from the classification procedure followed.

In our analysis we also study the contribution of each sensor to the classification results. As already described the features used in our experiments come from physiological signals, video monitoring of driver's face and environmental information. As features are extracted from signals obtained from different sensors, features can be grouped into five groups each of them related to a specific sensor of the experimental setting. Such an analysis can give a significant insight for the importance of each sensor when building a system for driver state monitoring. Physiological features are grouped in features coming from RRV, features coming from EDA and features coming from respiration. The other two groups are the features from video and environmental features, respectively. We then evaluate the contribution of each group of features in the classification performance, with the following two procedures: (i) we perform the classification with the whole feature set, removing each time a group of features belonging to a specific sensor and we measure the decrement in accuracy. (ii) We perform classification using only features coming from a specific sensor. In Figs. 6.9(a) and 6.9(b) we present the results with the two procedures. The conclusions from both procedures are identical. For fatigue classification, the most

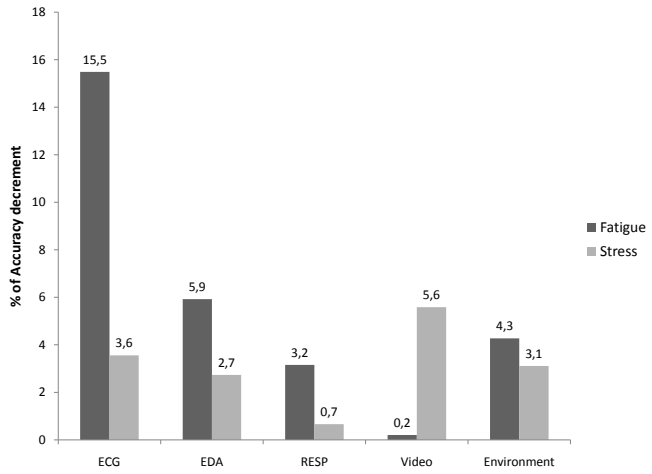

(a)

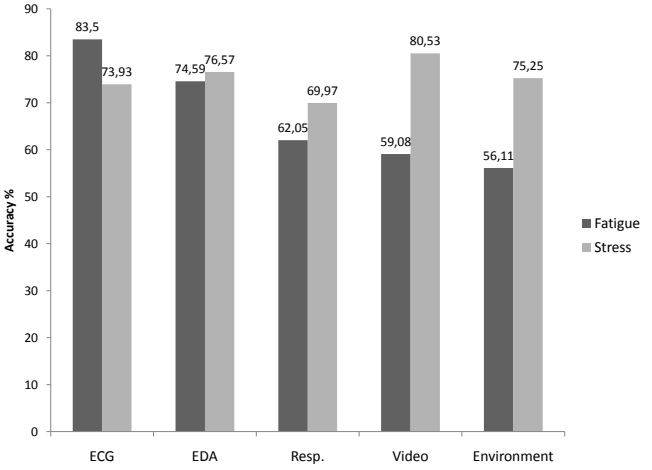

(b)

Figure 4.5: (a) The percentage of accuracy reduction after removing groups of features from the original feature set and (b) the accuracy obtained using only features from the specific sensor. RRV denotes features that are extracted from the RRV signal, EDA features that are extracted from the EDA signal, RESP features that are extracted from respiration, VIDEO features from video processing and Environment for features indicating environmental conditions.

Table 4.4: Results for the *fatigue* classification problem using three feature sets. For each classifier, the sensitivity (Sens.) and the specificity (Spec.) per class are given as well as the total accuracy (Acc.).

		Normal		*Low Fatigue*		*High Fatigue*		
		Sens.	Spec.	Sens.	Spec.	Sens.	Spec.	Acc.
Physiological features	*SVM*	0.87	0.82	0.71	0.81	0.96	0.90	0.85
	Decision Trees	0.76	0.76	0.73	0.72	0.94	0.95	0.81
	Naive Bayes	0.81	0.74	0.49	0.67	0.92	0.79	0.74
	Bayes Classifier	0.88	0.74	0.50	0.74	0.94	0.83	0.77
		Sens.	Spec.	Sens.	Spec.	Sens.	Spec.	Acc.
Physiological +Video features	*SVM*	0.85	0.85	0.76	0.82	0.99	0.92	0.87
	Decision Trees	0.74	0.74	0.70	0.70	0.94	0.95	0.79
	Naive Bayes	0.70	0.83	0.63	0.64	0.92	0.78	0.75
	Bayes Classifier	0.79	0.79	0.64	0.70	0.92	0.85	0.78
		Sens.	Spec.	Sens.	Spec.	Sens.	Spec.	Acc.
Physiological +Video +Environmental features	*SVM*	0.89	0.87	0.79	0.84	0.96	0.92	0.88
	Decision Trees	0.74	0.74	0.71	0.70	0.94	0.95	0.80
	Naive Bayes	0.70	0.86	0.65	0.64	0.92	0.79	0.76
	Bayes Classifier	0.76	0.83	0.73	0.71	0.93	0.88	0.81

significant sensor is the ECG, whereas in stress classification no sensor appears to be dominant. Thus, a reliable fatigue detection system, could be solely based on an ECG sensor. On the other hand, for a stress detection system, the fusion of more information sources seems inevitable.

4.5 Physiological state and driving performance

Our proposed methodology showed good performance even in the detection of early stages of fatigue (*low* fatigue state). In order to investigate whether these early fatigue stages are worth recognizing, we performed a study to examine the impact of driver's fatigue levels on driving performance. The goal of our study was to verify that the detected fatigue levels are associated with the deterioration of driving performance. A simulation environment was developed to measure driving performance in terms of subject's sensorimotor functions (i.e. perception and reaction times). The simulation driving world was based on the Microsoft XNA framework as it is shown in Fig. 4.6. The vehicle is controlled by the Logitech's Momo racing wheel. The subject was asked to focus on the driving task, i.e. keep the vehicle within the road lane and avoid crashes with pedestrians which appeared unexpectedly on the road, by pressing the brake pedal and stopping the vehicle. From this primary task, measurements of steering control and reaction times are monitored. In addition to the primary driving task, a secondary-task request is used following the well-established PDT (Peripheral Detection Task) technique [55]. During the experiments

Table 4.5: Results for the *stress* classification problem using three feature sets. For each classifier, the sensitivity (Sens.) and the specificity (Spec.) per class are given as well as the total accuracy (Acc.).

		Normal		*Stress*		
		Sens.	Spec.	Sens.	Spec.	Acc.
Physiological features	*SVM*	0.79	0.78	0.78	0.79	0.78
	Decision Trees	0.78	0.76	0.75	0.77	0.76
	Naive Bayes	0.79	0.63	0.54	0.72	0.66
	Bayes Classifier	0.85	0.63	0.49	0.77	0.67
		Sens.	Spec.	Sens.	Spec.	Acc.
Physiological +Video features	*SVM*	0.80	0.90	0.91	0.82	0.86
	Decision Trees	0.80	0.81	0.81	0.80	0.81
	Naive Bayes	0.82	0.71	0.66	0.79	0.74
	Bayes Classifier	0.85	0.71	0.65	0.82	0.75
		Sens.	Spec.	Sens.	Spec.	Acc.
Physiological +Video +Environmental features	*SVM*	0.88	0.85	0.84	0.88	0.86
	Decision Trees	0.82	0.81	0.80	0.81	0.81
	Naive Bayes	0.85	0.76	0.74	0.83	0.79
	Bayes Classifier	0.86	0.76	0.73	0.83	0.79

apart from pedestrians, other objects (animals) randomly appeared outside the roadway. Once the objects perceived, the subject respond by pressing one of the control buttons of the steering wheel, and the respective reaction time is measured.

The physiological signals monitored in the laboratory experiments are similar to the ones measured during real-world experiments (ECG, EDA and respiration). The same off-the-shelf equipment (Biopac MP-100) is used in this type of experiments. In the laboratory testing, a single camera is used to take video recordings from the driver's face. The same annotation method based on self-reporting is followed. Furthermore, the subject was asked to report the time he got awake and the hours of sleep. The total number of sessions gathered is 24 and each session duration is 12 minutes. From those sessions, in 12 the subject was in *normal state*, 7 in *low* fatigue and 6 in *high* fatigue. Each session is split in two 5 minute intervals (first and last minute are excluded).

4.5.1 Fatigue and driving performance measures

Some useful measures for driving performance are extracted, based on the task involved in the experimental protocol. The first category of measures involves the reaction time of the driver both on primary and secondary tasks. The reaction time is a good measure of subject's alertness. In order to evaluate the reaction time, the time passed from the moment that the object appeared on the screen until the subject presses the brake pedal (for the primary task) or the button (for the secondary task) is measured. The association of the fatigue levels with driving performance, is evaluated using the following measures:

Table 4.6: Results for the *stress* classification problem using three feature sets. For each classifier, the sensitivity (Sens.) and the specificity (Spec.) per class are given as well as the total accuracy (Acc.).

	Normal		*Stress*		
	Sens.	Spec.	Sens.	Spec.	Acc.
SVM	0.78	0.90	0.96	0.90	0.90
Decision Trees	0.84	0.87	0.94	0.92	0.90
Naive Bayes	0.77	0.78	0.89	0.89	0.85
Bayes	0.80	0.79	0.89	0.90	0.86

Table 4.7: Results for the *stress* classification problem using three feature sets. For each classifier, the sensitivity (Sens.) and the specificity (Spec.) per class are given as well as the total accuracy (Acc.).

	Normal		*Low Fatigue*		*High Fatigue*		
	Sens.	Spec.	Sens.	Spec.	Sens.	Spec.	Acc.
SVM	0.73	0.92	0.87	0.70	0.92	0.95	0.86
Decision Trees	0.72	0.90	0.89	0.72	0.93	0.96	0.86
Naive Bayes	0.62	0.78	0.72	0.58	0.89	0.91	0.77
Bayes	0.59	0.75	0.72	0.58	0.89	0.92	0.77

mean and standard deviation of reaction time on primary task, mean and standard deviation of reaction time in secondary task and standard deviation of the vehicle position from the center of the lane.

In Table 4.9, the *mean*$\pm$*standard deviation* of the driving performance measures, for *normal*, *low* and *high* fatigue states are given, as those are self reported by the subject. The P value using the hypothesis that driving performance is not better in the *normal* state is also given. When the subject is in *low fatigue* state, a significant decrease in driving performance is observed, expressed in average reaction times for both primary and secondary tasks. In the *high* fatigue state all performance measures are significantly worse, as expected. Our analysis verifies that changes in driver's state that are detected by our methodology do correspond to driving performance changes.

4.5.2 Prediction of driving performance

During the experiments we also gathered the physiological signals described before, and we extracted the same feature set, summarized in Table 4.1. In Table 4.10 we present the correlation of the physiological features with the driving performance measures. We also present the correlation of the physiological measures with the hours of sleep and hours of awake, as well as the correlation between driving performance measures. We

Table 4.8: Confusion Matrix, Sensitivity (Sens.) and specificity (Spec.) for each class for the classification of *normal* (N), *low fatigue* (LF) and *high fatigue* (HF) classes for the four classifiers and use of physiological, video and environment features.

SVM				**Decision Tree**			
	N	LF	HF		N	LF	HF.
N	89.12	12.82	0.08	*N*	74.14	25.12	1.60
LF	10.88	78.90	3.86	*LF*	25.76	70.54	4.56
HF	0.00	8.28	96.06	*HF*	0.74	0.71	93.84
Acc.	**0.88**			Acc.	**0.80**		
Class	Sens.	Spec.		Class	Sens.	Spec.	
N	0.89	0.87		N	0.74	0.74	
LF	0.79	0.84		F	0.71	0.70	
HF	0.96	0.92		L.F	0.94	0.95	
Naive Bayes				**Bayes**			
	N	LF	HF		N	L.F	HF
N	69.54	11.40	0.00	*N*	75.84	15.06	0.00
LF	28.84	65.12	8.04	*LF*	23.24	72.86	7.20
HF	1.62	23.48	91.96	*HF*	0.92	12.08	92.80
Acc.	**0.76**			Acc.	**0.81**		
Class	Sens.	Spec.		Class	Sens.	Spec.	
N	0.70	0.86		N	0.76	0.83	
LF	0.65	0.64		L.F.	0.73	0.71	
HF	0.92	0.79		H.F.	0.94	0.81	

Table 4.9: The mean ± std of driving performance measures for *normal*, *low* and *high* fatigue states. The fourth and sixth columns are the P values using the hypothesis that performance measures are significantly better (i.e. lower mean and std of reaction times) in *normal* state (N.), compared to *low* (L.F) and *high* (H.F.) fatigue states, respectively.

Reaction Time	*N.* (N=22)	*L.F.* (N=14)	P-value	*H.F.* (N=12)	P-value
Primary Task mean RT	0.90±0.15	1.03±0.18	0.0353	1.19±0.24	0.0002
Secondary Task mean RT	0.52±0.05	0.72±0.23	0.0005	0.79±0.10	0.0000
Primary Task std RT	0.12±0.07	0.15±0.11	0.3047	0.32±0.17	0.0000
Secondary Task std RT	0.12±0.06	0.24±0.16	0.0019	0.25±0.07	0.0000
Std of Position	0.62±0.11	0.70±0.14	0.0575	0.78±0.10	0.0003

observe significant correlations between physiological features and driving performance measures. This outcome indicates the potential of predicting driver's reaction time based on physiological features. To test this hypothesis we used two common regression models: i) stepwise linear fit and ii) neural networks. For each model two predictors are tested: the first based on the time of experiment, hours of sleep and hours of awake and the second on physiological features. In lack of sufficient amount of data, the probability of

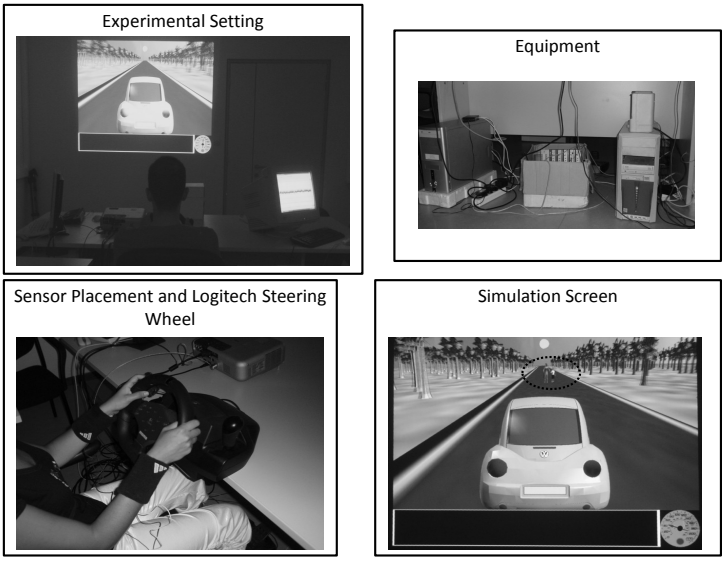

Figure 4.6: The developed simulation environment.

overfitting is high. In order to overcome this problem, the following procedure is adopted:

1. Consider a dataset D.
2. For each session i of the dataset, let D_i the two samples of the specific session. D_i is considered as the testing dataset and the rest $D' = D \setminus i$ as the training dataset.
3. From the training dataset D' produce a larger dataset D'' (2000 samples) sampling according to the mean and covariance of the original training set.
4. Train the prediction model using D''.
5. Estimate the value of D_i samples based on the trained model.

For the neural networks, after experiments we concluded to a 5-5-1 architecture (with the physiological feature set the five features F1, F2, F4, F6 and F14 since EDA features did not had significant correlation with reaction time), while for the neural network using alertness features, a 3-3-1 architecture is used. In Fig. 5.7 the output of all predictors is given as well as the actual reaction time of the subject for each session. For each session the actual and estimated reaction times are the average of the two 5-minute samples of the session. In Table 4.11 the correlation between actual time and predictions is given, as well as the mean squared error (MSE) of the prediction for each method. All four predictors (based on physiological or alertness features) are statistical better than the mean-value predictor. The neural network with the physiological featurws as input has the smaller mean squared error.

Table 4.10: The correlation of physiological features with the driving performance measures and subject's hours of sleep and hours been awake for the dataset collected in the simulation environment.

	P1	P2	P3	P4	P5	T1	T2
F1	0.70	0.71	0.48	0.62	0.53	-0.47	0.75
F2	0.72	0.54	0.66	0.50	0.38	-0.38	0.38
F3	-0.12	-0.20	-0.27	-0.29	0.14	0.17	-0.38
F4	-0.64	-0.49	-0.39	-0.50	-0.38	0.35	-0.64
F5	0.36	0.50	0.21	0.46	0.50	-0.22	0.54
F6	-0.42	-0.43	-0.19	-0.41	-0.40	0.25	-0.53
F7	-0.04	0.08	0.01	0.00	0.13	-0.10	0.09
F8	0.19	0.20	0.09	0.07	0.07	-0.06	0.36
F9	0.03	0.07	0.18	0.10	-0.28	0.20	0.20
F10	-0.39	-0.39	-0.15	-0.31	-0.41	0.34	-0.40
F11	-0.05	-0.05	0.10	-0.05	0.06	-0.16	-0.18
F12	0.20	0.20	0.12	0.19	0.17	0.15	0.26
F13	-0.13	-0.17	-0.01	-0.24	0.02	0.21	-0.24
F14	-0.63	-0.68	-0.54	-0.62	-0.28	0.30	-0.81
P1						-0.61	0.73
P2						-0.60	0.76
P3						-0.52	0.60
P4						-0.65	0.71
P5						-0.60	0.46

4.6 Discussion

In this work we presented a methodology for simultaneous fatigue and stress detection in realistic driving conditions. Our methodology follows three steps for the identification of driver's state: (i) preprocessing and feature extraction, (ii) feature selection and (iii) classification. The information used in our methodology comes from physiological signals, video monitoring of the driver's face and environmental conditions. A large number of features was initially extracted. Features are evaluated with respect to their discrimination power of fatigue and stress states. The best indicators of fatigue and stress are selected. Four classifiers are used in order to evaluate the accuracy of the proposed methodology using three different feature sets: (i) physiological features, (ii) physiological and video features, (iii) physiological, video and environmental features. Furthermore, the contribution of each sensor on both stress and fatigue classification is evaluated. Finally, we demonstrated, using a simulation environment, that detection of even earlier stages of fatigue, is of high importance, since a significant deterioration in performance is observed. Finally, a detailed study indicated that the achieved through our methodology detection of even earlier stages of fatigue, is of high importance, since a significant deterioration in performance is observed.

Performing real-time monitoring of driver's physiological activity is still quite difficult,

Table 4.11: The correlation between reaction time predictors. T-S and T-NN are for predictors based on time features (hours been awake, hours of sleep and time of the experiment) using stepwise linear fit and Neural networks respectively. P-S and P-NN are for predictors based on physiological features (RRV, respiration, EDA) using stepwise linear fit and Neural networks respectively. RT is the actual reaction time, MSE is the mean square error of the predictors. Mean RT is a predictor with constant output value, the mean reaction time of the driver, which is used as a basis predictor. In the last column the last column the P-value of the MSE of other predictors against the basis predictor is given.

Fit	T-NN	P-S	P-NN	RT	MSE	P
T-S	1.00	0.55	0.58	0.69	1.56E-02	4.77E-02
T-NN	-	0.52	0.56	0.68	1.60E-02	5.33E-02
P-S	-	-	0.92	0.70	1.52E-02	3.10E-02
P-NN	-	-	-	0.77	1.21E-02	3.84E-02
Mean RT					2.88E-02	

since this requires special sensor equipment attached to the driver, which in a real-car application would raise a number of safety related issues concerning the obtrusive driver monitoring procedure. Some research projects [129] addressed the implementation of the unobtrusive driver monitoring paradigm, by collecting biosignals from sensors embedded on the steering wheel or adjusted on the driver's seat. Although many approaches on affective state recognition (either stress or fatigue) have presented promising results in the field of biomedical and/or other special applications, still they are not considered suitable for an automotive application. In our work, from the large group of biosignals used in similar studies, we have chosen to exploit only a limited set of them (ECG, EDA, respiration) having in mind that the unobtrusive monitoring of the selected biosignals could be feasible in professional or even commercial vehicles of the near future. Apart from biosignals our approach incorporates information from driver's face video as well as the driving environment, we achieved comparable results. However, direct comparison with other methods is not feasible mainly for two reasons. First because other methods focus on the estimation of a single psycho-physiological state and secondly because most relevant studies were performed on a simulation environment. In our approach we followed a quite different experimental protocol allowing us to address i) the simultaneous estimation of driver's stress and fatigue levels and ii) the driver monitoring on real-life conditions. Furthermore, we demonstrated, using a simulation environment, that detection of even earlier stages of fatigue, is of high importance, since a significant deterioration in performance is observed. Performing real-time monitoring of driver's physiological activity is still quite difficult, since this requires special sensor equipment attached to the driver, which in a real-car application would raise a number of safety related issues concerning

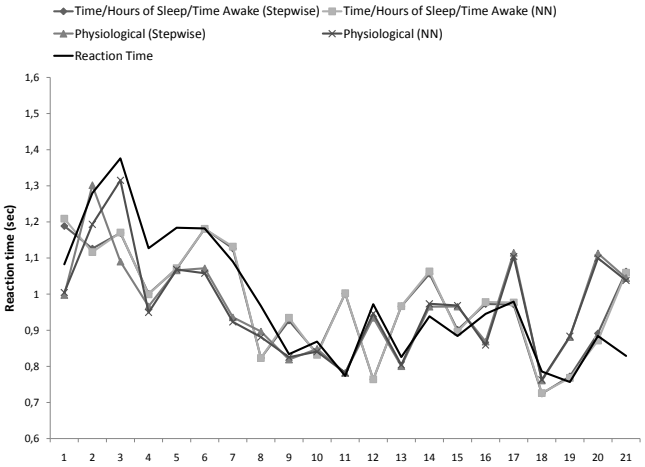

Figure 4.7: The actual reaction time for each session, and the estimated reaction time using different predictors based on different feature set (physiological features and alertness features) and estimation method (stepwise linear fit and neural networks).

the obtrusive driver monitoring procedure. Some research projects [129] addressed the implementation of the unobtrusive driver monitoring paradigm, by collecting biosignals from sensors embedded on the steering wheel or adjusted on the driver's seat. Although many approaches on affective state recognition (either stress or fatigue) have presented promising results in the field of biomedical and/or other special applications, still they are not considered suitable for an automotive application. In our work, from the large group of biosignals used in similar studies, we have chosen to exploit only a limited set of them (ECG, EDA, respiration) having in mind that the unobtrusive monitoring of the selected biosignals could be feasible in professional or even commercial vehicles of the near future.

Concerning the performance of the employed classifiers, SVM is the one presenting the best results in all classification problems, followed by Decision trees and Bayesian classifier. Naive Bayes had the worst accuracy. The reason for this, as depicted in Table 4.3, is that the assumption of feature independence does not hold, thus making the Naive Bayes classifier weak for all classification problems examined.

Classification using physiological features shows very good performance (the highest accuracy, 85%, is obtained using the SVM classifier). The incorporation of additional features merely improves the initial results. In contrast, removing RRV related features, a 15.5% decrease in accuracy is observed (Fig. 6.9). Using the SVM classifier and physiological and video features a 99% accuracy in *high* fatigue classification is achieved. Considering, that this state is more related to driving performance and accident provocation than the others, we consider that the success in its accurate detection is crucial. We also notice that the main source of misclassification is between the low fatigue class and the other two classes (*normal* and *high* fatigue). This is expected since the discrimination

of fatigue in discrete levels is quite abstract, given that fatigue is commonly considered as a continuous variable. The discrimination of fatigue in classes might cause errors due to annotation errors from the subject who could misjudge his state. This problem is enhanced considering the long duration of the experiments and thus the probability of variation of the fatigue criteria as those are defined by the subject. Stress classification was expected to be more difficult, since no features, proved to sufficiently discriminate stress levels. Using only physiological signals, a 78% accuracy is obtained with the SVM classifier. The incorporation of additional information, increases significantly the accuracy of all classifiers. Furthermore, we observe in Fig. 6.9 that no group of variables has a very good discrimination power, thus concluding that a reliable system for stress detection must be based on the fusion of several information sources. Direct comparison of the obtained results using our methodology with existing ones in the literature, is not feasible mainly for two reasons. First because other methods focus merely on the estimation of a single psycho-physiological state and secondly because most relevant studies were performed on a simulation environment. In our approach we followed a quite different experimental protocol allowing us to address i) the simultaneous estimation of driver's stress and fatigue levels and ii) the driver monitoring on real-life conditions.

An important step in our methodology is feature selection, since a large number of features can be extracted from the information sources used. In Fig. 4.4(a) we observe that the *mean RR* (F1) and the *std of RR* (F2) are very good discriminators for fatigue levels, while more complex RRV features (DFA and Lyapunov exponents) lack discrimination power. However, those features are used more in medical applications, extracted from long recordings, and are related to problematic heart function [99, 140]. For within individual variations, simple RRV characteristics have proved to be rather informative [46]. Respiration rate which is highly correlated with heart rate, as well as EDA features are also good indicators of fatigue. From video features, std of eye activation (V2) and PERCLOS (V4) are the best fatigue indicators, especially in discriminating *high* fatigue. The relation of PERCLOS with late stages of fatigue is well established in the literature. Regarding stress, *mean RR* (F1), LF/HF ratio (F6) and the ratio of heart rate to respiration rate (F14) are the best indicators among the physiological features, but still their discrimination power is not so high. A possible explanation for this, may be the low impact of stress on the physiological signals compared to that of circadian rhythm. From video features, the standard deviation of head movement (V3) was the best stress indicator. Still, since the head movement is a behavioural parameter, the correlation of this feature with stress is expected to vary significantly between individuals. Environmental conditions were expected to be rather correlated with stress levels. From the examined driving environment variables, only weather conditions did have a contribution to stress classification.

An important aspect of this work was the association of driving performance with early fatigue stages. In a series of simulation experiments we demonstrated that driving performance decreased statistically under *low fatigues* states. We cannot claim with certainty

that this decrease could potentially increase the probability of an accident. However, this performance decrease is important information that modern driving assistance systems should take into account, and adapt their decision functions and behavior accordingly. A further step in this direction is the prediction of driver's reaction times, based on features extracted from physiological signals. Model based on neural networks could predict driver's reaction time based on physiological signals. A very appealing feature of neural networks is the ability for online learning. For example in a special equipped vehicle, capable of monitoring both physiological signals and reaction times in specific conditions, could learn the mapping from physiological signals to reaction time, for each individual driver, and use this mapping for predicting driver's performance.

It should be noted that in this work a single subject is monitored during ordinary work days, without any restrictions related to sleep hours or external stimuli. The driver experiences a number of different conditions, both from the physiological aspect as well as from the environmental point of view. We therefore consider that this study truly depicts the actual physiological status of the particular subject during driving. Extension of our study to several subjects as well as development of automated methods for the adaptation to each driver's physiology are in our future work plans.

Chapter 5

Real time Driver's Stress Event Detection

5.1 Introduction

According to the American Highway Traffic Safety Administration, high stress influences adversely drivers' reaction in critical conditions, thus, it is one of the most important reasons for car accidents along with fatigue, intoxication and aggressive driving [139]. Stress, according to [1], is "the total assessable influence impinging upon a human being from external sources and affecting it mentally". Recent findings have shown that stress is not only tightly intertwined neurologically with the mechanisms responsible for cognition, but also plays a vital role in decision making, problem solving and adaptation to unpredictable environments, such as driving [88]. Driving in real traffic conditions is a complex task, since fast decisions need to be taken given limited information. The driving task poses differing demands on the driver. Following a road requires primarily lateral control, following a preceding car additionally requires longitudinal control actions, whereas more complex maneuvers, such as overtaking, require higher cognitive and control effort as well as driving skills. Specific events occurring during the driving task can incorporate some kind of safety risk for the driver. For example in the task of following a preceding car, the

sudden reduction of the speed of the preceding car, urges the follower for a hard braking; an overtaking may become life-threatening if a vehicle from the opposite direction appears. Defining them as driving events, such events usually increase the stress levels of the driver. The level of increase depends on the individual's perception of life-threatening situations and its duration may be temporary or even long-term, affecting the driver's physiological state and behavior thereafter.

Therefore, we can define stress events as the physiological reactions of the driver to the driving events. It has been noticed that when subjects experience stress events, they have specific reactions, mapped to their physiological signals, like an increase in heart rate and skin conductivity. Thus, the detection of stress events is possible, through the monitoring of driver's physiological reactions to driving events. This allows for measuring the driving events' impact on drivers' psychophysiological state and driving behavior. These measurements can be used by adaptive systems in various ways to help drivers cope with their stress. Automatic management of non-critical in-vehicle information systems such as radio, cell phones and on-board navigation aids according to the level of stress are practical application of the abovementioned adaptive systems [19]. For example, when a stress state is detected, the system could undertake specific actions to minimize additional causes of workload increase, such as blocking incoming calls from the mobile phone, or postponing non critical navigation information. Furthermore, the knowledge of the possible causes of driver's stress may be useful information for the next generation of navigation systems. For example, if a hard braking caused an increase of stress level, this information could be exploited by a collision warning system to adjust its strategy accordingly. Thus, not only detection of stress events, but also their association with specific driving events is rather important.

A limited number of approaches has been presented during the last years for driver stress monitoring: Healey and Picard [46] specified an experimental protocol for data collection which was initially described in [44]. Each driver followed a pre-specified route containing 15 different events, from which four stress level categories were created according to the results of the subjects self report questionnaires. In total, 545 one-minute segments were classified. A linear discriminant function was used to rank each feature individually based on recognition performance and a sequential forward floating selection (SFFS) algorithm was used to find an optimal set of features for recognizing driver stress. Skin conductance variation and mean heart rate was among the selected features. In another study, Healey and Picard [45] presented a method for data collection and analysis in real driving conditions for the detection of driver stress state. Data from 24 drives of at least 50-min duration were collected for analysis. The data were analyzed in two ways. In the first case they used features from 5-min intervals of data during rest, highway and city driving conditions in order to distinguish three levels of driver stress for multiple drivers and during several days. In the second case they compared continuous features, calculated at 1-second intervals throughout the entire drive with a metric of observable stressors created by independent coders from videotapes. The results showed that skin

conductivity and heart rate metrics are most closely correlated to driver stress level. Next we shortly describe approaches reported in literature, aiming on stress detection, but not related to the driving task. In the following approaches the experiments were performed in a laboratory setting, where it is relatively easy to detect stress, since the sources and the number of stimulations are restricted and the increase of sympathetic activity is related to a specific stimulation. However, in non-restricted environments, such as the driving one, the frequency and the sources of stimulations vary significantly, making more difficult the monitoring and consequently stress event detection.

Zhai *et al.* [163] developed a system for stress detection using blood volume pressure, skin temperature variation, electrodermal activity and pupil diameter[1]. Data were collected from 32 healthy subjects demonstrating significant correlation between stress and the above mentioned physiological signals; the classification of stress was performed using a Support Vector Machine (SVM). Rani *et al.* [120] presented a real time method for stress detection based on heart rate variability using Fourier and Wavelet analysis. Liao *et al.* [86] presented a probabilistic model for stress detection based on influence diagrams. Stress detection was based on probabilistic inference from features extracted from multiple sensors. These feature include physiological measures, physical appearance and performance measures. The main outcome of this work is that the Bayesian framework is suitable for information fusion and provision of a reliable stress metric.

All the above findings indicate that physiological signals can be exploited in order to provide a metric of driver stress in the car of the near future and to perform real time driver stress monitoring. Stress monitoring could serve the management of the non critical in-vehicle information systems and could also provide a continuous measure of the way that road and traffic conditions affect drivers. However, a number of limitations deteriorate the applicability of the reported approaches in real life driving conditions. The first one lies on the processing of the physiological signals. In all previously described works the methods used for signal processing can hardly be used in real time systems since they do not cope with the real time estimation of the signal baseline. The most common approach used in literature is normalization, using an initial phase where the driver is supposed to be relaxed [45], in order to estimate the baseline of the signals. In our work the physiological features are extracted in real-time, and the estimation of the baseline of each feature is also estimated in real-time. This estimation involves the online adaptation of the parameters of the stress detection model, thus commonly used classifiers such as SVM or decision trees cannot be applied. Instead, BNs are employed here since there are robust methods for online BN parameter adaptation. Another shortcoming of the works reported in literature, is that they have been evaluated either on simulation environments, or in restricted real-world environments. In this work instead, the dataset is collected in real unconstrained driving conditions. This increases the driver's stimulations and makes characterization much harder. Another important contribution of this work is

[1]The measure through the center of the adjustable opening in the iris of the eye, terminated at both ends by its circumference.

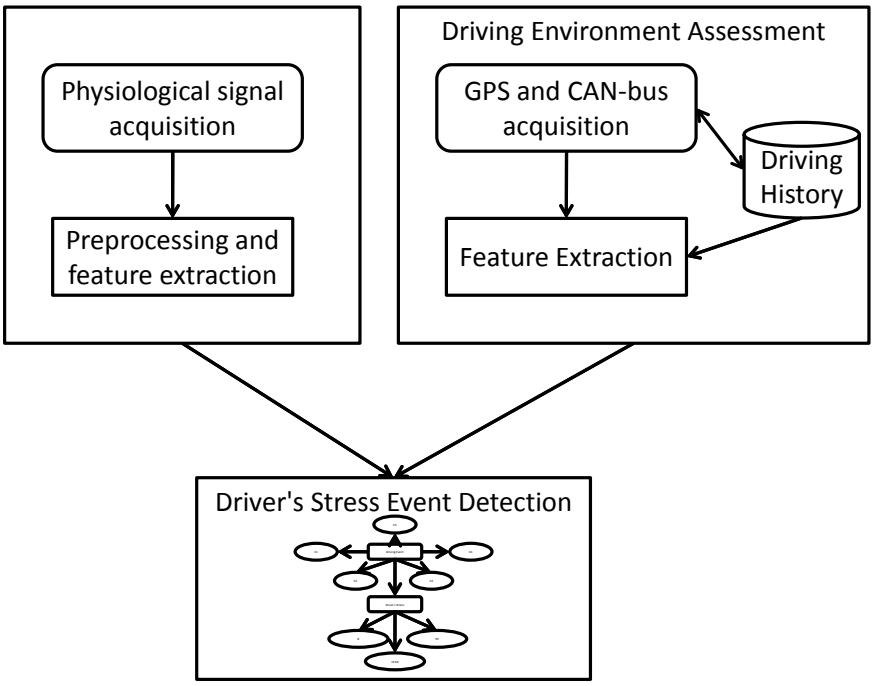

Figure 5.1: The three basic steps of our methodology.

the incorporation of the cause-effect relationship. The effect is the driver's stress event and the cause in our case is the driving event. We propose a mechanism for building a driving history of the driver for specific tours based on information from GPS[2] and the vehicle's CAN-bus[3] and then extract features which can be used in order to detect overtake and hard braking events, which consequently may cause a stress event. This information is incorporated into the model to improve the detection of stress events and to provide reasoning for the cause of such events. The reasoning ability is an additional reason for choosing BN for detecting stress events. In the following sections, we first describe the proposed methodology; next, the description of the data collection follows; then, we present the results of the proposed methodology and the discussion.

5.2 Materials and Methods

The proposed methodology consists of three basic steps (Fig. 5.1):

- Biosignal acquisition, preprocessing and feature extraction.

[2]Global Positioning System (GPS).

[3]Controller-area network (CAN) is a vehicle bus standard designed to allow microcontrollers and devices to communicate with each other within a vehicle without a host computer.

- Driving environment assessment.
- Incorporation of information in a BN and stress detection.

The method proposed initially performs a real time processing of the physiological signals. In our approach we exploit ECG, EDA and respiration. Features from those signals are extracted using 10 second windows. A variation of the Kalman smoother is applied to estimate the trend of the heart rate variability (HRV) signal which is extracted from the ECG. From the EDA a normalized measure of the differences of the skin conductivity is extracted and from respiration the entropy of the spectrum is calculated. Moreover, information for current driving environment is extracted, using GPS and the vehicle's CAN-bus data, as well as the driving behavior history. All this information is then incorporated into a BN for stress detection. Different BN models are employed.

5.2.1 Biosignal acquisition, preprocessing and feature extraction

For data acquisition we use the Biopac MP-100 system. The ECG signal is acquired at 300Hz sampling frequency, whereas the EDA and the Respiration signal are acquired using 50 Hz sampling rate. The resolution is set to 12-bit for all signals.

ECG

The most common measure related with stress events and increased mental load is the increase in the heart rate. The heart rate over a period of time is extracted from the HRV. We first extract from the ECG the R-R variability signal (RRV) from which the HRV is calculated as $HRV = 60/RRV$. In order to extract the RRV signal from the ECG, the R peaks are detected, using the procedure described in [119]. The R-R intervals are estimated as the time differences between successive R peaks. Those R-R intervals constitute the RRV signal. The RRV signal (as well as HRV signal) has two main components: i) a baseline component of low frequency which has some sudden variations due to stress events and ii) a periodic component including parasympathetic and the sympathetic activities. The latter can be modeled by an autoregressive process (AR) of order P [143]. Thus the R-R interval at time i denoted as rr_i is given as:

$$rr_i = \sum_{k=1}^{P} a_i^k rr_{i-k} + b_i + \epsilon, \tag{5.1}$$

where b and a are the baseline of the signal and the AR coefficients, respectively, whereas ϵ is the Gaussian distributed noise. The baseline b is the variable which is affected by the stress events and used for stress detection, whereas the AR coefficients which correspond to periodic RRV variation are not exploited in our methodology. The i index denotes that those variables are time varying:

$$b_i = b_{i-1} + \epsilon_b, \tag{5.2}$$

$$a_i^k = a_{i-1}^k + \epsilon_a, \tag{5.3}$$

where ϵ_b and ϵ_a are Gaussian distributed noise. The state space form of the above is:

$$\mathbf{x}_i = \mathbf{x}_{i-1} + R, \tag{5.4}$$

$$y_i = H_i x_i + Q, \tag{5.5}$$

where $\mathbf{x}_i = [a_1, a_2, ..., a_P, b_i]$, $y_i = rr_i$, R is the process noise, Q is the observation noise and the matrix $H_i = diag[rr_{i-1}, rr_{i-2}, ..., rr_{i-P}, 1]$. In order to estimate $\mathbf{x}_i$ we can use the ordinary Kalman filter equations [149] for each new sample y_i. These equations are:

$$x_i = x_{i-1}, \tag{5.6}$$

$$V_i = \tilde{V}_{i-1} + R, \tag{5.7}$$

$$S = H_i V_i H_i^T + Q, \tag{5.8}$$

$$K = V_i H_i^T S^{-1}, \tag{5.9}$$

$$\tilde{x}_i = x_i + K(y_i - H_i x_i), \tag{5.10}$$

$$\tilde{V}_i = (I - K H_i) V_i \tag{5.11}$$

where K is the Kalman Gain matrix, and $\tilde{x}_i$ and $\tilde{V}_i$ are the Kalman filter estimations of hidden state and error covariance matrix, respectively, at time step i. In order to have a better estimation of the hidden states of the model, the Kalman smoother could be applied. The Kalman smoother makes use of the collected statistics from all the time series and updates the estimation of the Kalman filter for the hidden states, using a backward recursion. Thus, it can be considered as an offline estimation method. The Kalman smoother update equations are:

$$\hat{x}_i = \tilde{x}_i + V_i^*(\hat{x}_i - \tilde{x}_{i+1}), \tag{5.12}$$

$$\hat{V}_i = V_i - V_t^*(\hat{V}_{i+1} - \tilde{V}_{i+1})V^*T, \tag{5.13}$$

$$V_i^* = \tilde{V}_i \tilde{V}_{i+1}^{-1}, \tag{5.14}$$

where $\hat{x}_i$ and $\hat{V}_i$ are the Kalman smoother estimations of hidden state and error covariance matrix at time step i, respectively. In our method we use windows of specific length for the calculation of the features from the physiological signals. Since, we are interested in having a good estimation of the hidden states included in the specific window, given the information at that time, we apply the Kalman smoother for each new window only on the past observations contained in the window. We call this procedure Window Kalman smoother and it can be considered as a partially applied Kalman smoother. With this procedure the estimation is expected to be better than Kalman filtering and worse than a Kalman smoother which uses all data. In our experiments we use an AR(6) process. The initial estimation of the AR coefficients and observation noise R, as well as the initial estimation of the baseline can be extracted using an initial segment of the signal. We used the first five minutes of the signal for all the initializations. The remaining step is to define the process noise Q. We consider a diagonal Q and after experiments the elements corresponding to AR coefficients are set to 10^{-8}, whereas the element corresponding to baseline is set to 10^{-6}.

From the Kalman filter the parameter of interest is the baseline parameter b. This parameter varies with time, and this variation as already described is caused by two factors: a very slow variation, and a more rapid variation due to stress events. The average baseline value b_i is calculated over a specific window. This new feature, denoted as B_k, where k is the window indicator, inherits the varying behavior of b_i and is also dominated by two components, the very slow varying and the stress related. Since the first component is very slow varying we assume that B_k follows a Gaussian distribution $N(\mu_k, \sigma_0)$, whereas in cases of external stimulations a rapid increase is expected:

$$B_k = \begin{cases} N(\mu_k, \sigma_1), \text{ No stress} \\ N(\mu_k + \delta, \sigma_2), \text{ Stress,} \end{cases} \tag{5.15}$$

where δ is the average increase of the heart rate in stress events. The μ_k is also time-varying. The estimation of μ_k is performed in the BN context (described in Section 5.2.3), decomposed from the Kalman filter and the estimation of b_i.

Electrodermal activity

The EDA signal is originally downsampled at 1 Hz. A smoothing filter is then applied, since in many cases noise is evident in the signal. The signal of EDA is composed by two main components. A slow varying one, i.e. the skin conductance level (SCL) and one related with sudden increase in mental load, the skin conductance response (SCR). A common measure of these rapid increases is the first absolute difference (FAD):

$$FAD = \frac{1}{N-1} \sum_{i=1}^{N-1} |s_{i+1} - s_i|, \tag{5.16}$$

where s_i in this case is the EDA at time i. A drawback of this feature is that is highly dependent on the SCL. A common practice is to use a normalization method after observing all the data, such a min-max normalization:

$$s_i' = \frac{s_i - \min\limits_k s_k}{\max\limits_k s_k - \min\limits_k s_k}, \tag{5.17}$$

or the standardization method:

$$s_i' = \frac{s_i - \mu_s}{\sigma_s^2} \tag{5.18}$$

where μ_s, σ_s are the mean and standard deviation of the time series, respectively. The above methods can only be applied in offline processing. One other approach in order to eliminate the impact of the SCL on the SCR is to divide the FAD measure with the current SCL level. The advantage of this approach is that it can be easily applied on real time estimation. The transformation applied with this method to the FAD measure is $1/SCL_l$ which is a non-linear function of SCL_l and $SCL_l = (1/N)\sum_i^N s_i$. This function reduces the FAD when SCL_l is large ($1/SCL_l < 1$) and magnifies it when SCL_l is small

$(1/SCL_l > 1)$. We consider the use of a logistic function of SCL_l which has a similar behavior. This logistic function is given as:

$$g(SCL_l) = \frac{1}{1 + \exp(-\alpha \cdot (SCL_l - \beta))}, \tag{5.19}$$

and the transformed FAD ($nFAD$) is given as $nFAD = FAD \cdot g(SCL_l)$.

The parameters α and β are optimized in order to obtain the higher correlation with a stress metric derived from the annotation (described in Section 5.3).

Respiration

The respiration is initially downsampled at 10 Hz and the mean of the signal is removed. Then a fast fourier transform is applied and the power spectrum of the signal is calculated. The extracted feature is the entropy of the resulting spectrum (RE),

$$p(f) = \frac{P(f)}{\sum_{f'} P(f')}, \tag{5.20}$$

$$RE = \sum_f p(f) \log p(f), \tag{5.21}$$

where $P(f)$ is the spectrum energy at frequency f. In a normal behavior the respiration of the subject should follow an almost periodic pattern, thus we expect to have a dominant peak in the spectrum and low spectrum entropy. Instead, in stress events the respiration usually freezes for a small period and then we have an increased respiration frequency, leading to a more complex spectrum with higher entropy.

Similar to the HRV case, for the RE we use a model as that of Eq. (5.15):

$$RE_k = \begin{cases} N(\mu_k, \sigma_1), \text{ No stress} \\ N(\mu_k + \delta, \sigma_2) \text{ Stress}, \end{cases} \tag{5.22}$$

where μ_k is slow time varying and δ is the average increase of respiration entropy in stress events.

It should be noted that there is a delay between the occurrence of a stress event and the result on the physiological signals. This delay is different for each physiological signal. Thus, since we extract features in a constant window it is very likely to have information loss due to this time offset. From the three signals in our study we found that EDA has 2-5 seconds delay, whereas the delay of HRV and respiration is negligible, compared to the window length. In our approach we align EDA with HRV, using cross-correlation analysis. From cross-correlation analysis we detect the offset having the largest correlation and then delay EDA by that offset. It should be noted that this approach does not affect the online application of the method; during a burn-in phase or even online, we can calculate the cross-correlation and the offset of the two signals.

5.2.2 Driving environment assessment

Apart from the processing of physiological signals, in our methodology we also incorporate an approach for modeling driving expected behavior and detecting common events based on GPS information (latitude, longitude, speed and heading) and vehicle information from CAN-bus (engine's rounds per minute-RPM, throttle).

The approach proposed here is based on building a driver's profile for each tour. This profile contains information about the typical behavior of the driver for each part of the tour, in terms of average speed, acceleration, throttle, etc. More specifically, for each tour a number of control points is assigned and for each control point a number of statistics are calculated. In order to calculate these statistics, the basic assumption is that we have a significant number of samples around each control point. This assumption is rather reasonable, since the majority of driver's repeat specific tours each day with only small variations. Thus, any GPS system could gather necessary information about the most often routes.

The reasoning for building a profile of each session is that under similar conditions the driver has an expected behavior, in terms of speed, braking before turns, etc. Variations on the expected behavior could be strongly related to specific driving events. For example, a braking which was more intense than normal could be considered by the driver as a hard braking, or speeds lower than expected followed by unexpected acceleration could infer a possible overtake. Of course, those events could be more reliably detected with more sophisticated hardware such as camera or radars, but the goal of this method is to build an event detector which works without special equipment and to demonstrate the added value of such a system in driver's stress estimation.

Next, we describe in detail the driving event detection. From the database of the GPS positions we need to derive a small subset of positions which describe the tour. We use the fuzzy K-means algorithm [56]. The number of initial centers, denoted as C_i, is 200 for a tour of about 60 kilometers which originally had about 3000 samples for each tour. Then using the membership function for each sample we estimate a number of statistics per point. The approach is similar for any measure of interest m. The average of the measure m for each control point i denoted as M_i is calculated as

$$M_i = \frac{\sum_j w_{ij} m_j}{\sum_j w_{ij}} \tag{5.23}$$

where w_{ij} is the weighted distance of control point i from the sample j.

The measures for each control point i calculated with the aforementioned way include:

- Average Speed (AMS_i).
- Average Deceleration (AD_i).
- Average Magnitude in Heading Changes ($AMHC_i$). The differences of the heading direction are calculated. Since, we are not interested in the direction of the change we take the square of those differences (magnitude).

- Average Throttle (AT_i). The average throttle is expressed in percentage, acquired from the CAN-bus.
- Average RPM ($ARPM_i$). The average RPM of the engine acquired also from the CAN-bus.
- Average Overtaking (AO_i). For each sample in the dataset we have a variable denoting the frequency of overtaking events at a specific point. This estimation is used as prior estimation of overtaking events. This is quite useful since in rural roads there are specific parts of the road where overtaking is considered safe. The points where an overtake occurs are extracted from the annotation of the dataset.

Using the above information and the current readings from the GPS and CAN-bus we extract a number of features. The first set of features is the weighted average of the measures $AMS_i, AD_i, AT_i, AMHC_i$, and $ARPM_i$, where the weights refer to the distance of the current position from each control point i. These can also be considered as the expected values of speed, deceleration, heading change, throttle and RPM, respectively. The second set of extracted features includes the average of the current readings (i.e. speed, deceleration, heading change, throttle and RPM) in a specific window, as well as the average difference of these readings with their expected values. Finally, we also use as feature the presence of a preceding vehicle. This info is manually extracted from the video annotation. Using the features described above we first examine how good indicators these features are for overtaking and braking detection. We consider a classifier using only one feature at a time and we calculate the area under curve (AUC) of that classifier. The N features having the largest AUC are considered as the best candidate set. N is experimentally chosen so as to get the best classification results. The features with the highest ranking for discriminating overtake events are the presence of a preceding vehicle (C_1), the frequency of overtakes on the specific location (C_2), the current throttle (C_3), the current RPM (C_4) and the difference between current and average RPM (C_5). For hard braking detection the best feature set consists of the current deceleration (C_6) and the difference of current deceleration and the average deceleration on the specific location (C_7). In order to detect driving events (overtaking and hard braking) we use the Naive Bayes classifier, which can be easily merged with the BN for stress detection (described in the next section), which also yields satisfactory results for the problem under consideration.

5.2.3 Bayesian Networks for stress detection

BNs are widely used for knowledge representation and reasoning under uncertainty in intelligent systems [112]. The structure of a BN is a directed acyclic graph. Its nodes correspond to random variables of interest while the directed arcs represent direct causal or influential relation between nodes. The uncertainty of the interdependence of the variables is represented locally by the conditional probability table $P(X_i|Pa_{X_i})$ associated with each

node X_i, given its parents Pa_{X_i}. The graphical structure of a BN allows the representation of interdependency between variables, which together with an independence assumption, lead to the joint probability distribution of $X = \{X_1, X_2, \cdots, X_D\}$, one of the most important features of BNs. The joint probability distribution can be factored out as a product of the conditional distributions in the network:

$$Pr(X) = \sum_{i=1}^{D} Pr(X_i|Pa(X_i)), \tag{5.24}$$

where D is the number of variables.

Many well known models (Kalman Filters, AR models, Naive Bayes classifier) can be represented as graphical models and BNs. BNs have also been used for classification problems. If we assume that the class is represented as random variable in the model ($Class$), then in order to get a classification output we need to estimate the probability:

$$P(Class|X = E), \tag{5.25}$$

where X is the variable set that is used in the model and E are the values of the variables for the specific instance. In the general case this probability is estimated using inference algorithms for BNs [79].

In our study we examine three models for driver's stress detection. The first model (BN1) includes only physiological features. This model is depicted in Fig. 5.2. The variables of our model are the *Driver's stress* class variable and the feature variables extracted from the physiological signals. *Driver's stress* is a discrete variable following a multinomial distribution with two states (*normal* and *stress*). Feature variables are continuous variables following a conditional Gaussian distribution, since they have always a discrete parent (the *Driver's stress* variable) and potentially other Gaussian variables (other feature variables).

In the second model (BN2) we extend the first model (BN1) which uses only physiological information by adding a new variable corresponding to the driving events, named *Driving Event*. This is due to the fact that stress events that we are studying are directly related to specific driving events. The information of the occurrence of a driving event, should improve the performance of stress event detection. The *Driving Event* variable has three states: (i) *overtaking*, (ii) *hard braking*, (iii) *other*, where *other* includes both no-event or events of other types with very low frequency. Then a direct arc from *Driving Event* to *Driver's stress* is added. The BN2 model is shown in Fig. 5.3. The value of the *Driving Event* is extracted from the video annotation of the sessions. Thus, we may consider this variable as the output of an advanced driving detector with a 100% accuracy and it is expected to have the best results.

As such a driving detector is not available in practice, in the third model we are using the driving event detection described in Section 5.2.2. There are two possible approaches. The simplest one is to initially detect the events and then provide the outcome as input to the abovementioned model (in the *Driving Event* variable). This implies a one directional

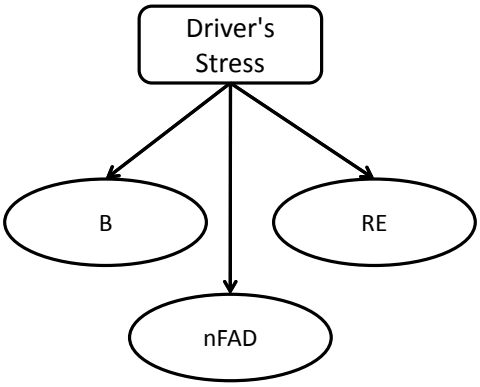

Figure 5.2: The BN1 model for Stress detection using only physiological features. B corresponds to the heart rate, $nFAD$ corresponds to the normalized first differences of the EDA signal and RE to respiration entropy.

relation between stress and events. We followed a more complex approach, to merge the event and stress detection models in one, which allows for a bidirectional relation between stress and event detection. For example when there is no evidence of stress in physiological signals, then the probability of overtaking is lower. The merge of the driving event and stress event detection implies the merge of the BN2 model with the two Naive Bayes classifiers for detecting overtaking and hard braking. Since both Naive Bayes classifier and BNs are based on Bayesian theory and graphical models, this merging is feasible. The outline of the merging procedure and the resulting model, namely BN3, are depicted in Fig. 5.4.

In our experiments we first train the BN models in an offline (batch) mode using the training set and then we evaluate them online on the test set. The offline learning of the parameters of the model is based on the maximum likelihood (ML) estimation. The learning of the BN parameters is described in [106]. The parameter adaptation in online mode is necessary, since as already described, both the conditional distributions of feature B and RE extracted from HRV and respiration are time varying (the μ_k parameter in Eqs. (5.15) and (5.22)). The conditional Gaussians which are used as the distribution of continuous variables with discrete parents, after the propagation of evidence collapse to

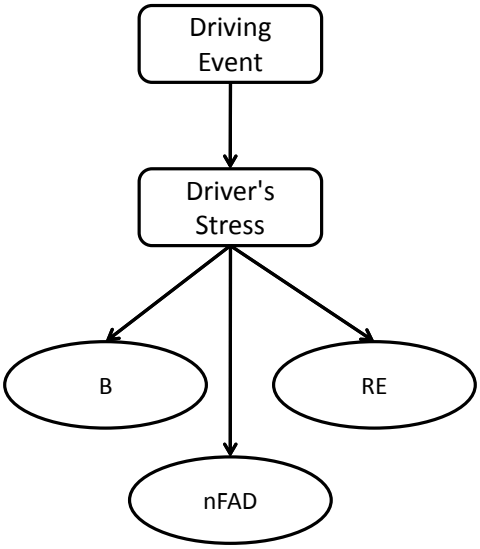

Figure 5.3: The BN2 model for Stress detection using physiological features and driving event information. B corresponds to the heart rate, $nFAD$ corresponds to the normalized first differences of the EDA signal and RE to respiration entropy.

mixture of Gaussians. Thus, we could use the same parameter adaptation techniques as those used in the mixture of Gaussian models. A K-component mixture Gaussian model is described as:

$$P(x) = \sum_{k=1}^{K} \pi_k N(x; \mu_k, \sigma_k), \tag{5.26}$$

where μ_k, σ_k and π_k are the mean, the standard deviation and the prior probability of the k component, respectively. The probability that an evidence x comes from the component k is given as:

$$p_k(x) = \frac{\pi_k \cdot N(x; \mu_k, \sigma_k)}{\sum_j \pi_k \cdot N(x; \mu_j, \sigma_j)}. \tag{5.27}$$

The standard online update equations for a mixture Gaussian model are of the form:

$$\mu_k^T = (1 - \lambda \cdot p_k(x))\mu_k^{T-1} + \lambda \cdot p_k(x) \cdot x, \tag{5.28}$$

$$(\sigma_k^T)^2 = (1 - \lambda \cdot p_k(x))(\sigma_k^{T-1})^2 + \lambda \cdot p_k(x) \cdot (x - \mu_k^T)^2, \tag{5.29}$$

where λ is the learning rate, T the current and $T-1$ the previous estimation of a parameter. We followed the approach of [82] where the learning rate is not constant but it is

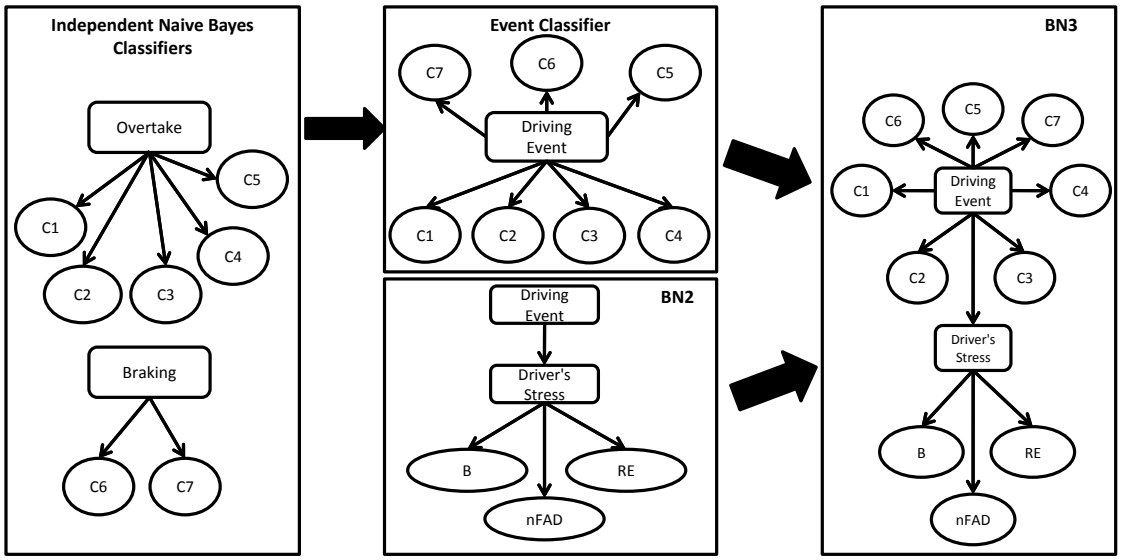

Figure 5.4: The merging procedure of the two Naive Bayes models for overtake and hard braking detection with BN2 model for stress detection, resulting in the BN3 model. B corresponds to the heart rate, $nFAD$ corresponds to the normalized first differences of the EDA signal, RE to respiration entropy and $C1 - C7$ to the seven features selected for overtake and hard braking detection.

given by the following equations:

$$c_k = c_k + p_k(x), \tag{5.30}$$

$$\nu_k = p_k(x) \cdot (\frac{1-\lambda}{c_k} + \lambda). \tag{5.31}$$

In Eqs. (5.28) and (5.29), $\lambda \cdot p_k(x)$ is replaced with the ν_k of Eq. (5.31).

Applying the above update rules in the update of the μ_k which is described in the Appendix, we obtain the following online update equation:

$$\mu_k^T = (1-\nu_k)\mu_k^{T-1} + \nu_k[\frac{p_1(x_k)x_k/\sigma_1^2 + p_2(x_k)(x_k-\delta)/\sigma_2^2}{p_1(x_k)/\sigma_1^2 + p_2(x_k)/\sigma_2^2}], \tag{5.32}$$

since σ_1, σ_2 and δ are considered fixed.

Table 5.1: Description of the dataset. In the first four columns we give the dataset description per subject. In the last two columns the frequency of an event per hour of driving is given (statistics for Subject 1).

	Subject	Subject 2	Subject 3	Subject 4	Event	Frequency
Number of tours	25	1	1	1	Overtake	13.7
Average Duration	55 min.	52 min.	55 min.	54 min.	Hard Braking	2.4
No Stress Events	5926	392	232	361	Cross road	2.4
Low Stress Events	301	11	12	1	Unexpected	1.6
Medium Stress Events	159	3	7	10		
High Stress Events	20	1	0	0		

5.3 Dataset

The experiments were performed in real driving conditions, at a specific route and the duration of each session was approximately 50 minutes. The equipment that was used in order to acquire the needed information included: i) a Biopac MP-100 for signal acquisition of the driver (ECG, EDA and Respiration). This equipment was installed on the back seat of the vehicle and the sensors were attached to the driver. ii) A camera monitoring the road that was used only for annotation reasons, iii) The vehicle's CAN-bus which provided car data (Speed, RPM and Throttle).

Four subjects participated in the experiments: three male and one female. The majority of the data is coming from Subject 1 who is considered as the train and validation subject, while the rest of the subjects are used as test data. The above strategy is based on the fact that the physiology of a stress event is similar to all humans and only the possible causes and the magnitude of changes on physiological signals are expected to change from subject to subject. The dataset description per subject is given in Table 5.1. For Subject 1, a number of useful statistics can be extracted, related to the number of events per session (Table 5.1) and the probability of each stress level given a driving event (Fig. 5.5). We observe that for Subject 1 our dataset includes a large number of events with different stress levels. We should here notice that events annotated as high stress events are usually life threatening and such events are very rarely monitored in the literature, due to safety reasons. We should also notice that due to unpredictable malfunctions, for very few sessions the GPS and/or CAN-bus information is not available. The annotation of the events and the stress caused is performed by a microphone and a voice recognition software based on Microsoft speech API. The vocabulary of the program was restricted to the most often events, and other events were categorized as "unknown". The stress level was discriminated into four categories: i) no stress, ii) low stress, iii) medium stress and iv) high stress. The driver was instructed to first say the type of the event and next, with a small pause, the stress level caused, for example "turn low", "overtake medium", "brake high". Non-annotated instances were also classified as no stress level. From the self-annotation of stress level, we extract a continuous stress metric. The annotated stress

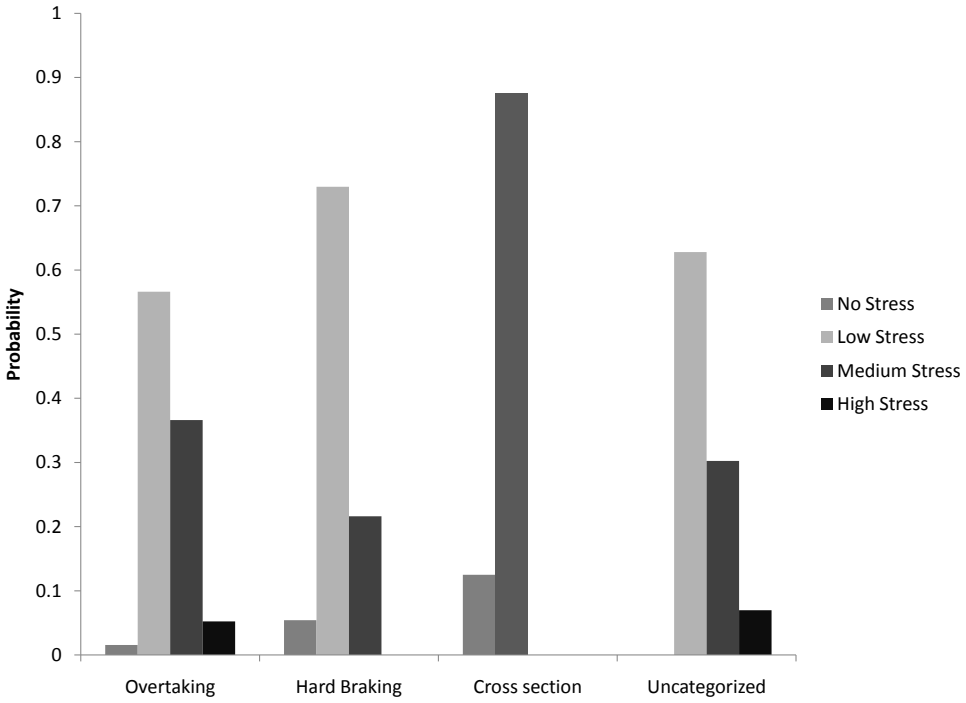

Figure 5.5: The probability of occurrence of a stress event (*Normal*, *Low/Medium/High Stress*) after a driving event (*overtaking*, *hard braking*, *cross-road* and *uncategorized*), according to driver's annotation.

events are assigned at specific time segments, producing a signal $s(t)$ where

$$s(t) = \begin{cases} 0, \text{ if no stress reported at time } t \\ 1, \text{ if low stress reported at time } t \\ 2, \text{ if medium stress reported at time } t \\ 3, \text{ if high stress reported at time } t. \end{cases} \tag{5.33}$$

However, the produced signal does not take into account the impact of the stress event on neighboring time segments. To extend the effect of stress event to adjacent segments, we take the convolution of the $s(t)$ signal with a hamming window of length 3. The convolved signal is considered as the stress metric.

In the experiments for stress event detection we aggregate the four stress levels into two classes, the no-stress class and the stress class. More specifically, the stress class contains both medium and high stress events which constitute stressful events. Moreover, as indicated in Table 5.1 the number of high stress events is quite low and therefore, the high stress cannot constitute a separate class. Thus, it is merged with the medium stress class, which has a significant number of events. Low stress events are considered as unlabeled data, since in cases when drivers were not confident about their stress level,

Table 5.2: The mean and standard deviation of the correlation on all RRV signals of the Kalman filter, the Kalman smoother and the proposed Window Kalman smoother, with the Butterworth filter considered as ground truth in estimating the RRV baseline. For the Window Kalman smoother, the smoothing window is 10 seconds.

	Correlation (mean/std)
Kalman filter	0.82/0.078
Kalman smoother	0.94/0.066
Window Kalman smoother	0.86/0.070

Table 5.3: The correlation of the proposed and different EDA normalization methods with the stress metric derived from the annotated dataset.

Method	Correlation with stress metric
No normalization	0.134
Standardization	0.245
Min-max	0.216
$1/SCL_l$	0.227
Proposed	0.263

tended to use the low stress class, so as to provide a mild estimation. This was also confirmed by the inspection of the impact of those events on the physiological signals of the subjects.

5.4 Results

We first present results on the methods used for physiological signal preprocessing and feature extraction. In this section we also test the adaptation procedure described in Section 5.2.3. Next we present the results obtained regarding the driving environment assessment and finally the stress event detection is evaluated using the three examined BN models.

5.4.1 Physiological signal preprocessing and feature extraction

Initially, we estimate the HRV trend extracted from the ECG using the Window Kalman smoother for real-time trend estimation. The window used for the Window Kalman smoother is 10 seconds. In Table 5.2 we compare the Window Kalman smoother with i) the Kalman Filter and ii) the Kalman smoother, in terms of their correlation with a Butterworth filter with cutoff frequency at 0.05Hz (the RRV sampling frequency is 1 Hz) which is considered to provide the ground truth for HRV trend. The Kalman smoother has the highest correlation with the Butterworth filter, but as described in Section 5.2.1

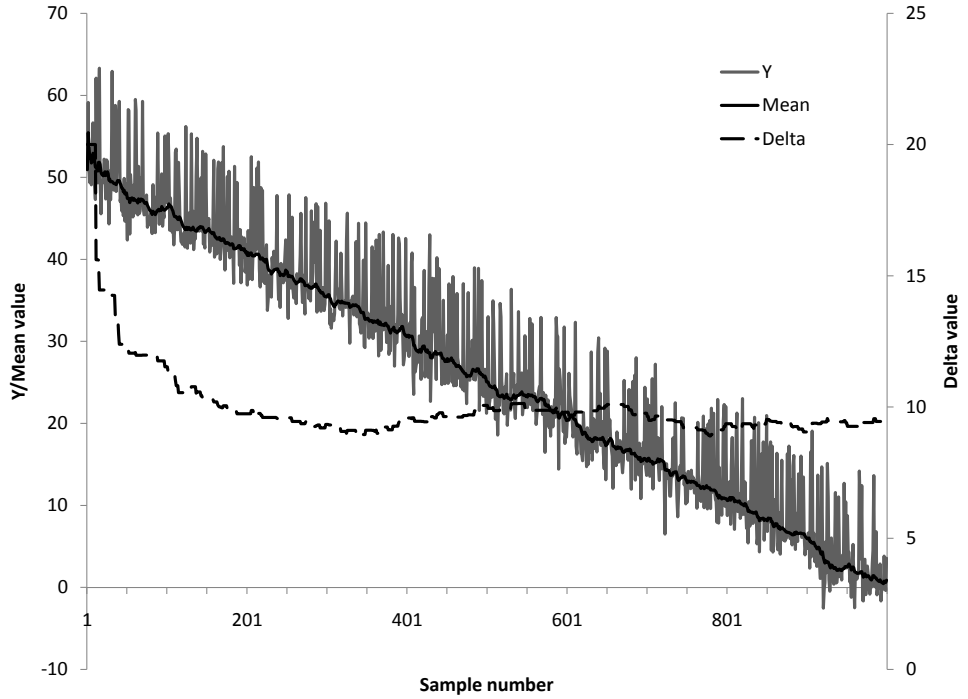

Figure 5.6: The adaptation of the model in the signal Y. *Mean* is the mean of the first mixture Gaussian component and *Delta* the offset of the second component.

it cannot be applied for real time estimation. Therefore, we employ the Window Kalman smoother which is a windowed version of Kalman smoother (applicable in real time) and as we can see in Table 5.2 has a slightly worse performance than the Kalman smoother but superior to the Kalman filter.

Next, we evaluate the proposed normalization method of the EDA. We perform a leave one out method, each time holding one session for test and the other for training of the logistic function's parameters α and β. In Table 5.3 we present the correlation of the normalized feature $nFAD$ with the stress metric; for comparison purposes we also provide the respective correlation of the other methods described in Section 5.2.1. Table 5.3 confirms the suitability of our approach based on the logistic function, since it has higher correlation with the stress metric compared to the other methods.

In Section 5.2.3 we described the method for online learning of the distribution parameters of the B and RE variables extracted from the HRV and the respiration signal, respectively. For testing we employ a time series model with similar behavior as that of a typical HRV signal. The employed model is the following:

$$Y_k = \begin{cases} (1000-k)/20 + \mathbf{N}(0,2), p_k < 0.8 \\ (1000-k)/20 + \mathbf{N}(10,2), p_k > 0.8 \end{cases}, k = \{1,2,,1000\}, \tag{5.34}$$

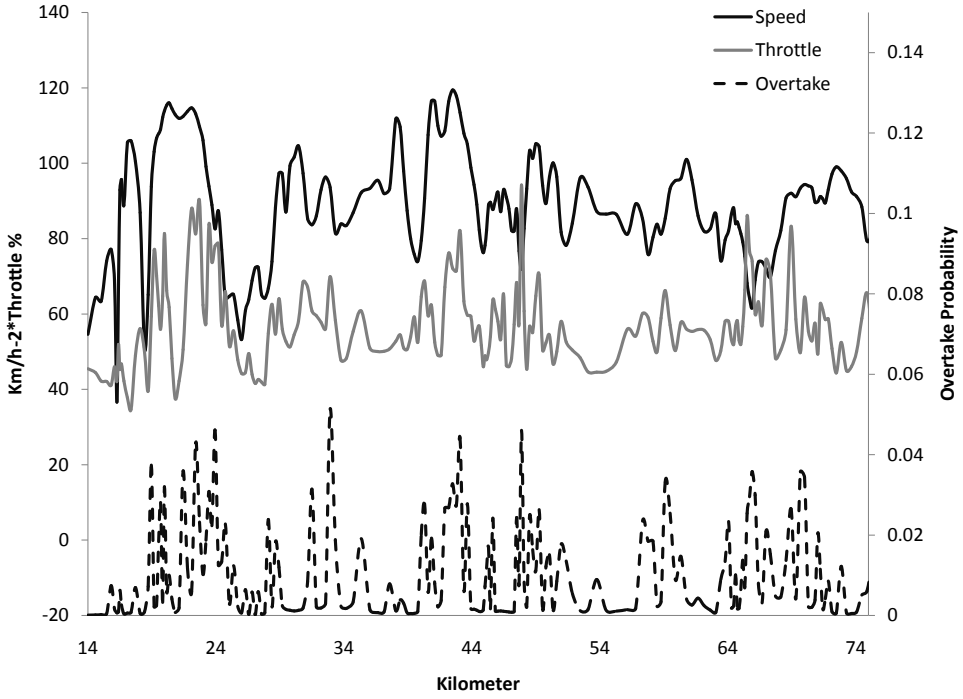

Figure 5.7: The average speed, the average throttle and the overtake probability at each point of the tour.

where p_k is a random number in [0,1]. We test the adaptation of the model described in Eq. (5.15) using the online update of μ_k described in Eq. (5.32) and δ described in Appendix. The standard deviations σ_1 and σ_2 are considered known and initially $\mu_k = 100$ and $\delta = 20$. The learning rate λ in Eq. (5.31) is set to 0.1. In Fig. 5.6 we present the adaptation process of the mean μ_k and δ. We observe that the adaptation is achieved relatively fast and the variations from the actual value are small.

5.4.2 Driving Environment assessment

In this stage we use the information of driving history and the current readings from GPS and CAN-bus to detect critical events, i.e. overtaking and hard braking. In Fig. 5.7 we provide some of the measures extracted from driving history, described in Section 5.2.2. The measures presented are the average speed, the average throttle and the average overtake of each control point of the tour. We observe that points with increased probability of overtaking have also high average throttle and speed. The driver usually attempts overtaking only when high speed can be achieved (open road ahead) while safety conditions are met.

Next we present the results of the overtake detection. The total number of overtake

Table 5.4: Confusion Matrix, Sensitivity and Specificity for each class and total accuracy for the classification of hard braking (H.B) and overtaking (Ovt) events using the Naive Bayes Classifier.

Hard Braking			Overtaking		
Confusion Matrix (mean/std)			Confusion Matrix (mean/std)		
	Non H. B.	H. B.		Non Ovt	Ovt
Classified as Non H. B.	34.61/2.73	13.58	Classified as Non Ovt	121.94/18.21	24.06
Classified as H. B.	5.39	26.42/5.77	Classified as Ovt	28.07	125.95/1.25
Sensitivity	0.87	0.66	Sensitivity	0.81	0.84
Specificity	0.72	0.83	Specificity	0.84	0.82
Overall Accuracy	**0.76**		Overall Accuracy	**0.83**	

events in the dataset is 150 which corresponds to the 5% of the dataset leading to a significant class imbalance. To this end we take all the overtake samples and select randomly equal number of none overtake samples. Then we join the two sample sets in a new balanced dataset and we perform ten-fold cross validation using the Naive Bayes classifier. In order to obtain more reliable results we perform the above procedure 200 times. In Table 5.4 we provide the confusion matrix and compute sensitivity, specificity and the total accuracy for the average of the 200 ten-fold cross validations. The obtained accuracy is 83% and which is rather high, especially considering that no sophisticated hardware was used for monitoring the driving environment.

A similar procedure is also followed for hard braking detection. The annotated hard braking events constitute the 0.7% of the total dataset. Thus, we performed the procedure described for overtake detection 500 times instead of 200. The results are also given in Table 5.4. The obtained accuracy is 76% which is statistically higher than a random guess.

5.4.3 Bayesian Network models and stress detection

The last step of our methodology incorporates all previously reported information into the BN models. The evaluation is performed in online mode using a leave one out method. For Subject 1, we keep one session for testing at a time and we train the BN parameters offline, using the remaining sessions. For the other subjects (test subjects), the model is trained using all the sessions of Subject 1.

The first model, BN1, includes only physiological features. The results of this model for all four subjects are given in Table 5.5. The accuracy of stress event detection is 88% for Subject 1 and for the validation subjects 92%, 89% and 84% respectively. Hence, no statistical difference between the accuracy on the train subjects and validation subjects is observed. This is a strong indication of good generalization performance, considering also that the validation was performed on data of subjects not used in the training. We observe though, that for stress detection we have low specificity for all subjects. The reason of this, is that the impact of stress events on the physiological signals is similar to

Table 5.5: Confusion Matrix, Sensitivity and Specificity for each class and total accuracy for the classification of Stress events for the four subjects in our study using the BN1 model.

Subject 1			Subject 2		
Confusion Matrix			Confusion Matrix		
	Non S	S		Non S	S
Classified as Non S.	5232	45	Classified as Non S.	362	0
Classified as S.	694	134	Classified as S.	30	4
Sensitivity	0.88	0.75	Sensitivity	0.92	1.00
Specificity	0.99	0.16	Specificity	1.00	0.12
Overall Accuracy	**0.88**		Overall Accuracy	**0.92**	
Subject 3			Subject 4		
Confusion Matrix			Confusion Matrix		
	Non S	S		Non S	S
Classified as Non S.	205	0	Classified as Non S.	307	1
Classified as S.	27	7	Classified as S.	59	9
Sensitivity	0.88	1.00	Sensitivity	0.84	0.90
Specificity	1.00	0.21	Specificity	1.00	0.13
Overall Accuracy	**0.89**		Overall Accuracy	**0.84**	

that of increased workload, i.e. increase in heart rate and EDA. The difference lies in the magnitude of this increase, which in stress events is expected higher. However, the larger increase, considering also the effect of noise in RRV estimation and the possible errors in self annotation does not seem sufficient to discriminate the two states. A feasible solution is the incorporation of additional information such as the possible causes of a stress event, in order to reduce the false positives, which is performed in the next models.

In the second BN model (BN2) we have incorporated the driving event information. In this case the information of the driving event is extracted manually from the video of the road scenery. This equals to capturing driving events with an optimal detector. In order to test stress detection accuracy, also with non-optimal detectors, we artificially introduce errors in the driving event detection. The information inserted in the *Driving Event* variable is given according to the following rule

$$P(DrivingEvent) = \begin{cases} 1 & \text{if there is an obstacle and } p < T1 \\ & \text{or there is no obstacle and } p > T2 \\ 0 & \text{if there is an obstacle and } p > T1 \\ & \text{or there is no obstacle and } p < T2 \end{cases}, \tag{5.35}$$

where p is a random number and $T1$ and $T2$ are the specificity and sensitivity of the event detection system, respectively. We consider three such systems with $T1 = \{0.9, 0.8, 0.7\}$ and $T2 = \{0.99, 0.9, 0.8\}$. Then we compare the sensitivity and specificity of stress event detection using i) only the driving event detection, assuming that every time an event occurs we also have a stress event and ii) driving event detection and physiological features (BN2). The results of both models are presented in Fig. 5.8. The sensitivity of the stress event detection is always higher for the model using both driving events and

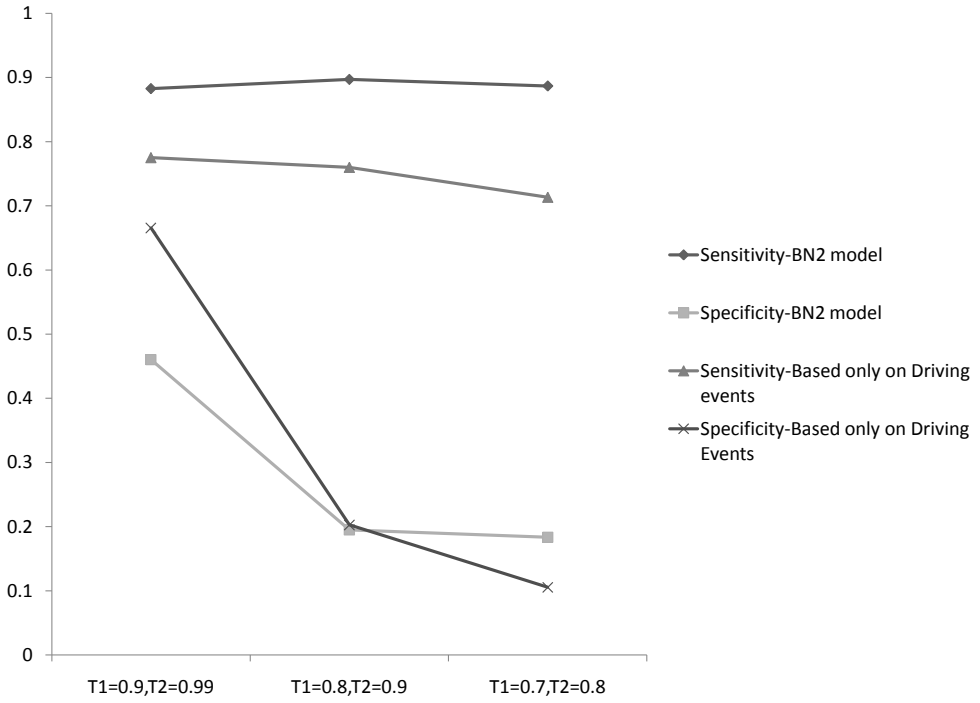

Figure 5.8: The sensitivity and specificity are presented for the BN2 model and stress detection based only on driving events, where we assume that there are three possible systems providing the driving events. $T1$ is the sensitivity and $T2$ the specificity of these systems.

physiological features compared to the model using only driving events. Furthermore, it is not influenced by the deterioration of the driving event detection accuracy. On the other hand, the specificity of both models is affected by the accuracy of the driving event detection but the effect on the specificity for the BN2 model becomes negligible.

In the third model (BN3) the driving event detection is based on features extracted from the driving environment. Having collected a significant number of sessions from Subject 1, we were able to build a driving history model for this subject and incorporate it to the enhanced model (BN3). The evaluation of the enhanced model is therefore performed only on the specific subject. Using Bayesian inference, we extracted both the probability of driver's stress event and the occurrence of a driving event. In Table 5.6 we present the detection accuracy of driving and stress events. Comparing the results of BN3 and BN1 models in Tables 5.6 and 5.4, respectively, we observe a significant increase in stress event detection accuracy (95% compared to 88%). The main reason of this increase in accuracy is the significant reduction of the false detected stress events using the driving event information.

Table 5.6: Confusion Matrix, Sensitivity and Specificity for each class and total accuracy for the classification of Stress Events (Stress), Overtaking (Ovt) and Hard Braking (H.B.) events using the BN3 model.

Driving Event			
Confusion Matrix			
	None .	Ovt	H.B.
Classified as None	2564	75	24
Classified as Ovt	69	78	0
Classified as H.B	62	0	13
Sensitivity	0.95	0.51	0.35
Specificity	0.96	0.53	0.17
Overall Accuracy	**0.92**		
Stress			
Confusion Matrix			
	Non S	S	
Classified as Non S.	2578	36	
Classified as S	111	36	
Sensitivity	0.96	0.50	
Specificity	0.99	0.24	
Overall Accuracy	**0.95**		

In Section 5.2.3 we claimed that the incorporation of driving event and driver's stress event detection in the same model could yield to a better detection performance of both driving and stress events. As presented earlier the obtained results confirm this for the stress event detection problem. As far as the driving events are concerned, Table 5.7 presents the driving event detection results for a three class problem (overtake, hard braking and none) using the Naive Bayes Classifier (as a benchmark) and the same training and testing procedure. Comparing Tables 5.7 and 5.6 we observe that BN3 significantly reduces the false positives of the driving event detection and increases the accuracy (92% compared to 65%). This can be explained since the probability of a driving event is lower in the absence of a physiological reaction.

5.5 Discussion

A methodology for driver stress estimation based on physiological signals (ECG, EDA and respiration) and driving behavior was presented. The RRV signal was modeled as a time varying AR model and using a variation of Kalman smoother we estimate the trend of the signal in real time. The information used is the trend of the signal since for stress detection we are interested in the baseline of the signal and not in the periodic variations. From the EDA the first absolute difference were used as a measure of skin conductance response. In order to improve this feature as stress indicator we employed a normalization method than can be applied in real time and reduce significantly the effect of the skin conductance level on the magnitude of the differences. Window analysis was then applied,

Table 5.7: Confusion Matrix, Sensitivity and Specificity for each class and total accuracy for the classification of Driving Events as a three class problem using a Naive Bayes classifier.

Driving Event			
Confusion Matrix (mean/std)			
	None	Ovt	H.B.
Classified as None	1719	22	9
Classified as Ovt	441	120	2
Classified as H.B	535	11	26
Sensitivity	0.64	0.78	0.70
Specificity	0.98	0.21	0.05
Overall Accuracy	**0.65**		

for feature extraction. Additionally we employed a method for building a driving history and exploited this information to improve the driver's stress event detection.

In order to fuse all the above information we employed the Bayesian framework. We examined three BN models, one with only physiological features, one incorporating driving events which are extracted based on annotation of video monitoring and a last one where the driving events are detected using information from the GPS and the CAN-bus of the vehicle. All models are tested in a dataset gathered in real driving conditions. We used one subject for training and testing, which performed a large number of experiments and four other for validation purposes. The accuracy of the BN model using only physiological features, was in average for all subjects approximately 88%. The results obtained on the validation subjects, reveal the good generalization behavior of the proposed method. This first model has a significant number of false positives since in particular segments an increased heart rate and/or skin conductance is observed without drivers actually experiencing an increased stress. These segments may be considered as moments of increased workload. In our work focusing on the detection of stress events, this may be considered as a drawback. However, for a system aiming at detecting increased workload, the solely usage of physiological signals could be sufficient.

The other two models include also driving event information. From Table 5.1 and Fig. 5.5 we observe that the event with the higher frequency is overtaking, as the driving context is a rural road. Furthermore, we observe that overtaking along with hard braking have the higher probability of medium and high stress events. This is expected since overtaking is the most frequent, and risk involved event and hard braking, on the other hand, is usually caused by driver's inattention or sudden events occurring on road, and thus it is always related to high crash risk. This is also the reason, focusing on the detection of these two events in our work.

With the second model (BN2) we examined how driving event detection could improve the stress events detection accuracy, reducing false positives. This was verified in the third model (BN3) where we used the driving environment information from GPS measurements and CAN-bus data in order to detect driving events. Introducing the driv-

ing event detection into the same model employed for the stress event detection, both the accuracy of driving and stress event detection are improved. This model is highly correlated with the driver's perception of stress and a 92% accuracy in stress event detection is achieved.

Most of the related works reported in the literature make use of data collected in simulation environments. However, subjects' responses to driving events occurring in a safe environment (simulation) are quite different from those in real conditions. For this reason, we have constructed a dataset with real drivers' reactions (stress events) to actual driving events. Since we are referring to real-world experiments, there is always the difficulty in controlling the driver's state because it highly depends on the prevailing driving environment. Moreover, driver's self annotation during real time presents practical difficulties (i.e. discrimination between low and medium stress level). These shortcomings of the annotation procedure are inherited in the increased number of false positives and for some cases of medium or low stress events there was no evidence of increase in heart rate and/or skin conductivity. In many cases drivers seem to over or under estimate their stress level. Thus, we suggest that for similar studies, apart from driver's self annotation, more reliable stress metrics should be used, based for example on electroencephalogram (EEG) or biomarkers [160]. In other cases, since driving events are accompanied by intense driver's movements, significant movement noise is introduced in the ECG. This noise affects the RR estimation and the value of the features extracted. On the other hand, in cases of very low SCL level the increase in EDA activity was not evident, apart from very intense events. Thus, for monitoring drivers physiological signals on real driving conditions, the choice of the sensors and sensor placement is crucial.

A major advantage of the proposed approach is that it can be applied in real time and does not need an initial relaxation phase for estimating signals baseline. Moreover, using the online adaptation of the model parameters, we obtain a good generalization performance. Furthermore, we discriminate the increase workload from stress events, based mainly on detecting both the cause, which is usually a driving event and the effect which is a stress event accompanied by an impact on physiological signals. Therefore, the proposed method can be effectively used to detect driver's stress events which can be further exploited by advanced driving support systems.

Appendix

We consider a mixture model of the population $\mathbf{X}$

$$x_i \sim \begin{cases} N(x_i; \mu_1, \sigma_1), \text{ if } x_i \text{ comes from the } C_1 \text{ component} \\ N(x_i, \mu_1 + \delta, \sigma_2), \text{ if } x_i \text{ comes from the } C_2 \text{ component} \end{cases} . \tag{5.36}$$

The mixing probability of each component is defined as π_1 and π_2. The ML estimation of the parameters of the model is based on the EM method. The EM estimation of the

ML parameters of the model, is based on the maximization of the following function:

$$\begin{aligned} L &= \sum_i \left[w_{i1}[c_1 + \log \sigma_1^{-2} + (x_i - \mu_1)^2/\sigma_1^2] \right. \\ &\quad \left. + w_{i2}[c_2 + \log \sigma_2^{-2} + (x_i - \mu_1 - \delta)^2/\sigma_2^2] \right], \end{aligned} \tag{5.37}$$

where c_1 and c_2 are constants and

$$w_{i1} = \frac{\sum_i \pi_1 N(x_i; \mu_1, \sigma_1)}{\sum_i [\pi_1 N(x_i; \mu_1, \sigma_1) + \pi_2 N(x_i; \mu_1 + \delta, \sigma_2)]}, \tag{5.38}$$

$$w_{i2} = \frac{\sum_i \pi_2 N(x_i; \mu_1 + \delta, \sigma_2)}{\sum_i [\pi_1 N(x_i; \mu_1, \sigma_1) + \pi_2 N(x_i; \mu_1 + \delta, \sigma_2)]}. \tag{5.39}$$

The calculation of w_{i1} and w_{i2} is the E-step of the EM algorithm. In the M-step we find μ_1 and δ which maximize Eq. (5.37). Regarding only the terms involving μ_1, Eq. (5.37) can be written as:

$$\begin{aligned} L &= C + \sum_i w_{i1}(x_i - \mu_1)^2/\sigma_1^2 \\ &\quad + \sum_i w_{i2}(x_i - \mu_1 - \delta)^2/\sigma_2^2, \end{aligned} \tag{5.40}$$

where C summarizes all other terms. Taking the derivative with respect to μ_1, we obtain:

$$\begin{aligned} \frac{\vartheta L}{\vartheta \mu_1} &= 2[-\sum_i w_{i1} x_i/\sigma_1^2 + \sum_i w_{i1}\mu_1/\sigma_1^2 \\ &\quad - \sum_i w_{i2} x_i \sigma_2^2 + \sum_i w_{i2}\mu_2/\sigma_2^2 \\ &\quad + \sum_i w_{i2}\delta/\sigma_2^2]. \end{aligned} \tag{5.41}$$

Setting to zero and solving with respect to μ_1 we obtain:

$$\mu_1 = \frac{(\sum_i w_{i1} x_i/\sigma_1^2 + \sum_i w_{i2} x_i/\sigma_2^2) - \sum_i w_{i2}\delta/\sigma_2^2}{(\sum_i w_{i1}/\sigma_1^2 + \sum_i w_{i2}/\sigma_2^2)}. \tag{5.42}$$

We follow the same procedure for δ. Taking the derivative of Eq. (5.37) with respect to δ we obtain:

$$\begin{aligned} \frac{\vartheta L}{\vartheta \delta} &= -\sum_i w_{i2} x_i/\sigma_2^2 + \sum_i w_{i2}\mu_1/\sigma_2^2 \\ &\quad + \delta(\sum_i w_{i2}/\sigma_2^2). \end{aligned} \tag{5.43}$$

Setting also to zero and solving with respect to δ we obtain:

$$\delta = \frac{\sum_i w_{i2} x_i/\sigma_2^2 - \sum_i w_{i2}\mu_1/\sigma_2^2}{(\sum_i w_{i2}/\sigma_2^2)}. \tag{5.44}$$

Chapter 6

Adaptation of a driver state detection system on new drivers

6.1 Introduction

Mixture models are well studied in the literature and applications exist in several domains, such as density estimation [11], clustering [5, 37], classification [97], image registration [34, 61], regression [4, 15], etc. The most widely used mixture model is the Gaussian mixture model (GMM). There are two main problems in the application of mixture models. The first is the estimation of model parameters. Parameter estimation is based on the *maximum likelihood* (ML) or *maximum a posteriori* (MAP) estimation of the parameters using the expectation-maximization algorithm (EM) [27, 33, 123] or

the variational extensions of the EM (VEM) [54, 133]. The second is the choice of the number of components, of the mixture model. There are some cases where the number of components is known a priori, (e.g. classification problems), however in the majority of cases this number is unknown (e.g. image clustering and segmentation). There have been several heuristic methods for an unsupervised estimation of the number of components [90, 146, 21, 13, 111].

In this work we address a different problem. We assume that the number of components as well as the model parameters are already estimated in an initial training dataset. Then this initial model is applied on a new dataset which is a transformation of the original one and there is a one-to-one mapping between the components of the initial dataset and the components of the new one. This problem is encountered in many domains, such as model adaptation [28], image registration [34] and tracking [158]. One may consider to simply retrain the model using the new dataset, but without any restrictions or constraints, this could lead to a violation of the one-to-one mapping. A commonly used approach is the application of constraints on the new parameters, such as the assumption that the new population is a geometric transformation of the original one. In Fig. 6.1 we present an example of this transformation. This assumption imposes that the new GMM parameters are also geometric transformations of the original ones. Usually, (as it is shown in Fig. 6.1) the geometric transformation consists of a rotation and a scaling matrix (matrix A in Fig. 6.1 is the product of a rotation and a scaling matrix), and a translation vector $\mathbf{b}$. Digalakis *et. al* [28, 130] treated this problem under the additional constraint that the transformation matrix A as well as the covariance matrices are diagonal. Use of a diagonal transformation matrix implies only scaling only across the dimensions of the population. Moss and Hancock [102] addressed also this constrained transformation problem. However, they were limited to the image registration problem, thus in 2D dimensional mixture models, and they treated the M-step for all transformation parameters, as an optimization problem.

In this work we treat the general D-dimensional problem, with non-diagonal rotation and covariance matrices, and the transformation parameters are identified employing the EM algorithm. The EM algorithm consists of two basic steps: i) the expectation step and ii) the maximization step, which are derived for the problem under investigation. An optimization method is applied only for the rotation angles in the maximization step. We also consider the special case of spherical covariance matrices. As already described, the method is based on the EM algorithm introduced by Dempster *et. al* [27]. EM gained great attention the last two decades mainly due to its simplicity, the natural handling of the probabilistic constraints and the certain convergence to a local minimum. Redner and Walker [121] criticized the EM as a first-degree rather "slow" algorithm, compared to Newton and quasi-Newton methods. However, the performance of the EM algorithm has proven to depend on the overlap of the mixture of Gaussian, and in the cases of minimum overlap the convergence rate becomes super-linear [159]. In this work, we apply the findings of [159] in the problem under consideration and we also propose an initialization

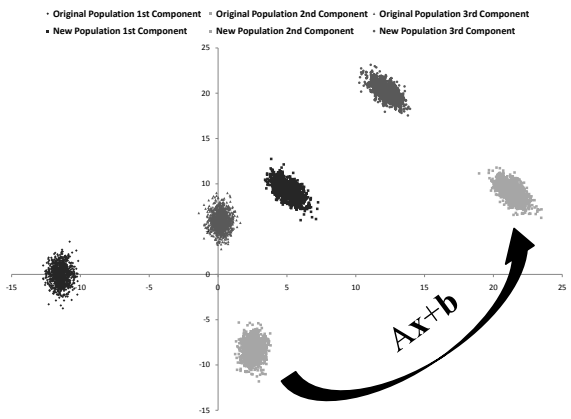

Figure 6.1: Example of a geometric transformation of a population.

method for a multiple start EM algorithm, which increases the probability of the correct solution identification.

The assumption of a unique transformation applied on all mixture components, may hold for a large number of problems. However, it could be of great interest to allow each component to have an individual transformation. For better understanding, the unique transformation could be applied to the estimation of a camera motion capturing a still scenery. However if some objects are also moving, then in order to estimate both motions we need to consider transformations to individual components.

In what follows, in Section 6.2 the problem is defined and in Section 6.3 we derive the expectation and maximization steps of the EM algorithm for both full and spherical covariance cases. In Section 6.3.4 we study the likelihood function, considering the overlapping of the initial GMM components and we propose a global minimum criterion. In the experiments performed in Section 6.6 the algorithm's behavior and the correct solution identification as a function of the mixture overlapping are examined. In Section 6.5 we examine the case of both global and local transformation, using a MAP EM approach. Finally, the results and the proposed methodology are discussed in Section 6.8.A summary of the notations used hereby is given in Table 6.1.

6.2 Background on the Geometric Transformation of a Gaussian Mixture model

Suppose an initial sample $\mathbf{X}^0$ of a D-dimensional space $\mathfrak{R}^D$, whose distribution is approximated as a GMM with L components. Any probability density can be accurately approximated with a mixture of Gaussians having a proper number of components [84].

The density of sample $\mathbf{X}^0$ is expressed as:

$$P(\mathbf{X}^0) = \prod_{\mathbf{x}\in\mathbf{X}^0} \sum_{i}^{L} p_i \mathbf{N}(\mathbf{x}|\boldsymbol{\mu}_i, \Sigma_i), \tag{6.1}$$

where p_i, $\boldsymbol{\mu}_i$ and Σ_i are the prior, the mean and covariance matrix of the i-th mixture component, respectively. Furthermore it holds that $\sum_i^L p_i = 1$. The problem examined which is examined here is the geometric transformation of a GMM. We consider a new sample $\mathbf{X}$ with n samples, which is produced according to:

$$\mathbf{X}^0 \overset{A(\cdot)+\mathbf{b}}{\Longrightarrow} \mathbf{X}, \tag{6.2}$$

where $A(\cdot)$ is the rotation and scaling function and $\mathbf{b}$ is the translation. The distribution of the new sample $\mathbf{X}$, under the transformation $A(\cdot) + \mathbf{b}$ is:

$$P(\mathbf{X}) = \prod_{\mathbf{x}\in\mathbf{X}} \sum_{i} p_i \mathbf{N}(\mathbf{x}|A\boldsymbol{\mu}_i + \mathbf{b}, A^T \Sigma_i A). \tag{6.3}$$

The matrix A is the product of a number of elementary transformation matrices:

$$A = S[\prod_{i=1}^{P} R_i]. \tag{6.4}$$

S is a diagonal scaling matrix, and the coefficients $s_{i,i}$ scales the mixture components across dimension i and R_i is an elementary rotation matrix with angle denoted as ϕ_i.

In this work we consider a slightly different transformation, where scaling is only applied on the covariance matrices and not in the mean of the Gaussian distributions. Thus, we do not shrink or enlarge the whole distribution space but rather the range of each component. The GMM described the new population is thus written as:

$$P(\mathbf{X}) = \prod_{\mathbf{x}\in\mathbf{X}} \sum_{i} p_i \mathbf{N}(\mathbf{x}|A\boldsymbol{\mu}_i + \mathbf{b}, A^T S \Sigma_i S A), \tag{6.5}$$

and

$$A = [\prod_{i=1}^{P} R_i]. \tag{6.6}$$

However for all the derivations following, the extension to the case of (6.3) is trivial. The parameters describing the original GMM model are:

$$\begin{aligned} \mathbf{M} \;=\; & \{\{p_1, \boldsymbol{\mu}_1, \mathbf{vec}[\Sigma_1]\}, \{p_2, \boldsymbol{\mu}_2, \mathbf{vec}[\Sigma_2]\}, ..., \\ & \{p_L, \boldsymbol{\mu}_L, \mathbf{vec}[\Sigma_L]\}\}. \end{aligned} \tag{6.7}$$

and the transformation parameters are:

$$\boldsymbol{\Theta} \;=\; \{\{\phi_1, \cdots, \phi_P\}, \{s_1, \cdots, s_D\}, \tag{6.8}$$

$$\{b_1, \cdots, b_D\}\}. \tag{6.9}$$

There is no closed solution for the maximum likelihood estimation of the transformation parameters $\boldsymbol{\Theta}$. The main tool for solving similar problems is the expectation-maximization (EM) algorithm [27]. The application of the EM in the specific problem, is described in the next section.

Table 6.1: Symbols used in this work and their meaning.

Symbols	Meaning
$\boldsymbol{x}, \boldsymbol{y}, \boldsymbol{b}$	Vectors
A, R	Matrices
$\mathbf{X}$	Variable set
$P(\mathbf{X})$	Probability distribution
$\pi(\mathbf{X})$	Prior probability distribution
$\mathfrak{L}$	Log-likelihood
$e(M*)$	Overlapping of a GMM model
n	Population samples
D	Problem's dimension
L	Number of GMM components
$\mathbf{N}$	Gaussian Distribution
$\boldsymbol{\mu}$	Mean of Gaussian
Σ	Covariance of Gaussian
$vec[\cdot]$	Vectorize matrix
$tr(\cdot)$	Trace of matrix
$E[\cdot]$	Expectation operator

6.3 EM approach

The EM algorithm as denoted by his name consists of two step: i) the expectation step and ii) the maximization step. The goal of the EM algorithm is to maximize at each step k the expected log-likelihood of the complete data with respect to model's parameters:

$$\mathbf{\Theta}^k = \arg\max_{\mathbf{\Theta}} E[\log p(\mathbf{X}, \Omega|\mathbf{\Theta}, \mathbf{M})|\mathbf{X}, \mathbf{\Theta^{k-1}}], \tag{6.10}$$

where $\mathbf{\Theta}^{k-1}$ is the previous estimation of parameters, $\mathbf{M}$ is the initial model considered and Ω denotes the collection of the corresponding unobserved mixture indices.

The expected log-likelihood, can be written as:

$$\begin{aligned}
\mathfrak{L}(\mathbf{\Theta^k}|\mathbf{\Theta^{k-1}}, \mathbf{M}) &= E[\log p(\mathbf{X}, \Omega|\mathbf{\Theta}, \mathbf{M})|\mathbf{X}, \mathbf{\Theta^{k-1}}] \\
&= \sum_{x\in\mathbf{X}} \sum_i p(\omega_i|x, \mathbf{\Theta}^{k-1}) p(x|\omega_i, \mathbf{\Theta}^{k-1}) \\
&+ \sum_{x\in\mathbf{X}} \sum_i p(\omega_i|x, \mathbf{\Theta}^{k-1}) p(\omega_i) \qquad (6.11) \\
&= \sum_{x\in\mathbf{X}} \sum_i p(\omega_i|x, \mathbf{\Theta}^{k-1}) \left[-\frac{1}{2} \log |\Sigma_i'| \right. \\
&- \left. \frac{1}{2}(x-\mu_i')^T (\Sigma_i')^{-1} (x-\mu_i') \right] \qquad (6.12) \\
&+ \sum_{x\in\mathbf{X}} \sum_i p(\omega_i|x, \mathbf{\Theta}^{k-1}) p(\omega_i|\mathbf{\Theta}^{k-1}), \qquad (6.13)
\end{aligned}$$

where $\mu_{\mathbf{i}}' = A\mu_i + b$ and $\Sigma_i' = A^T S\Sigma_i SA$. The term (6.13) does not depend on the transformation parameters $\mathbf{\Theta}$ and thus not need to be included in further derivations. The first term (6.12), denoted as $\mathfrak{J}$, following [28] can be written as:

$$\begin{aligned}\mathfrak{J} &= \sum_i \pi_i(\mathbf{X})\Big[2\log|A| \\ &+ \boldsymbol{y}^T S^{-1}\Sigma_i^{-1}S^{-1}\boldsymbol{y} \\ &+ \mathrm{tr}\big[AS^{-1}\Sigma_i^{-1}S^{-1}A^T\hat{\Sigma}_i[\mathbf{X}]\big]\Big],\end{aligned} \tag{6.14}$$

where $\boldsymbol{y} = (A^T E_i[\mathbf{X}] - \boldsymbol{\mu}_i - A^T\mathbf{b})$ and $\pi_i(\mathbf{X})$ is:

$$\pi_i(\mathbf{X}) = \sum_{\mathbf{x}\in\mathbf{X}} h_i(\mathbf{x}), \tag{6.15}$$

where

$$\begin{aligned}h_i(\mathbf{x}) &\equiv p(\omega_i|x,\Theta^{k-1}) \\ &= \frac{p_i P(\mathbf{x}|\boldsymbol{\mu}_i',\Sigma_i')}{\sum_{j=1}^{L} p_j P(\mathbf{x}|\boldsymbol{\mu}_j',\Sigma_j')}\end{aligned} \tag{6.16}$$

$E_i[\mathbf{X}]$ and $\hat{\Sigma}_i[\mathbf{X}]$ are the sufficient statistics which are defined in Section 6.3.1 and calculated in the **E**-step of the EM algorithm.

In this section we present the derivation of the **E** and **M** steps of the EM based algorithm for the estimation of the parameter vector $\mathbf{\Theta}$. Using an initial guess for $\mathbf{\Theta}$, $\mathbf{\Theta}^0$, the algorithm repeats the **E** and **M** steps until the convergence criteria are met. A more sophisticated method for parameter initialization is described in Section 6.4. The termination criterion used is:

$$\|\Theta^k - \Theta^{k-1}\| < \epsilon, \tag{6.17}$$

where $\mathbf{\Theta}^k$ is the parameter vector at step k. Next the derivation of **E**-step and **M**-step is described in more detail. We consider two cases for the M-step: i) a general case where the covariance matrices are full positive definite matrices and ii) the spherical covariance case.

6.3.1 E-step

In the **E**-step we estimate the expected sufficient statistics of the data, given the current estimation of the parameter vector $\mathbf{\Theta}^{k-1}$ [28]:

$$E_j[\mathbf{X}] = \frac{\sum_{i=1}^{n}\mathbf{x}_i P(\mathbf{x}_i|A\boldsymbol{\mu}_j+\mathbf{b},(SA)^T\Sigma_j SA)}{\sum_{i=1}^{n}\sum_{k=1}^{L} P(\mathbf{x}_i|A\boldsymbol{\mu}_k+\mathbf{b},(SA)^T\Sigma_k SA)}, \tag{6.18}$$

$$E_j[\mathbf{X}\mathbf{X}^T] = \frac{\sum_{i=1}^{n}\mathbf{x}_i\mathbf{x}_i^T P(\mathbf{x}_i|A\boldsymbol{\mu}_j+\mathbf{b},(SA)^T\Sigma_j SA)}{\sum_{i=1}^{n}\sum_{k} P(\mathbf{x}_i|A\boldsymbol{\mu}_k+\mathbf{b},(SA)^T\Sigma_k SA)}, \tag{6.19}$$

$$\hat{\Sigma}_i[\mathbf{X}] = E_j[\mathbf{X}\mathbf{X}^T] - E_j[\mathbf{X}]E_j[\mathbf{X}]^T. \tag{6.20}$$

6.3.2 M-step under the general case

The update equations for all the transformation parameters (translation vector, scale vector and rotation angles) are employed in the M-step. We do not update the mixture model membership probabilities p_i, assuming that the new sample comes from the transformed components with the same proportion.

Translation vector

Taking the derivative of Eq. () with respect to the translation vector $\mathbf{b}$ and setting the derivative to zero we obtain the following update equation:

$$\mathbf{b} = C^{-1}D, \tag{6.21}$$

where C and D are defined as:

$$C = \left[\sum_i \pi_i(\mathbf{X})\Sigma_i^{-1}S^{-1}A^T\right], \tag{6.22}$$

$$D = \left[\sum_i \pi_i(\mathbf{X})\Sigma_i^{-1}S^{-1}A^T(E_i[\mathbf{X}] - A\boldsymbol{\mu}_i)\right]. \tag{6.23}$$

Scale vector

Taking the derivative of Eq. () with respect to the scale $\mathbf{s}_j$ and setting the derivative to zero, we obtain:

$$a\mathbf{s}_j^2 + b\mathbf{s}_j + c = 0, \tag{6.24}$$

where a, b and c are defined as:

$$\begin{aligned} a &= 1, \\ b &= \sum_i \frac{\pi_i(\mathbf{X})}{n}\left\{\boldsymbol{x}_{ij}^T\boldsymbol{y}_{ij} + tr(A^T S^{1j}\Sigma_i S^{2j}A\hat{\Sigma}_i[\mathbf{X}])\right\}, \\ c &= \sum_i \frac{\pi_i(\mathbf{X})}{n}\left\{\boldsymbol{x}_{ij}^T\boldsymbol{x}_{ij} + tr(A^T S^{2j}\Sigma_i S^{2j}A\hat{\Sigma}_i[\mathbf{X}])\right\}. \end{aligned}$$

In the above equations $\boldsymbol{x}_{ij}$ and $\boldsymbol{y}_{ij}$ are defined as:

$$\boldsymbol{x}_{ij} = L_i S^{1j}\left[A^T(E_i[\mathbf{X}] - \mathbf{b}) - \boldsymbol{\mu}_i\right], \tag{6.25}$$

$$\boldsymbol{y}_{ij} = L_i S^{2j}\left[A^T(E_i[\mathbf{X}] - \mathbf{b}) - \boldsymbol{\mu}_i\right], \tag{6.26}$$

where L_i is derived from the Cholesky decomposition of the covariance matrix Σ_i^{-1}:

$$\Sigma_i^{-1} = L_i^T L_i. \tag{6.27}$$

S^1 and S^2 are diagonal matrices, defined as:

$$S_{ij}^{1k} = \begin{cases} 0, \text{ if } i=j=k \\ s_i, \text{ if } i=j \neq k \\ 0, \text{ otherwise} \end{cases}, \tag{6.28}$$

$$S_{ij}^{2k} = \begin{cases} 1, \text{ if } i=j=k \\ 0, \text{ otherwise} \end{cases}. \tag{6.29}$$

It can be shown that $|c| >> |b|$ and $c < 0$ and thus $b^2 - 4c > 0$, whereas:

$$\mathbf{s}_j^2 = \frac{b \pm \sqrt{b^2 - 4c}}{2}, \tag{6.30}$$

has one positive and one negative solution. We always select the positive one.

Rotation angles

The derivation of the angle update formula is more complicated. For simplicity $\mathfrak{J}$ is split as the sum of two terms:

$$\mathfrak{J} = \sum_i \pi_i(\mathbf{X})[\mathfrak{J}_i^a + \mathfrak{J}_i^b], \tag{6.31}$$

where $\mathfrak{J}_i^a$ and $\mathfrak{J}_i^b$ are defined as:

$$\mathfrak{J}_i^a = \mathbf{F}^T S^{-1} S_i^{-1} S^{-1} \mathbf{F}, \tag{6.32}$$

$$\mathfrak{J}_i^b = tr(A S^{-1} \Sigma_i^{-1} S^{-1} A \hat{\Sigma}_i[\mathbf{X}]), \tag{6.33}$$

where $\mathbf{F}$ in Eq. (6.32) is defined as:

$$\mathbf{F} = (A^{-1} E_i[\mathbf{X}] - \boldsymbol{\mu}_i - A^{-1}\mathbf{b})^{\mathbf{T}}. \tag{6.34}$$

We consider the matrix A to be a product of elementary transformations (see Eq. (6.4)):

$$A = R_1 R_2 \cdots R_j \cdots R_{D-1}, \tag{6.35}$$

and R_j is:

$$R_j^{(D\times D)} = \begin{array}{c} \\ \\ \\ \\ \\ \\ \\ \end{array} \begin{array}{c} \\ j \\ \\ \\ \\ \\ \\ \end{array} \begin{pmatrix} & & j & & & \\ 1 & \cdots & 0 & 0 & \cdots & 0 \\ \vdots & \ddots & \vdots & \vdots & \iddots & 0 \\ 0 & \cdots & \cos(\phi_j) & \sin(\phi_j) & \cdots & 0 \\ 0 & \cdots & -\sin(\phi_j) & \cos(\phi_j) & \cdots & 0 \\ \vdots & \iddots & \vdots & \vdots & \ddots & \vdots \\ 0 & \cdots & 0 & 0 & \cdots & 1 \end{pmatrix}, \tag{6.36}$$

where ϕ_j the rotation angle. The results following, can be extended to more generic forms of R_j, as we will see in the experiments for the estimation of a 3D geometric

transformation, where the number of angles exceed the problems dimensionality ($P > n-1$). However, at the moment we follow this definition for simplicity. Either case, R_j can be decomposed as:

$$R_j = (I_j \cos(\phi_j) + J_j \sin(\phi_j) + K_j), \tag{6.37}$$

where I_j, J_j and K_j are matrices defined in Appendix 6.8. The partial derivative of $\mathfrak{J}$ with respect to ϕ_j is given as (see Appendix 6.8):

$$\begin{aligned}
\frac{\partial \mathfrak{J}}{\partial \phi_j} &= \sum_i \pi_i(\boldsymbol{x}) \left[[(\boldsymbol{x}_{ij}^T \boldsymbol{x}_{ij} - \boldsymbol{y}_{ij}^T \boldsymbol{y}_{ij}) \right. \\
&+ tr(A_j^c \Sigma_i^{-1} A_j^c \hat{\Sigma}_i[\mathbf{X}]) \\
&- tr(A_j^s \Sigma_i^{-1} A_j^s \hat{\Sigma}_i[\mathbf{X}])] \sin(2\phi_j) \\
&+ 2[\boldsymbol{x}_{ij}^T \boldsymbol{y}_{ij} + tr(A_j^s S_i^{-1} A_j^c \hat{\Sigma}_i[\mathbf{X}])] \cos(2\phi_j) \\
&+ 2[\boldsymbol{x}_{ij}^T (\boldsymbol{z}_{ij} + \boldsymbol{w}_i)] \sin(\phi_j) \\
&- \left. 2[\boldsymbol{y}_{ij}^T (\boldsymbol{z}_{ij} + \boldsymbol{w}_i)] \cos(\phi_j) \right] .
\end{aligned} \tag{6.38}$$

The vectors $\boldsymbol{x}_{ij}, \boldsymbol{y}_{ij}, \boldsymbol{z}_{ij}$ and $\boldsymbol{w}_i$ are defined as:

$$\boldsymbol{x}_{ij} = L_i^T A_j^c (E_i[\mathbf{X}] - \mathbf{b}), \tag{6.39}$$

$$\boldsymbol{y}_{ij} = L_i^T A_j^s (E_i[\mathbf{X}] - \mathbf{b}), \tag{6.40}$$

$$\boldsymbol{z}_{ij} = L_i^T A_j^k (E_i[\mathbf{X}] - \mathbf{b}), \tag{6.41}$$

$$\boldsymbol{w}_i = L_i^T \boldsymbol{\mu}_i, \tag{6.42}$$

where L_i is the Cholesky decomposition of the covariance matrix Σ_i^{-1}. The matrices A_j^c, A_j^s, and A_j^k are defined as:

$$A_j^c = R_{D-1}^T \cdots I_j^T \cdots R_2^T R_1^T S^{-1}, \tag{6.43}$$

$$A_j^s = R_{D-1}^T \cdots J_j^T \cdots R_2^T R_1^T S^{-1}, \tag{6.44}$$

$$A_j^k = R_{D-1}^T \cdots K_j^T \cdots R_2^T R_1^T S^{-1}. \tag{6.45}$$

Setting Eq. (6.38) to zero we obtain an equation of the following form:

$$a \cos(2\phi) + b \sin(2\phi) + c \cos(\phi) + d \sin(\phi) = 0, \tag{6.46}$$

where

$$\begin{aligned}
a &= \sum_i \pi_i(\boldsymbol{x}) \left[(\boldsymbol{x}_{ij}^T \boldsymbol{x}_{ij} - \boldsymbol{y}_{ij}^T \boldsymbol{y}_{ij}) \right. \\
&+ tr(A_j^c \Sigma_i^{-1} A_j^c \hat{\Sigma}_i[\mathbf{X}]) \\
&- \left. tr(A_j^s \Sigma_i^{-1} A_j^s \hat{\Sigma}_i[\mathbf{X}]) \right] , \\
b &= 2 \sum_i \pi_i(\mathbf{X}) [\boldsymbol{x}_{ij}^T \boldsymbol{y}_{ij} + tr(A_j^s \Sigma_i^{-1} A_j^c \hat{\Sigma}_i[\mathbf{X}])], \\
c &= 2 \sum_i \pi_i(\mathbf{X}) [\boldsymbol{x}_{ij}^T (\boldsymbol{z}_{ij} + \boldsymbol{w}_i)] \sin(\phi_j), \\
d &= -2 \sum_i \pi_i(\mathbf{X}) [\boldsymbol{y}_{ij}^T (\boldsymbol{z}_{ij} + \boldsymbol{w}_i)] \cos(\phi_j).
\end{aligned}$$

In order to solve Eq. (6.46) for ϕ, we use a non-linear optimization method (Levenberg-Marquardt).

6.3.3 M-step under the spherical covariance case

We consider the special case where spherical covariances $\Sigma_i = \sigma^2 I$ and spherical scaling $S = sI$ are employed. We derive the update equations for scale vector and rotation angles (the derivation of the translation vector is the same).

Scale vector

The parameter s^* is given as:

$$s^* = \sqrt{\frac{\sum_i \pi_i(\mathbf{X}) \left[tr(\hat{\Sigma}_i[\mathbf{X}])/(D\sigma^2) + \boldsymbol{z}^T \boldsymbol{z}/\sigma_i \right]}{D}}, \tag{6.47}$$

where $\boldsymbol{z} = [A^T(\hat{\Sigma}_i[\mathbf{X}] - \mathbf{b}) - \boldsymbol{\mu}_i]$.

Rotation Angles

From the definition of the matrices J_i and I_i (see Appendix 6.8) we obtain the following identities:

$$\begin{aligned} tr(A_j^c S_i^{-1} A_j^c \hat{\Sigma}_i[\mathbf{X}]) &= tr(A_j^s S_i^{-1} A_j^s \hat{\Sigma}_i[\mathbf{X}]), & (6.48)\\ tr(A_s S_i^{-1} A_c \hat{\Sigma}_i[\mathbf{X}]) &= 0, & (6.49)\\ \boldsymbol{x}_{ij}^T \boldsymbol{x}_{ij} &= \boldsymbol{y}_{ij}^T \boldsymbol{y}_{ij}, & (6.50)\\ \boldsymbol{x}_{ij}^T \boldsymbol{y}_{ij} &= 0. & (6.51) \end{aligned}$$

Incorporating Eqs. (6.48)-(6.51) into Eq. (6.38) we obtain:

$$\begin{aligned} \frac{\partial \mathfrak{J}}{\partial \phi_i} &= 2[\boldsymbol{x}_{ij}^T(\boldsymbol{z}_{ij} + \boldsymbol{w}_i)] \sin(\phi_j) \\ &- 2[\boldsymbol{y}_{ij}^T(\boldsymbol{z}_{ij} + \boldsymbol{w}_i)] \cos(\phi_j)]. \end{aligned} \tag{6.52}$$

Setting to zero and solving with respect to ϕ_j, we obtain a solution ϕ_i^* which is given as:

$$\phi_i^* = -atan(\frac{\boldsymbol{y}_{ij}^T(\boldsymbol{z}_{ij} + \boldsymbol{w}_i)}{\boldsymbol{x}_{ij}^T(\boldsymbol{z}_{ij} + \boldsymbol{w}_i)}), \tag{6.53}$$

where $\boldsymbol{x}_{ij}, \boldsymbol{y}_{ij}, \boldsymbol{z}_{ij}$ and $\boldsymbol{w}_{ij}$ are defined in Equations (6.87), (6.88), (6.89) and (6.90), respectively.

6.3.4 Local maxima

Since EM can be considered as a local optimization method, the existence of many local maxima could have a serious effect on the method performance. In the case of a unique maximum the algorithm is guaranteed to convergence to this maximum. Thus, it is of great interest to study the shape of the likelihood function, given the parameters of the problem.

One of the factors influencing the number of local maxima of the log-likelihood function, is the sparsity of the mixture components. This is verified theoretically in [89, 91]. The more dense the distribution, the larger the number of local maxima in the search of the optimal transformation parameters which fit the data.

We follow the measure of the Gaussian overlap introduced in [89]. We define $\gamma_{ij}(\mathbf{x})$ as:

$$\gamma_{ij}(\mathbf{x}) = (\delta_{ij} - h_i(\mathbf{x}))h_j(\mathbf{x}) \text{ for } i,j = \{1,...,L\}, \tag{6.54}$$

where δ_{ij} is the Kronecker function and $h_i(\mathbf{x})$ is defined in Eq. (6.16). The overlap measure of two mixture components is defined as:

$$e_{ij}(\mathbf{M}^*) = \int_{\mathbf{R}^d} |\gamma_{ij}(x)| P(\mathbf{x}|\mathbf{M}^*)dx \text{ for } i,j = \{1,...,L\}, \tag{6.55}$$

where $\mathbf{M}$ is the GMM model considered and $e_{ij}(\mathbf{M}^*) \leq 1$ since $|\gamma_{ij}(x)| \leq 1$. The maximum overlapping $e(\mathbf{M}^*)$, is defined as:

$$e(\mathbf{M}^*) = \max_{ij} e_{ij}(\mathbf{M}^*). \tag{6.56}$$

More details can be found in [89]. Next we prove that $e(\mathbf{M}^*)$ is invariant under the transformation $A(\cdot) + \mathbf{b}$.

Lemma 6.1. *The measure of Gaussian overlapping $e(\mathbf{M}^*)$ is invariant under the transformation $Ax + b$, where A is the product of rotation and scaling matrices.*

Proof. Since the measure of overlap $e(\mathbf{M}^*)$ is governed by the overlapping of different components, we examine only the cases $e_{ij}(M^*)$, where $i \neq j$. Under the transformation $x' = A\mathbf{x} + \mathbf{b}$ and the new parameter vector $\mathbf{M}^{*'}$, $\mathbf{P}(\mathbf{x}'|A\boldsymbol{\mu}_i^* + b, A\Sigma_i A^T)$ can be written as:

$$\begin{aligned}
\mathbf{P}(\mathbf{x}'|A\boldsymbol{\mu}_i^* + \mathbf{b}, A\Sigma_i A^T) &= \mathbf{N}(A\mathbf{x} + b|A\boldsymbol{\mu}_i^* + b, A\Sigma_i A^T) \\
&= (|2\pi|^{-d/2}|\Sigma_i|^{-1}|S|^{-1}) \\
&\cdot \exp\big[-(A\mathbf{x} + \mathbf{b} - (A\boldsymbol{\mu}_i^* + b))^T \\
&\quad A^{-T}\Sigma_i^{-1}A^{-1} \\
&\quad (A\mathbf{x} + \mathbf{b} - (A\boldsymbol{\mu}_i^* + b))\big] \\
&= |2\pi|^{-d/2}|\Sigma_i|^{-1}|S|^{-1} \\
&\cdot \exp -\frac{(\mathbf{x} - \boldsymbol{\mu}_i^*)^T\Sigma_i^{-1}(\mathbf{x} - \boldsymbol{\mu}_i^*)}{2\sigma_i^2|S|^2} \\
&= |S|^{-1}\mathbf{P}(\mathbf{x}|\boldsymbol{\mu}_i^*, \Sigma_i).
\end{aligned} \tag{6.57}$$

For $i \neq j$, defining $P_i \equiv P(A\mathbf{x}+\mathbf{b}|A\boldsymbol{\mu}_i^* + b, A^T\Sigma_i^* A)$ and using the property that $|R| = 1$, and the variable transformation $\mathbf{x}' = A\mathbf{x} + \mathbf{b}$ we obtain:

$$\begin{aligned} e_{ij}(\mathbf{M}^{*'}) &= \int_{\mathbf{R}^d} h_i'(\mathbf{x}')h_j'(\mathbf{x}')P(\mathbf{x}'|M^{*'})d\mathbf{x}' \\ &= \int_{\mathbf{R}^d} \frac{\pi_i^*\pi_j^* P_i P_j}{\sum_{k=1}^L \pi_k^* P_k}|SR|d\mathbf{x}. \end{aligned} \tag{6.58}$$

Given that $R^T R = I$, we obtain:

$$\begin{aligned} e_{ij}(\mathbf{M}^{*'}) &= \int_{\mathbf{R}^d} \frac{\pi_i^*\pi_j^* P(\mathbf{x}|\boldsymbol{\mu}_i^*, \Sigma_i^*)P(\mathbf{x}|\boldsymbol{\mu}_j^*, \Sigma_j^*)}{|S|\sum_{k=1}^L \pi_k^* P(\mathbf{x}|\boldsymbol{\mu}_k^*, \Sigma_k^*)}|S|d\mathbf{x} \\ &= e_{ij}(\mathbf{M}^*). \end{aligned} \tag{6.59}$$

∎

In [89] is proved that if the initial guess of the parameters lies in the neighbor of the correct solution $\mathbf{N}(\mathbf{M}^*)$ then, given sufficient samples, the EM converges to the correct solution. The range of $\mathbf{N}(\mathbf{M}^*)$ has been shown to be related to $e_{ij}(\mathbf{M}^*)$. Since this in invariant under the transformation $A\mathbf{x}+\mathbf{b}$, it is also expected that the range of $\mathbf{N}(\mathbf{M}^*)$ will be also invariant under the same transformation. This is very important, since studying the initial model, we could infer the range of the transformation parameters, where the model converges to the true solution and we could therefore construct an optimal grid on the parameter space to obtain the correct solution. Here, we use a more naive approach, which is described in the next section.

6.4 EM with multiple starts

For a D dimensional problem we consider P rotation angles. For a 2D dimensional problem, $P = 1$, whereas for a 3D dimensional problem $P = 3$. Thus we have a $\Re^P$ angle space $\boldsymbol{\Phi}$. However considering only the space $[-\pi, \pi]$ for each angle the angle space is a hypercube. We produce a grid of this hypercube splitting the range of each angle in K equal distant intervals. Thus we have K^P possible initializations for the rotation angles. The optimal value of K depends on the problem complexity. The larger the K the higher the probability of identifying the global maximum, and of course the higher the computational cost.

We then consider scale parameters initialization. A large value is initially assigned to scale parameters. The rationale for this choice, is that the new sample should be covered by all initial mixtures, thus no mixture is favored to cover a different chunk of the sample.

Furthermore, from the numerical stability point of view, if we assume that the new model is far out of the initial's model region, then the estimation of likelihood of the new data, given the initial model, can create numerical problems.

The method proposed is summarized in Algorithm 6. The algorithm is named *msEM* (EM with multiple starts). Starting from different initializations as those are produced by

Produce a grid of the rotation angle space $\mathbf{\Phi}$
for all $\phi_0 \in \mathbf{\Phi}$ **do**
  $k = 0$
  $\mathfrak{J}_{max} = -\infty$
  while $\|\mathbf{\Theta}^k - \mathbf{\Theta}^{k-1}\| < \epsilon$ **do**
    Calculate expected statistics in **E**-step
    Update transformation $\mathbf{\Theta}^k$ parameters in **M**-step
    $k = k + 1$
  $\mathbf{M}^* = \Theta^k(\mathbf{M}^0)$
  if $\mathfrak{J}(\mathbf{M}^*) > \mathfrak{J}_{min}$ **then**
    $\mathfrak{J}_{max} = \mathfrak{J}(\mathbf{M}^*)$
    $\mathbf{\Theta}^{opt.} = \mathbf{\Theta}^k$

Algorithm 2: msEM

the grid of the transformation parameter space, we perform the EM steps until convergence in the tranformation parameters. From all solutions Θ^{EM} we keep the optimal one $\mathbf{\Theta}^{opt.}$, the solution that was closer to the expected log-likelihood of the transformed model and scaled according to S^{EM}.

6.5 Global and Local Transformation

The assumption of a unique transformation for all mixture model components, may hold for some problems, but in many others could be a very strict constraint. In order to add more flexibility in the model, we could allow each component to have an individual (local) transformation as well. We will consider the 2-D case, but the following results are easily extendable to the more general case. We start from the definition of the both global and local transformation in rotation, scaling and translation. The new rotation matrix $R_j^{(GL)}$ for a 2-D case can be written as:

$$R_j^{(GL)} = \begin{pmatrix} \cos(\phi + \phi_j) & -\sin(\phi + \phi_j) \\ \sin(\phi + \phi_j) & \cos(\phi + \phi_j) \end{pmatrix}, \tag{6.60}$$

where ϕ the rotation applied to all components and ϕ_j the rotation applied to the specific $j-th$ component. Obviously R_j can be also express as the product of a local and a global rotation:

$$\begin{aligned} R_j^{(GL)} &= R^{(G)} \cdot R_j^{(L)} \\ R^{(G)} &= \begin{pmatrix} \cos(\phi) & -\sin(\phi) \\ \sin(\phi) & \cos(\phi) \end{pmatrix} \\ R_j^{(L)} &= \begin{pmatrix} \cos(\phi_j) & -\sin(\phi_j) \\ \sin(\phi_j) & \cos(\phi_j) \end{pmatrix}. \end{aligned} \tag{6.61}$$

For the translation vector we can write:

$$b_j^{(GL)} = b^{(G)} + b_j^{(L)} \tag{6.62}$$

and for scaling

$$S_j^{(GL)} = \begin{pmatrix} s_1^{(G)} \cdot s_1^{(L)} j & 0 \\ 0 & s_2^{(G)} \cdot s_{2j}^{(L)} \end{pmatrix}. \tag{6.63}$$

The basic assumption of those local transformation are that are in magnitude smaller than the global ones. Thus in order to apply this constrained in their estimation we choose to apply a prior distribution on those parameters. Thus we assume that:

$$\phi_j^{(L)} \propto \mathbf{N}(0, \sigma_\phi^2), \tag{6.64}$$

$$s_{kj}^{(L)} \propto \mathbf{N}(0, \sigma_s^2), \tag{6.65}$$

$$\mathbf{b} \propto \mathbf{N}(\mathbf{0}, \sigma_{\mathbf{b}}^2 \mathbf{I}). \tag{6.66}$$

The new set of transformation parameters and the incorporation of the prior on the distribution of local transformations, leads to an MAP EM estimation and the optimization of the new auxiliary log-likelihood function:

$$\begin{aligned} \mathfrak{J} &= \sum_i \pi_i(\mathbf{X}) \Big[2 \log |A_i^{(GL)}| \\ &+ \boldsymbol{y}^T (S_i^{(GL)})^{-1} \Sigma_i^{-1} (S_i^{(GL)})^{-1} \boldsymbol{y} \\ &+ \operatorname{tr}\big[A_i^{(GL)} (S_i^{(GL)})^{-1} \Sigma_i^{-1} (S_i^{(GL)})^{-1} (A_i^{(GL)})^T \hat{\Sigma}_i[\mathbf{X}] \big] \Big] \\ &- \log c_1 + \sum_{j=1}^{P} \lambda_\phi (\phi_{ij}^{(L)})^2 \\ &- \log c_2 + \sum_{j=1}^{n} \lambda_s (s_{ij}^{(L)})^2 \\ &- \log c_3 + \lambda_{\mathbf{b}} \mathbf{b}^{\mathbf{T}} \mathbf{b}, \end{aligned} \tag{6.67}$$

with respect to both local and global transformation parameters. The c_1, c_2 and c_3 are terms not involving transformation parameters, P is the number of angles in the transformation, D the problem's dimension, $\lambda_\phi = 1/(2\sigma_\phi^2)$, $\lambda_s = 1/(2\sigma_s^2)$ and $\lambda_s = \sigma_{\mathbf{b}}^2$. Furthermore, $\boldsymbol{y} = [(A_i^{(GL)})^T E_i[\mathbf{X}] - \boldsymbol{\mu}_i - (A_i^{(GL)})^T \mathbf{b}]$. The expectation $E_i[\mathbf{X}]$, as well as $E_i[\mathbf{X}\mathbf{X}^T]$ calculated in the **E**-step, are now defined as:

$$E_j[\mathbf{X}] = \frac{\sum_{i=1}^{n} \mathbf{x}_i P(\mathbf{x}_i | A_i^{(GL)} \boldsymbol{\mu}_j + \mathbf{b}, \Gamma_i^T \Sigma_j \Gamma_i)}{\sum_{i=1}^{n} \sum_{k=1}^{L} P(\mathbf{x}_i | A_i^{(GL)} \boldsymbol{\mu}_k + \mathbf{b}, \Gamma_i^T \Sigma_k \Gamma_i)}, \tag{6.68}$$

$$E_j[\mathbf{X}\mathbf{X}^T] = \frac{\sum_{i=1}^{n} \mathbf{x}_i \mathbf{x}_i^T P(\mathbf{x}_i | A_i^{(GL)} \boldsymbol{\mu}_j + \mathbf{b}, \Gamma_i^T \Sigma_j \Gamma_i)}{\sum_{i=1}^{n} \sum_{k=1}^{L} P(\mathbf{x}_i | A_i^{(GL)} \boldsymbol{\mu}_k + \mathbf{b}, \Gamma_i^T \Sigma_k \Gamma_i)}, \tag{6.69}$$

$$\Gamma_i \equiv S_i^{(GL)} A_i^{(GL)}. \tag{6.70}$$

The update equation of the global transformation parameters, taking place in the **M**-step, is similar to those presented in Section 6.3.2. The only changes are the definition of the matrices A_j^c, A_j^s, and A_j^k defined in Eqs. (6.71),(6.71) and (6.71), respectively:

$$\begin{aligned} A_{ji}^c &= (R_{P,i}^{(GL)})^T \cdots I_j^T (R_{j,i}^{(L)})^T \cdots (R_{1,i}^{(GL)})^T (S_i^{(GL)})^{-1}, \\ A_{ji}^s &= (R_{P,i}^{(GL)})^T \cdots J_j^T (R_{j,i}^{(L)})^T \cdots (R_{1,i}^{(GL)})^T (S_i^{(GL)})^{-1}, \\ A_{ji}^k &= (R_{P,i}^{(GL)})^T \cdots K_j^T (R_{j,i}^{(L)})^T \cdots (R_{1,i}^{(GL)})^T (S_i^{(GL)})^{-1}, \end{aligned}$$

where j refers to the j-th rotation angle, whereas i to the i-th component.

Furthermore in all equations presented for the global transformation we should replace the transformation parameters with the new ones containing both global and local transformations. We proceed with the update equations of the local transformations.

Translation vector

Taking the derivative of the log-likelihood (6.67) with respect to the translation vector $\mathbf{b}^L$ and setting the derivative to zero we obtain the following update equation:

$$\mathbf{b}_i^L = (C_i + \lambda'_\phi I)^{-1} D_i, \tag{6.71}$$

where $\lambda'_{\mathbf{b}} I) = 1/(\sigma_{\mathbf{b}}^2)$, and C_i, D_i are defined as:

$$C_i = \left[\Sigma_i^{-1}\Gamma_i^{-1}\right], \tag{6.72}$$

$$D_i = \left[\Sigma_i^{-1}\Gamma_i^{-1}(E_i[\mathbf{X}] - A_i^{(GL)}\boldsymbol{\mu}_i - \mathbf{b}^{(\mathbf{G})})\right], \tag{6.73}$$

where Γ_i defined in Eq. (6.70).

Taking the derivative of the log-likelihood with respect to the scale $\mathbf{s}_{ij}^{(L)}$ of the i-th component at j-th dimension and setting the derivative to zero, we obtain:

$$(\mathbf{s}_{ij}^{(L)})^2 + (b + \lambda_s)\mathbf{s}_{ij}^{(L)} + c - \lambda_s = 0, \tag{6.74}$$

where a, b and c are defined as:

$$a = 1, \tag{6.75}$$

$$b = \boldsymbol{y}_{ij}^T \boldsymbol{y}_{ij} + tr[(A_i^{(GL)})^T S_i^{1j} \Sigma_j S_i^{2j} A_i^{(GL)} \hat{\Sigma}_i[\mathbf{X}]], \tag{6.76}$$

$$c = \boldsymbol{x}_{ij}^T \boldsymbol{x}_{ij} + tr[(A_i^{(GL)})^T S_i^{2j} \Sigma_j S_i^{2j} A_i^{(GL)} \hat{\Sigma}_i[\mathbf{X}]. \tag{6.77}$$

In the above equations $\boldsymbol{x}_{ij}$ and $\boldsymbol{y}_{ij}$ are defined as:

$$\boldsymbol{x}_{ij} = L_i S^{1j} \left[(A_i^{(GL)})^T (E_i[\mathbf{X}] - \mathbf{b}_i^{GL}) - \boldsymbol{\mu}_i\right], \tag{6.78}$$

$$\boldsymbol{y}_{ij} = L_i S^{2j} \left[(A_i^{(GL)})^T (E_i[\mathbf{X}] - \mathbf{b}_i^{GL}) - \boldsymbol{\mu}_i\right], \tag{6.79}$$

The matrices S^1 and S^2 are defined as:

$$(S_p^{1k})_{ij} = \begin{cases} s_{kp}^{GL}, \text{ if } i = j \neq k \\ 0, \text{ otherwise} \end{cases}, \tag{6.80}$$

$$(S_p^{2k})_{ij} = \begin{cases} s_{kp}^{G}, \text{ if } i = j = k \\ 0, \text{ otherwise} \end{cases}. \tag{6.81}$$

Similarly to Eq. (6.24), Eq. (6.74) has two possible solutions for $\mathbf{s}_{ij}^{(L)}$: one negative and one positive. We again select the positive one.

Rotation angles

In a similar derivation as that of Section 6.3.2 we obtain an equation of the following form:

$$a\cos(2\phi_{ij}^{(L)}) + b\sin(2\phi_{ij}^{(L)}) + c\cos(\phi_{ij}^{(L)}) + d\sin(\phi_{ij}^{(L)}) + \lambda'_{\phi}(\phi_{ij}^{(L)}) = 0, \tag{6.82}$$

where $\lambda'_{\phi} = 1/(\sigma_{\phi}^2)$ and

$$\begin{aligned} a &= \big[(\boldsymbol{x}_{ij}^T\boldsymbol{x}_{ij} - \boldsymbol{y}_{ij}^T\boldsymbol{y}_{ij}) \\ &+ tr(A_j^c\Sigma_i^{-1}A_j^c\hat{\Sigma}_i[\mathbf{X}]) \\ &- tr(A_j^s\Sigma_i^{-1}A_j^s\hat{\Sigma}_i[\mathbf{X}])\big], \end{aligned} \tag{6.83}$$

$$b = 2[\boldsymbol{x}_{ij}^T\boldsymbol{y}_{ij} + tr(A_j^sS_i^{-1}A_j^c\hat{\Sigma}_i[\mathbf{X}])], \tag{6.84}$$

$$c = 2[\boldsymbol{x}_{ij}^T(\boldsymbol{z}_{ij} + \boldsymbol{w}_i)]\sin(\phi_j), \tag{6.85}$$

$$d = -2[\boldsymbol{y}_{ij}^T(\boldsymbol{z}_{ij} + \boldsymbol{w}_i)]\cos(\phi_j). \tag{6.86}$$

The vectors $\boldsymbol{x}_{ij}, \boldsymbol{y}_{ij}, \boldsymbol{z}_{ij}$ and $\boldsymbol{w}_i$ are defined as:

$$\boldsymbol{x}_{ij} = L_i^TA_j^c(E_i[\mathbf{X}] - \mathbf{b}_i^{GL}), \tag{6.87}$$

$$\boldsymbol{y}_{ij} = L_i^TA_j^s(E_i[\mathbf{X}] - \mathbf{b}_i^{GL}), \tag{6.88}$$

$$\boldsymbol{z}_{ij} = L_i^TA_j^k(E_i[\mathbf{X}] - \mathbf{b}_i^{GL}), \tag{6.89}$$

$$\boldsymbol{w}_i = L_i^T\boldsymbol{\mu}_i, \tag{6.90}$$

The non-linear Eq. 6.82 is also solved using the Levemberg-Marquardt method. The MAP-EM algorithm estimating both global and local transformations is given in Algorithm 3.

Prior distribution on local transformation parameters

The variance in the prior distribution of the transformation parameters is the parameter governing the freedom given on those parameters. If we use a vary large variation then the model diverges from the initial assumption of a geometric transformation of an initial

while $\|\mathbf{\Theta}^k - \mathbf{\Theta}^{k-1}\| < \epsilon$ **do**
E-step: Calculate expected statistics.
M-step:
Update all global rotations $\phi_i^{(G)}$ using the solution of Eq. (6.46).
Update all global scale coefficients $s_i^{(G)}$ using Eq. (6.30).
Update all local rotations $\phi_{ij}^{(L)}$ using the solution of Eq. (6.82).
Update all local scale coefficients $s_{ij}^{(L)}$ using the positive solution of Eq.(6.74).
Update global translation $\mathbf{b^{(G)}}$ using Eq. (6.21).
Update local translations $\mathbf{b_i^{(L)}}$ using Eq. ().
$k = k + 1$

Algorithm 3: Global/Local MAP-EM

population. Each component will probably converge to the closest component of the new population. On the other hand, using a very small initial variance, we restrict the model and we are in-fact neglicting local transformation parameters. A desired behavior would be, if initially we restrict the local transformation parameters and progressively, while the global transformation converges to the actual solution, loose the constraints and allow the adaption of the local parameters as well. This behavior can be achieved using a iteration varying λ defined as:

$$\lambda_k = \lambda_0 \exp(-\gamma k) + \lambda_0'. \tag{6.91}$$

The parameters λ_0, λ_0' and γ for each prior distribution are experimentally chosen. The γ parameter in a large degree defines the behavior of the algorithm, outlined in Algorithm 3. If γ is large then the constraints are quickly dropped and this algorithm is equivalent with an algorithm where at each iteration we seek for both local and global transformation parameters without constraints. On the other hand if γ is very small and we also have implied large constraints λ_0 the algorithm initially fits the global transformation, and after a large number of iterations starts to fit the local ones.

6.6 Results

We performed a series of experiments in order to investigate the estimation of the transformation parameters, using the EM approach and the multiple-start EM for the global transformation cases, as well as experiments for the MAP-EM approach for estimating both local and global transformations.

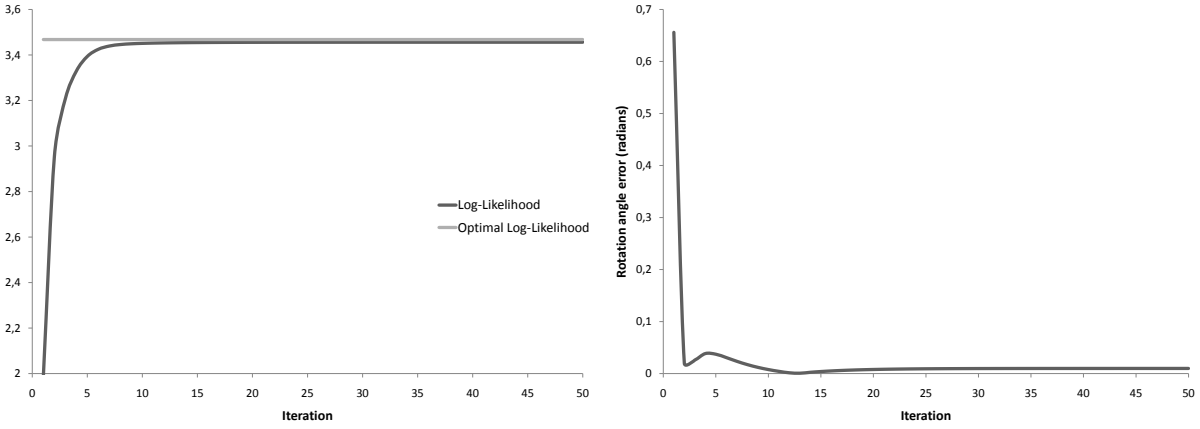

(a) (b)

Figure 6.2: (a) The log-likelihood of the estimated model and the log-likelihood of the actual one and (b)the rotation error, vs the number of iterations, for a 2D problem with three components.

6.6.1 EM approach

A 2D problem is initially studied with three mixture components. The parameters of the initial mixture component are:

$$\mu_{\mathbf{1}} = \begin{bmatrix} 0 \\ 0 \end{bmatrix}, \mu_{\mathbf{2}} = \begin{bmatrix} 2 \\ 2 \end{bmatrix}, \mu_{\mathbf{2}} = \begin{bmatrix} 5 \\ 0 \end{bmatrix}$$

and

$$\mathbf{\Sigma_1} = \mathbf{\Sigma_2} = \mathbf{\Sigma_3} = \begin{bmatrix} 1 & -0.2 \\ -0.2 & 1 \end{bmatrix}.$$

The transformation parameters $\mathbf{\Theta}^*$, which transformation is applied to the initial mixture model, are:

$$\{\mathbf{\Theta}^*\} = \left\{ \begin{array}{c} \phi = 60^\circ \\ \beta_1 = 10 \\ \beta_2 = 10 \\ s_1 = 1.5 \\ s_2 = 1.5 \end{array} \right\}.$$

In Fig. 6.2(a) we present the log-likelihood of the estimated model for each iteration step. For comparison we also provide the log-likelihood of the target model. We observe a fast convergence for the specific case, with an expected monotonically increase in the estimated model's log-likelihood. The fast convergence to the correct model is also demonstrated by the rotation angle error depicted in Fig. 6.2(b).

Next we examine a 3D case and a GMM with five components. The original component means are randomly sampled as:

$$\mu_i \in [0, 40] \text{ and } \|\mu_i - \mu_j\| > 15 \text{ for } i, j \in \{1...L\}, i \neq j,$$

And the covariance of all components was:

$$\mathbf{\Sigma_i} = \begin{bmatrix} 1 & -0.3 \\ -0.3 & 1 \end{bmatrix}. \text{ for } i \in \{1...L\}$$

We must notice here that the rotation matrix A used in this case was:

$$\begin{aligned} A &= R_x(\phi_x) \cdot R_y(\phi_y) \cdot R_z(\phi_z), \qquad (6.92) \\ R_x(\phi_x) &= \begin{pmatrix} 1 & 0 & 0 \\ 0 & \cos\phi_x & -\sin\phi_x \\ 0 & sin\phi_x & \cos\phi_x \end{pmatrix}, \\ R_y(\phi_y) &= \begin{pmatrix} \cos\phi_y & 0 & -\sin\phi_y \\ 0 & 1 & 0 \\ \sin\phi_y & 0 & \cos\phi_y \end{pmatrix}, \\ R_z(\phi_z) &= \begin{pmatrix} \cos\phi_z & -\sin\phi_z & 0 \\ \sin\phi_z & \cos\phi_z & 0 \\ 0 & 0 & 1 \end{pmatrix}. \end{aligned}$$

In the examined case $\phi_x = \phi_y = \phi_z = \pi/4$, the scale coefficients were all set to 2 and translation vector $\mathbf{b}$ uniformed sampled at $[0, 50]$.

In Figs. (6.3(a)), (6.3(b)) we present the log-likelihood of the estimated model and the rotation error for the three angles in Eq. (6.92). The method also proved to correctly converge to the actual transformation parameters. We observe that the convergence is slower compared to the 2D case, which is due to higher problem's complexity and mixture component overlapping.

In order to test the robustness of the algorithm with respect to the distance of the initial guess and actual value of the parameters, we examine a 2D and a more complex 5D case.

(i) *2D case*: The varying parameters in the first experiment are the number of components and the rotation angle (a unique parameter in $2D$ case). Each mixture component is equally sampled with 500 samples ($\pi_i = \frac{1}{L}$, for $i = 1, \cdots L$). The covariance of the components are spherical and fixed to $\Sigma_i = I$, for $i = \{1, ...L\}$. The mean of the components is randomly selected according to:

$$\mu_i \in [0, 100] \text{ and } \|\mu_i - \mu_j\| > 20 \text{ for } i, j \in \{1...L\}, i \neq j. \qquad (6.93)$$

The translation and scale vectors are also randomly selected: the first in the range $[-10, 10]$ and the second in the range $[1, 3]$. In Fig. 6.4(a) we present the rotation error

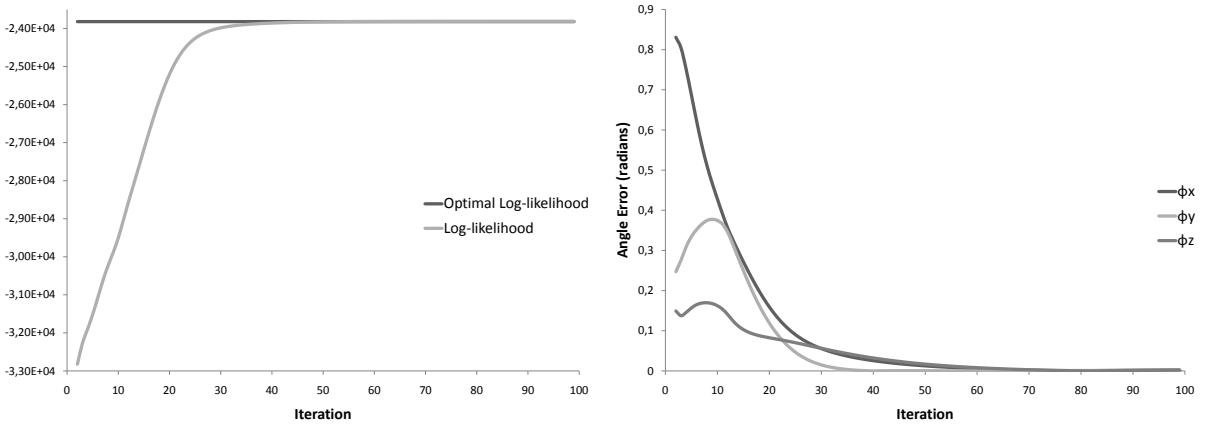

(a) (b)

Figure 6.3: (a) The log-likelihood of the estimated model and the log-likelihood of the actual one and (b)the rotation error, vs the number of iterations, for a 3D problem with five components.

$|\phi^{EM} - \phi^*|$ as a function of true rotation angle ϕ^*. ϕ^{EM} is the estimation of the rotation angle.

(ii) *5D case*: A similar series of experiments is conducted for a 5D problem. The varying parameters are again the number of components and the rotation angles (all angles have the same value). We should notice that the rotation matrix adopted for the 5D case is of the form described in Eq. (6.36) and thus we have four rotation angles. The covariance of the components is spherical and fixed to $\Sigma_i = I,$ for $i = \{1, ...L\}$. The mean of the components are randomly selected according to:

$$\mu_i \in [0, 100] \text{ and } \|\mu_i - \mu_j\| > 20 \text{ for } i, j \in \{1...L\}, i \neq j.$$

The translation and scale vectors are also randomly selected, the first in the range $[-10, 10]$ and the second in the range $[1, 3]$. In Fig. 6.4(b) the rotation error $|\phi^{EM} - \phi^*|$ as a function of true rotation angle ϕ^* is presented. ϕ^{EM} is the estimation of the rotation angle.

6.6.2 Multiple start EM approach

A number of experiments are conducted using the *msEM*. We examine 2D, 3D and 4D problems, since for higher dimensionality problems the possible number of initializations becomes very large. We examine the effect of the overlapping of the initial mixture model in the performance of the algorithm, as well as the K parameter of the EM-algorithm. The number of the components is equal to the dimension of the problem in all cases. We expect that with higher K and less overlapping between the mixture components, the algorithm must perform better. The overlapping between the components is split in 5 ranges according to the min and max distance between components $L_1 \leq \|\mu_i - \mu_j\|] \leq$

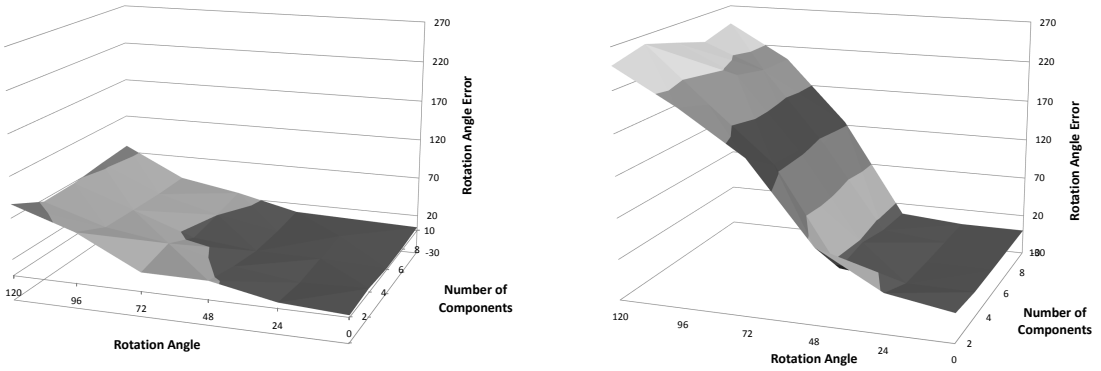

(a) (b)

Figure 6.4: (a) The estimated rotation error for a 2D case as a function of the mean component distance and the rotation angle of the new mixture model, and (b) the estimated rotation error for a 5D case as a function of the mean component distance and the rotation angle of the new mixture model.

L_2 for $i, j = \{1, ...L\}, i \neq j$, where $L_1 \in \{0.5, 1, 2, 3, 5\}$ and $L_2 \in \{1, 1.5, 3, 5, 10\}$ In Fig. 6.5 we show that overlapping $e(\mathbf{M})$ is a function of the distance between components (with fixed covariance matrices). For each case (dimension, number of initialization and initial distance between components) we run 100 cases with an initial rotation angles $2\pi/5$, translation vectors uniform sampled in the space $[0, 10]$ and scales uniform sampled in the space $[1, 3]$. The average rotation, translation and scale errors, as well as the average likelihood are given in Table 6.2. Furthermore, in Fig. 6.6 we show graphically the rotation error and the translation error, in order to provide a better overview of the method behavior as a function of the problem's dimensionality, overlapping and number of initializations. We observe that the rotation error is increased with higher dimensionality and overlapping. Increasing the number of initializations the error is reduced, which is explained, since with more trials starting from different locations, the probability of finding the global minimum, i.e. the correct solution, is higher. A similar behavior is observed in the translation error. The only difference is that translation error is increased with less overlapping, i.e. larger distance between components. The larger the distance between components, the larger the expected translation error in case of wrong solution identification.

6.6.3 MAP-EM approach for global and local transformation

We next examine the convergence of the MAP-EM method for estimating both global and local transformations, for a 2D case.

We test the impact of the parameter γ on the correct solution identification. In this

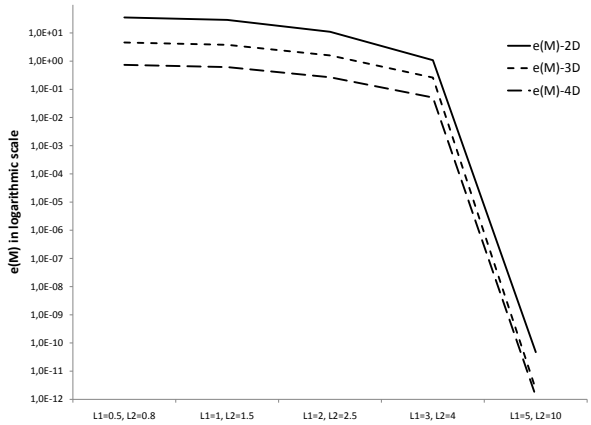

Figure 6.5: $e(M)$ as a function of the distance between the components $L_1 \leq \|\mu_i - \mu_j\|] \leq L_2$ for $i = \{1, ...L\}, i \neq j$, for 2D, 3D and 4D problems (the $e(M)$ axis is in logarithmic scale).

example we only allow local rotations, in order to have a more restricted problem. For the local rotations, $\lambda^k = 50e^{-\gamma \cdot k} + 1$ and $\gamma \in [0.01, 0.02, 0.05, 0.07, 1, 5]$. We have 20 initial components with randomly distributed means according to:

$$\mu_i \in [0, 80] \text{ and } \|\mu_i - \mu_j\| > 15 \text{ for } i, j \in \{1...L\}, i \neq j.$$

and identity covariance matrices for all components. In Fig. 6.7(a) we present the mean squared error of the estimation of the new components. We observe that for this example and for $\gamma < 1$, the error is relatively small and the estimated components, correspond to the true ones. For $\gamma > 1$ the model converges to false components. Furthermore, in Fig. 6.7(b) we demonstrate the average error in the estimation of both local and global rotations at each iteration, for $\gamma < 1$. We observe a similar behavior, however for larger γ faster convergence was achieved, as expected.

Table 6.2: (a) The rotation error (R), (b) the scaling error (S), (c) the translation error (T) and (d) difference of the estimated log-likelihood from the actual models.

	$L_1 = 0.5, L_2 = 0.8$				$L_1 = 1, L_2 = 1.5$				$L_1 = 2, L_2 = 2.5$			
	R	S	T	L	R	S	T	L	R	S	T	L
2D/1	46.4	0.81	1.68	-8502	43.34	0.74	2.41	-8233	45.32	0.8	3.77	-8625
2D/2	28.94	0.54	0.97	-81874	21.78	0.39	1.13	-8394	12.94	0.23	1.49	-8638
3D/1	105.78	1.25	2.04	-18575	107.52	1.17	2.71	-18789	107.64	1.14	6	-19276
3D/2	52.78	0.68	1.55	-18440	50.58	0.7	2.18	-18590	47.83	0.65	3.71	-19397
3D/4	25.21	0.34	0.79	-18264	19.05	0.23	0.74	-18376	8.46	0.12	0.88	-19615
4D/1	108.91	1.33	3.19	-32499	109.7	1.3	5.26	-32912	114.58	1.28	9.59	-34441
4D/2	38.05	0.42	1.26	-32547	42.66	0.55	2.35	-32838	54.7	0.58	5.35	-33654
4D/3	8.33	0.09	0.5	-32584	4.86	0.07	0.47	-32623	8.22	0.11	1.17	-33948
	$L_1 = 3, L_2 = 4$				$L_1 = 5, L_2 = 10$							
	R	S	T	L	R	S	T	L				
2D/1	28.18	0.59	4.41	-9133	1.36	0.08	2.17	-9720				
2D/2	6.88	0.13	0.95	-8912	0.3	0.04	0.13	-9534				
3D/1	93.96	1.09	9.03	-20732	54.68	2.24	19.94	-24330				
3D/2	28.49	0.33	3.9	-20362	4.39	0.1	2.27	-21725				
3D/3	6.92	0.1	1.16	-20340	1.29	0.05	0.77	-21654				
4D/1	111.82	1.38	14.63	-36394	80.2	3.36	30.62	-44601				
4D/2	35.97	0.52	6.68	-35687	16.18	0.47	9.81	-38659				
4D/3	8.71	0.12	2.01	-35610	3.39	0.07	2.82	-37974				

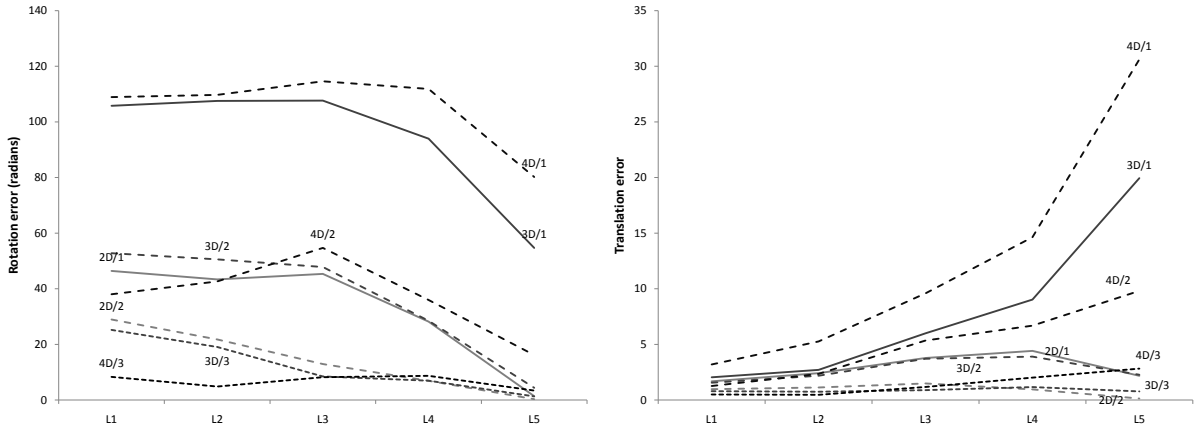

(a) (b)

Figure 6.6: (a) The estimated rotation error, and (b) the estimated translation error for 100 runs of different dimension problems with different initial distance between mean of the components. In the legend notation aD/b, a denotes the problem's dimension and b the number of angle space splits.

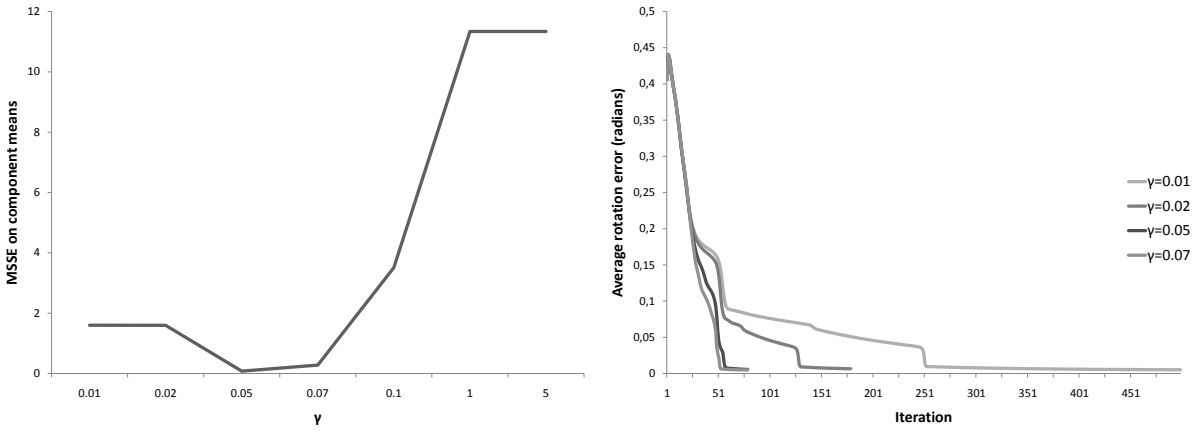

(a) (b)

Figure 6.7: (a) The mean squared error on the estimation of the component means as a function of the γ. (b) The rotation angle error for each iteration step for different γ.

6.7 Application to new driver adaptation

The problem as defined before and the methodology presented may be applied on a variety of applications, such as image and point set registration, tracking etc. However the problem related with this thesis is the adaptation of an initial model, designed to discriminate driver states, to new drivers. We can use the following two approaches:

1. Use a GMM model for classification, where each component is assigned for each driver state of interest.

2. Use an arbitrary classifier, trained on the original feature space $\mathbf{F} \in \mathfrak{R}^D$, where D the number of features. We approximate the feature space density as a GMM model with arbitrary number of components. In order to estimate the number of components and the parameters we could use the approach presented in [21]. We assume that the new feature space (e.g. the physiological features of the new driver) is a space $\mathbf{F}'$ and there is a mapping function f from the original feature space $\mathbf{F}$ to $\mathbf{F}'$:

$$\mathbf{F} \overset{f(\cdot)}{\longrightarrow} \mathbf{F}'. \tag{6.94}$$

   We assume that f consists of global and local transformations described in the previous sections. Using the described methodology we could estimate those transformation parameters and then apply inverse mapping to the original feature space. This approach is described in detail, in section 6.7.2.

For both approaches, the training of the initial classification model (either the GMM model or the arbitrary classifier) is based on *supervised learning*, where for every sample we are also aware of the target class, whereas the adaptation procedure is based on *unsupervised learning*, where the target class of each sample is not available. In the following sections, we demonstrate the two approaches, the first using real drivers data and the second one on both real and artificial data.

6.7.1 Application on real data

In this section we demonstrate the application of the described methodology where we assume a GMM based classifier. We used the simulation dataset, where one subject was used for training whereas a second subject was used for testing. We are restricted to two only subjects since those two subjects had sufficient data, for both states (*fatigue* and *normal*) in order to apply the method. In the examined case the *low fatigue* and *high fatigue* are merged in one class (*fatigue*), due to limited data from the *high fatigue* class. The physiological features used, are the mean heart rate and the std of RR intervals, extracted at 5 minute intervals. Those features proved to be very indicative of fatigue state (see Chapter 4), and the restriction to a 2D feature space allows an easier visualization of the GMM models.

In Figs. 6.8(a), 6.8(b) we present the distribution of the features for the the two subjects. The GMM model has two components, the first describing the feature space

for the *normal* state (C_1) and the second one describing the feature space for the *fatigue* state (C_2). The GMM parameters are estimated using the following equations:

$$\mu_{\mathbf{1}} = \frac{1}{|\mathbf{x} \in \mathbf{C_1}|} \sum_{\mathbf{x} \in \mathbf{C_1}} \mathbf{x}, \tag{6.95}$$

$$\Sigma_1 = \frac{1}{|\mathbf{x} \in \mathbf{C_1}|} \sum_{\mathbf{x} \in \mathbf{C_1}} (\mathbf{x} - \mu_{\mathbf{1}})(\mathbf{x} - \mu_{\mathbf{1}})^{\mathbf{T}}, \tag{6.96}$$

$$\mu_{\mathbf{2}} = \frac{1}{|\mathbf{x} \in \mathbf{C_2}|} \sum_{\mathbf{x} \in \mathbf{C_2}} \mathbf{x}, \tag{6.97}$$

$$\Sigma_2 = \frac{1}{|\mathbf{x} \in \mathbf{C_2}|} \sum_{\mathbf{x} \in \mathbf{C_2}} (\mathbf{x} - \mu_{\mathbf{2}})(\mathbf{x} - \mu_{\mathbf{2}})^{\mathbf{T}}, \tag{6.98}$$

where $\mu_{\mathbf{1}}$, $\mu_{\mathbf{2}}$ the mean of the first and second component, respectively, whereas Σ_1, Σ_2 the covariance of the first and second component, respectively. $\mathbf{x} \in \mathbf{C_1}$ and $\mathbf{x} \in \mathbf{C_2}$ are the samples belonging to *normal* and *fatigue* classes respectively, whereas $|\mathbf{x} \in \mathbf{C_1}|$ and $|\mathbf{x} \in \mathbf{C_2}|$ the number of samples belonging to each class respectively. In order to assign a new sample $\mathbf{x}$ to a specific class we use the following Bayesian criterion:

$$C(x) = \begin{cases} C_1, p(x|C_1)p(C1) > p(x|C_2)p(C_2) \\ C_2, \text{ otherwise} \end{cases}, \tag{6.99}$$

where $p(x|C_1) = \mathbf{N}(\mu_1, \Sigma_1)$, $p(x|C_2) = \mathbf{N}(\mu_2, \Sigma_2)$, and $p(C_1)$, $p(C_2)$ the prior probabilities of each state, extracted from the annotated data.

In the two approaches examined, the GMM model is fitted to the data of the first subject and then this initial model is adapted to the second subject's data, using: i) the global transformation approach, ii) global and local transformations approach. The results of the adaptation are depicted in Figs. 6.8(c) and 6.8(d), respectively. In Table 6.3 we present the classification results (confusion matrix, sensitivity, specificity and accuracy) for both approaches. For comparison reasons, we also present the results of fitting the GMM on the data of the second subject using the labeled data and the Eqs. 6.95-6.98, which can be considered as the training error of a *supervised* method. We observe that the global and local transformation approach gives slightly better results than the global transformation approach. The error of 17% achieved with the global and local transformation approach is relatively small, considering it as the generalization error, and taking into account that the training error was 12%. This justifies the assumption that at least for specific features, the feature space between different subjects can be described under the geometric transformation assumption, and furthermore this method can achieve very good generalization results.

6.7.2 Use of an arbitrary classifier and GMM for density estimation

In this section we describe the second approach, where an arbitrary classifier is built upon a original dataset, and a GMM model with L components is used to model the

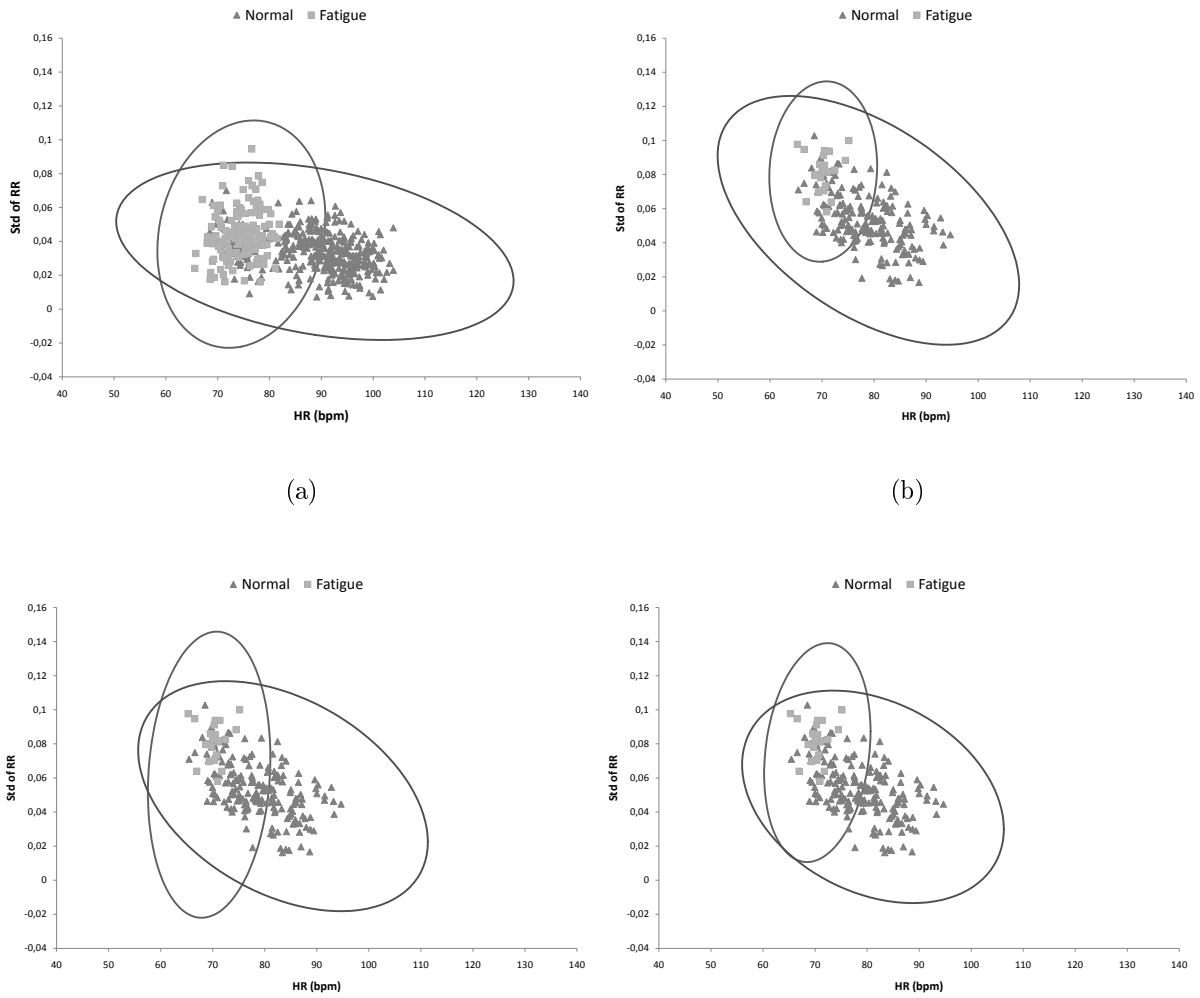

Figure 6.8: (a) The feature space of the first subject and the fitted Gaussian components using labeled data. (b)-(c)-(d) The feature space of the second subject with (b) the fitted Gaussian components using labeled data, (c) the GMM model of the first subject adapted based on global transformation and (d) the GMM model of the first subject adapted based on both global and local transformations

density of the original dataset. The basic idea of this approach is that instead of trying to adapt the parameters of a classifier on a new data, which in some cases could be very complicated, we could map the data to the classifier's parameters. A common technique in this direction is the normalization of the data, either using the min-max normalization or the standardization of the data. However those approaches do not use any prior information about the data distribution and they cannot handle changes occurring in specific regions of the feature space. Our approach could overcome these limitations.

We first demonstrate the above method in an artificial dataset. This dataset consists of a 2D GMM with three components. Each component corresponds to different class.

Table 6.3: The classification results for: (*GMM*) learn a GMM using the class labels of the second subject, (*G. Trans.*) fit a GMM on the data of the first subject and adapt on the second subject's data using the global transformation approach and (*G.L. Trans.*) fit a GMM on the data of the first subject and adapt on the second subject's data using the global and local transformations approach.

	GMM		*G. Trans.*		*G.L. Trans.*	
	Normal	*Fatigue*	*Normal*	*Fatigue*	*Normal*	*Fatigue*
Classified as *Normal*	20	22	22	39	22	36
Classified as *Fatigue*	2	165	0	148	0	151
Sensitivity	0.91	0.88	1	0.79	1	0.81
Specificity	0.48	0.99	0.36	1	0.38	1
Accuracy	**89**%		**81**%		**83**%	

The mean and covariance of each component are properly selected in order to give a well seperated classification problem. For each component we produce 300 samples. Then we produce a new dataset transforming the original dataset:

$$\mathbf{x}'_{ij} = A_j^{(GL)}\mathbf{x}_{ij} + \mathbf{b}_j^{(GL)}, \tag{6.100}$$

where $\mathbf{x}_{ij}$ the i-th sample coming from the j-component.

$$A_1^{(GL)} = \begin{pmatrix} 0.39 & -0.92 \\ 0.92 & 0.39 \end{pmatrix} \tag{6.101}$$

$$A_2^{(GL)} = \begin{pmatrix} 0.68 & -0.73 \\ 0.73 & 0.68 \end{pmatrix} \tag{6.102}$$

$$A_3^{(GL)} = \begin{pmatrix} 0.63 & -0.78 \\ 0.78 & 0.63 \end{pmatrix} \tag{6.103}$$

$$\mathbf{b_1^{(GL)}} = \begin{pmatrix} 1.88 \\ 1.51 \end{pmatrix} \tag{6.104}$$

$$\mathbf{b_2^{(GL)}} = \begin{pmatrix} 1.56 \\ 2.27 \end{pmatrix} \tag{6.105}$$

$$\mathbf{b_3^{(GL)}} = \begin{pmatrix} 1.87 \\ 2.12 \end{pmatrix} \tag{6.106}$$

After estimating $A_j^{(GL)}$ and $\mathbf{b_j^{(GL)}}$ we can map the $\mathbf{X}'$ in the original space $\mathbf{X}$ using the following:

$$\mathbf{x}''_i = \frac{\sum_{j=1}^{L} p(\mathbf{x}_i|C_j)((A_j^{(GL)})^{-1}(\mathbf{x}_i - \mathbf{b_j^{(GL)}}))}{\sum_{j=1}^{L} p(\mathbf{x}_i|C_j)} \tag{6.107}$$

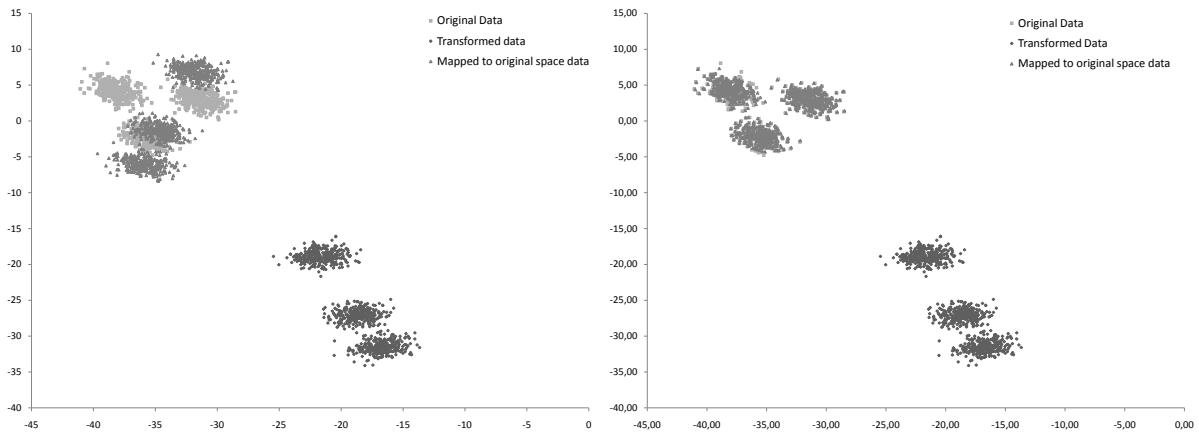

(a) (b)

Figure 6.9: In the above figure, we present the original population $\mathbf{X}$, the transformed population $\mathbf{X}'$ and the mapped to the original space population $\mathbf{X}''$ using (a) global transformation (b) global and local transformations.

Table 6.4: The classification results for the artificial dataset, using inverse mapping with global transformation and using both global and local transformations.

	G. trans.			*G.L. trans.*		
	C_1	C_2	C_3	C_1	C_2	C_3
Classified as C_1	0	4	0	299	0	0
Classified as C_2	0	296	1	0	300	0
Classified as C_3	300	0	299	1	0	300
Sensitivity	0	0.99	1	1	1	1
Specificity	0	1	0.5	1	1	1
Accuracy		**66**%			**100**%	

The mean squared error of the mapping of $\mathbf{X}''$ to the original population using global transformation is 21.19 (Fig. 6.9(a)), whereas using both global and local transformations is 0.04 (Fig. 6.9(b)). This is also depicted in the classification performance. Using a Naive Bayes model trained in the original population, the classification error on the dataset produced by the inverse mapping using the global transformation was 33.89%, whereas using both global and local transformations, the error was 0.1%. The results are presented in detail in Table 6.4.

We also applied the above methodology on the previous problem with the real driver's data. We again used the same data described in the previous section. We present the results of four different approaches, for comparison purposes:

A1 10-cross validation on the data of the first subject, using the SVM classifier.

A2 (a) Train an SVM with the original data of the first subject. (b) Fit a GMM model

with two components to the data of the first subject. (c) Fit the GMM model of the first subject to the data of the second subject using only the global transformation approach. (d) Apply the inverse mapping using Eq. 6.107. (e) Test using the new mapped data.

A3 (a) Train an SVM with the original data of the first subject. (b) Fit a GMM model with two components on the data of the first subject. (c) Fit the GMM model of the first subject to the data of the second subject using the approach with both global and local transformations. (d) Apply the inverse mapping using Eq. 6.107. (e) Test using the new mapped data.

A4 (a) Normalize the data of the first subject. (b) Train an SVM classifier using the normalized data of the first subject. (c) Normalize the data of the second subject. (d) Test using the normalized data of the second subject. For normalization we used the min-max approach for each feature:

$$x' = \frac{x - x_{min}}{x_{max} - x_{min}}, \tag{6.108}$$

where x_{min} and x_{max}, the minimum and maximum value of the feature, respectively.

In all cases we use radial basis function (RBF) kernel for the SVM. In order to fit a GMM model on the original data density, we need to estimate the number of mixture components as well as each component's parameters. We use the method presented in [21], which gives very good results (the estimated number of components was two).

In Table 6.5 we present the confusion matrix, specificity and accuracy per class, as well as the accuracy of the classifier. We observe that the approach using both local and global transformations outperforms dramatically the approach using the simple min-max normalization. Moreover, compared to the global transformation approach, although it has lower accuracy, the error is better balanced between the two classes. Furthermore, compared to the approach presented in the previous section, the SVM gives better results for the global and local transformation approach. The advantage of the use of a more complicated classifier compared to GMM, is expected to be greater in more complex problems, with more features.

6.8 Discussion

In this work we initially addressed the problem of estimating the parameters of a GMM from a sample, which is a geometric transformation of an original, considered known, GMM. The method proposed here is based on the EM framework. We considered both cases of full positive definite and spherical covariance matrices. The main difference from other similar approaches presented in the literature is first that no restrictions are assumed on the covariance matrix and second that we examined a rather generic transformation matrix, which is a product of elementary rotation and scaling matrices. We examined the

Table 6.5: The classification results of the four approaches (**A1**, **A2**, **A3** and **A4**) for evaluating the performance of different mapping methods of the data of new drivers, to the original space where the classifier is trained.

	A1		**A2**	
	Normal	*Fatigue*	*Normal*	*Fatigue*
Classified as *Normal*	137	60	13	10
Classified as *Fatigue*	17	134	9	177
Sensitivity	0.89	0.84	0.59	0.95
Specificity	0.7	0.95	0.57	0.95
Accuracy	**85**%		**91**%	
	A3		**A4**	
	Normal	*Fatigue*	*Normal*	*Fatigue*
Classified as *Normal*	20	26	22	69
Classified as *Fatigue*	2	161	0	118
Sensitivity	0.91	0.86	1	0.63
Specificity	0.43	0.99	0.24	1
Accuracy	**87**%		**67**%	

case of a 3D problem with a full 3D rotation matrix and demonstrated that the estimation of such transformations is feasible with our approach. Next we performed experiments in order to indicate the method's behavior regarding to the dimensionality of the problem, the initial model's and transformation's complexity. Intuitively, the larger the complexity of the problem, the larger the number of the local maxima of the log-likelihood function. Consequently, the larger the complexity of the problem, the smaller the probability that the algorithm converges to the actual solution. In the 2D case, the number of components did not have a significant effect on the rotation error and the correct solution identification. This can be explained in the sense that the problem is quite well-posed, the number of parameters is quite limited (5 parameters) and the number of local maxima is expected to be rather low. The main parameter affecting the correct solution identification is the rotation angle. The algorithm starting from an initial guess of zero rotation, identified the correct solution in cases where the true rotation angle was smaller than $\pi/2$. For larger angles, the algorithm identified the symmetric one. However these two solutions have the same log-likelihood if the covariance matrices are spherical. For 2D problems, such as image registration, this method is expected to give very good results. In higher dimensional problems the number of components has a more significant effect. From the 5D case experiments, we observed that in problems with fewer components than the problem's dimension, we have a larger error in the rotation angles. Moreover, the number of cases that the algorithm did not correctly identify the true solution is higher. We observe that the range where the algorithm gives very good results is in the range of $0-\pi/4$ degrees, compared to $0-\pi/2$ degrees of the 2D case. This is expected, considering the higher number of local maxima in a more complex problem with larger number of

parameters. This problem was tackled using the *msEM*.

Using the *msEM* algorithm (the respective results are summarized in Table 6.2), we observe that even in cases with high mixture overlapping and large rotation angle, the algorithm can identify the correct solution with relatively small error. In 2D cases for $K = 2$ we obtain very good results, which indicate that this value of K is sufficient for 2D problems. In higher-dimension problems, the higher K gives better results, but with inevitable impact on computational cost.

Then we presented an approach for estimating both global and local transformations. This approach could be suitable for example in image registration or tracking where both camera and objects in the scene are moving. Our approach is based on MAP-EM estimation method with progressive relaxing of the constraints on the local transformations. Initial experiments indicated the impact of the relaxing rate on the correct solution estimation.

In the last section we described two different approaches, using the proposed methodology, for the unsupervised adaptation of a classifier to a new sample. The first method adapts the parameters of the classifiers (a GMM model) to the new sample, whereas the second adapts the data to the classifier's parameters, through inverse mapping to the original data space, used for training the classifier. Both methods were evaluated in terms of the adaptation of a classifier for *normal* and *fatigue* states discrimination, trained on a specific subject and adapted to a second one. The data of both subjects were acquired during our simulation experiments. Both methods had similar results, however the use of the second one could be more beneficial in more complex problems. Although our first results are quite promising, more experiments, are required in order to investigate the advantages and disadvantages of each approach as well as to evaluate the proposed method for the adaptation of a driver physiological state recognition system to new drivers.

Appendix A: Solution of $\frac{\partial J}{\partial \phi_j} = 0$ with respect to ϕ_j.

We introduce the following matrices:

$$I_j^{(n\times n)} = \begin{array}{c} \\ j \end{array} \begin{pmatrix} & & \overset{j}{} & & & \\ 0 & \cdots & 0 & 0 & \cdots & 0 \\ \vdots & \ddots & \vdots & \vdots & \iddots & 0 \\ 0 & \cdots & 1 & 0 & \cdots & 0 \\ 0 & \cdots & 0 & 1 & \cdots & 0 \\ \vdots & \iddots & \vdots & \vdots & \ddots & \vdots \\ 0 & \cdots & 0 & 0 & \cdots & 0 \end{pmatrix}, \tag{6.109}$$

$$J_j^{(n\times n)} = \begin{array}{c} \\ j \\ \\ \\ \\ \\ \end{array} \begin{array}{c} \begin{array}{cccccc} & & j & & & \end{array} \\ \begin{pmatrix} 0 & \cdots & 0 & 0 & \cdots & 0 \\ \vdots & \ddots & \vdots & \vdots & \iddots & 0 \\ 0 & \cdots & 0 & 1 & \cdots & 0 \\ 0 & \cdots & -1 & 0 & \cdots & 0 \\ \vdots & \iddots & \vdots & \vdots & \ddots & \vdots \\ 0 & \cdots & 0 & 0 & \cdots & 0 \end{pmatrix} \end{array}, \tag{6.110}$$

$$K_j^{(n\times n)} = \begin{array}{c} \\ j \\ \\ \\ \\ \\ \end{array} \begin{array}{c} \begin{array}{cccccc} & & j & & & \end{array} \\ \begin{pmatrix} 1 & \cdots & 0 & 0 & \cdots & 0 \\ \vdots & \ddots & \vdots & \vdots & \iddots & 0 \\ 0 & \cdots & 0 & 0 & \cdots & 0 \\ 0 & \cdots & 0 & 0 & \cdots & 0 \\ \vdots & \iddots & \vdots & \vdots & \ddots & \vdots \\ 0 & \cdots & 0 & 0 & \cdots & 1 \end{pmatrix} \end{array}. \tag{6.111}$$

We split Eq. () as the sum of two terms:

$$\mathfrak{J} = \sum_i \pi_i(\mathbf{X})[\mathfrak{J}_i^a + \mathfrak{J}_i^b], \tag{6.112}$$

where J_i^b and J_i^a are given by Eqs. (6.32) and (6.33), respectively. J_i^a can be written in an expanded form as:

$$\begin{aligned} \mathfrak{J}_i^a &= \boldsymbol{x}_{ij}^T\boldsymbol{x}_{ij}\cos(\phi_j)^2 + \boldsymbol{y}_{ij}^T\boldsymbol{y}_{ij}\sin(\phi_j)^2 \\ &+ 2\boldsymbol{x}_{ij}^T\boldsymbol{y}_{ij}\cos(\phi_j)\sin(\phi_j) \\ &+ 2\boldsymbol{x}_{ij}^T(\boldsymbol{z}_{ij}+\boldsymbol{w}_i)\cos(\phi_j) \\ &+ 2\boldsymbol{y}_{ij}^T(\boldsymbol{z}_{ij}+\boldsymbol{w}_i)\sin(\phi_j), \end{aligned} \tag{6.113}$$

where $\boldsymbol{x}_{ij}$, $\boldsymbol{y}_{ij}$, $\boldsymbol{z}_{ij}$ and $\boldsymbol{w}_{ij}$ are defined in Eqs. (6.87), (6.88), (6.89) and (6.90), respectively. Taking the derivative of J_i^a with respect to ϕ_j we obtain:

$$\begin{aligned} \frac{\partial\mathfrak{J}_i^a}{\partial\phi_j} &= 2[(\boldsymbol{x}_{ij}^T\boldsymbol{x}_{ij} - \boldsymbol{y}_{ij}^T\boldsymbol{y}_{ij})]\cos(\phi_j)\sin(\phi_j) \\ &+ 2\boldsymbol{x}_{ij}^T\boldsymbol{y}_{ij}\sin(\phi_j)^2 - 2\boldsymbol{x}_{ij}^T\boldsymbol{y}_{ij}\cos(\phi_j)^2 \\ &+ 2\boldsymbol{x}_{ij}^T(\boldsymbol{z}_{ij}+\boldsymbol{w}_i)\sin(\phi_j) \\ &- 2\boldsymbol{y}_{ij}^T(\boldsymbol{z}_{ij}+\boldsymbol{w}_i)\cos(\phi_j) \\ &= (\boldsymbol{x}_{ij}^T\boldsymbol{x}_{ij} - \boldsymbol{y}_{ij}^T\boldsymbol{y}_{ij})]\sin(2\phi_j) \\ &+ 2\boldsymbol{x}_{ij}^T\boldsymbol{y}_{ij}\cos(2\phi_j) + 2\boldsymbol{x}_{ij}^T(\boldsymbol{z}_{ij}+\boldsymbol{w}_i)\sin(\phi_j) \\ &- 2\boldsymbol{y}_{ij}^T(\boldsymbol{z}_{ij}+\boldsymbol{w}_i)\cos(\phi_j). \end{aligned} \tag{6.114}$$

The term $\mathfrak{J}_i^b$ can be written in expanded form as:

$$\begin{aligned}
\mathfrak{J}_i^b &= tr(AS_i^{-1}A\hat{\Sigma}_{ij}[\mathbf{X}]) \\
&= tr(A_j^c S_i^{-1} A_j^c \hat{\Sigma}_{ij}[\mathbf{X}])\cos(\phi_j)^2 \\
&+ tr(A_j^s S_i^{-1} A_j^s \hat{\Sigma}_{ij}[\mathbf{X}])\sin(\phi_j)^2 \\
&+ 2tr(A_j^s S_i^{-1} A_j^c \hat{\Sigma}_{ij}[\mathbf{X}])\cos(\phi_j)\sin(\phi_j) \\
&+ 2tr(A_j^c S_i^{-1} A_j^k \hat{\Sigma}_{ij}[\mathbf{X}])\cos(\phi_j) \\
&+ 2tr(A_j^s S_i^{-1} A_j^k \hat{\Sigma}_{ij}[\mathbf{X}])\sin(\phi_j). \qquad (6.115)
\end{aligned}$$

Then we consider the derivative of $\mathfrak{J}_i^b$ with respect to ϕ_j:

$$\begin{aligned}
\frac{\partial \mathfrak{J}_i^b}{\partial \phi_j} &= (tr(A_j^c S_i^{-1} A_j^c \hat{\Sigma}_{ij}[\mathbf{X}])\sin(2\phi_j) \\
&- tr(A_j^s S_i^{-1} A_j^s \hat{\Sigma}_{ij}[\mathbf{X}])\sin(2\phi_j) \\
&+ 2tr(A_j^s S_i^{-1} A_j^c \hat{\Sigma}_{ij}[\mathbf{X}])\cos(2\phi_j) \\
&+ 2tr(A_j^c S_i^{-1} A_j^k \hat{\Sigma}_{ij}[\mathbf{X}])\sin(\phi_j) \\
&- 2tr(A_j^s S_i^{-1} A_j^k \hat{\Sigma}_{ij}[\mathbf{X}])\cos(\phi_j). \qquad (6.116)
\end{aligned}$$

The last two terms containing the A_j^k matrix, which is defined by Eq. (6.71), give zero in the diagonal, thus we obtain:

$$\begin{aligned}
\frac{\partial \mathfrak{J}^b}{\partial \phi_j} &= (tr(A_j^c S_i^{-1} A_j^c \hat{\Sigma}_{ij}[\mathbf{X}])\sin(2\phi_j) \\
&- tr(A_j^s S_i^{-1} A_j^s \hat{\Sigma}_{ij}[\mathbf{X}])\sin(2\phi_j) \\
&+ 2tr(A_j^s S_i^{-1} A_j^c \hat{\Sigma}_{ij}[\mathbf{X}])\cos(2\phi_j). \qquad (6.117)
\end{aligned}$$

Replacing Eqs. (6.114) and (6.117) in Eq. (6.113) we finally obtain:

$$\begin{aligned}
\frac{\partial \mathfrak{J}}{\partial \phi_i} &= \sum_i n_i[[(\boldsymbol{x}_{ij}^T \boldsymbol{x}_{ij} - \boldsymbol{y}_{ij}^T \boldsymbol{y}_{ij}) + tr(A_j^c S_i^{-1} A_j^c \hat{\Sigma}_{ij}[\mathbf{X}]) \\
&- tr(A_j^s S_i^{-1} A_j^s \hat{\Sigma}_{ij}[\mathbf{X}])]\sin(2\phi_j) \\
&+ 2[\boldsymbol{x}_{ij}^T \boldsymbol{y}_{ij} + tr(A_j^s S_i^{-1} A_j^c \hat{\Sigma}_{ij}[\mathbf{X}])]\cos(2\phi_j) \\
&+ 2[\boldsymbol{x}_{ij}^T (\boldsymbol{z}_{ij} + \boldsymbol{w}_i)]\sin(\phi_j) \\
&- 2[\boldsymbol{y}_{ij}^T (\boldsymbol{z}_{ij} + \boldsymbol{w}_i)]\cos(\phi_j). \qquad (6.118)
\end{aligned}$$

Setting Eq. (6.118) to zero an equation of the following form is obtained:

$$a\cos(2\phi) + b\sin(2\phi) + c\cos(\phi) + d\sin(\phi) = 0, \qquad (6.119)$$

where a, b, c and d are defined in Eqs. (6.83), (6.84), (6.85) and (6.86), respectively.

Appendix B: Estimation of the Rotation Angles in the case of Spherical Covariance matrices.

From the definition of the matrices J_i and I_i in Eqs. (6.110) and (6.109), respectively, we obtain the following properties:

$$\begin{aligned} I_i^T I_i &= I_i & (6.120)\\ J_i^T J_i &= I_i & (6.121)\\ I_i^T J_i &= J_i & (6.122)\\ J_i^T I_i &= J_i^T & (6.123) \end{aligned}$$

First we show that:

$$tr(A_j^c S_i^{-1} A_j^c \hat{\Sigma}_i[\mathbf{X}]) - tr(A_j^s S_i^{-1} A_j^s \hat{\Sigma}_i[\mathbf{X}]) = 0, \quad (6.124)$$

where A_j^c, A_j^s, Σ_i and $\hat{\Sigma}_i[\mathbf{X}]$ are defined in Section 6.2. The first term, $tr((A_j^c)^T S_i^{-1} A_j^c \hat{\Sigma}_i[\mathbf{X}])$, in the case of spherical covariance ($\Sigma_i = \sigma_i^2 I$) can be written as:

$$tr((A_j^c)^T \Sigma_i^{-1} A_j^c \hat{\Sigma}_i[\mathbf{X}]) = \frac{n}{\sigma_i^2} tr((A_j^c)^T A_j^c \hat{\Sigma}_i[\mathbf{X}]), \quad (6.125)$$

where n is the dimension of the matrix Σ_i. For $(A_j^c)^T A_j^c$ we observe that:

$$\begin{aligned} (A_j^c)^T A_j^c &= R_{n-1}^T \cdots I_j^T \cdots R_1^T R_1 \cdots I_i \cdots R_{n-1} \\ &= R_{n-1}^T \cdots I_j \cdots R_{n-1}, & (6.126) \end{aligned}$$

and defining

$$A_j^p \sim R_{n-1}^T \cdots I_j \cdots R_{n-1}, \quad (6.127)$$

we can replace $(A_j^c)^T A_j^c$ with A_j^p in Eq.(6.125), obtaining:

$$tr((A_j^c)^T S_i^{-1} A_j^c \hat{\Sigma}_i[\mathbf{X}]) = \frac{n}{\sigma_i^2} tr((A_j^p)^T \hat{\Sigma}_i[\mathbf{X}]). \quad (6.128)$$

For $tr(A_j^s \Sigma_i^{-1} A_j^s \hat{\Sigma}_i[\mathbf{X}])$ we have:

$$tr((A_j^s)^T \Sigma_i^{-1} A_j^s \hat{\Sigma}_i[\mathbf{X}]) = \frac{n}{\sigma_i^2} tr((A_j^s)^T A_j^s \hat{\Sigma}_i[\mathbf{X}]). \quad (6.129)$$

For $(A_j^s)^T A_j^s$ we have:

$$\begin{aligned} (A_j^s)^T A_j^s &= R_{n-1}^T \cdots J_j^T \cdots R_1^T R_1 \cdots J_j \cdots R_{n-1} \\ &= R_{n-1}^T \cdots I_j \cdots R_{n-1} = A_j^p. & (6.130) \end{aligned}$$

Replacing $(A_j^s)^T A_j^s$ with A_j^p in Eq. (6.129) we obtain:

$$tr((A_j^s)^T \Sigma_i^{-1} A_j^s \hat{\Sigma}_i[\mathbf{X}]) = \frac{n}{\sigma_i^2} tr(A_j^p \hat{\Sigma}_i[\mathbf{X}]), \quad (6.131)$$

which is the same as $tr((A_j^c)^T S_i^{-1} A_j^c \hat{\Sigma}_i[\mathbf{X}])$ and Eq. (6.124) is proved.

Furthermore $tr(A_j^s \Sigma_i^{-1} A_j^c \hat{\Sigma}_i[\mathbf{X}])$ is zero since:

$$tr((A_j^s)^T S_i^{-1} (A_j^c) \hat{\Sigma}_i[\mathbf{X}]) = \frac{n}{\sigma_i^2} tr((A_j^s)^T A_j^c \hat{\Sigma}_i[\mathbf{X}]), \tag{6.132}$$

and

$$\begin{aligned} (A_j^s)^T A_j^c &= R_{n-1}^T \cdots J_j^T \cdots R_1^T R_1 \cdots I_j \cdots R_{n-1} \\ &= R_{n-1}^T \cdots J_j^T I_j \cdots R_{n-1} \\ &= R_{n-1}^T \cdots J_j^T \cdots R_{n-1}. \end{aligned} \tag{6.133}$$

Since J_j^T has only zeros in the diagonal the trace in Eq. (6.132) equals zero:

$$tr((A_j^s)^T \Sigma_i^{-1} (A_j^c) \hat{\Sigma}_i[\mathbf{X}]) = \emptyset. \tag{6.134}$$

Finally based on the derivations (6.126), (6.130) and (6.133) it is straightforward to show that $\boldsymbol{x}_{ij}^T \boldsymbol{x}_{ij}$ equals $\boldsymbol{y}_{ij}^T \boldsymbol{y}_{ij}$ and $\boldsymbol{x}_{ij}^T \boldsymbol{y}_{ij} = 0$. For $\boldsymbol{x}_{ij}^T \boldsymbol{x}_{ij}$ we have:

$$\begin{aligned} \boldsymbol{x}_{ij}^T \boldsymbol{x}_{ij} &= (E_i[\mathbf{X}] - B)^T A_j^c L_i^T L_i A_j^s (E_i[\mathbf{X}] - B) \\ &= \frac{1}{\sigma^2} (E_i[\mathbf{X}] - B)^T R_{n-1} \cdots J_i^T \cdots \\ &\quad R_2^T R_1^T S^{-1} S^{-1} R_1 R_2 \\ &\quad \cdots J_i \cdots R_{n-1}^T (E_i[\mathbf{X}] - B) \\ &\overset{S^{-1}=\frac{1}{s^2}I}{=} \frac{1}{s^4\sigma^2} (E_i[\mathbf{X}] - B)^T R_{n-1}^T \cdots I_i^T \\ &\quad \cdots R_2^T R_1^T R_1 R_2 \\ &\quad \cdots I_i \cdots R_{n-1} (E_i[\mathbf{X}] - B) \\ &\overset{R_i^T R_i = I}{=} \frac{1}{s^4\sigma^2} (E_i[\mathbf{X}] - B)^T R_{n-1}^T \cdots \\ &\quad I_i^T I_i \cdots \\ &\quad R_{n-1}^T (E_i[\mathbf{X}] - B) \\ &\overset{I_i^T I_i = I_i}{=} \frac{1}{s^4\sigma^2} (E_i[\mathbf{X}] - B)^T (E_i[\mathbf{X}] - B). \end{aligned} \tag{6.135}$$

Similarly for $\boldsymbol{y}_{ij}^T\boldsymbol{y}_{ij}$ we have:

$$\begin{aligned}
\boldsymbol{y}_{ij}^T\boldsymbol{y}_{ij} &= (E_i[\mathbf{X}]-B)^T A_j^c L_i^T L_i A_j^s (E_i[\mathbf{X}]-B) \\
&= \frac{1}{\sigma^2}(E_i[\mathbf{X}]-B)^T R_{n-1}^T \cdots I_i^T \cdots \\
&\quad R_2^T R_1^T S^{-1} S^{-1} R_1 R_2 \\
&\quad \cdots J_i \cdots R_{n-1}^T (E_i[\mathbf{X}]-B) \\
&\overset{S^{-1}=\frac{1}{s^2}I}{=} \frac{1}{s^4\sigma^2}(E_i[\mathbf{X}]-B)^T R_{n-1}^T \cdots I_i^T \\
&\quad \cdots R_2^T R_1^T R_1 R_2 \\
&\quad \cdots J_i \cdots R_{n-1}^T (E_i[\mathbf{X}]-B) \\
&\overset{R_i^T R_i=I}{=} \frac{1}{s^4\sigma^2}(E_i[\mathbf{X}]-B)^T R_{n-1}^T \cdots \\
&\quad J_i^T J_i \cdots \\
&\quad R_{n-1}^T (E_i[\mathbf{X}]-B) \\
&\overset{J_i^T J_i=I_i}{=} \frac{1}{s^4\sigma^2}(E_i[\mathbf{X}]-B)^T (E_i[\mathbf{X}]-B). \qquad (6.136)
\end{aligned}$$

We observe that indeed $\boldsymbol{x}_{ij}^T\boldsymbol{x}_{ij}$ equals $\boldsymbol{y}_{ij}^T\boldsymbol{y}_{ij}$. Finally, for $\boldsymbol{x}_{ij}^T\boldsymbol{y}_{ij}$ we have:

$$\begin{aligned}
\boldsymbol{x}_{ij}^T\boldsymbol{y}_{ij} &= (E_i[\mathbf{X}]-B)^T A_j^c L_i^T L_i A_j^s (E_i[\mathbf{X}]-B) \\
&= \frac{1}{\sigma^2}(E_i[\mathbf{X}]-B)^T R_{n-1}^T \cdots J_i^T \cdots \\
&\quad R_2^T R_1^T S^{-1} S^{-1} R_1 R_2 \\
&\quad \cdots J_i \cdots R_{n-1}^T (E_i[\mathbf{X}]-B) \\
&\overset{S^{-1}=\frac{1}{s^2}I}{=} \frac{1}{s^4\sigma^2}(E_i[\mathbf{X}]-B)^T R_{n-1}^T \cdots J_i^T \cdots R_2^T R_1^T \\
&\quad R_1 R_2 \cdots J_i \cdots R_{n-1}^T (E_i[\mathbf{X}]-B) \\
&\overset{R_i^T R_i=I}{=} \frac{1}{s^4\sigma^2}(E_i[\mathbf{X}]-B)^T R_{n-1}^T \cdots \\
&\quad I_i^T J_i \cdots \\
&\quad R_{n-1}^T (E_i[\mathbf{X}]-B) \\
&\overset{y^T J_i y=0}{=} 0. \qquad (6.137)
\end{aligned}$$

According to the above, and incorporating Eqs. (6.128), (6.131) and (6.134) into Eq. (6.38) we obtain:

$$\begin{aligned}
\frac{\partial J}{\partial \phi_i} &= 2[\boldsymbol{x}_{ij}^T(\boldsymbol{z}_{ij}+\boldsymbol{w}_i)]\sin(\phi_j) \\
&- 2[\boldsymbol{y}_{ij}^T(\boldsymbol{z}_{ij}+\boldsymbol{w}_i)]\cos(\phi_j)]. \qquad (6.138)
\end{aligned}$$

Setting Eq. (6.138) to zero and solving with respect to ϕ, we obtain a solution ϕ_i^*:

$$\phi_i^* = -atan(\frac{\boldsymbol{y}_{ij}^T(\boldsymbol{z}_{ij}+\boldsymbol{w}_i)}{\boldsymbol{x}_{ij}^T(\boldsymbol{z}_{ij}+\boldsymbol{w}_i)}), \qquad (6.139)$$

where $\boldsymbol{x}_{ij}$, $\boldsymbol{y}_{ij}$, $\boldsymbol{z}_{ij}$ and $\boldsymbol{w}_{ij}$ are defined in Eqs. (6.87), (6.88), (6.89) and (6.90), respectively.

Chapter 7

Advanced Driver Support and driver physiological state

7.1 Introduction

During the last decades, the development of driver assistance systems is of growing importance as these systems are expected to improve road safety and traffic efficiency. The Advanced Driver Assistance Systems (ADAS) partly support or take over the driver's tasks. ADAS can be defined as in-vehicle system that has a direct supporting interaction with the driver or the driver task. The way of support may vary from informative to controlling [58, 74]. ADAS operates from inside the car, but may be connected to external sources. Several ADAS, such as Adaptive Cruise Control (ACC), Lane Departure Warning (LDW) and Intelligent Speed Assistance (ISA) are already popular among car manufacturers. ADAS is part of a technology called Intelligent Transportation Systems (ITS). ITS incorporates intelligence in both roadways and vehicles in order to improve the traffic flow. Co-operative road-vehicle systems and vehicle-vehicle systems are also emerging worldwide. Intelligent vehicles and roads are the future standard and specialized research addresses the identification of their impact as well as their adaptation to the real user needs for safer and efficient transportation services. Currently, ADAS are designed to support drivers in maintaining safety thresholds or ensuring compliance with

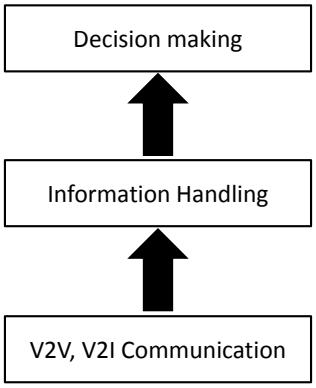

Figure 7.1: The basic building blocks of a next generation ADAS system.

formal driving rules, such as maintaining safe time headways in car-following situation or adhering to speed limits [71, 114].

The next generation of ADAS systems is going to adverse more information and apply different strategies in order to cope with changing environments and user's needs. A significant factor refers to changes in driver's performance and ability to continue the driving task. Since the most important variable influencing driver's performance is the driver's physiological state, this information would be certainly exploited by future ADAS systems. In this Chapter we study the extension of ADAS systems in three directions:

- Cooperative driving that exploits V2V ad V2I communication for extended perception of the driving environment.
- Enhanced situation assessment based on the advanced information fusion and extraction of valuable notification messages.
- Extension of the classic rule based warning strategies with advanced probabilistic decision making, incorporating environment information, as well as the driver's state.

In Fig. 7.1 we present the building blocks of a next generation ADAS system, which are studied in this Chapter. In Section 7.2 we present a simulation study, on the potential improvement of driving safety using V2V and V2I communication. In this first study a naive schema for information fusion is used. In Section 7.3 we present a more intelligent method for incorporation and handling information from low confidence sensors (other vehicles) as well as from sensors with high confidence (road infrastructure). Finally in Section 7.4 a decision making method based on Dynamic Bayesian Networks is presented for deciding whether to notify the driver about a potential hazard as well as how intrusive the warning should be.

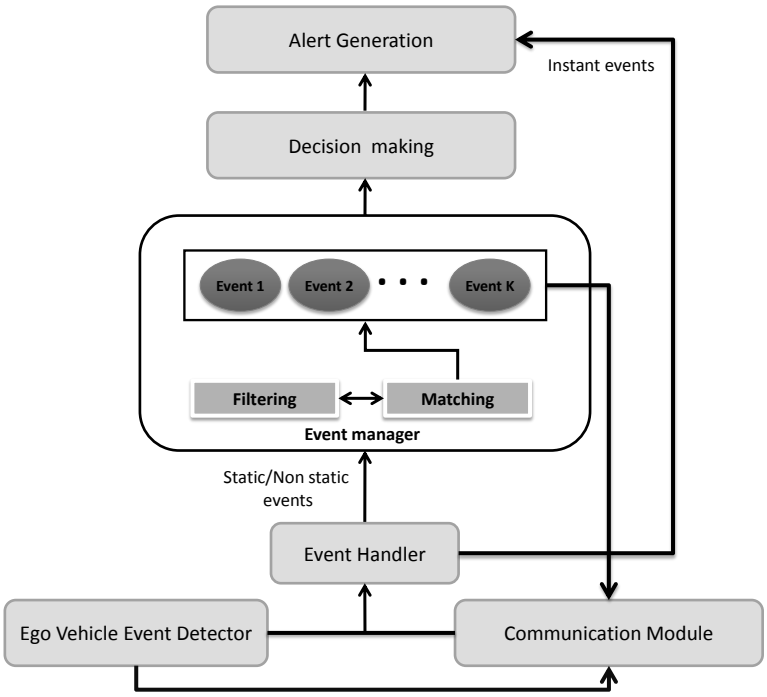

Figure 7.2: The basic components of a co-operative driver support system.

7.2 A simulation study on co-operative driving systems

One main advantage of co-operative vehicles, which are able to communicate with other vehicles or infrastructure, is the extension of driver's perception and eventually the reduction of accident risk. In order to test this hypothesis we consider a co-operative driver support system with an architecture presented in Fig. 7.2. In this section we will examine the following basic modules of this system:

- *Communication module*,
- *Ego-vehicle event detector*,
- *Event Handler module*.
- *Event Manager module*,

The *decision maker* and the *alert manager* (shown in Fig. 7.2), responsible for driver notification, are considered void components for the purposes of this first study, and are examined in next sections.

7.2.1 Ego-vehicle event detector

The Ego-Vehicle Event detector is the in-vehicle embedded platform, responsible to recognize events and conditions in the local environment using on board sensors (e.g. traffic

conditions, narrow road, lane invasion, static or slow moving obstacles, etc.). The ego-vehicle can then act as a scouter by communicating the detected events to other vehicles and the road infrastructure. To thin end the ego-vehicle detected events feed the Communication Module for broadcasting and also pass to the Event Handler for further processing.

7.2.2 Communication module

The communication between vehicles (V2V) and infrastructure and vehicles (I2V and V2I) is biderectional and the exchange of messages among them is achieved through the communication module. We discriminate two kind of vehicles: i) co-operative vehicles (i-vehicles) which have communication ability and ii) common vehicles without communication ability. Each i-vehicle produces a number of messages related to potential hazards either detected by the ego-vehicle or received as messages by other i-vehicles or the road infrastructure. In this work we do not focus on communication details and only the average delay (as a function of distance and relative speed) is considered.

7.2.3 Event Handler

Incoming messages arriving from Communication Module and ego-vehicle feed the Event Handler (the classification of events, as well as the source of information, are shown in Table 7.1). Three types of events are considered:

- Static events: Those are the events reported from infrastructure or other vehicles, which are located to a fixed position on the highway. Those events are not removed from the Event List until the vehicle reaches their location.
- Non-static events (such as slow moving vehicles, slowing down traffic etc.): Those are events reported from other vehicles or road infrastructure, but their presence is not guaranteed by the time that the ego-vehicle reaches their reported location.
- Instant Events: Those are critical events either detected from Ego-Vehicle Detector (i.e. lane invasion) or received from other vehicles (i.e. sudden braking) occurring in short distance from the ego-vehicle.

The first two categories refer to events on the highway which are potential obstacles for the ego-vehicle. That is, if the vehicle approaches the event with a speed over a safe limit, this event becomes threat for the driver. Let the obstacle speed (or the safe speed limit) be u_0 and the ego-vehicle speed u_e. The risk measure is considered as the braking effort required in order to reach obstacle's speed, multiplied by a constant, defined as:

$$r = c\frac{u_r^2}{2d}, \tag{7.1}$$

where r is the risk, $u_r = u_0 - u_e$ the relative speed between ego-vehicle and the obstacle, d the distance between ego-vehicle and the obstacle and c is a constant depending on the

Table 7.1: Event Classification

Event	Event Category	Source
Road works	Static	I2V
Accident	Static	I2V
Road Narrow	Static	V2V/I2V
Road condition	Static	V2V/I2V
Traffic	Non-Static	V2V/I2V
Fixed or Slow Moving Vehicle	Non-static/Instant	V2V/I2V/ Ego-vehicle detector
Sudden brake of foregoing Vehicle	Instant	V2V
Lane invasion	Instant	Ego-vehicle detector

$IS - MERGED = FALSE$
if $FilterPass(E) == FALSE$ **then**
  for each $E' \in A$ **do**
    if $Merge(E, E') == FALSE$ **then**
      $IS - MERGED = TRUE$
  if $!IS - MERGED$ **then**
    $AddInList(E)$

Algorithm 4: Handling new Event Procedures

vehicle and the weather conditions. This constant is common for all events. The last category of events requires an instant warning; thus they are directly forwarded to the *Alert generator* without processing by the *Event Manager*.

7.2.4 Event Manager

The Event Manager is responsible to keep a list of incoming events and sort them according to their risk. Each node of the list corresponds to a particular event which in turn consists of the variables: (i) distance (d) which is the distance between the event and the ego-vehicle, (ii) relative speed (u_r) which is the relative speed between ego-vehicle and an obstacle, (iii) category (c) and iv) type (t). An example of category is Static/Non-Static and for type is road works, road narrowing etc. When a new event is received by the Communication Module and the Event Manager, undertakes the following tasks; initially the Event filtering procedure removes irrelevant to ego-vehicle events, while the relevant ones (*Filter Pass*) are directed to the matching procedure. During this procedure the incoming events are compared to existing events (nodes in the list) and are merged with nodes referring to the same event (*Merge*). If no merge occurs, the incoming event is added as a new node in the list. The overall procedure is outlined in Algorithm 4. The *Filter Pass* and *Merge* procedures are described below:

Filter Pass

This is the function within Event filtering which determines whether the incoming event is worth reported in terms of relevance to the ego-vehicle. This function reduces computational cost by avoiding irrelevant information.

The criteria to consider an event as non-worth reporting are:

1. The events whose reported position is either backward or in opposite highway direction from the ego-vehicle. Hence, such events are not considered forthcoming hazards.

2. For the non-static events we consider the possibility of being no longer valid when ego-vehicle approaches their reported location. To handle this case, an expire horizon is assigned to non-static events, according to the relative speed and distance.

$$t_{expire} = \frac{u_r}{s} + T_0, \tag{7.2}$$

where T_0 is a constant indicating a time margin used to assure the event expiration. When *time-to-live* of the message in the Event List becomes equal to t_{expire}, then the message is discarded.

Merge

In this simulation environment a simple method for handling events is adopted. The need of such a mechanism rises from the fact that the same information may arrive from different sources. Thus we need a mechanism to derive which messages refer to the same event. More formally, *Merge* is a function of the matching procedure which removes multiple nodes from the Event List referring to the same event. For instance, suppose a vehicle detecting a narrow road in some distance ahead. If the same event is already a node in the Event List (provided by another source through the communication module) we can merge or ignore the message coming from the Ego-Vehicle Event Detector.

Another important feature of the *Merge* function is its ability to provide high level information from individual messages. Consider for example the scenario of a queue of K vehicles in some distance ahead from the ego-vehicle detector. Each i-vehicle in the queue recognizes a slow moving vehicle in front and broadcasts a message. Therefore, a number of messages with overlapping information is received. This scenario reveals the necessity of an aggregation mechanism which combines single incoming messages about slow moving objects and generates high level information such as heavy traffic. The usual information coming from other vehicles is about obstacles (slow moving vehicles or fixed objects). Moreover the ego-vehicle is able to detect other vehicles in the vicinity (near lanes) and monitor their relative speed. Using the above information the *Merge* function can infer traffic situation using different approaches such as rules or probabilistic inference. In this work a simple rule-based approach is considered, following the principles below:

- All highway lanes are occupied by detected vehicles.

for each $E' \in A$ **do**
  if *Expired*(E') **then**
    Delete(E')
  else
    Update Position and Risk of E'
Re-sort List(E')

Algorithm 5: Update list

- The relative speed between ego-vehicle and other vehicles approaches zero.
- The ego-vehicle speed is below a threshold (typical 15 m/s).

If all the above conditions are satisfied then traffic jam event is inferred. Another level of merging information is the reasoning about specific non-static events. For example merging traffic jam (non-static event) with road works (static event) in near location, traffic jam is due to road works is concluded. Thus, the driver could be notified through a single message containing high-level information instead of two separate messages. In Section 7.3 a more advanced method of information fusion is described.

Prioritization

The Prioritization function is responsible for storing the new event in the list (*Add Node*) keeping the priority order. This involves the re-estimation of all events' risk according to Eq. (7.1). The Event List is then re-sorted in descending order. The highest risk event (top entry) is then forwarded to the *decision making* (see Section 7.4), which decides whether and in which way to notify the driver.

Update list

A periodic update of the Event List is performed to ensure that contained events are still relevant according to the ego-vehicle current position (outlined in Algorithm 5). The *Expired* routine determines when the nodes of the Event List are no longer valid and the *Delete* routine removes them. The events are considered non-valid when the criteria described in section 7.2.4 are met. Those are summarized below:

1. If the event type is *static* and the distance is smaller than zero, $E_d < 0$.
2. If the obstacle type is *non static* and $t_w > t_{expire}$ where t_w is the *time-to-live* of the message in the Event List.

If the event is not deleted, we update the distance of the event $E_d = E_d - E_{u_r}$ and the risk is calculated again. After all events' risks are updated the list is re-sorted.

Broadcasting handler

For efficient scouting functionality, a continuous broadcasting of the forthcoming events (nodes in the Event List) is necessary due to communication range limitations (max 500 meters for V2V). If detected events are broadcasted only once, the currently out of range vehicles will not be updated for potential hazards. Hence, all nodes in the Event List have to pass to the communication module for broadcasting. Using no reduction strategy the total number of messages is $(N-1)^2$. To confront with bandwidth limitations, we apply a simple reduction strategy: If the position information of an incoming event (message from Communication module) is close to ego-position with respect to communication range, we consider that other vehicles within the range of the ego-vehicle are already aware of the event and thus, this particular message is not broadcasted.

7.2.5 Simulation Environment

In order to test the outcomes of the co-operative driving, we developed an environment [31, 69] for a macroscopic simulation of the traffic behavior on a highway road. The simulation environment has been developed in $C\#$. A brief description of the environment is given below.

Vehicle Behaviour Model

To model the vehicle behavior in a highway environment we used the Intelligent Driving Model (IDM) [144]. The following equations describe the model:

$$\frac{dv}{dt} = a[1 - (\frac{v}{v_0})^{\delta} - (\frac{s^*}{s})^2] \tag{7.3}$$

$$s^* = s_0 + (vT + \frac{v\Delta v}{2\sqrt{ab}}), \tag{7.4}$$

where, v_0 is the desired speed of the vehicle, s^* is the desired dynamical distance between two vehicles, s the actual gap, T is the safety time headway when following other vehicles, a is the acceleration in everyday traffic, b is the "comfortable" braking deceleration everyday traffic, s_0 is the minimum bumper-to-bumper distance to the front vehicle, δ is the acceleration exponent and Δu is the relative speed. To produce a more realistic model we have expanded the IDM to allow lane changing, obstacle and potential hazard detection:

- *Lane Change*: Vehicles are allowed to change lanes if they are following a vehicle with speed lower than the desired. In a K lane highway each lane has a low and an upper speed limit. Each vehicle aims to reach the appropriate lane according to desired speed u_0.

- *Obstacle detection*: In each time instance, vehicles detect obstacles ahead in a range R. If an obstacle is detected at distance d, the actual gap s in equation (7.3) is set to d. Otherwise s is set to a maximum value indicating that no obstacle exists.

- *Potential hazard detection*: Vehicles detect obstacles in their current and adjacent (± 1) lanes. We characterize an obstacle as potential hazard if the speed of the obstacle is lower than a predefined threshold. If all adjacent lanes are occupied by slow moving obstacles then we assume traffic congestion. Furthermore, if ego-vehicle is slow moving, it's status is directly forwarded to the communication module described above.

Communications Simulation

The communication characteristics considered in the simulation, are the following:

- The communication ranges of V2V, V2I and I2V.
- The latency as a function of distance and type of communication (V2V, V2I and I2V).

Vehicles produce three types of messages: i) obstacle detected by ego-vehicle (slow moving vehicles or fixed obstacles), ii) traffic detected by ego-vehicle when many slow moving vehicles are present in adjacent lanes and iii) events reported by other vehicles. These messages are broadcasted to road infrastructure and neighboring vehicles. Whenever vehicles come into the range of an i-vehicle or a road infrastructure base station a new session is initialized and messages are received within dT (latency time). The message delivery fails if the source and target distance exceeds the communication range. i) obstacle detected by ego-vehicle (slow moving vehicles or fixed obstacles), ii) traffic detected by ego-vehicle when many slow moving vehicles are present in adjacent lanes and iii) events reported by other vehicles. These messages are broadcasted to road infrastructure and neighboring vehicles. Whenever vehicles come into the range of an i-vehicle or a road infrastructure base station a new session is initialized and messages are received within dT (latency time). The message delivery fails if the source and target distance exceeds the communication range.

7.2.6 Simulation Results

We used the simulation environment to relate communication characteristics (range, latency) with driving risk (braking effort gain) as well as to demonstrate the way that information received from different sources (nearby i-vehicles or road infrastructure) is merged. The latency of the communication is constant, i.e. if the broadcasting duration set to T, the communication delay is dT, the actual broadcasting duration is $T + dT$. Initially we provide results, concerning the range and broadcasting frequency of communication and their impact on risk reduction. We consider 10 i-vehicles moving on the highway and a slow moving vehicle being in some distance ahead. Moreover, we suppose that all vehicles are moving in the same lane and lane changes are not allowed. The distance between i-vehicles is initially set to 1.5 km. For comparison purposes, we introduce for each i-vehicle a corresponding Zombie vehicle (conventional vehicle without

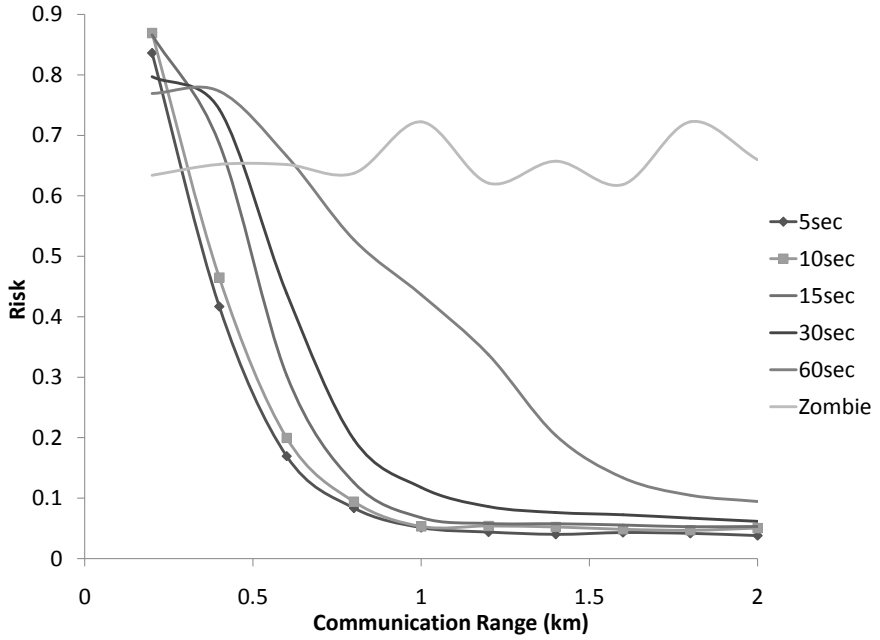

Figure 7.3: The risk according to the range of communication for different update intervals (Slow moving vehicle speed = $20m/s$).

communication ability). Each Zombie vehicle has the same initial position, speed and IDM parameters (as described in Eq. (7.3)) with its corresponding i-vehicle. To illustrate the performance (in terms of mean breaking effort) we consider two cases; In the first case, the speed of the slow moving vehicle is set to 10 m/s and in the second 20 m/s. In both cases, all other vehicles have an initial speed of 35 m/s. Visibility (the maximum distance where an obstacle or a foregoing vehicle is detected) is set to 200 m.

In Figs. 7.3,7.4 we provide the mean braking effort of the Zombie vehicles and i-vehicles with broadcasting duration 5, 15, 30 and 60 secs for both cases of slow moving vehicle speed. We observe that the braking effort in the first case is very high (a safe value for normal conditions is 0.2 [53]) while in the second case the safety requirement is achieved with a communication range of 600 m and broadcasting duration smaller than 15 sec. From the above scenario we conclude that for the second case is almost impossible to ensure safety with only V2V communication. Then we examine the case of I2V and V2I communication. The great benefit is that the communication range for this case is almost unlimited, because when a infrastructure station receives a message from a vehicle it can broadcast it to all other stations using a LAN. In Fig. 7.5, we provide the braking effort of the i-vehicles with and without infrastructure communication and for Zombie vehicles for comparison. We observe a significant reduction in braking effort. Moreover, in this case we can achieve the safety margin of 0.2 braking effort even in the extreme case of an obstacle with speed of 10 m/s.

Next we provide qualitative results for the function of the *Event manager*, using screen-

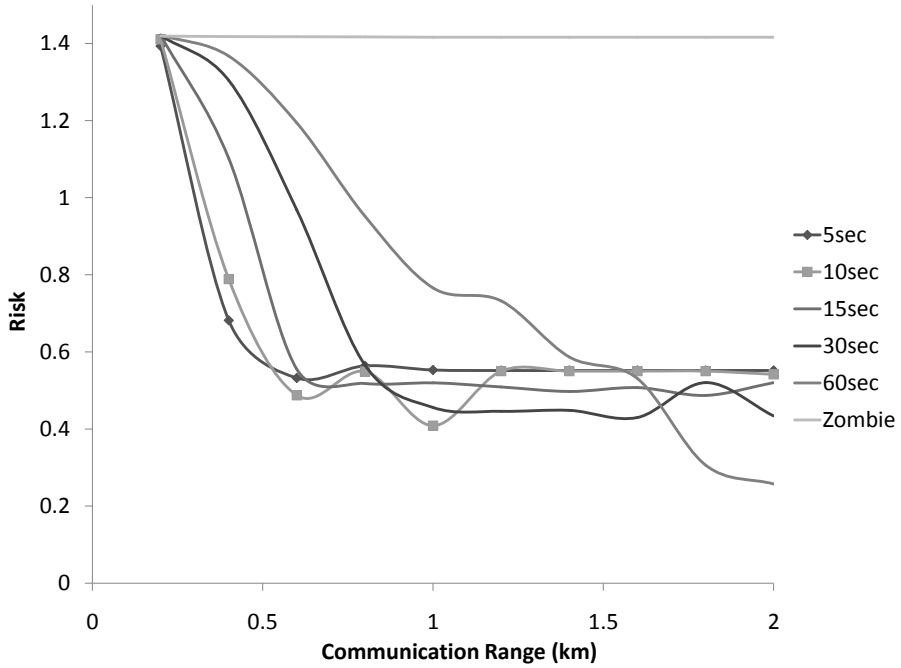

Figure 7.4: The risk according to the range of communication for different update intervals (Slow moving vehicle speed = $10m/s$).

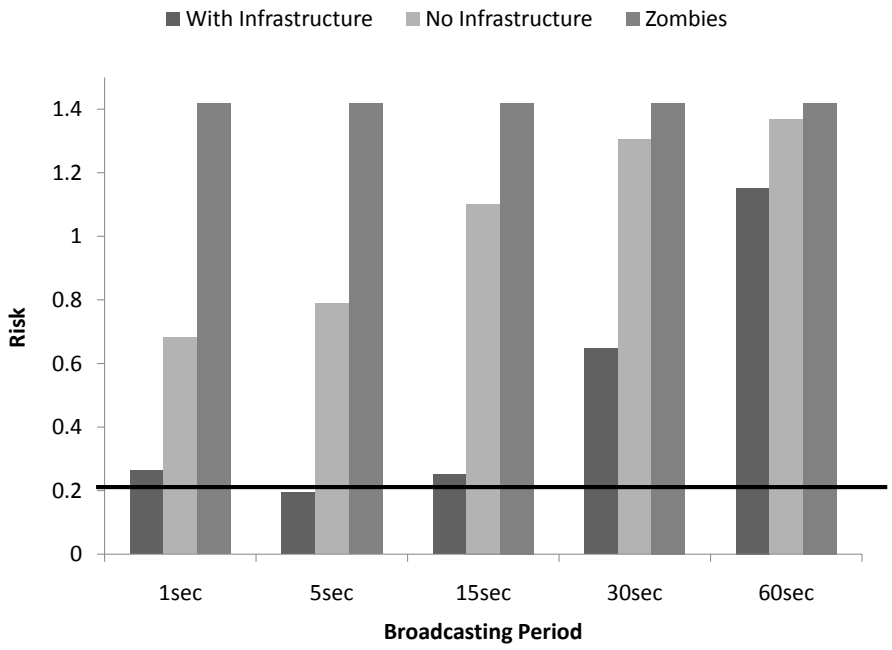

Figure 7.5: The risk of Zombie and i-vehicles with and without road infrastructure communication. Communication range is set to $400m$ and visibility to $200m$.

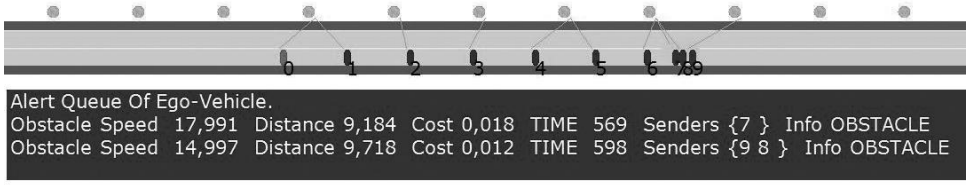

Figure 7.6: Ego-vehicle receives through the road infrastructure messages reported by i-vehicles with id numbers 7, 8 and 9.

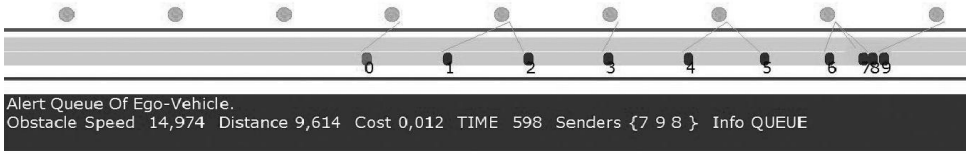

Figure 7.7: When three vehicles are very close they are considered as a queue. Ego-vehicle receives road infrastructure messages reporting an obstacle and a queue of vehicles.

shots from the simulation of the slow moving vehicle scenario. In this simulation V2I communication is allowed and information fusion is performed and broadcasted. The simulation illustrates a mini-map of the highway, where the vehicles are shown as ellipses with an id number assigned, while road infrastructure base stations are indicated as ellipses above the highway. In the bottom of the screenshot we provide a log display where the Event List of the ego-vehicle (id 0) is indicated. Early in the simulation when no queue is formed yet, two obstacle messages are reported to the road infrastructure. The first comes from i-vehicle with id 8 which also merged the message from the slow moving vehicle (id 9) and the other from the i-vehicles with id number 7 (Figure 7.6). The road infrastructure broadcasts this information, which in turn is received by the ego-vehicle. Later when the queue has been formed (from vehicles 7,8,9), the broadcasted messages from individual vehicles are merged (into vehicle 7) inferring a queue situation (Figure 7.7) forwarded through infrastructure to ego-vehicle.

Furthermore, we developed a second, more complicated scenario, in order to demonstrate the merging process when many events are present. We assume road works taking place in two out of the four lanes of the highway. Furthermore, near the road works event we deploy a large number of vehicles with different speed in order to create a traffic congestion. In this case, the ego-vehicle receives a large number of messages about slow moving vehicles along with a message from road infrastructure reporting road works in the same area. The Event Manager of the ego-vehicle merges the aforementioned messages producing a high level message, hense *"Traffic due to Road Works"*. A screenshot of this complex scenario simulation is illustrated in Fig. 7.8. Also, the log display demonstrating the Event List of the ego-vehicle sorted by the estimated events' risk is provided.

We tested in a simulation environment an ADAS system exploiting V2V and V2I communication and a significant reduction in the braking effort (risk) was observed for co-operative vehicles in relation to vehicles without communication capabilities. In this

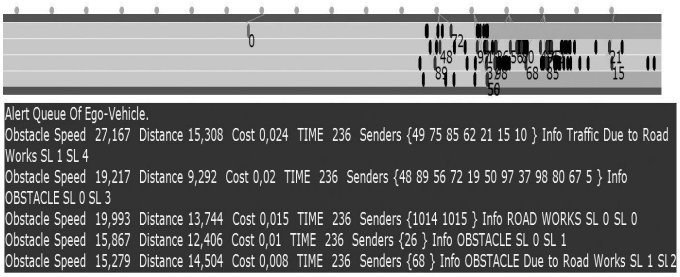

Figure 7.8: A more complicated scenario. The Event List of the ego-vehicle contains a number of messages sorted by their risk.

first approach, we used a rather simplistic information handling method, based on rules. In the following section we present a more advanced information handling method, based on Bayesian network inference.

7.3 Advanced Information Handling

Using V2V and V2I communication for driving environment assessment, there is a variety of information sources with different reliability level. Co-operative vehicles, may broadcast information coming from other sources or from the in-vehicle sensors. This information may be of low credibility, due to sensor limitations, or may be rather low level (for example detect road works as an obstacle). In order to handle this information and furthermore, extract high level information, we propose the use of Bayesian networks instead of the rule based method previously presented. The information is exchanged between vehicles (V2V) and infrastructure (V2I) in the form of messages. Those messages contain information about the type of the event as well as geographical information (GI), i.e. the longitude and latitude of the event. Events detected from the ego-vehicle are considered to have a GI similar to the ego-vehicle, while events coming from other sources (V2V, I2V) have their own GI. In order to handle those events more efficiently we split the horizon of our vehicle in virtual circles which we call geographic areas (GAs). This approach allows to handle groups of events and provide reasoning about possible causes of events or to extract more important and usable information. This reasoning is based mainly on expert knowledge (as reported in the literature) but it can easily extended to incorporate information from statistical data obtained by road management systems.

We consider the GA as a circle with radius R. Considering the ranges of the radar and the V2V communication, we assume R to have an approximate value of 150m. This is the maximum sensing range achieved by the i-vehicle .The ego-vehicle position determines the center of the first GA, while sequential tangent GAs are virtually created to cover a distance of about 1.5 km. This is regarded as the maximum safety distance, above which no warning message is considered necessary. This representation can be interpreted as follows: The 1st GA is the area where the ego-vehicle resides, and thus it constitutes the

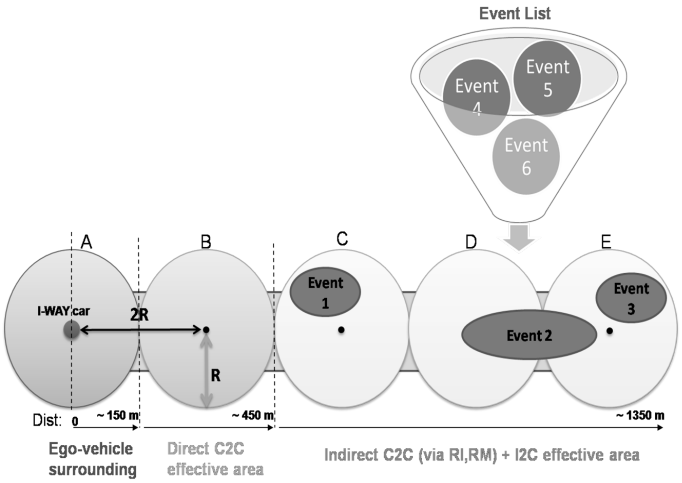

Figure 7.9: Geo-referenced events representation using virtual GAs.

local environment of the ego-vehicle. In the local GA the driving context information resides such as traffic, road narrow and local weather, detected by the ego-vehicle. This information is not part of the notifications issued to the driver, since he/she is assumed to be already aware of.

Considering that the direct V2V communication range is approximately 450-500m, we could interpret the second GA as the sphere where direct V2V communication is enabled, given the communication range of the antenna installed in the vehicle. However the vehicle-originated messages can be propagated also via the RI infrastructure communication channels (indirect V2V). The discrimination between direct and indirect V2V communication is useful in the sense that not all V2V messages involve the same confident level with respect to the ego-vehicle. For instance the vehicle-originated messages about detected obstacles (produced from slow moving cars) or collision warning (produced from safety distance violations) are only relevant to the ego-vehicle when sent through direct V2V communication (close distance to the ego-vehicle) otherwise there is high probability that they would have become obsolete (non-valid) by the time the ego-vehicle reaches their reported position.

All other forthcoming events either vehicle-originated (both direct and indirect) or infrastructure-originated which are reported at a distance $D < 1.5$km from the ego-vehicle reside to one of the rest GAs according to their exact geo-position. Although we have defined the 1.5 km distance as the maximum distance for notifications generation, some I2V messages contain information that could affect driver's trip plans. For example if there is a road closure/ traffic jam etc. the driver may select to change his route. Such information is considered valuable for the driver to know well in advance, hence those types of I2V messages hold the lowest priority and should provided to the driver in the form of informative messages.

The forthcoming events are stored into a list (event list E) and their geographic position is checked periodically; when an event resides in a GA, its start and end position is

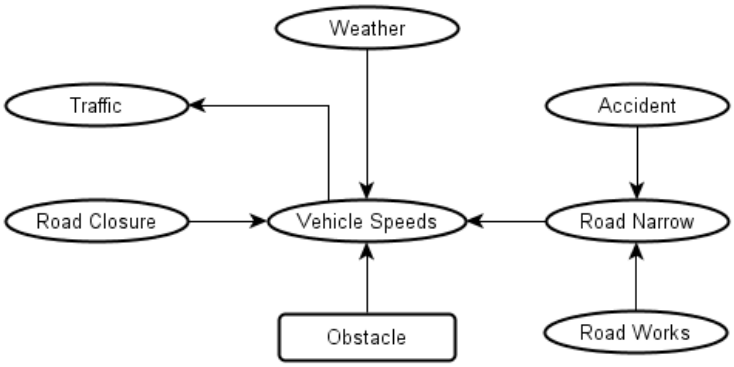

Figure 7.10: The graphical model of the relation between driving environment variables.

represented in the corresponding virtual circle and the event is removed from the list. There may be also a case, when a reported event lies in two or more successive GAs (event 2 in Figure 7.9). Consider for example "Road Works" covering 0.5 km distance. This event enters two successive GAs, so that in the end it covers the actual geo-area (from start to end position). The entering of an event into a GA is called geo-referenced event representation. During the geo-referenced representation the merging of similar events (with same Event IDs) is also possible within a GA. This allows for efficient handling of redundant information either from multiple messages sent by the same source (RI, same vehicle) or from different sources (different vehicles). Considering the case where the same message for "road works" is reported by many other co-operative vehicles. This is merged within the corresponding geo-area and is presented only once to the driver.

7.3.1 Inference of new information

Our approach is based on the assumption that the messages coming from different information sources (other vehicles, infrastructure) contain information which may provide evidence about the presence of another event. Thus they could lead either to the refinement of the perceived situation or to the extraction of new valuable information. This consideration allows for the exploitation of events interrelationships in order to:

i) extract new valuable information from the available data

ii) increase confidence of information coming from low-confident sources

iii) generate compact notifications from accumulated geo-related information

For instance, the presence of Road Works in a geo-area leads to Narrow Road event, which in turn reduces the expected average vehicle speeds in the particular geo-area. The decrease in vehicle speeds constitutes a possible symptom of traffic congestion in the area.

Moreover the correlations between individual events could be exploited to increase credibility of low-confidence information. In general terms, the events reported from the

infrastructure are credited with high confidence while the V2V messages are considered low-confident information sources. During the geo-reference event representation every forthcoming event reported by V2V/I2V, which lies within the range of a GA it enters the GA with a confidence value assigned. Given the information existing in a GA, we use the model of Figure 7.3.1 in order to make inferences that increase the credibility of low-confident information. For instance, the vehicle-originated messages reporting obstacles (slow moving cars), together with the car velocity data enclosed in these messages, can be fused with statistical traffic flow data in particular days and time of day and/or weather data to reveal information about the average vehicle speed in a geo-area or infer "heavy traffic".

Finally using the same model it is possible to avoid the generation of individual notifications of different events in the same geo-area but produce instead compact notification messages that enclose all the available information lying in the area. For example in Figure 7.9 assuming that Event 3 refers to "accident" and Event 2 refers to "traffic queue" then the extracted notification message for the geo-area E is "Traffic queue due to Accident". The two events although seem individual, they are combined in a single consolidated message revealing also their inter-dependencies. The methodology for performing information fusion is described in the next section.

7.3.2 Fusion of low-confident information sources

In this chapter we describe how the information coming from different sources lying in the same geo-area (GA) is used in order to increase confidence of the information lying within a GA range.

In general terms, the events reported from the infrastructure are credited with high confidence while the V2V messages are considered low-confident information sources. In order to deal with both redundant and missing information we developed a methodology based on Bayesian networks.

Bayesian Networks, are widely used for knowledge representation and reasoning under uncertainty in intelligent systems [112]. The structure of a BN is a directed acyclic graph (DAG). Its nodes correspond to random variables of interest while the directed arcs represent direct causal or influential relation between nodes. The uncertainty of the interdependence of the variables is represented locally by the conditional probability table (CPT) $P(X_i|Pa_{X_i})$ associated with each node X_i, given its parents Pa_{X_i}. The graphical structure of BN allows the representation of interdependency between variables, which together with an independence assumption leads to the joint probability distribution of $\mathbf{X} = \{X_1, X_2, \cdots, X_n\}$, one of the most important features of BN. The joint probability distribution can be factored out as a product of the conditional distributions in the network:

$$Pr(X) = \prod_{i=1}^{n} P(X_i|Pa_{X_i}), \tag{7.5}$$

where n the number of variables. Causality and inference are two of the main properties

Table 7.2: The conditional distribution table of accident, road works and weather.

Accident	Probability	Road Works	Probability	Weather	Probability
No	0.95	No	0.95	Good	0.8
Yes	0.05	Yes	0.05	Bad	0.15
				Very bad	0.05

Table 7.3: The conditional distribution table of Traffic.

		Road Narrow	
Road Works	Accident	No	Yes
No	No	0.9	0.1
Yes	No	0	1
No	Yes	0.1	0.9
Yes	Yes	0	1

of Bayesian theory, which make those models appealing for our purpose. In our approach, we designed a model that encapsulates the causalities between different events, based on common sense, and expert knowledge. The initial BN model has the structure presented in Fig. 7.3.1. After defining the structure the next step is to define the parameters of the model. In the following tables we give the probability tables of each of the variable.

7.3.3 Evidence in the model

As described earlier every forthcoming event reported by V2V/I2V, which lies within the range of a GA it enters the GA with a confidence value assigned. In principle, the events reported by other cars have lower confidence than those reported from the infrastructure. Given the information existing in a GA, we can use the model described here in order to make inferences that increase the credibility of low-confident information.

The information in classical Bayesian network theory is called evidence and the goal of the inference is to estimate the posterior probability of the variables given the evidence E and the model M

$$P(X|E,M) = \sum_i P(X_i|Pa_{X_i},E) \tag{7.6}$$

where X_i the variables of the environment incorporated in the model and Pa_{X_i} the parents of the variables X_i as denoted by the structure of the model.

To perform inference in Bayesian networks there are two large families of algorithms in the literature: the exact inference algorithms and the approximate inference algorithms. Both families have their pros and the cons. In our case, given a small model with discrete only variables we selected to use the Junction tree inference algorithm [79] developed in

Table 7.4: The conditional distribution table of Vehicle speeds.

			Vehicles Speeds		
Weather	Road Narrow	Road Closure	Low	Medium	High
Good	No	No	0.1	0.2	0.7
Bad	No	No	0.2	0.4	0.4
Very Bad	No	No	0.3	0.4	0.3
Good	Yes	No	0.2	0.5	0.3
Bad	Yes	No	0.3	0.5	0.2
Very Bad	Yes	No	0.4	0.4	0.2
Good	No	Yes	0.2	0.3	0.5
Bad	No	Yes	0.3	0.4	0.3
Very Bad	No	Yes	0.4	0.4	0.2
Good	Yes	Yes	0.2	0.4	0.4
Bad	Yes	Yes	0.3	0.5	0.2
Very Bad	Yes	Yes	0.5	0.4	0.1

Table 7.5: The conditional distribution table of Traffic.

	Traffic		
Vehicle Speeds	No Traffic	Traffic	Queue
Low	0.05	0.15	0.85
Medium	0.2	0.7	0.1
High	0.7	0.25	0.05

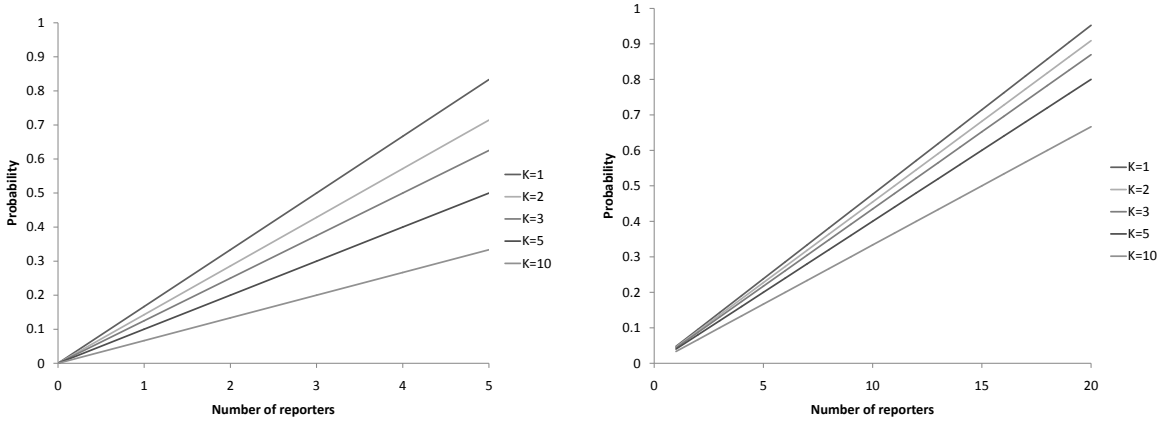

(a) (b)

Figure 7.11: The confidence on Traffic evidence, given the number of i-vehicles reporting Traffic. Total number of senders: a) 5 and b) 20.

C++. In the following we describe the main steps followed in our approach, while a more detailed description of the algorithm is included in the Appendix.

In the following we examine the evidence for each one of the variables: i) Traffic, ii) Road Narrow iii) Low Speeds and iv) Weather for the cases when only V2V communication is present (the I2V information is inserted as hard evidence in the model).

Traffic evidence

For the Traffic event, which we expect to be reported by all the senders in the affected area, we apply the following formula

$$P(E) = \frac{N^R}{N + K} \tag{7.7}$$

where N^R are the senders reported the same event, N the sum of the senders of the area and K a constant that reduces the reliability of the senders' information.

Fig. 7.11(a) and Fig. 7.11(b) illustrates the confidence of the traffic event with respect to the number of the incoming V2V messages reporting traffic in the same area.

Road narrow evidence

The road narrow event reported from vehicles actually refers to the narrowing of the ego-lane. It is therefore expected that not all i-vehicles will recognize and broadcast this type of event. For instance in a highway with L the number of lanes, the probability of a vehicle moving in the narrowing lane is $1/L$. Thus, the probability we assign to a road

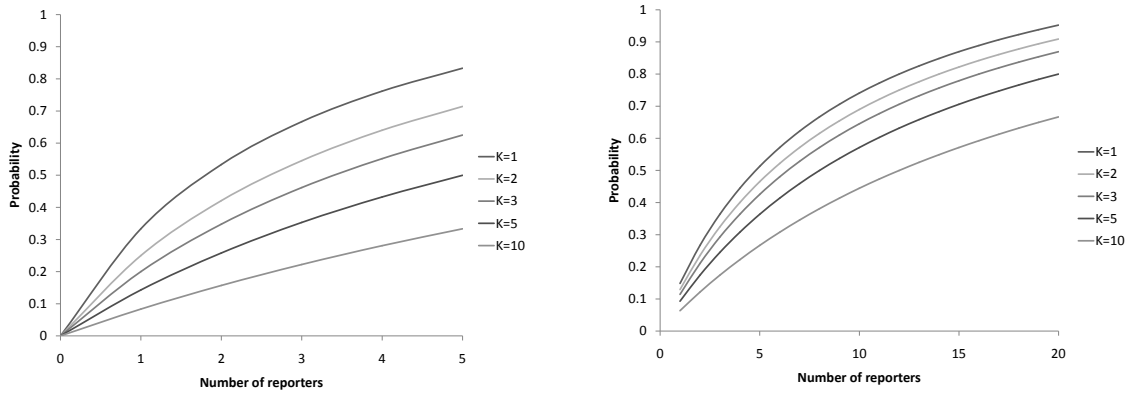

(a) (b)

Figure 7.12: The confidence on road narrow evidence, given the number of i-vehicles reporting road narrow. Total number of senders: a) 5 and b) 20.

narrow event reported by V2V messages is given by the following formula:

$$P(E = RoadWorks) = \frac{N^R}{N^R + \frac{N'}{L} + K} \quad (7.8)$$

$$= \frac{N^R}{N^R + \frac{N - N^R}{L} + K} \quad (7.9)$$

$$= \frac{N^R}{\frac{L-1}{L} N^R + \frac{N/L}{+} K} \quad (7.10)$$

where N' are the co-operative vehicles that did not send a road narrow message.

In Figs. 7.12(a) and 7.12(b) we illustrate the confidence of road narrow event with respect to the number of the incoming V2V messages reporting road narrow in the same area.

Low Speeds Evidence

Suppose we have N incoming V2V messages. Each one of them incorporates a field regarding the sender's speed, u_i. In case the messages refer to obstacles (assuming slow moving vehicles) the information about the obstacle's speed (at least, an estimation) is also included. Taking all this into consideration we could say that we have a collection of N speed samples for the specific region (here N is the number of senders as well as the obstacles reported). In order to have a more precise estimation of the actual average speed, given that we have few samples (number of i-vehicles) we incorporate to our estimation a prior estimation of the average speed, based on speeds observed in the past.

In *road management systems* resides a large database of observed average speeds in the past. Those speeds are dependent mainly on the road section, on the hour of the day

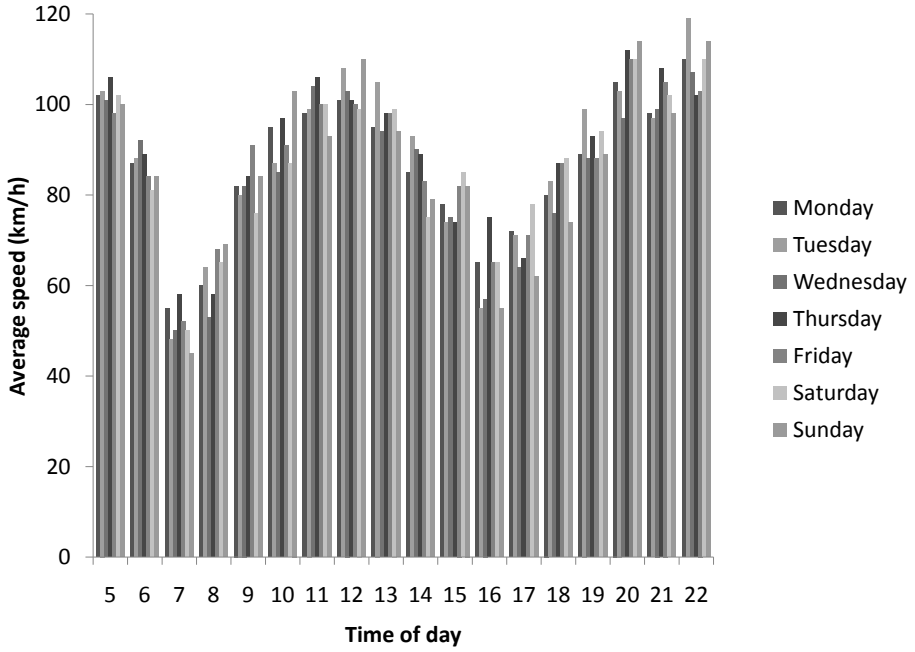

Figure 7.13: A sample histogram (not real data) of a road section.

(Rush hours) and the day of the week. Given this information we equip our model with histograms of average speeds and time, referring to different road sections and different days of week.

We need an estimation of the average speed (AS) of a specific geo-area. In order to reduce the effect of possible few samples we add K "virtual" senders with speed calculated from the specific bin of the histogram database, and the average speed is estimated according to the following equation

$$AS = \frac{\sum_{i=1}^{i=N} u_i + K \cdot AS'(position, time, DayOfWeek)}{N + K} \tag{7.11}$$

The K defines how are we going to rely on the statistics. If K is large (relative to the N) then we always estimate the average speed from the statistics (the histograms stored). If K is small (relative to the N) then we ignore the statistics and rely only on the i-vehicles. A good compromise is to set at each time $K = N$ in order to rely equal on both information sources. AS' is a look up function which relates the current information of geographic area (position, time and Day of Week) with a specific bin in the stored histograms and return the expected average speed. In Fig. 7.3.3 we give an idea of how those histograms seems. This does not refer to real data, but it is a common pattern, presenting two main rush hours (morning and afternoon) with low speeds. Such statistic data could to be exploited in order to have an estimation of expected average speed.

After calculating the average speed, we use a softmax function in order to get the

probability of the *Vehicle speeds* (V.S) state:

$$P(V.S. = Verylow = as) = \gamma + (1-\gamma)\frac{e^{\alpha_1 \cdot (as-\beta_1)}}{\sum_{i\in[1,2,3]} e^{\alpha_i \cdot (as-\beta_i)}} \quad (7.12)$$

$$P(V.S. = Medium|AS = as) = \gamma + (1-\gamma)\frac{e^{\alpha_2 \cdot (as-\beta_2)}}{\sum_{i\in[1,2,3]} e^{\alpha_i \cdot (as-\beta_i)}} \quad (7.13)$$

$$P(V.S. = High|AS = as) = \gamma + (1-\gamma)\frac{e^{\alpha_3 \cdot (as-\beta_3)}}{\sum_{i\in[1,2,3]} e^{\alpha_i \cdot (as-\beta_i)}} \quad (7.14)$$

$$(7.15)$$

where γ is a constant that modifies the credibility we give to our estimation of the average speed (AS).

Weather Evidence

The major source of information about weather conditions is the Road Infrastructure. There are several types of weather conditions typically reported by road infrastructure but in our model we grouped those values in three categories (*Good*, *Bad* and *Very Bad* weather conditions).

7.3.4 Information value

Taking advantage of the reasoning abilities of Bayesian Networks and the causalities denoted in the BN model of Fig. 7.3.1. We proceed with the extraction of the usable information for the driver, which defines the content of a potential notification message. The content of notification messages derive from the information existing within the GAs. As already mentioned, the GA A represents the ego-vehicle surroundings and the information lying there constitutes the driving context. The rest of the GAs cover the area where a possible notification message could be extracted. In order to decide whether the information (event) lying into a GA generates a notification message we have to consider the following:

1. The validity of the information.
2. The information gain.
3. The current driving context

In the following we describe the approach followed to manage the three issues above mentioned.

1) The validity of information is estimated from the posterior probability of each variable X given the evidence E and the $P(X|E)$. Invalid information can be derived from vehicle-originated messages which are propagated via the RI infrastructure

Table 7.6: Information Ranking.

Event	Source of Info	Priority Order
Critical obstacle ahead	Ego-vehicle	1
Lane invasion	Ego-vehicle	2
Slow down traffic	V2V	7
Slow moving car	V2V	11
Road narrow	V2V	10
Safety dist. violation	V2V	4
Weather conditions	I2V	8
Road closure	I2V	9
Accident	I2V	3
Road works	I2V	5
Traffic Queue	I2V	6

communication channels (indirect V2V). For instance the vehicle-originated messages about moving obstacles (slow cars) or collision warnings are only relevant to the ego-vehicle when sent through direct V2V communication (close distance to the ego-vehicle) otherwise there is high probability that they would have become obsolete (non-valid) by the time the ego-vehicle reaches their reported position.

2) The Information Gain (IG) is a parameter introduced to express how worthy the information is for the driver. It is a qualitative measure of the usefulness of the information, derived from a questionnaire to a number of drivers. Table 7.6 depicts the priority order of specific events (1 indicates highest priority) according to their criticality. From Table 7.6 we extract the Information Gain after a rating normalization.

3) Concerning the current driving context this is actually the information lying in the surrounding of the ego-vehicle (GA: A). Our goal is to avoid the generation of notifications about events the driver is already aware of. Take for instance a traffic congestion event recognized by the in-vehicle sensing system; this resides in the ego-vehicle's GA. Consider also a traffic congestion event reported by I2V which is expanded in the next 3 GAs (A, B, C). Apparently there is no need to provide a notification about forthcoming traffic congestion since the driver experiences it already. To tackle this issue we define the Temporal Information Gain (TIG) as the Information Gain of a variable given the current driving context. When the configuration of a variable in the driving context is the same with the evidence of that variable in the GA, the Temporal Information Gain is equal to zero otherwise it is equal to the Information Gain.

To address all three aforementioned considerations in a similar way, for a configuration j of a variable X_i we estimate the Expected Temporal Information Gain (ETIG) as following:

$$ETIG_i^j = P(X_i = x_i^j) \cdot TIG_i^j \tag{7.16}$$

This parameter defines the worth-reporting information and allows the management of priorities in the sense that the information assigned with high ETIG (over a threshold value) is included in the notification message.

The procedure is the following:

Step1 : Every time an event enters a GA, its corresponding information gain is assigned to it.

Step2 : Given the current driving context and the evidence for each model variable derived from the information fusion we estimate the ETIG for all model variables of the total number of GAs.

Step3 : All the variables within a GA with $ETIG >= Th$ (Th=threshold) are combined and generate a compact notification message.

Step4 : The extracted notification message passes to the Decision Making, which determines when the message will be provided to the driver.

7.3.5 Experiments and results

In this section we test the inference capability of the BN model. Suppose we have K incoming messages about potential obstacles. Combining those events with the statistical data available we have an estimation of the average speeds (AS) on a specific GA. We then examine two cases:

- 1st case: no other evidence (i.e. no message from RI) is available
- 2nd case: two additional messages are received from RI, one reporting an Accident and the other reporting Heavy Rain (interpreted as bad weather).

In the first case the only information is the Average speed which mainly affects the probability of Traffic variable. Figure 7.14 illustrates the probability (a) and the Expected Information Gain (b) of the Traffic variable (No Traffic, Traffic and Queue) in relation to our estimation of AS. As Traffic we imply the "slow down traffic" while as queue the traffic congestion forming a queue of vehicles. The straight lines in both diagrams correspond to the probability of Traffic variable, without the information of AS.

Fig. 7.14 illustrates the probability (a) and the Estimated Information Gain (b) of the Traffic variable (No Traffic, Traffic and Queue) in relation to our estimation of AS given also the other evidence about accident and bad weather. Again the straight lines refer to the probability of Traffic variable, without the information of AS.

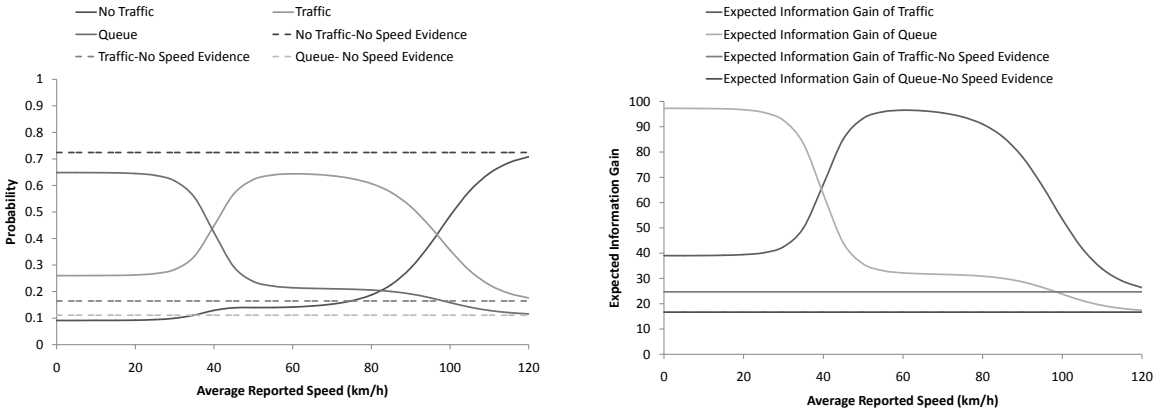

(a) (b)

Figure 7.14: The probability of Traffic states (a) and their Expected Information Gain (b) with the Average Speed (AS) when there is no other evidence ($\gamma = 0.8$).

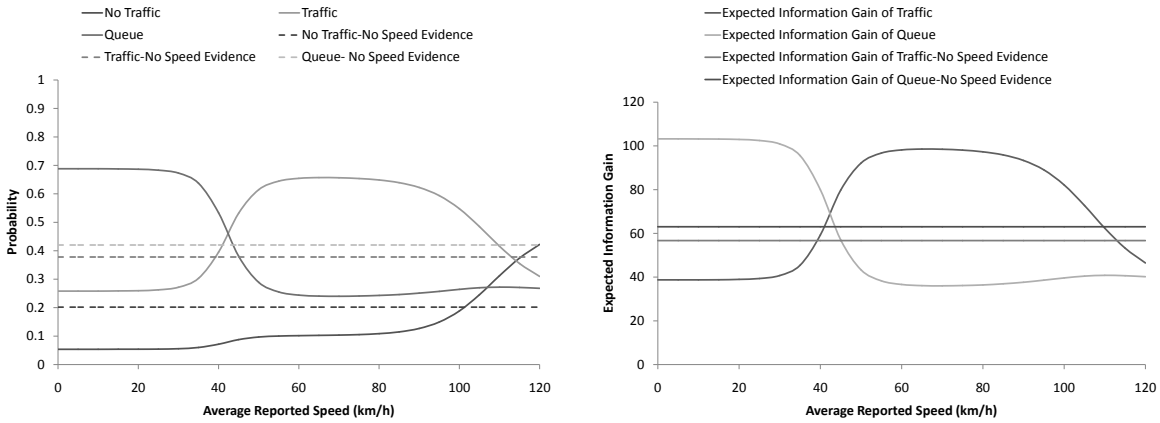

(a) (b)

Figure 7.15: The probability of Traffic states (a) and their Expected Information Gain (b) with the Average Speed (AS) when there is evidence of Accident and Bad Weather ($\gamma = 0.8$).

We notice that in the second case the probability of Queue and Traffic (i.e. slow down traffic) is increased and the probability of No-Traffic does not grow as rapidly as in the first case with the Average Reported speed. The Average Reported speed however is considered as a non accurate metric, thus it does not necessarily correspond to the real speeds occurring on the road. This is enforced by the constant γ. Setting $\gamma = 1$, we treat the Average Reported speed as the only reliable indicator of the expected speed on the road.

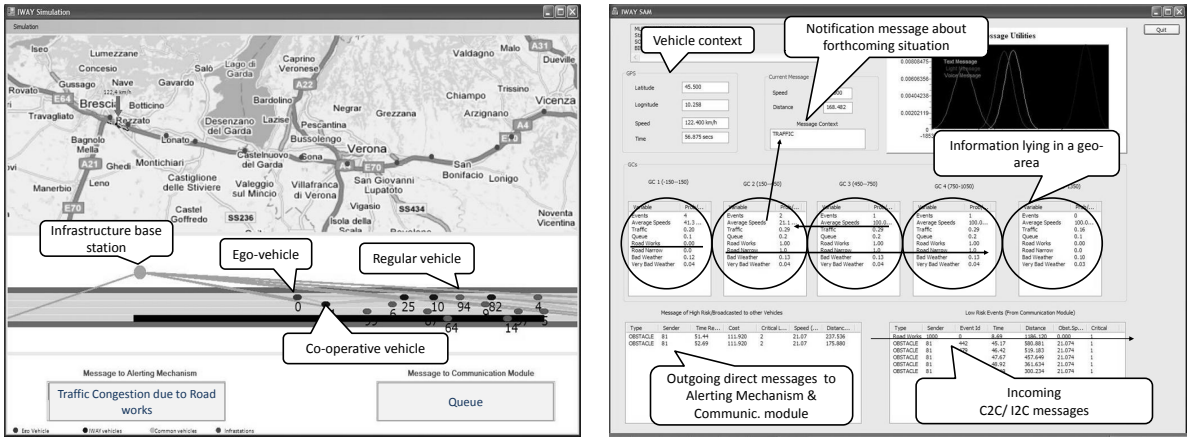

(a) (b)

Figure 7.16: (a) A long-range view of the traffic simulation and (b) a snapshot of the visual interface of the information handling.

In order to test the information handling in more complicated scenarios, we extended the simulator developed in section 7.2. The basic modification lies on the information handling that is performed according to the method described above instead of the initially developed rule based method.

Figures 7.16(a) and 7.16(b) constitute a time instance of an experiment execution that demonstrates the whole functionality of the information handling. In more detail, the incoming messages stored in the list refer to Obstacles detected by other cars and to Road Works event sent by the RI. The probabilities of all model variables within a geo-area are computed according to the evidence of specific events. Here the Road Works probability is 1 (high confidence) and the probability of slow traffic is increased with the number of incoming Obstacles messages in a geo-area. Then the Estimated Temporal Information Gains determine the valuable pieces of information given the current driving context (1st left circle). In the illustrated example the worth-reporting events are the Road Works and the Slow traffic which, given their interdependency, are combined in a single message "Slow traffic due to road works" (Fig. 7.16(a)).

7.4 Advanced Decision Making

In this section we present a methodology for advanced decision making based on Dynamic Bayesian networks. The goal is to provide the driver with tailored messages about critical forthcoming events. The types of messages vary according to a number of parameters like the severity of a given event (which is interpreted by the braking effort required by the driver until he reaches the safety limit), the driver state (stress and fatigue levels), the local weather and traffic conditions, etc. A sophisticated decision making is necessary to

ensure that the driver is aware of forthcoming events well in advance so he has enough time to react while at the same time the alerting system is as less distractive or irritating as possible. The possible actions of the Decision Maker are: no notification, text Message with information, light vocal message and intense vocal message. The decision making is based on the idea of Influence diagrams [60] and dynamic Bayesian networks. Dynamic Bayesian Networks (DBN) [106], are temporal extensions of the Bayesian Networks. When constructing a DBN for modelling changes over time, we include all variables $\mathbf{X} = \{X_1, X_2, , X_n\}$, at each time slice. If the current time step is represented by t, the previous time step by $t-1$, and the next step by $t+1$.

While in Bayesian Networks we have a unique structure G, denoting dependencies among variables, in DBNs we have two structures, the first one G_0, defines dependencies among variables on the same time slice, and the second one variables G_{trans}, defines time dependencies among variables in successive time slices. To construct a DBN model, the same basic steps must be followed, as those for constructing a simple Bayesian Network:

1. Define which variables are inserted in the model.
2. Define the structure of G_0 and G_{trans}.
3. Define the parameters of the variables involved in the model.

After completion of these three steps, one could modify both structure and parameters using experimental data and existing training algorithms.

DBNs, like simple static Bayesian Networks can be used to estimate the expected configuration of all or some of the variables, maybe given some evidence (information about the state of some variables). However in DBNs, those variables may lie on a future time slice, and represent a future configuration of the environment.

In order to have a Decision making model we need to add on the existing DBN model, two additional types of variables:

- The Decision Node (which decision to make)
- The Utility Nodes (negative costs on specific configurations of the model)

The Decision Node is usually a multinomial random variable, where the number of configurations is equal to the number of decisions we are able to make. The Utility Nodes are usually children of discrete variables and they consist of a table where we assign a cost for each possible configuration of the parent variables. However in our case, we have both discrete variables, so one can consider the utility nodes, as utility functions on some or all of the variables:

If X_i is continuous

$$R(X_i) = f(X_i), \text{ if } X_i \text{ continuous}, \tag{7.17}$$

and if X_i is discrete the utility function is given as:

$$R(X_i) = \begin{cases} w_0, \text{ if } X_i = x_{i0} \\ w_1, \text{ if } X_i = x_{i1} \\ \vdots \\ w_k, \text{ if } X_i = x_{ik} \end{cases} . \tag{7.18}$$

where x_ij the jth configuration of variable X_i and w_j the utility assigned to that configuration. Of course X_i can be one or more variables that are involved in the function R.

In the following sections we describe the variables inserted in the model, the structure and the parameters of the model, as well as the sampling technique used to estimate the risk function in future time slices. Finally, we examine the behavior of the decision making model, in predefined scenarios, using a simulation environment.

7.4.1 Variables of the model

First of all the variables of our decision making model are defined. A description of those is given in the following table. The variables are categorized into discrete and continuous. Next we describe how we threat the two different categories.

Discrete Variables

In the case of a discrete variable with only discrete parents its distribution follows a multinomial distribution:

$$P(X = x_i | Pa_{X^{ds}} = x_j^{ds}) = \theta_{ij}, \tag{7.19}$$

where x_i is the ith configuration of X, $Pa_{X^{ds}}$ the set of discrete parents of the X, x_j^{ds} the jth configuration of the parents and θ_{ij} the probability ($\sum_j \theta_{ij} = 1$). In the case of a discrete variable with both continuous and discrete parents its distribution is a softmax distribution

$$P(X = x_i | Pa_{X^c} = x^c, Pa_{X^{ds}} = x_j^{ds}) \sim \frac{e^{a_{ij}(x_i - b_{ij}x^c)}}{\sum_j e^{a_{ij}(x_i - b_{ij}x^c)}}, \tag{7.20}$$

where Pa_{X^c} the set of continuous parents of X.

From the above equation it holds that:

$$\sum_i P(X = x_i | Pa_{X^c} = x^c, Pa_{X^{ds}} = x_j^{ds}) = 1, \tag{7.21}$$

for each configuration x_j^{ds} of the discrete parents of X.

Continuous Variables

We model continuous variables as general conditional Gaussian distributions: If the variable X has no parents or only continuous parents:

$$X \sim N(f(Pa_{X^C}, \Delta t), \sigma \Delta t^2) \tag{7.22}$$

If the variable X has discrete parents with K possible configuration then the variable is distributed according to the following table:

$$X \sim \begin{cases} (N(f_1(Pa_(X^C), \Delta t), \sigma_1 \Delta t^2) \text{if } Pa_(X^d s) = x_1^d \\ \vdots \\ N(f_k(Pa_(X^C), \Delta t), \sigma_K \Delta t^2) \text{if } Pa_(X^d s) = x_K^d) \end{cases} \tag{7.23}$$

where Pa_{X^C} are the continuous parents of X and $Pa_{X^{ds}}$ the discrete parent of X and Δt the time interval between two successive time slices.

Model Structure Definition

Having defined which variables are used in our model, we then describe the structure of the model considering the inter- and intra- dependencies of our variables. The structure of G_0 is given in Fig. 7.17(a) and of $G_t rans$ in Fig. 7.17(b). We briefly describe hereby the reasoning of our structure: We first examine the intra-dependencies of the model (the dependencies in the same time-slice). In the first time slice, the speed of the vehicle depends only on the traffic conditions. The probability of the driver being distracted is related to the driver state and to the traffic conditions, since it is more likely to be distracted when there are a lot of stimulations around. The probability of driver seeing the obstacle, depends on the driver's state and the distance from the obstacle. The parameter of visibility is incorporated in the See's distribution parameters.

The Acknowledgment depends on the Decision we make (e.g. generate notification), if the driver is distracted or not, as well as on the driver's state.

The Memory variable, can be considered as a history variable, and contains the information about whether the driver has been notified with any message in the past. Obviously this variable depends only on the Decision variable.

In the following we examine the time-dependencies between the variables. For instance:

- If the driver sees the obstacle in the previous time slice then it also sees it in the next time slice.
- If the driver is aware (acknowledged) of the obstacle in time slice, then he will be aware also in the next time slice.
- If the driver reacts to the potential hazard in the previous time slice then it also Reacts in the next time slice.
- The reaction time increases when the driver is aware of the obstacle.

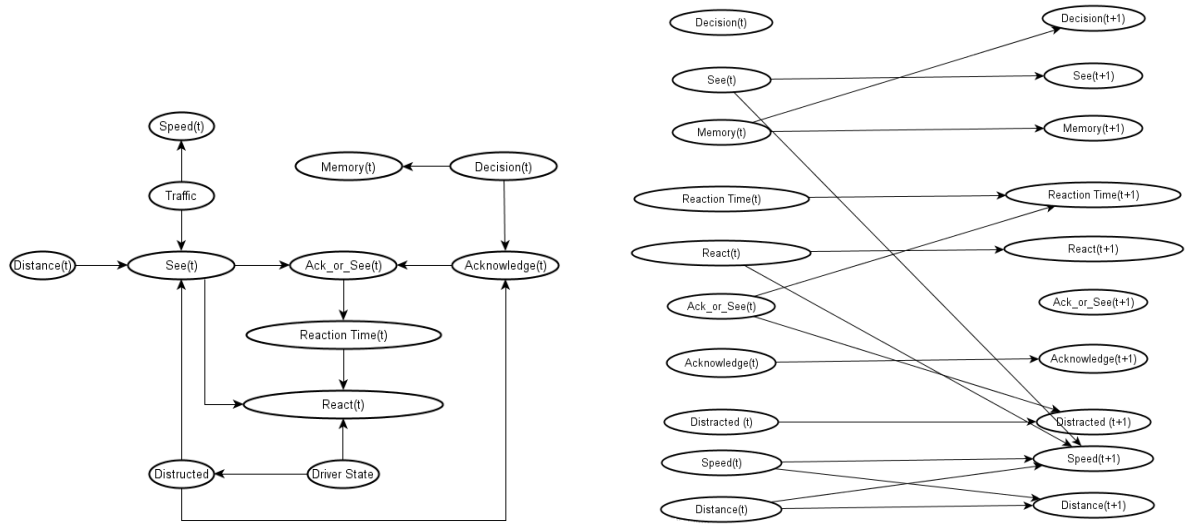

(a) (b)

Figure 7.17: (a) The structure of G_0 and (b) the structure of G_{trans}.

7.4.2 Variable Distributions

In Section 7.4.1 we gave an overview of the variables that are inserted in the model. For each of them we have to define the parameters of their distribution function, for both the G_0 and G_{trans}. Here we give some insight about the most important ones.

Decision

The Decision is treated as a random discrete variable. We have four possible decisions (Table 7.8) and obviously the discrete variable corresponding to the Decision shall have four states. We always estimate the expectations given the Decision in the first time slice D_0. In the first time slice all actions (Decision states) have the same probability. For the next time slices we give a large probability to the No-Message action and small to the other, in order to take the "optimal" decision, without let the model depend on future actions.

Speed

We have two different functions for the speed change. The first one is the free model when the driver does not react to the potential hazard:

$$f_f = V_{t-1}, \tag{7.24}$$

and the second one is the model according to which driver decelerates when acknowledged about the hazard:

Table 7.7: The parameters of speed distribution of G_trans.

React	See	Traffic	f	a_{max}	V_0
No	No	No	f_f	-	-
No	No	Yes	f_f	-	-
No	Yes	No	f_v	$\mu_f \cdot g$	Obstacles Speed
No	Yes	Yes	f_v	$\mu_f \cdot g$	Obstacles Speed
Yes	No	No	f_v	$(\mu_f \cdot g)/c$	20 m/s
Yes	No	Yes	f_v	$(\mu_f \cdot g)/c$	12 m/sec
Yes	Yes	No	f_v	$\mu_f \cdot g$	Obstacles Speed
Yes	Yes	Yes	f_v	$\mu_f g$	Obstacles Speed

$$f_V = V_{t-1} - a_{max} \cdot \Delta t \cdot e^{-b(a - a_{max}/2)}, \tag{7.25}$$

where

$$a = \min(0, \frac{(V_{t-1} - V_0)^2}{2 \cdot S_{t-1}} \tag{7.26}$$

The a_{max} and V_0 are the only values that change according to discrete parents configuration.

In Table 7.7 we the a_{max} and V_0 according to different configurations of discrete parents.

Where μ_f is the friction constant which depends on the weather conditions, g the gravity speed and c a constant ($c > 1$) which implies that the driver tend to decelerate more softly when not seeing the obstacle.

Distance

As far as the distance variable is concerned, the prediction of the distance in the future time slices is significantly important. The function of distance is obviously:

$$f_s = S_(t-1) - V_(t-1) * \Delta t \tag{7.27}$$

React

The react function is a softmax CPD used to model the cumulative distribution of the log-normal distribution of the Reaction Time of the driver. The React variable has a continuous parent (the Time to React) and three discrete parents:

- React $(t-1)$: If the driver is supposed to react in the previous time slice, then with high probability he will also react on the current time slice
- Driver State: The average reaction time increases when the driver is fatigue.
- Traffic: The average reaction time increases when there is traffic.

For each configuration of the above mentioned we have different expected reaction time distribution and we fitted the softmax function on the cumulative distribution of that distribution. In Fig. 7.18 we illustrate the cumulative distribution of the Log normal distribution (mean 1.2 with standard deviation 0.2) and the corresponding softmax function.

Time to React (RT_t)

If the driver is acknowledged about the obstacle, or "sees" the obstacle, then we consider that there is a time interval until the driver do react (we observe some speed reduction). If the driver Sees or is Aware of the obstacle, the function of time to react is considered as:

$$f_R T = RT_(t-1) + \Delta t, \tag{7.28}$$

otherwise

$$f_R T = 0. \tag{7.29}$$

Acknowledge

The Acknowledge variable describes the probability of the driver being aware of the potential Hazard. The basic rules used to derive the probability table are: i) the driver cannot be acknowledged if we give a Text Message and he is distracted, ii) there is a smaller probability for the driver to be acknowledged when he is tired (fatigue) and the notification is a Text Message and iii) moreover the driver tends to forget (slowly) the information, so the probability of acknowledged at $(t+1)$, given that he is acknowledged in (t) is less than 1.

Memory

Memory variable is used as the history of the past decision we made. It has two states (No Message Given/Message Given). When a Decision for a message is taken, the Memory takes the state Message Given. For the next time slice the Memory variable has the same state as in the previous time slice, so if at some point we decide to give a message, thereafter the Memory variable will always have the Message Given state, otherwise it will always have the No Message Given state.

Utility Functions

Having defined the parameters of the model, we need also to define the cost functions according to which the decisions are made. We have two basic categories for utility functions: safety related system acceptance related In the following we briefly describe the utilities functions for each of the two categories.

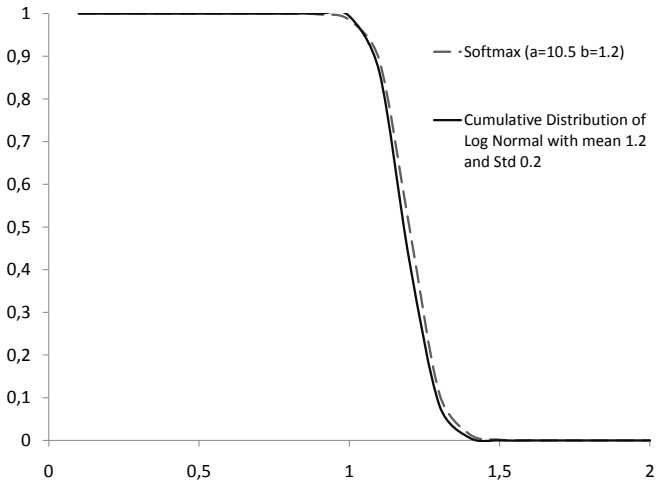

Figure 7.18: The cumulative distribution of the Log normal distribution (mean 1.2 with standard deviation 0.2) and the corresponding softmax function.

Table 7.8: The variables of the DBN model.

Variable	Description	Type	Notation
Decision	No Message/ Text Message/ Voice Message/ Intense Voice Message	Discrete	D
Memory	A variable indicating if we provided message on the past	Discrete	M
Driver State	If the driver is in fatigue or stress state in fatigue or stress state	Discrete	Ds
Weather	Good/Bad/Very Bad	Discrete	W
Traffic	Traffic condition	Discrete	T
Distracted	An estimation if the driver is distracted or not	Discrete	Da
Acknowledged	An estimation if the driver is aware of the hazard	Discrete	Ack
See	If the driver sees the obstacle	Discrete	See
Acknowledged or See	A combination of the two variables	Discrete	$AcqOrSee$
React	If the driver reacts to the potential Hazard	Discrete	R
Reaction Time	Time passed from the time driver has been acknowledged about the hazard	Continuous	Rt
Speed	Speed of the Vehicle	Continuous	V
Distance	Distance from the Hazard	Continuous	S
Time of Day	Day/Night	Discrete	Day

7.4.3 Safety Related Utility Functions

Reaction Time

The first function used to meet safety requirements is a function of the reaction time of the driver according to the estimated speed and distance in different time slices

$$B_t = \frac{S_t - \frac{(V_t - V_0)^2}{2\mu_f \cdot g}}{V_t} \tag{7.30}$$

$$R_t = \frac{C}{1 + e^{a(B_t - b)}} \tag{7.31}$$

$$\tag{7.32}$$

C is a multiplicative factor, that depends on the context. In our first approach this factor depends on weather conditions. However almost all the other variables (e.g. driver state) are also involved in this utility function, since they contribute in the estimation of speed in next time slices.

Driver State

A utility is assigned to voice messages when the driver state is stress. This utility is magnified in traffic conditions and very high speeds (where a nervous reaction could cause accident). This should lead to strategies where Voice messages are produced earlier in order to avoid possible invocation of intense voice messages.

A utility is also assigned to intense voice messages when the driver state is fatigue. This is to ensure that the driver is alerted about the forthcoming event.

Driver Distraction

When the speeds are high or an obstacle is close, the Text Message has an additional cost, because it can distract the driver.

7.4.4 System acceptance Utilities

Message Repetition

In order to avoid unnecessary messages to the driver we assign negative utilities (cost) to the Text Message (-100), Voice Message (-200) and Intense Voice Message (-300).

Information Provision

We also assign a very large utility to the state of Memory variable corresponding to "message provided". This enforces the system to produce at least one message, since it is not acceptable to hide information from the driver.

for all $j = 1 \cdots M$ where M the number of samples **do**
  for all $d = 1 \cdots D$ where D the number of possible decisions **do**
    $V^0 = E^0, d$
    $w_j = 1$
    Get the i variable in the elimination order El.
    if the variable X_i^0 is Evidence **then**
      $w_j = w_j \cdot P^0(X_i^0 = E_i | Pa_{X_i^0} \in V_j^0)$
    else
      Sample the X_i^0 variable (according to X_i^0's distribution) given the sampled values of its parents:
      $x_{ij}^0 \sim P^0(X_i^0, Pa_{X_i^0} \in V_j^0)$
      $V_j^0 = V_j^0 \cup x_{ij}^0$
    for all $t = 1 \cdots K$ where K the number of time slices **do**
      $V^t = E^t$
      Get the i variable in the elimination order El.
      if the variable X_i^0 is Evidence **then**
        $w_j = w_j \cdot P^t(X_i^t = E_i | Pa_{X_i^t} \in V_j^t, Pa_{X_i^{t-1}} \in V_j^{t-1})$
      else
        Sample the X_i^0 variable (according to X_i^0's distribution) given the sampled values of its parents:
        $x_{ij}^0 \sim P^0(X_i^0, Pa_{X_i^0} \in V_j^0)$
        $V_j^0 = V_j^0 \cup x_{ij}^0$

Algorithm 6: Sampling(El:Elimination order of G_0,E:Evidence)

7.4.5 Utility estimation for each possible action

The next step is the estimation of the expected utility of each decision. This is not trivial in case of both discrete and continuous variables, so we use approximate inference instead, based on sampling.

After applying the sampling procedure we get a set of samples for each time slice. Using those samples we can estimate the expectation of the utility function according to the following equation:

$$E[R(X_i^t)|D = d] = \frac{\sum_j \text{ where } {}_{d_j=d}\, w_j R(x_{ij}^t)}{\sum_j \text{ where } {}_{d_j=d}\, w_j} \tag{7.33}$$

$$E[R(X_i^t)] = \frac{\sum_j w_j R(x_{ij}^t)}{\sum_j w_j} \tag{7.34}$$

In a similar way we can estimate the variance of our variables:

$$
\begin{aligned}
Var[R(X_i^t)|D=d] &= E[R(X_i^t)|D=d] - E[R(X_i^t)|D=d] \cdot E[R(X_i^t)|D=d] && (7.35)\\
&= \frac{\sum_j \text{ where } {}_{d_j=d}\, w_j R(x_{ij}^t)^2}{\sum_j \text{ where } {}_{d_j=d}\, w_j} && (7.36)\\
&\quad -E[R(X_i^t)|D=d] \cdot E[R(X_i^t)|D=d] && (7.37)\\
Var[R(X_i^t)] &= \frac{\sum_j w_j R(x_{ij}^t)^2}{\sum_j w_j} - E[X_i^t] \cdot E[X_i^t] && (7.38)
\end{aligned}
$$

We should notice one potential drawback of the above-mentioned algorithm. In many cases when the evidence is very unlikely the w_j's could be very small, or even zero and our estimation of $E[X_i^t]$ is far from accurate. This could be magnified if we had evidence in far time slices. However in our case, due to the nature of evidence and the model design, this is not the case and we are always able to take a fair estimation of the $E[X_i^t|D=d]$. Moreover, there is an additional advantage of our solution. The approximate inference algorithms are in many cases also called any-time inference algorithms. The reason is that at any time you can stop the procedure and use the samples that are already produced for at least a poor estimation.

The total utility of any decision is a sum over all the different utility functions.

$$\mathbf{R}_d^t = \sum_j R_{jd}^t = \sum_j E[R_j(X_j^t)|D=d] \tag{7.39}$$

where X_j^t the variables involved in the utility function R_j in time slice t.

The average utility of a decision d over P time slices is given as

$$\mathbf{R}_d = \frac{1}{P}\sum_{t=1}^{t=P} R_d^t \tag{7.40}$$

The action d that the system does is the one with the higher R_d.

7.4.6 Driver warning simulator

In order to test the decision making mechanism and the driver warning we extended the simulator used for the fatigue study presented in Section (3). The simulation environment (Fig. 7.19) supports a short-range view of the ego-vehicle and its surroundings. The simulator contains the following parts:

1. A 3d environment
2. The ego-car sensor emulators
3. An HMI emulator.

In the following we describe the development of the 3 main parts of the simulator.

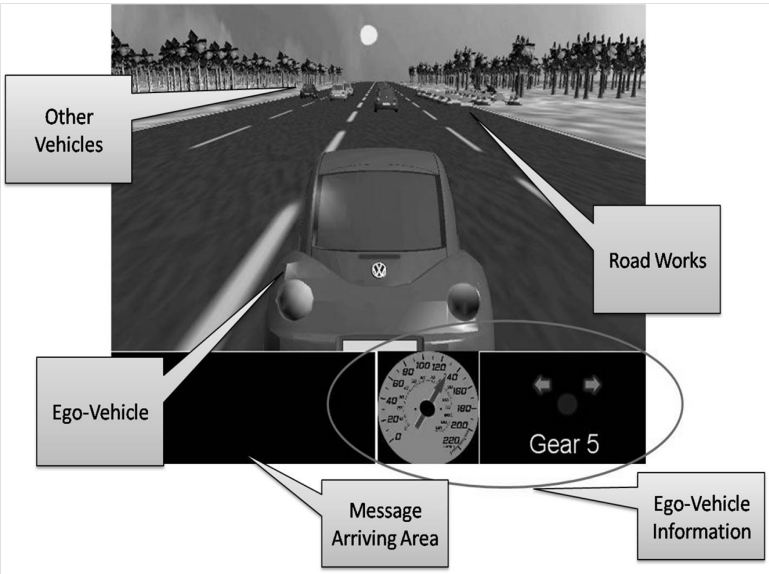

Figure 7.19: The simulation environment

The 3D environment

For the development of a realistic 3d environment we used the Microsoft XNA framework, which is based on the Directx3d and provides many higher level utilities for a developer of 3d engines. The world on this environment consists of:

- A highway Road (with four lanes)
- Surrounding Environment (sky, trees, grass, sun)
- Other vehicles (eventually some of those, will be other vehicles)
- Potential Obstacles (e.g. road works)

The user has control over the ego-vehicle. The camera follows that vehicle, and for vehicle controlling we use the Logitech Steering Wheel, which includes:

- Steering wheel: used to steer the vehicle.
- Gear: each gear has a maximum and minimum speed, as well as different maximum acceleration. The change of gear is manual.
- Acceleration and brake pedals: used to accelerate and decelerate the vehicle.
- Buttons on the steering wheel: used to emulate other functions (activating right and left indicators)

Furthermore since we have a vehicle controlled by the user (steering angle, acceleration), we needed a vehicle dynamics model to simulate the behavior of the vehicle, according to the input of the driver. Those dynamics are described in detail in [35, 101]. For the other

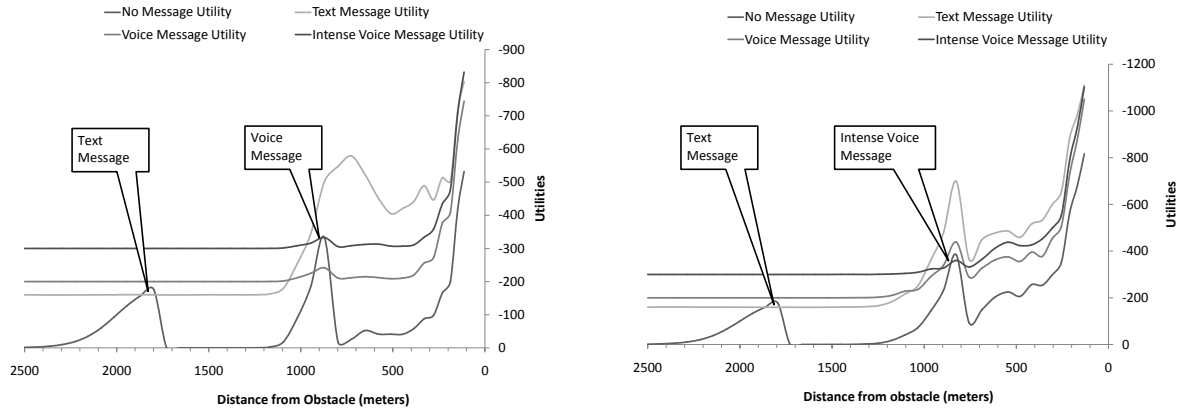

(a) (b)

Figure 7.20: The utility of each decision as a function of the distance from the obstacle. We also demonstrate the time instances where the system makes a decision different from *no message*.

vehicles in the environment we used the IDM model [144]. This model calculates the acceleration and deceleration of vehicles on a single lane in order to keep a safety distance between them. In order to produce a more realistic environment we added a simple lane change behavior to those vehicles as described in Section 7.2.

Ego-Vehicle Sensor Emulators

The sensors emulated are: i) a radar sensor for detection of preceding vehicles (distance and speed) and ii) a video sensor for lane detection and lateral vehicle position estimation.

Can-Bus/Radar Sensor Emulators

Those two sensors are more easily emulated. The basic information of the can-bus (speed, left/right indicator etc) are extracted from the simulation context.

GPS Emulation

The GPS information (latitude, longitude, speed and heading) are extracted from the simulation context. Our road is straight, and starts from a specific latitude and longitude position with a specific angle. All vehicles have the same heading. The current position of a vehicle is extracted from the position on the road (distance traveled) and the starting position. This holds also for the ego-vehicle.

Using the information of the above sensors we detect events in the proximity of the vehicle, whereas a list of various long range messages, corresponding to infrastructure or other vehicles, is stored in a database and provided to the vehicle at specific time instances. In Figs. 7.20(a) and 7.20(b) we present the behavior of the decision making

for two scenarios. In both cases we have received a message of an obstacle ahead and we instructed the driver to keep a constant speed near 35 m/sec as approaching the virtual obstacle, and to decelerate once arriving at a specific distance from it. In the first scenario the driver state is considered normal, whereas the weather is considered good. We observe that the system produces two messages: one text message and one regular voice message. In the second scenario, the driver is considered in fatigue state and the weather rainy. We observe that the system instead of a regular voice message produces an intense voice message.

7.5 Discussion

We have presented three studies on individual parts of an advanced cooperative driving system. A cooperative driving system is an advanced driver assistance system (ADAS) that exploits wireless communications (vehicle -to- vehicle communication and road infrastructure -to- vehicle communication) with the scope to extend driver's perception through the information coming from the external environment and to develop more accurate pre-crash warning systems. In the first study we focused on the communication requirements (range, latency, broadcasting frequency) of a driving cooperative system that need to be met, in order to achieve a safety gain. An enhanced situation assessment was also achieved through the merging of different information sources and the evaluation of individual risks, which was tested through a long-range simulation environment, specially built for testing purposes. In the second study an intelligent information handling mechanism was developed. It is designed to perform information fusion and reasoning and to extract high-level worth-reporting information for the driver. For the information fusion we followed an approach based on geo-reference representation of the ego-vehicle and forthcoming events while for the inference on the road situation and the definition of the notification content, we developed a methodology based on Bayesian networks. The proposed methodology supports the management of low-confident or missing information sources (e.g. absence of road infrastructure), as well as the generation of consolidated messages about geo-related events (e.g. Traffic due to Road Works, Accident caused Road Closure, etc). The validity and prioritization of forthcoming events are also tackled through the Information Gain, a parameter introduced as a measurable indicator of notification importance, given the current driving context. The outcome of the advanced information handler is the generation of enhanced notification messages. These enhanced notifications are further used by a decision making mechanism [124] in order to provide the driver with an optimal warning strategy about forthcoming hazards. This is described in the third study of this chapter. The decision making is based on sampling of Dynamic Bayesian networks for driving risk evaluation and decides upon the best warning strategy, taking into account both environmental conditions and driver's state. The decision mechanism was evaluated on a user interactive simulation environment. The conducted experiments showed that the information of the driver psycho-physiological state if incorporated into the pre-crash

warning systems, can evolve further this technology by increasing the safety margins with the provision of alerts tailored to the current driver status.

Chapter 8

Conclusions and Future Work

8.1 Conclusions

We presented a study on the detection of driver's fatigue and stress levels. Our estimation of fatigue levels is feasible using only physiological signals (ECG, Respiration, EDA) with a 86% accuracy on three fatigue levels. Stress detection, based only on physiological signals proved a more difficult problem. By incorporating more information into the system, such as video features or environmental factors, wthe accuracy in fatigue and stress levels estimation is increased (87.5% accuracy on three fatigue levels and 85% accuracy on two stress levels).

The main difference from similar works, is that drivers were monitored during ordinary work days, without restriction on sleep hours or external stimulations, for a long period of time. Thus, we consider that this study truly depicts the actual physiological status of the particular subject during driving, and the obtained results correspond to near optimum performance of a real (personalized) driver status monitoring system. In a simulation environment it was verified that both *low* and *high* fatigue states lead to driving performance impairment. Furthermore the relation of physiological signals and driving performance was studied. Our results indicate that using only drivers' physiological measurements, a prediction of reaction time is possible. This implies that an in-vehicle system capable of monitoring driver's physiological signals, could be trained to predict the reaction times of the driver prior to events and adjust accordingly the safety margins of a driver assistance system.

The physiological state of stress is strongly associated with driving conditions and the presence of specific increased-risk driving events. Towards this direction, we proposed a methodology, applicable in real-time, for assessing drivers' stress events based

on physiological signals' monitoring (ECG, EDA and respiration) and a driving history which is built upon information from GPS and CAN-bus. The information extracted is incorporated into a BN model for stress event detection. The proposed methodology was evaluated in real driving conditions and demonstrated good generalization performance, mainly due to the online parameter estimation. The proposed methodology, associating driver's stress events with specific driving events, could exploit Bayesian Framework's reasoning ability and answer to queries of the type "is the driver stressed when overtaking?". Such queries reveal valuable information about driving behavior which can be exploited by the new generation of advanced driver assistance systems.

A very important issue in physiological state recognition systems, is the adaptation to new subjects-drivers. We presented an approach based on the estimation of the parameters of a geometric transformation applied on a Gaussian mixture model. The method proposed here is based on the EM framework. We considered both the cases of full positive definite and spherical covariance matrices. The original approach gives very good results, when the distance of the initial guess and the actual transformation parameters is relatively small. This is a restriction inherited from EM behavior, since it can be considered as a local optimization method. To overcome this problem, we extended the original EM approach to a multiple start one. The multiple-start EM had significant higher probability of finding the correct solution. Finally we extended the initial transformation model, allowing each component having an individual-local transformation, under the assumption that local transformations are smaller in magnitude than the global one. This assumption is incorporated in the EM framework using prior distribution on the local transformation parameters, leading to a MAP-EM approach. Finally we demonstrated how the described method can be applied for the adaptation of a driver state recognition system to new drivers, with very promising initial results.

Information about driver's physiological state is valuable for modern driver support systems, since they could adapt their strategies accordingly, increasing driving safety. In the last Chapter we perform a study on the basic functionalities of a new generation driver support system, which is able to assess driver's state, as well as the driving environment through in-vehicle sensors and communication with other vehicles and road infrastructure. We initially conducted a series of experiments in a macroscopic traffic simulator to investigate the safety gain from such systems and derive some minimum requirements in communication characteristics in order to maximize this gain. An emerging need for those systems is the advanced information fusion, since there is incoming information from different sources with low confidence and credibility (other vehicles) as well from high confidence sources (road infrastructure). We propose a solution based on Bayesian networks, which is suitable for both information fusion and evidence explanation. Using the proposed solution we could extract the messages which are more informative for the driver. Furthermore, we investigate the use of Dynamic Bayesian networks for optimal warning strategy selection, replacing the simplistic non-adaptive rule based methods employed by the state-of-the-art alerting mechanisms.

8.2 Future Work

In the recognition of driver's physiological state, there are several future directions. The first one is to search for physiological signal characteristics that could discriminate better different fatigue and stress levels. We could also use more information, such as facial expressions, or to investigate new sensors such as thermal imaging. Next we should test the adaptation methodology proposed in a large set of drivers.

Concerning stress event detection, the discrimination of stress events in a larger scale could be very beneficial, since events including higher risk are more probably to lead to changes in the physiological state and driving behavior. In order to distinguish stress event in a larger scale, we need a more precise annotation method, a better physiological signal acquisition equipment, neglecting noise due to drivers movements, and probably incorporate additional information, such as facial expressions and head movements. Another possible extension of the proposed methodology is the prediction and evaluation, in terms of the risk involved, of specific driver actions, i.e. overtaking. We observed that prior to such an event there is an activation of the nervous system, related to the decision making process. Using the evidence of this activation and the driving behavior of the driver we could estimate driver's intension for overtaking. Having also a better assessment of the driving environment we could evaluate the risk of such a decision and either warn the driver or simply evaluate his driving behavior (aggressive, passive etc.). Regarding the proposed method for estimating the geometric transformation on a Gaussian Mixture mode, we should study more comprehensively the convergence criteria of this method. Concerning the global and local transformations estimation, we progressively relax the constraints imposed on local transformation parameters. However, there could more advanced methods for constraints adaptation, for example relaxing and tightening according to the increase in the log-likelihood function. Finally, the proposed method, is quite generic and can be easily applied to other problems, such as image and point set registration.

Finally for the system proposed for advanced driver support systems, the information fusion and the decision making should be reshaped using data collected from an improved and even more realistic simulation environment, which will truly reveal drivers' responses to the outputs of a warning system.

Bibliography

[1] ISO 10075-3:2004. Ergonomic principles related to mental workload – part 3: Principles and requirements concerning methods for measuring and assessing mental workload. Technical report.

[2] P.A. Hancock and W.B. Verwey. Fatigue, workload and adaptive driver systems. *Accid Anal Prev*, 29(4):495–506, 1997.

[3] R. Lazarus and S. Folkman. *Stress, Appraisal, and Coping*. Springer Publishing Company, March 1984.

[4] M. Aitkin. A general maximum likelihood analysis of overdispersion in generalized linear models. *Statistics and Computing*, 6(3):251–262, 1996.

[5] M. Aitkin. Likelihood and Bayesian analysis of mixtures. *Statistical Modeling*, 1(4):287–304, 2001.

[6] T. Akerstedt. Work hours, sleepiness and the underlying mechanisms. *J Sleep Res*, 4(S2):15–22, 1995.

[7] K. Anderson and P.W. McOwan. A real-time automated system for the recognition of human facial expressions. *IEEE Transactions on Systems, Man and Cybernetics*, 36(1):96–105, 2006.

[8] S. Asteriadis, N. Nikolaidis, and I. Pitas. Facial feature detection using distance vector fields. *Pattern Recognition*, 42(7):1388–1398, 2009.

[9] R.W. Backs and K.A. Seljos. Metabolic and cardiorespiratory measures of mental effort: the effects of level of difficulty in a working memory task. *Int J Psychophysiol*, 16(1):57–68, 1994.

[10] Inc. Biopac.

[11] C.M. Bishop. *Neural Networks for Pattern Recognition*. Oxford University Press, November 1995.

[12] R. Bittner, P. Smrcka, M. Pavelka, P. Vysok, and L. Pousek. Fatigue indicators of drowsy drivers based on analysis of physiological signals. *ISMDA '01: Proceedings of the Second International Symposium on Medical Data Analysis*, pages 62–68, 2001.

[13] K. Blekas, A. Likas, N. P. Galatsanos, and I. E. Lagaris. A spatially constrained mixture model for image segmentation. *Neural Networks, IEEE Transactions on*, 16(2):494–498, 2005.

[14] E.R.B. Bojorges-Valdez, J.C. Echeverria, R. Valdes-Cristerna, and M.A. Pena. Scaling patterns of heart rate variability data. *Physiol Meas*, 28(6):721–30, 2007.

[15] S.S. Brandt. Maximum likelihood robust regression by mixture models. *J. Math. Imaging Vis.*, 25(1):25–48, 2006.

[16] B. Brenner and M.L. Selzer. Risk of causing a fatal accident associated with alcoholism, psychopathology, and stress: further analysis of previous data. *Behav. Sci*, 14(6):490–5, 1969.

[17] H. Breu, J. Gil, D. Kirkpatrick, and M. Werman. Linear time euclidean distance transform algorithms. *IEEE Transactions on Pattern Analysis and Machine Intelligence*, 17:529–533, 1995.

[18] I.D. Brown. Driver fatigue. *Hum Factors*, 36(2):298–314, 1994.

[19] P. Burns and T.C. Lansdown. E-distraction: The challenges for safe and usable internet services in vehicles. Technical report, NHTSA Driver Distraction Internet Forum, 2009.

[20] M. Chipman and Y.L. Jin. Drowsy drivers: The effect of light and circadian rhythm on crash occurrence. *Safety Science*, In Press, Corrected Proof, 2009.

[21] C. Constantinopoulos and A. Likas. Unsupervised learning of gaussian mixtures based on variational component splitting. *IEEE transactions on neural networks*, 18(3):745–755, 2007.

[22] T. Cootes, G. Edwards, and C. Taylor. Active appearance models. In *Computer Vision ὐ ECCV'98*, pages 484–498. 1998.

[23] A. Crawford. Fatigue and driving. *Ergonomics*, 4:143–54, 1961.

[24] P.E. Danielsson. Euclidean distance mapping. *Computer Graphics and Image Processing*, 14(3):227–248, 1980.

[25] D.R. Davies and R. Parasuraman. *The psychology of vigilance.* Academic, London, 1982.

[26] M.E. Dawson, A.M. Schell, and D.L. Filion. *Handbook of psychophysiology.* Cambridge University Press, New York, 2000.

[27] A.P. Dempster, N.M. Laird, and D.B. Rubin. Maximum likelihood from incomplete data via the em algorithm. *Journal of the Royal Statistical Society Ser. B*, 39, 1977.

[28] V. Digalakis, D. Rtischev, L. Neumeyer, and Edics Sa. Speaker adaptation using constrained estimation of gaussian mixtures. *IEEE Transactions on Speech and Audio Processing*, 3:357–366, 1995.

[29] C. Dussault, J.C. Jouanin, M. Philippe, and C.Y. Guezennec. Eeg and ecg changes during simulator operation reflect mental workload and vigilance. *Aviat Space Environ Med*, 76(4):344–51, 2005.

[30] J.C. Echeverria, M.S. Woolfson, J.A. Crowe, B.R. Hayes-Gill, G.D. Croaker, and H. Vyas. Interpretation of heart rate variability via detrended fluctuation analysis and alphabeta filter. *Chaos*, 13(2):467–75, 2003.

[31] S. Eichler, B. Ostermaier, C. Schroth, and T. Kosch. Simulation of car-to-car messaging: analyzing the impact on road traffic. *Modeling, Analysis, and Simulation of Computer and Telecommunication Systems, 2005. 13th IEEE International Symposium on*, pages 507–510, 27-29 Sept. 2005.

[32] I. Fasel, B. Fortenberry, and J. Movellan. A generative framework for real time object detection and classification. *Computer Vision and Image Understanding*, 98(1):182–210, 2005.

[33] C. Fraley and A. Raftery. Bayesian regularization for normal mixture estimation and model-based clustering. *Journal of Classification*, 24(2):155–181, 2007.

[34] D. Gerogiannis, C. Nikou, and A. Likas. The mixtures of student's t-distributions as a robust framework for rigid registration. *Image Vision Comput.*, 27(9):1285–1294, 2009.

[35] T.D. Gillespie. *Fundamentals of Vehicle Dynamics*. Society of Automotive Engineers, Inc., Warrendale, PA, 1992.

[36] C.J. Golden. Stroop color and word test: A manual for clinical and experimental uses. *Unknown Journal*, pages 1–32, 1978.

[37] L.A. Goodman. Exploratory latent structure analysis using both identifiable and unidentifiable models. *Biometrika*, 61(2):215–231, 1974.

[38] E. Grandjean. Fatigue in industry. *Br J Ind Med*, 36(3):175–86, 1979.

[39] E. Grandjean. *Fitting the task to the man: a textbook of occupational ergonomics (4th ed.)*. Taylor & Francis/Hemisphere, 1989.

[40] E. Gulian, G. Matthews, A.I. Glendon, D.R. Davies, and L.M. Debeney. Dimensions of driver stress. *Ergonomics*, 32(6):585–602, 1989.

[41] R.I. Hammoud and H. Zhang. Alertometer: Detecting and mitigating driver drowsiness and fatigue using an integrated human factors and computer vision approach. In *Passive Eye Monitoring: Algorithms, Applications and Experiments*. Springer Berlin Heidelberg, 2008.

[42] T.C. Hankins and G.F. Wilson. A comparison of heart rate, eye activity, eeg and subjective measures of pilot mental workload during flight. *Aviat Space Environ Med*, 69(4):360–7, 1998.

[43] J. Healey. *Wearable and Automotive Systems for Affect Recognition from Physiology*. PhD thesis, M.I.T, 2000.

[44] J. Healey, J. Seger, and R. Picard. Quantifying driver stress: developing a system for collecting and processing bio-metric signals in natural situations. *Biomed Sci Instrum*, 35:193–8, 1999.

[45] J.A. Healey and R.W. Picard. Detecting stress during real-world driving tasks using physiological sensors. *Intelligent Transportation Systems, IEEE Transactions on*, 6:156–166, 2005.

[46] J.A. Healey and R.W. Picard. Smartcar: Detecting driver stress. In *Pattern Recognition,15th International Conference on*, volume 4, pages 218–221, 2000.

[47] K. Heaton, S. Browning, and D. Anderson. Identifying variables that predict falling asleep at the wheel among long-haul truck drivers. *Aaohn J*, 56(9):379–85, 2008.

[48] A. Heino, H.H. van der Molen, and G.J.S. Wilde. Traffic research centre. Technical Report VK 90-22, University of Groningen, 1990.

[49] R.J. Heslegrave and J.J. Furedy. Sensitivities of hr and t-wave amplitude for detecting cognitive and anticipatory stress. *Physiol Behav*, 22(1):17–23, 1979.

[50] J.D. Hill and L.N. Boyle. Driver stress as influenced by driving maneuvers and roadway conditions. *Transportation Research Part F: Traffic Psychology and Behaviour*, 10(3):177–186, 2007.

[51] E. Hjelmas and B.K. Low. Face detection: A survey. *Computer Vision and Image Understanding*, 83(3):236–274, 2001.

[52] M. Horvath, E. Frantik, K. Kopriva, and J. Meissner. Eeg theta activity increase coinciding with performance decrement in a monotonous task. *Activitas Nervosa Superior*, 18(3):207ỏ210, 1976.

[53] http://www.safespeed.org.uk/. Last visited 10-3-2008.

[54] Q. Huang, J. Yang, and Y. Zhou. Variational bayesian method for speech enhancement. *Neurocomputing*, 70(16-18):3063–3067, 2007.

[55] G. Jahn, A. Oehme, J.F. Krems, and C. Gelau. Peripheral detection as a workload measure in driving: Effects of traffic complexity and route guidance system use in a driving study. *Transportation Research Part F: Traffic Psychology and Behaviour*, 8(3):255 – 275, 2005.

[56] C.B. James. *Pattern Recognition with Fuzzy Objective Function Algorithms*. Kluwer Academic Publishers, 1981.

[57] M. James, T.C. Doege, R.M. Davis, and M.A. Williams. Sleepiness, driving, and motor vehicle crashes. *JAMA*, 279:1908–1913, 1998.

[58] W.H. Janssen, H. Alm, J.A. Michon, and A. Smiley. Driver support. pages 53–66, 1993.

[59] J.R. Jennings, J.C. Stringfellow, and M. Graham. A comparison of the statistical distributions of beat-by-beat heart rate and heart period. *Psychophysiology*, 11(2):207–10, 1974.

[60] F.V. Jensen. *Bayesian Networks and Decision Graphs*. Springer-Verlag New York, Inc., Secaucus, NJ, USA, 2001.

[61] B. Jian and B.C. Vemuri. A robust algorithm for point set registration using mixture of gaussians. In *ICCV '05: Proceedings of the Tenth IEEE International Conference on Computer Vision*, pages 1246–1251, Washington, DC, USA, 2005. IEEE Computer Society.

[62] P.G. Jorna. Spectral analysis of heart rate and psychological state: a review of its validity as a workload index. *Biol Psychol*, 34(2-3):237–57, 1992.

[63] P.G. Jorna. Heart rate and workload variations in actual and simulated flight. *Ergonomics*, 36(9):1043–54, 1993.

[64] D. Kahneman. *Attention and effort.* Prentice Hall, New Jersey, U.S.A., 1973.

[65] M. Kass, A. Witkin, and D. Terzopoulos. Snakes: Active contour models. *International Journal of Computer Vision*, V1(4):321–331, 1988.

[66] C.D. Katsis, G. Ganiatsas, and D.I. Fotiadis. An integrated telemedicine platform for the assessment of affective physiological states. *Diagnostic Pathology*, 1:1–16, 2006.

[67] C.D. Katsis, N. Katertsidis, G. Ganiatsas, and D.I. Fotiadis. Towards emotion recognition in car racing drivers: a biosignal processing approach. *IEEE Transactions on Systems, Man and Cybernetics, Part A: Systems and Humans*, 38(3):502–512, 2008.

[68] G. Kecklund, T. Akerstedt, D. Sandberg, M. Wahde, T. Dukic, and A. Anund. State of the art review of driver sleepiness. Technical report, Volvo, 2006.

[69] B.S. Kerner, S.L. Klenov, and A. Brakemeier. Testbed for wireless vehicle communication: a simulation approach based on three-phase traffic theory, 2007.

[70] D. Kim, Y. Seo, S. Kim, and S .Jung. Short term analysis of long term patterns of heart rate variability in subjects under mental stress. In *International Conference on BioMedical Engineering and Informatics (BMEI 2008)*, volume 2, pages 487–491, Sanya, 2008.

[71] T. Kim and D.J. Lovell. Observation of real driving behavior in car-following: preliminary results. *Vehicular Technology Conference, 2005. VTC 2005-Spring. 2005 IEEE 61st*, 5:2939–2943 Vol. 5, 30 May-1 June 2005.

[72] A. Kircher, M. Uddman, and J. Sandin. Vehicle control and drowsiness. Technical report, Swedish National Road and Transport Research Institute, 2002.

[73] S.G. Klauer, T.A. Dingus, V.L. Neale, J.D. Sudweeks, and D.J. Ramsey. The impact of previous driver inattention on near crash/crash risk: An analysis using the 100-car naturalistic driving study data, 2006.

[74] T. Kosilo, J. Kolakowski, and Z. Walczak. Project safespot (smart vehicles on smart roads). *Microwaves, Radar and Wireless Communications, 2006. MIKON 2006. International Conference on*, pages 215–215, 22-24 May 2006.

[75] A.F. Kramer. Physiological metrics of mental workload: A review of recent progress. In D.L. Damos, editor, *Multiple-Task performance*, pages 279–328. Taylor and Francis, London, 1991.

[76] H.H. Kramer, S. Rammos, O. Krogmann, L. Nessler, S. Boker, A. Krian, and W. Bircks. Cardiac rhythm after mustard repair and after arterial switch operation for complete transposition. *Int J Cardiol*, 32(1):5–12, 1991.

[77] L. Kunhui, H. Jiyong, C. Jiawei, and Z. Changle. Real-time eye detection in video streams, 2008.

[78] S.K. Lal, A. Craig, P. Boord, L. Kirkup, and H. Nguyen. Development of an algorithm for an eeg-based driver fatigue countermeasure. *J Safety Res*, 34(3):321–8, 2003.

[79] S. Lauritzen and F. Jensen. Stable local computation with conditional gaussian distributions. *Statistics and Computing*, 11(2):191–203, 2001.

[80] Y. Lecun, L. Bottou, Y. Bengio, and P. Haffner. Gradient-based learning applied to document recognition. *Proceedings of the IEEE*, 86(11):2278–2324, 2002.

[81] D. H. Lee and K. S. Park. Multivariate analysis of mental and physical load components in sinus arrhythmia scores. *Ergonomics*, 33(1):35–47, 1990.

[82] D. Lee. Effective gaussian mixture learning for video background subtraction. *IEEE Transactions on Pattern Analysis and Machine Intelligence*, 27(5):827–832, 2005.

[83] M.H. Lee, G. Yang, H.K. Lee, and S. Bang. Development stress monitoring system based on personal digital assistant (pda). In *Conf Proc IEEE Eng Med Biol Soc*, volume 4, pages 2364–7, 2004.

[84] J.Q. Li and A.R. Barron. Mixture density estimation. In *In Advances in Neural Information Processing Systems 12*, pages 279–285. MIT Press, 1999.

[85] Z. Li. Spectral analysis of heart rate variability as a quantitative indicator of driver mental fatigue. Technical report, SAE International, 2002.

[86] W. Liao, W. Zhang, Z. Zhu, and Q. Ji. A decision theoretic model for stress recognition and user assistance. In *AAAI*, pages 529–534, 2005.

[87] W. Liao, W. Zhang, Z. Zhu, and Q. Ji. A Real-Time Human Stress Monitoring System Using Dynamic Bayesian Network. In *CVPR*, 2005.

[88] C.L. Lisetti and F. Nasoz. Using noninvasive wearable computers to recognize human emotions from physiological signals. *EURASIP J. Appl. Signal Process.*, 2004(1):1672–1687, 2004.

[89] J. Ma and S. Fu. On the correct convergence of the em algorithm for gaussian mixtures. *Pattern Recognition*, 38(12):2602 – 2611, 2005.

[90] J. Ma and J. Liu. The BYY annealing learning algorithm for gaussian mixture with automated model selection. *Pattern Recognition*, 40(7):2029–2037, 2007.

[91] J. Ma, L. Xu, and M.I. Jordan. Asymptotic convergence rate of the em algorithm for gaussian mixtures. *Neural Comput.*, 12(12):2881–2907, 2000.

[92] A.W. MacLean, D.R.T. Davies, and K. Thiele. The hazards and prevention of driving while sleepy. *Sleep Medicine Reviews*, 7(6):507–521, 2003.

[93] D. Mascord, J. Walls, and G.A. Starmer. Fatigue and alcohol:interactive effects on human performance in driving-related tasks. In L. R. Hartley, editor, *Fatigue and Driving-Driver Impairment, Driver Fatigue and Driving Simulation*. Taylor and Francis, London, 1995.

[94] D.J. Mascord and R.A. Heath. Behavioral and physiological indices of fatigue in a visual tracking task. *Journal of Safety Research*, 23(1):19–25, 1992.

[95] G. Maycock. Sleepiness and driving: The experience of uk car drivers transport research library. *Journal of Sleep Research*, 5:229–237, 1996.

[96] R.E. Mayer and J.R. Treat. Psychological, social and cognitive characteristics of high-risk drivers: A pilot study. *Accident Analysis and Prevention*, 9(1):1–8, 1977.

[97] G.J. McLachlan and D. Peel. *Finite Mixture Models*. Wiley, New York, 2000.

[98] K. Messer, J. Matas, J. Kittler, and K. Jonsson. Xm2vtsdb: The extended m2vts database. In *In Second International Conference on Audio and Video-based Biometric Person Authentication*, pages 72–77, 1999.

[99] M. Meyer, A. Rahmel, C. Marconi, B. Grassi, P. Cerretelli, and J.E. Skinner. Stability of heartbeat interval distributions in chronic high altitude hypoxia. *Integr Physiol Behav Sci*, 33(4):344–62, 1998.

[100] J.C. Miller and R.R. Mackie. Some effects of long-term driving, irregular work schedules, and physical work on driver performance and psychophysiological arousal. In *19th International Congress of Applied Psychology*, 1978.

[101] W.F. Milliken and D.L. Milliken. *Race Car Vehicle Dynamics*. SAE International, 1995.

[102] S. Moss and E.R. Hancock. Cartographic matching with millimetre radar images. *Applications of Computer Vision, IEEE Workshop on*, 0:70, 1996.

[103] L.J. Mulder. Measurement and analysis methods of heart rate and respiration for use in applied environments. *Biol Psychol*, 34(2-3):205–36, 1992.

[104] L.J. Mulder. Measurement and analysis methods of heart rate and respiration for use in applied environments. *Biol Psychol*, 34(2-3):205–36, 1992.

[105] L.J. Mulder. *Assessment of cardiovascular reactivity by means of spectral analysis.* PhD thesis, 1988.

[106] K.P. Murphy. *Dynamic bayesian networks: representation, inference and learning.* PhD thesis, University of California, Berkeley, 2002.

[107] S. Nomura, T. Mizuno, A. Nozawa, H. Asano, and H. Ide. Salivary cortisol as a new biomarker for a mild mental workload. In *International Conference on Biometrics and Kansei Engineering (ICBAKE)*, pages 127–131, Cieszyn, 2009.

[108] O.G. Okogbaa, R.L. Shell, and D. Filipusic. On the investigation of the neurophysiological correlates of knowledge worker mental fatigue using the eeg signal. *Appl Ergon*, 25(6):355–65, 1994.

[109] F.G. Paas, J.J. Van Merrienboer, and J.J. Adam. Measurement of cognitive load in instructional research. *Percept Mot Skills*, 79(1 Pt 2):419–30, 1994.

[110] R. Parasuraman. *The Attentive Brain*. Cambridge, MA, and London: MIT Press, 1998.

[111] A. Penalver, F. Escolano, and J. Saez. Color image segmentation through unsupervised gaussian mixture models. In *Advances in Artificial Intelligence - IBERAMIA-SBIA 2006*, pages 149–158. 2006.

[112] J. Pearl. Bayesian networks. pages 149–153, 1998.

[113] C.K. Peng, S.V. Buldyrev, S. Havlin, M. Simons, H.E. Stanley, and A.L. Goldberger. Mosaic organization of dna nucleotides. *Phys. Rev. E*, 49(2):1685–1689, 1994.

[114] J. Piao and M. McDonald. Low speed car following behaviour from floating vehicle data. *Intelligent Vehicles Symposium, 2003. Proceedings. IEEE*, pages 462–467, 9-11 June 2003.

[115] S.W. Porges and E.A. Byrne. Research methods for measurement of heart rate and respiration. *Biol Psychol*, 34(2-3):93–130, 1992.

[116] J.H.A. Qader, L.M. Khadra, and H. Dickhaus. Nonlinear dynamics in hrv signals after heart transplantations. In *Signal Processing and Its Applications, 1999. ISSPA '99. Proceedings of the Fifth International Symposium on*, volume 1, pages 231–234, 1999.

[117] Ji Qiang, P. Lan, and C. Looney. A probabilistic framework for modeling and real-time monitoring human fatigue. *IEEE Transactions on Systems, Man and Cybernetics*, 36(5):862–875, 2006.

[118] R. Quinlan. *C4.5: Programs for Machine Learning (Morgan Kaufmann Series in Machine Learning)*. Morgan Kaufmann, 1993.

[119] R.M. Rangayyan. *Biomedical Signal Analysis: A Case-Study Approach*. NJ: IEEE press, 2001.

[120] P. Rani, J. Sims, R. Brackin, and M. Sarkar. Online stress detection using psychophysiological signals for implicit human-robot cooperation. *Robotica*, 20(6):673–685, 2002.

[121] R.A. Redner and H.F. Walker. Mixture densities, maximum likelihood and the em algorithm. *SIAM Review*, 26(2):195–239, 1984.

[122] L.A. Reyner and J.A. Horne. Falling asleep whilst driving: are drivers aware of prior sleepiness? *Int J Legal Med*, 111(3):120–3, 1998.

[123] D.A. Reynolds, T.F. Quatieri, and R.B. Dunn. Speaker verification using adapted gaussian mixture models. *Digital Signal Processing*, 10(1-3):19–41, 2000.

[124] G.Rigas, C.D. Katsis, P. Bougia, and D.I. Fotiadis. An intelligent decision support system for driver assistance based on vehicle, driver and road environment monitoring. In *7th European Congress and Exhibition on Intelligent Transport Systems and Services*, 2008.

[125] A.H.Roscoe. Assessing pilot workload. why measure heart rate, hrv and respiration? *Biol Psychol*, 34(2-3):259–87, 1992.

[126] M.R. Rosekind, P.H. Gander, K.B. Gregory, R.M. Smith, D.L. Miller, R. Oyung, L.L. Webbon, and J.M. Johnson. Managing fatigue in operational settings. 1: Physiological considerations and countermeasures. *Behav Med*, 21(4):157–65, 1996.

[127] M.R. Rosekind, E.L. Co, K.B. Gregory, and D.L. Miller. Crew factors in flight operations xiii: A survey of fatigue factors in corporate/executive aviation operations. Technical report, National Aeronautics and Space Administration (NASA), 2000.

[128] H. Rowley, S. Baluja, and T. Kanade. Neural network-based face detection. *IEEE Transactions on Pattern Analysis and Machine Intelligence*, 20(1):23–38, 1998.

[129] G. Rusconi, M.C. Brugnoli, P. Dosso, K. Kretzschmar, P. Bougia, D.I. Fotiadis, L. Salgado, F. Jaureguizar, and M. De Feo. I-way, intelligent co-operative system for road safety. *Intelligent Vehicles Symposium, 2007 IEEE*, pages 1056 –1061, 2007.

[130] E. Sa, V. Digalakis, and L. Neumeyer. Speaker adaptation using combined transformation and bayesian methods, 1995.

[131] K.Q. Shen, X.P. Li, C.J. Ong, S.Y. Shao, and E.P. Wilder-Smith. EEG-based mental fatigue measurement using multi-class support vector machines with confidence estimate. *Clin Neurophysiol*, 119(7):1524–33, 2008.

[132] L. Shen and L. Bai. A review on gabor wavelets for face recognition. *Pattern Analysis and Applications*, 9(2):273–292, 2006.

[133] W. Shinji, S. Atsushi, and N. Atsushi. Automatic determination of acoustic model topology using variational bayesian estimation and clustering for large vocabulary continuous speech recognition. *IEEE transactions on audio, speech, and language processing*, 14(3):855–872, 2006.

[134] M.R. Sikonja and I. Kononenko. Theoritical and empirical analysis of relieff and rrelieff. *Machine Learning*, 53:23–69, 2003.

[135] E.J. Sirevaag, A.F. Kramer, C.D. Wickens, M. Reisweber, D.L. Strayer, and J.F. Grenell. Assessment of pilot performance and mental workload in rotary wing aircraft. *Ergonomics*, 36(9):1121–40, 1993.

[136] M. Sivak. Human factors and highway-accident causation: Some theoretical considerations. *Accident Analysis and Prevention*, 13(2):61–64, 1981.

[137] H. Sjoberg. Physical fitness and mental performance during and after work. *Ergonomics*, 23(10):977–85, 1980.

[138] NCSDR/NHTSA Expert Panel on Driver Fatigue and Sleepiness. Drowsy driving and automobile crashes, 1998.

[139] R.G. Smart, E. Cannon, A. Howard, P. Frise, and R.E. Mann. Can we design cars to prevent road rage? *Int. J. Vehicle Information and Communication Systems*, 1:44–45, 2005.

[140] P.K. Stein, Q. Le, and P.P. Domitrovich. Development of more erratic heart rate patterns is associated with mortality post-myocardial infarction. *J Electrocardiol*, 41(2):110–5, 2008.

[141] H. Storm, K. Myre, M. Rostrup, O. Stokland, M.D. Lien, and J.C. Raeder. Skin conductance correlates with perioperative stress. *Acta Anaesthesiologica Scandinavica*, 46(7):887–895, 2002.

[142] H. Tan and Y.J. Zhang. Detecting eye blink states by tracking iris and eyelids. *Pattern Recogn. Lett.*, 27(6):667–675, 2006.

[143] M. Tarvainen, S. Georgiadis, P. Ranta-Aho, and P. Karjalainen. Time-varying analysis of heart rate variability signals with a kalman smoother algorithm. *Physiological Measurement*, 27(3):225–239, 2006.

[144] M. Treiber, A. Hennecke, and D. Helbing. Congested traffic states in empirical observations and microscopic simulations. *Physical Review E*, 62:1805, 2000.

[145] P. Viola and M. Jones. Robust real-time face detection. *International Journal of Computer Vision*, 57(2):137–154, 2004.

[146] N. Vlassis and A. Likas. A greedy em algorithm for gaussian mixture learning. *Neural Processing Letters*, 15(1):77–87, 2002.

[147] P. Wang and Q. Ji. Multi-view face and eye detection using discriminant features. *Computer Vision and Image Understanding*, 105(2):99–111, 2007.

[148] C.A. Waring and X. Liu. Face detection using spectral histograms and svms. *Systems, Man and Cybernetics, Part B, IEEE Transactions on*, 35(3):467–476, 2005.

[149] G. Welch and G. Bishop. An introduction to the kalman filter. Technical report, University of North Carolina at Chapel Hill, 1995.

[150] A. Wells and G. Matthews. *Attention and emotion.* LEA, London, 1994.

[151] C.M. Wickens and D.L. Wiesenthal. State driver stress as a function of occupational stress, traffic congestion, and trait stress susceptibility. *Journal of Applied Behavioural Research*, 10(2):83–97, 2005.

[152] C.J. Wientjes. Respiration in psychophysiology: methods and applications. *Biol Psychol*, 34(2-3):179–203, 1992.

[153] C.J. Wientjes. *Psychological Influences upon Breathing: Situational and Dispositional Aspects*. PhD thesis, 1993.

[154] A.M. Williamson, A.M. Feyer, and R. Friswell. The impact of work practices on fatigue in long distance truck drivers. *Accident Analysis and Prevention*, 28(6):709 – 719, 1996.

[155] G.F. Wilson. Applied use of cardiac and respiration measures: practical considerations and precautions. *Biol Psychol*, 34(2-3):163–78, 1992.

[156] A. Wisner. Fatigue and human reliability revisited in the light of ergonomics and work psychopathology. *Ergonomics*, 32(7):891–8, 1989.

[157] N. Wright, B. Stone, T. Horberry, and N. Reed. A review of in-vehicle sleepiness detection devices. Technical report, 2007.

[158] G. Xiong, C. Feng, and L. Ji. Dynamical gaussian mixture model for tracking elliptical living objects. *Pattern Recognition Letters*, 27(7):838–842, 2006.

[159] L. Xu and M.I. Jordan. On convergence properties of the em algorithm for gaussian mixtures. *Neural Computation*, 8:129–151, 1995.

[160] M. Yamaguchi and J. Sakakima. Evaluation of driver stress in a motor-vehicle driving simulator using a biochemical marker. *J Int Med Res*, 35(1):91–100, 2007.

[161] G. Yang, Y. Lin, and P. Bhattacharya. A driver fatigue recognition model using fusion of multiple features. In *Systems, Man and Cybernetics, 2005 IEEE International Conference on*, volume 2, pages 1777–1784, 2005.

[162] M. Yang, D. Kriegman, and N. Ahuja. Detecting faces in images: A survey. *IEEE Transactions on Pattern Analysis and Machine Intelligence*, 24(1):34–58, 2002.

[163] J. Zhai and A. Barreto. Stress detection in computer users based on digital signal processing of noninvasive physiological variables. *EMBS '06. 28th Annual International Conference of the IEEE*, pages 1355–1358, 2006.

[164] J. Zhai, A.B. Barreto, C. Chin, and C. Li. Realization of stress detection using psychophysiological signals for improvement of human-computer interactions. In *SoutheastCon, 2005. Proceedings. IEEE*, pages 415–420, 2005.

Author's Publications

Journal Publications

1. G. Rigas, C. Nikou, Y. Goletsis and D.I. Fotiadis, "A method for estimating Geometric transformations of Gaussian mixture models", (Submitted)

2. G. Rigas, Y. Goletsis and D.I. Fotiadis, "Real time Driver's Stress Event Detection", submitted in IEEE Transactions on Intelligent Transportation Systems

3. G. Rigas, Y. Goletsis, P. Bougia and D.I. Fotiadis, "Towards driver's state recognition on real driving conditions", Submitted in IEEE Transactions on System Man and Cybernetics, Part A.

4. A. Koutlas, G. Rigas, and D.I. Fotiadis, "A Fully Automated Methodology for Facial Expression Recognition", Submitted in IEEE Transactions on System Man and Cybernetics, Part B.

5. K.P. Exarchos, G. Rigas, C. Papaloukas and D.I. Fotiadis, "pCOMPARE: compare, visualize and annotate protein patterns", submitted.

6. K.P. Exarchos, T.P. Exarchos, C. Papaloukas, G. Rigas and D.I. Fotiadis, "Extraction of consensus protein patterns in regions containing non-proline cis peptide bonds and their functional ascertainment", submitted.

Conference Publications

1. G. Rigas, C.D. Katsis, G. Ganiatsas and D.I. Fotiadis. "A User Independent, Biosignal Based, Emotion Recognition Method". In Proceedings of the 11th international Conference on User Modeling, Corfu, Greece, July 25-29, 2007.

2. G. Rigas, C.D Katsis, P. Bougia and D.I. Fotiadis, "A reasoning-based framework for car driver's stress prediction", proceedings of IEEE Mediterranean conference on control and automation, MED08, Corsica, June 2008.

3. G. Rigas, A. Koutlas, C.D. Katsis, P. Bougia and D.I. Fotiadis, "An intelligent decision support system for driver assistance based on vehicle, driver and road en-

vironment monitoring", In Proceedings of the 7th European Congress on intelligent transport systems, ITS 2008, Geneva, Switzerland, June 2008.

4. G. Rigas, C.D. Katsis, P. Bougia and D.I. Fotiadis, "I-WAY: towards highway vehicle-to-vehicle communications and driver support", In Proceedings of the IEEE international conference on systems, man, and cybernetics, SMC 2008, Singapore, October 2008.

5. G. Rigas, C.D. Katsis, P. Bougia and D.I. Fotiadis, "An intelligent cooperative platform for enhancing drivers' perception on a highway environment", In Proceedings of the 1st Smart mobility Conference, Sophia-Antipolis, September 2008.

6. F. Dittmann, K.N. Geramani, G. Rigas, C.D. Katsis and D.I. Fotiadis, "Towards Advanced Information Fusion for Driver Assistant Systems of Modern Vehicles", proceedings of the 68th IEEE Vehicular Technology Conference, VTC Fall 2008, Canada September 2008.

7. G. Rigas, P. Bougia, G. Gkoletsis and D.I. Fotiadis. Towards advanced information extraction in cooperative driving support systems, 16th World Congress on ITS, 21-25 September 2009, Stockholm, Sweden.

8. G. Rigas, A.T. Tzallas, D. Tsalikakis, D.I. Fotiadis, Real-Time Quantification of Resting Tremor in the Parkinson's Disease. 31st Annual International IEEE Engineering in Medicine and Biology Society (EMBS 2009).

9. K.P. Exarchos, G. Rigas, Y Goletsis, D. Ardigo and D.I. Fotiadis, "Oral cancer reoccurrence prediction using Dynamic Bayesian Networks", IV International Conference on Computational BioEngineering (ICCB 2009), Bertinoro, Italy, 2009.

10. K.P. Exarchos, G. Rigas and D.I. Fotiadis, "Evolutionarily driven algorithm for the quantification of protein patterns' similarity", 17th Annual International Conference on Intelligent Systems for Molecular Biology and 8th European Conference on Computational Biology, (ISMB/ECCB 2009), Stockholm 2009.

11. G. Rigas, A.T. Tzallas, D. Baga, T.P. Exarchos, C.D. Katsis, D. Chaloglou, S. Konitsiotis and D.I. Fotiadis. "PERFORM: First steps in the assessment of patient motion status and support to treatment changes", 9th International Conference on Information Technology and Applications in Biomedicine (ITAB 2009), 2009.

12. K.P. Exarchos, G. Rigas and D.I. Fotiadis, "pCOMPARE: an evolutionarily driven algorithm for the quantification of protein patterns' similarity", ISMB Students Council Symposium 2009.

13. K.P. Exarchos, G. Rigas, Y. Goletsis, D. Ardigo and D.I. Fotiadis, "Oral cancer reoccurrence prediction using Dynamic Bayesian Networks", IV International Conference on Computational BioEngineering (ICCB 2009) 2009, Bertinoro, Italy.

14. K.P. Exarchos, G. Rigas and D.I. Fotiadis, "Evolutionarily driven algorithm for the quantification of protein patterns' similarity", 17th Annual International Conference on Intelligent Systems for Molecular Biology and 8th European Conference on Computational Biology, (ISMB/ECCB 2009), 2009.

15. K.P. Exarchos, G. Rigas, Y. Goletsis and D.I. Fotiadis, "Dynamic Bayesian Networks for disease evolution monitoring: the test case of oral cancer reoccurrence", 4th conference of the hellenic society for computational biology and bioinformatics (HSCBB09), 2009.

Short Vita

George Rigas was born in Aridaia, Greece in 1981. He reveived his Degree in Computer Science in 2003 and an McS in 2006 from the Computer Science Department, University Ioannina, Greece. Since 2006 has been a Ph.D. candidate in the Department of Computer Science, University of Ioannina, Greece.